DEVELOPMENT OF A CONTINUOUS PROCESS

FOR THE PRODUCTION OF

HEXAFLUOROPROPYL METHYL ETHER

Ashveer Krishen Domah

[BSc. (Eng.), UKZN]

University of KwaZulu-Natal

Durban

A thesis submitted in the School of Engineering

in fulfilment of the requirements for the degree

Master of Science in Engineering (Chemical)

October 2015

Supervisors: Doctor David Lokhat and Professor Deresh Ramjugernath

As the candidate's supervisor I agree to the submission of this thesis:

Dr. D. Lokhat

Prof. D. Ramjugernath

DECLARATION

I, Ashveer Krishen Domah, declare that:

The research reported in this dissertation/thesis, except where otherwise indicated, is my original work.

(i) This dissertation/thesis has not been submitted for any degree or examination at any other university.

(ii) This dissertation/thesis does not contain other persons' data, pictures, graphs or other information, unless specifically acknowledged as being sourced from other persons.

(iii) This dissertation/thesis does not contain other persons' writing, unless specifically acknowledged as being sourced from other researchers. Where other written sources have been quoted, then:

a) their words have been re-written but the general information attributed to them has been referenced;

b) where their exact words have been used, their writing has been placed inside quotation marks, and referenced.

(iv) Where I have reproduced a publication of which I am an author, co-author or editor, I have indicated in detail which part of the publication was actually written by myself alone and have fully referenced such publications.

(v) This dissertation/thesis does not contain text, graphics or tables copied and pasted from the Internet, unless specifically acknowledged, and the source being detailed in the dissertation/thesis and in the References sections.

Signed: 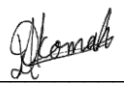

Date: _____

ACKNOWLEDGEMENTS

This research was undertaken as part of a large programme under the Fluorochemical Expansion Initiative (FEI) which has the backing of the Department of Science and Technology. This project was supported by the South African Research Chairs Initiative, the National Research Foundation, and Pelchem.

I would like to thank Professor D. Ramjugernath for his assistance and expertise in this project and impartment of knowledge. The utmost gratitude to Dr. D. Lokhat for his wealth of knowledge shared, technical support, friendship and guidance throughout the duration of this project.

I also acknowledge the assistance of the technical and laboratory staff of the University of KwaZulu-Natal, namely Sadha Naidoo and Ayanda Kanyele. Personal thanks go to my postgraduate colleague Kuveshan Padayachee for his friendship and support.

Lastly, I would like to thank my parents, Anita and Krishen Domah, and siblings for their encouragement and support.

ABSTRACT

Partially fluorinated dialkyl ethers are valuable intermediates for organofluorine syntheses. These compounds can be used for the preparation of perfluoroacrylic acids or the anhydrides, amides and esters thereof. They also serve as very effective solvents, particularly for the extraction of essential oils. A continuous process for producing 1,1 ,2,3,3,3-hexafluoropropyl methyl ether by reacting a liquid mixture of potassium hydroxide and methanol with gaseous hexafluoropropene in one or more microstructured devices was developed. The reaction of hexafluoropropene and potassium methoxide is highly exothermic, with higher operating temperatures favouring the formation of hexafluoropropyl methyl ether. The reactants are contacted for a prescribed time within a reaction zone having a high heat transfer area to reaction volume ratio and in intimate contact with a cooling medium, facilitating efficient dissipation of the exothermic reaction heat. The product mixture is contacted with water at below ambient temperature to extract the residual methanol and the raffinate is further purified by means of conventional distillation. The water and methanol mixture is fed to a distillation column that recovers methanol at a purity of 99%. The HME-methanol mixture is fed to another distillation column which produces HME at 98% purity. The methanol recovered from both distillation columns is recycled to the start of the process. The synthesis of hexafluoropropyl methyl ether using the aforementioned process was demonstrated experimentally using a falling film microreactor. Quadratic response surface methodology was used to probe for optimal reaction conditions for the yield of hexafluoropropyl methyl ether as well as the purity of the raw product.

TABLE OF CONTENTS

Chapter 3 – Materials, methods and procedures

Chapter 4 – Preliminary work – semi-batch gas-liquid reactor

Chapter 5 – Design of reaction section of the proposed process-synthesis of HME using falling-film microreactor technology

Appendix F – MatLab code

LIST OF SYMBOLS

Symbol	Description	
A	area	m^2
$a_{k/l}$	group Wilson parameter	
d	diameter	m
E	Extent of extraction	
F	response factor	
$F_{L/V}$	liquid-vapour flow factor	
F_o	Fourier number	
h	height	m
j_l	mean velocity	$m \cdot s^{-1}$
L_w	Liquid mass flow	$kg \cdot s^{-1}$
$m_{k/l}$	group pair parameters	
m	mass number	
M	mass	kg
n	moles	mol
$n_{k/l}$	group pair parameters	
P	pressure	Pa
R	universal gas constant	$J \cdot mol^{-1} \cdot K^{-1}$
R	correlation coefficient	
Re	Reynolds Number	
t	time	s
T	temperature	K
V	volume	m^3
V_w	vapour mass flow	$kg \cdot s^{-1}$
wt	weight	
x	mole fraction in liquid phase	
X	experimental factor	
X_o	stationary point	
y	mole fraction in vapour phase	
Y	response factor	
Y_o	response at stationary point	
z	charge number	

Greek letters

Symbol	Description
α	spacing for axial design point of central composite design
β	quadratic model coefficient
γ	activity coefficient
δ	thickness
λ	eigenvalue
μ	vapour velocity at weep point
ρ	density
Γ	group activity coefficient
ν	number of groups

Superscripts/subscripts

Symbol	Description
calc	calculated value
dc	downcomer
exp	experimental value
FH	size contribution
G	group contribution
i	species/factor *i*
is	internal standard
j	species/factor *j*
k	group *k*
l	liquid
obj	objective
ow	over weir
max	maximum
meth	methanol
min	minimum
r	residual
surf	surface
v	vial
v	vapour

LIST OF ABBREVIATIONS

ANOVA	Analysis of variance
ASOG	Analytical solution of groups
DIST	Distillate
DoF	Degrees of freedom
EXP	Experimental
FEI	Fluorochemical expansion initiative
FFMR	Falling-film microreactor
GC	Gas chromatography
GC-MS	Gas chromatography-mass spectrometry
GLR	Semi-batch gas-liquid reactor
HF	Hydrogen Fluoride
HFP	Hexafluoropropylene
HFPO	Hexafluoropropylene oxide
HME	Hexafluoropropyl methyl ether
HPU	HME purification unit
IS	Internal standard
KF	Potassium Fluoride
KOH	Potassium Hydroxide
LLE	Liquid-Liquid Extraction
LP	Low pressure
MRU	Methanol recovery unit
MS	Mean square
NDP	Number of data points
NECSA	South African Nuclear Energy Corporation
NRTL-RK	Non-random two liquid – Redliech-Kwong
PFDE	Partially flourinated dialkyl ethers
PID	Proportional-integral-derivative
PMP	(E)-1,2,3,3,3-pentafluoro-1-methoxy-prop-1-ene
SRE	Salt recovery evaporator
SRM	Surface Response Methodology
SS	Square sum
TFP	methyl 2,3,3,3 – tetrafluoropropionate
VLE	Vapour-Liquid equilibrium

LIST OF FIGURES

Chapter 1

Chapter 2

Chapter 3

Chapter 4

Chapter 5

Chapter 6

Chapter 7

Appendix A

Appendix B

LIST OF TABLES

Chapter 2

Chapter 3

Chapter 4

Chapter 5

Chapter 6

Appendix A

Appendix B

Appendix C

Appendix D

Appendix E

LIST OF PHOTOGRAPHS

Chapter 3

Chapter 4

1

CHAPTER ONE

1. INTRODUCTION

1.1 Project motivation and outline

In 2009, the Department of Science and Technology and Trade and Industry in collaboration with South African Nuclear Energy Corporation's (NECSA) chemical division launched the Fluorochemical Expansion Initiative (FEI). The purpose of the programme was to establish a fluorochemicals industry in the country that could produce higher-value fluorochemicals from an abundant feedstock of fluorspar (Pelchem, 2011).

Fluorspar (CaF_2) reserves in South Africa are in excess of 41 million tons yet, only about 5% is beneficiated to higher value fluoro-compounds while 95% is exported. Fluorspar is a precursor to almost all fluorochemicals produced industrially. South Africa is, at present, the second largest fluorspar producer globally (Pelchem, 2011).

The Fluorine Process Engineering and Separation Technology Chair at the University of KwaZulu- Natal has been involved in such projects in affiliation with NECSA and Pelchem. A process for the production of hexafluoropropylene oxide (HFPO), a valuable fluorochemical intermediate that is commonly converted to inert oils, high performance liquids, elastomers and membranes, from HFP was developed (Lokhat, 2012).

The Chair is now focusing on moving up the fluorochemical value-chain with further derivatives of HFP and HFPO being synthesized to even higher value chemicals following previous work developing processes to produce these base compounds. The chemicals produced at this level will be high value/low volume fine or specialty chemicals.

Partially fluorinated dialkyl ethers are valuable intermediates of organofluorine syntheses. These compounds can be used for the preparation of perfluoroacrylic acids or the anhydrides, amides

and esters thereof. They also serve as very effective solvents, particularly for the extraction of essential oils (Il'in, 2004).

Particular interest in this project was the synthesis of 1,1,2,3,3,3-hexafluoropropyl methyl ether (HME) which finds applications as an oil and water repellent, refrigerant, fertilizer, industrial solvent as well as a foam blowing agent (Il'in et al., 2004).

HME is produced via the reaction of HFP and an alcohol (methanol) in the presence of an alkali hydroxide (KOH). By-products in the form of alkenyl ethers and alkyl propionates are also formed. The process also yields small quantities of a salt, potassium fluoride, when potassium hydroxide catalyst is used. This is produced through the interaction of the reaction intermediates with the potassium hydroxide catalyst.

Unfortunately no large scale process is currently in operation for the synthesis of hexafluoropropyl methyl ether, the organofluorine compound of interest in this study, as a result of solid salt formation through an undesired side reaction which renders scale-up difficult.

1.2 Research hypothesis and objectives

The central hypothesis of the proposed research is that a continuous process for the production of HME can be designed using a falling film reactor and conventional separation technologies. Experimentation was performed to test the hypothesis and critical analysis was done to address the specified objectives, which are discussed below.

The first objective was to find optimal reaction conditions to maximize the yield and mole fraction of HME in the reactor effluent. Emphasis was placed on finding the appropriate reaction conditions that minimized the formation of undesired salt precipitate. This was conducted in a semi-batch gas-liquid reactor (GLR) of which the effect of reactor temperature, catalyst concentration and HFP mole fraction on the performance of the unit was examined.

The synthesis of HME was then conducted in a falling-film microreactor (FFMR). The results obtained from the preliminary work on the semi-batch apparatus served as a guideline for the experimental design. This was a continuous process as opposed to the aforementioned semi-batch process which poses greater economic viability. The reaction conditions investigated were reaction temperature, catalyst concentration, HFP mole fraction and liquid reagent flow rate.

These conditions were optimised to give appropriate levels of conversion, yield and selectivity. Scaling-up of the process may thereafter be realised by means of multiple FFMR's in parallel.
Experimental runs in the preliminary study on the GLR and some of the experimentation on the FFMR were carried out prior to this project in the Laboratory Project 1 (ENCH4LA) and Laboratory Project 2 (ENCH4LB) courses at the University of KwaZulu-Natal. This was a collaborative effort between myself and fellow laboratory partner Kuveshan Padayachee who is also using the experimentation as a basis for his post-graduate studies. His dissertation focuses primarily on kinetic model development and identification, whereas this dissertation focuses on a full process design and optimization of unit operations as well as an operating philosophy.

The second objective was to design a separation system to purify HME up to a purity level commercially salable (>98 mol%), using conventional technologies. This focussed on salt removal from the reactor effluent, extraction of the bulk of unreacted methanol and finally the distillation of HME to commercial level.

1.3 Process Overview

In Figure 1.1, a process flow diagram of the proposed process is illustrated. Fresh and recycled methanol will be added to a hopper with a separate feed of solid KOH catalyst and fed to the FFMR as liquid feed. This will be contacted with a gaseous feed stream of HFP and nitrogen. Unreacted gas may be vented and the liquid product will be sent to the salt recovery unit.

In the salt recovery unit, the lighter components in the feed stream will be evaporated which will concentrate the high boiling components in the unit. These components, consisting largely of water and dissolved salts, will be removed via a purge line.

The lighter boiling components from the salt recovery unit will be condensed and enter the liquid-liquid extraction phase of the process. The feed, which is primarily HME and unreacted methanol, will be contacted with water. Due to the miscibility of methanol in water and the hydrophobicity of HME, an aqueous phase of methanol and water will be formed together with an organic phase consisting, in large proportion, of HME. The organic phase will be sent to the HME purification unit to concentrate the HME in the product stream to >98 mol% composition. The aqueous phase is fed to the methanol recovery unit which will separate methanol and water.

The methanol from both units will be combined and recycled to the feed. The water removed in the methanol recovery unit will be recycled to the liquid-liquid extraction phase of the process. Each unit operation making up the process will be studied, designed and optimized.

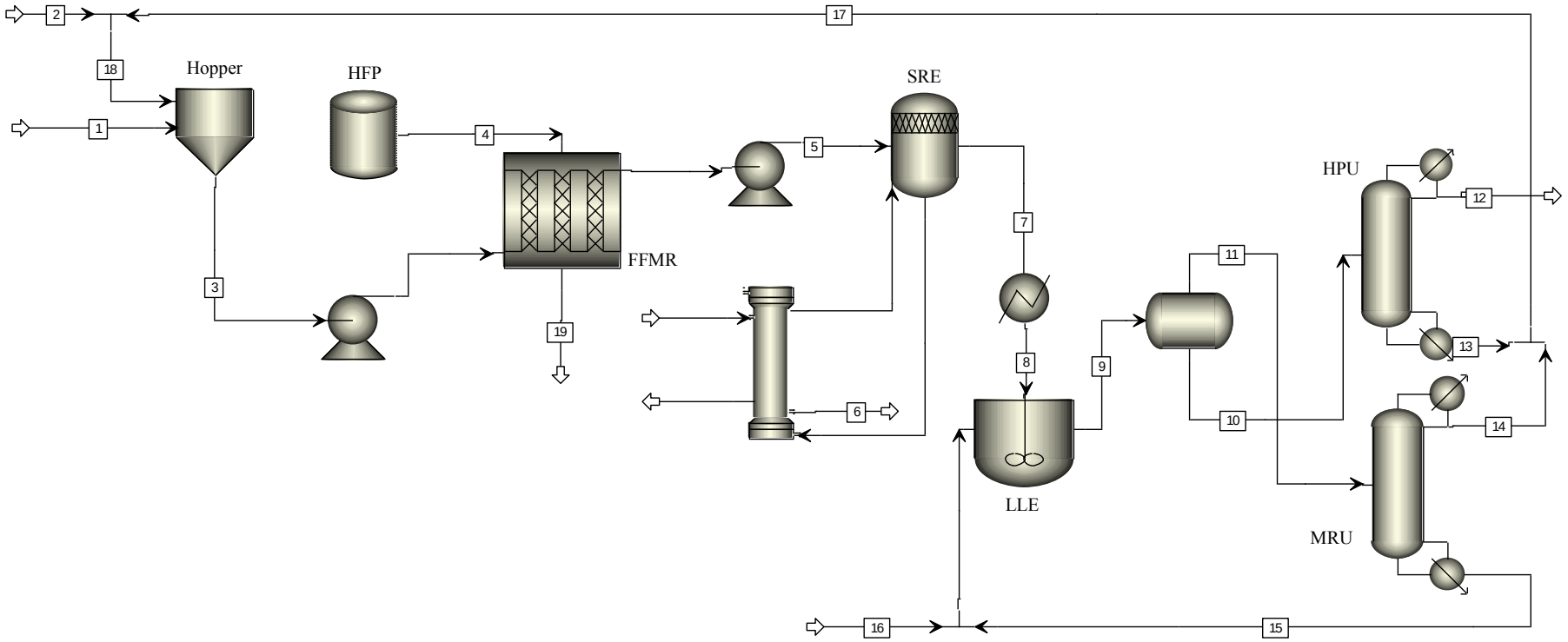

Figure 1.1: Conceptual process flow diagram

1.4 Report overview

The report comprises of 8 chapters and 7 appendices inclusive of the current chapter. Below is an elaboration on the components of the report.

Chapter 2 contains the literature survey with regards to the project undertaken. It provides the foundation for the project and includes a discussion of the synthesis of speciality organofluorine compounds as well as the experimental design method and surface response analysis.

Chapter 3, the materials, apparatus and methods section of the report, contains information on the procedures of the experimentation, the materials used in the experiment as well as the analytical techniques used for data analysis. Chapter 4 presents the results of the project and a discussion of the obtained results for preliminary work on a semi-batch gas-liquid reactor. In Chapters 5, the results from the FFMR experiments are discussed. Chapter 6 deals with the separation and purification procedures proposed to achieve a marketable composition of HME. Chapter 7 and 8 are the conclusions and recommendations respectively, for the project.

2

CHAPTER TWO

2. LITERATURE SURVEY

The purpose of this chapter is to give a brief history of similar experimentation performed to synthesize fluorinated ethers. It also elaborates on the commercial development and application of microreactor technology, the technology used to perform the experiments in this dissertation.

The theory behind the selection of process equipment and the design thereof are also presented herein. Vapour-liquid equilibrium data (VLE) and liquid-liquid equilibrium (LLE) are required for the design of industrial unit operations such as distillation columns and liquid-liquid extraction. Due to the novel nature of hexafluoropropyl methyl ether (HME), the compound of study in this dissertation, there is a general lack of kinetic information of systems involving HME. This chapter explains how VLE data was generated using the group-contribution method as well as how experimental results were used to scale-up the process because of the lack of LLE data.

2.1 Previous experimental studies on the synthesis of fluoroethers

Rendall et al. (1958) investigated the synthesis of partially fluorinated dialkyl ethers from various fluorinated compounds. According to the authors, this was the first investigation into the synthesis of these compounds. Gaseous hexafluoropropylene (HFP) served as the major fluorocarbon compound of interest and was bubbled through a solution of 10 wt% potassium hydroxide dissolved in methanol at approximately 303.15 K. The liquid product produced from the reaction was poured over crushed ice. Two distinct liquid layers were formed. The bottom layer was drawn off and was fractionally distilled. The major constituent component identified was 1,1,2,3,3,3-hexafluropropyl methyl ether (HME) which had a boiling point of 326.85 K. 1.92 kg of crude HFP was introduced into the system which resulted in 1.2 kg of HME being recovered after the fractionation. Ignoring the losses of product during the separation process, this corresponds to a yield of 62.4 wt% of HME with respect to the feed gas (Rendall et al., 1958).

The most recent experimental study of this system was reported by Il'in et al. (2004). They reported procedures to synthesise partially flourinated dialkyl ethers (PFDE) using HFP and a polyfluorinated alcohol in the presence of an alkali hydroxide. Similar to the experimental set-up mentioned previously, a flask with a 50 cm^3 solution of methanol with 12.5 wt% KOH dissolved was sparged with a gaseous flow of HFP at atmospheric pressure. An indication of the highly exothermic nature of the process was observed as the reaction temperature rapidly increased from 293.15 K to 313.15 K during the course of the experiment. The flow of HFP was stopped when the temperature showed minimal deviation as this indicated the reaction had reached completion in this batch set-up. The contents of the flask was then mixed with 400 cm^3 of cold water, agitated and two distinct liquid layers were formed. The bottom layer was extracted, washed again with 100 cm^3 of cold water and dried over calcium chloride ($CaCl_2$). The final product was distilled, analysed and a 98% yield was recorded of what was again identified as HME. The boiling point of the compound was reported to range between 327.15-328.15 K. The authors concluded that the formation of the ether product was via the addition of the alcohol across the double bond of HFP (Il'in et al., 2004).

Apart from the aforementioned efforts, there appears to be a general lack of kinetic information in the literature regarding this reaction system, including critical information on solid by-product formation and an appropriate operating envelope.

Hudlicky et al. (2000) investigated the preparation of fluorinated ethers via a reaction with bromine trifluoride. In seven different experiments different hydrocarbon ethers were used as starting reagents and reacted with bromine trifluoride to produce a fluorinated ether. The authors highlighted a general procedure for the preparation of ethers with bromine trifluoride. The reactant was placed in a dry 100 cm^3 round-bottomed flask which was equipped with a condenser, stir bar and septum in this batch set-up. The contents of the flask was charged with bromine trifluoride at room temperature and agitated by means of the stir bar. After the reaction had reached completion, the condenser was removed and the product was collected and washed with a 10% aqueous KOH solution followed by a 10% sodium sulphite solution and then dried over KOH. To concentrate the product, it was flash distilled. The flash distillation produced their respective products with purities in excess of 98% according to gas chromatography results (Hudlicky, et al., 2000).

Kato et al. (2003) proposed a new dechlorination process to reform chlorodifluoro methane ($CHClF_2$), commonly referred to as R-22, to difluoro methyl ether (CH_3OCHF_2). The reaction was performed in a batch system with a flask submerged in a water bath. The condenser used

maintained a constant temperature of 273 K by means of a chiller which was chosen to prevent solvent evaporation. A mixture of nitrogen and R-22 was charged to a solution of sodium methoxide and agitated with a magnetic stirrer. The reaction produced sodium chloride salt and a fluoroether (Kato, et al., 2003).

Chi et al. (1999) reported a method to synthesize partially fluorinated dialkyl ethers. The authors used perfluoropropoxyethylene as their base reagent and they investigated the reaction with the addition of different aliphatic alcohols (methanol, propanol, ethanol, n-butanol 2,2,2-trifluoroethanol, iso-propanol, iso-butanol, and 2-methoxyethanol). These reactions were performed in the presence of potassium hydroxide in a tetrahydrofuran (THF) solvent. It was stated that this had a significant effect in obtaining greater yields. Dioxane and acetonitrile were also proposed as alternative solvents to THF. The authors proposed a typical procedure for the preparation of partially fluorinated ethers. The base reagent (10 g) was dissolved in 15 cm^3 of the solvent, with THF used during these experimental runs. This solution was added to 38 cm^3 of alcohol for 30 minutes. The solution was then agitated at room temperature overnight. The solution was thereafter mixed with 200 cm^3 of water. The organic phase of the resulting solution was removed and washed again with 50 cm^3 of water. The crude product was finally distilled to further concentrate the fluoroether product (Chi, et al., 1999).

There have been various methods of synthesizing fluorinated ethers proposed in literature. Typical methods include fluorination of an ether with fluorine gas, fluorination using a metal fluoride, addition reaction with an alcohol and electro-chemical fluorination of an ether compound. Murata et al. (2002) states that an addition reaction of an alcohol to a fluorinated olefin is the most convenient method to synthesize fluorinated ethers. The authors reacted different fluorinated olefins with an alcohol and proposed a general experimental procedure to facilitate the addition reaction. The alcohol used in their study was 2,2,2-trifluoroethanol (1.0 mmol) which was mixed with 0.1 mmol of potassium hydroxide to form a solution. The reaction was performed in a stainless-steel reactor with a capacity of 10 cm^3. The reactor contents was initially cooled using liquid nitrogen and thereafter 7.5 mmol of the fluorinated olefin was introduced to the system and agitated. The reaction products were then fractionally distilled which allowed the saturated and unsaturated ethers to be separated (Murata, et al., 2002).

According to the studied literature, all attempts of synthesizing fluoroethers have been performed on batch systems on a very small scale. Commercialization has not been rapidly carried out due to inherent difficulties in the scaling-up of such processes (e.g. highly exothermic reactions, by-product precipitation, toxic reagents, etc.)

2.2 Synthesis of hexafluoropropyl methyl ether – reaction chemistry

Partially fluorinated dialkyl ethers are synthesized via the reaction between an organofluorine compound with an alcohol. This reaction occurs in the presence of an alkali hydroxide which serves as a catalyst to the reaction. In this investigation, hexafluoropropyl methyl ether (HME) which is a partially fluorinated ether, is synthesized via the reaction of gaseous hexafluoropropylene (HFP) with a liquid mixture of methanol and potassium hydroxide (KF) as shown in Reaction 2.1 (Il'in et al., 2004).

The reaction also results in by-products being formed as shown in the reaction scheme below. These include an alkenyl ether, 1,2,3,3,3-pentafluoro-1-methoxyprop-1-ene, and an alkyl tetrafluoropropionate, methyl 2,3,3,3-tetrafluoropropionate (Il'in et al., 2004).

$$CF_3CFCF_2 \xrightarrow{CH_3O^-} [CF_3CFCF_2OCH_3]^- \xrightarrow{+H^+} CF_3CFHCF_2OCH_3 \quad (2.1)$$

$$CF_3CFCF_2 \xrightarrow{CH_3O^-} [CF_3CFCF_2OCH_3]^- \xrightarrow{-F^-} CF_3CFCFOCH_3 \quad (2.2)$$

$$CF_3CFCF_2 \xrightarrow{CH_3O^-} [CF_3CFCF_2OCH_3]^- \xrightarrow{H_2O} CF_3CFHCOOCH_3 \quad (2.3)$$

During the synthesis of HME, another reaction, shown in Reaction 2.4, may occur and result in the formation of undesired potassium fluoride in addition to the side products shown in Reactions 2.1-2.3. The reaction shown in Reaction 2.4 is undesired for two reasons: KF has a low solubility in methanol and therefore forms a precipitate which makes large scale production of HME using conventional reactor configurations difficult. The reaction also consumes the alkali hydroxide catalyst, KOH. This impedes the conversion of reactants to the desired product due to a reduced rate (Il'in et al., 2004).

$$HF + KOH \rightarrow KF + H_2O \quad (2.4)$$

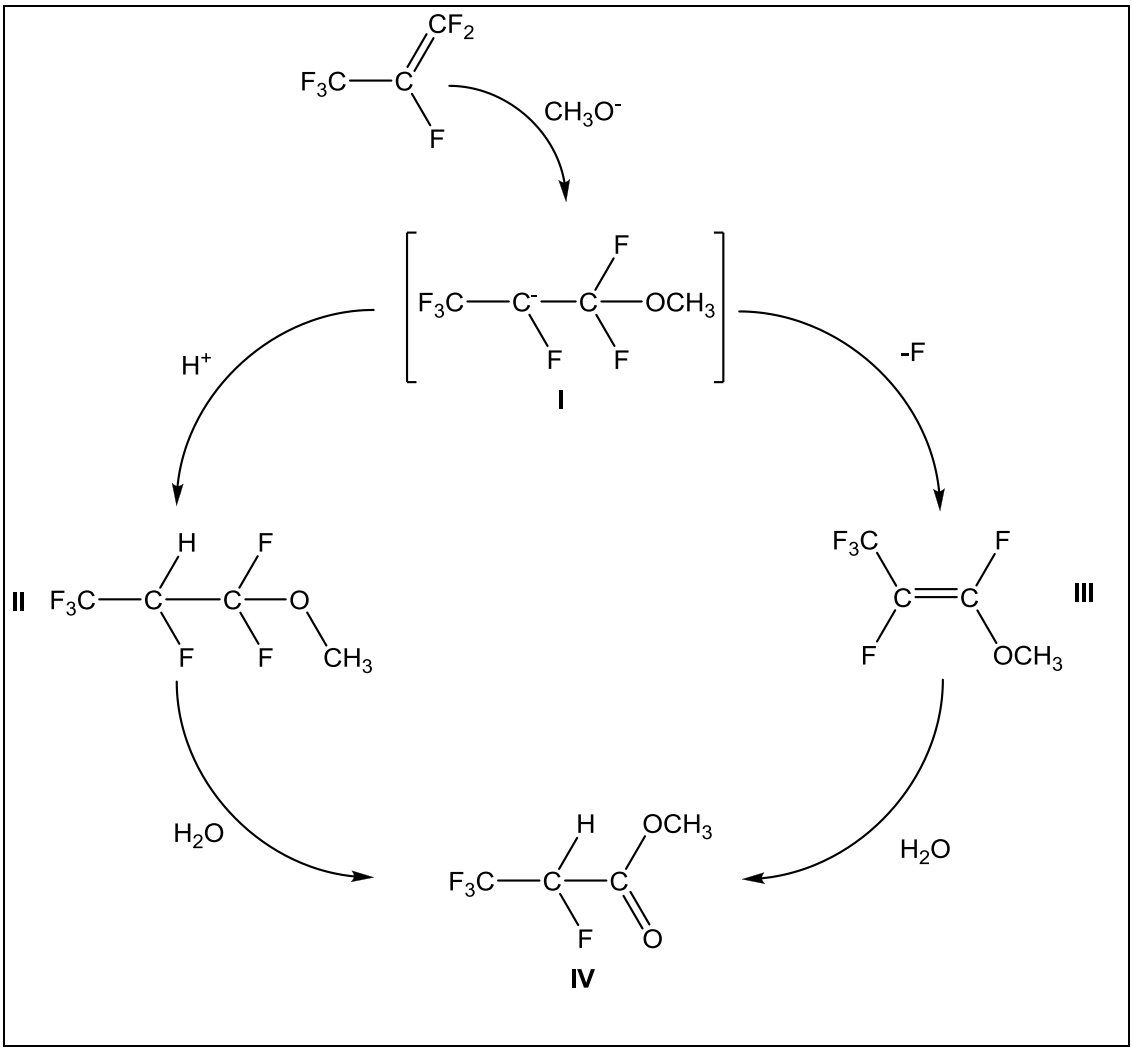

Figure 2.1: 1,1,2,3,3,3-hexafluoropropyl methyl ether reaction mechanism

The reaction mechanism for the formation of HME is illustrated in Figure 2.1. There is an addition reaction between an alkoxy anion, from the methanol, and HFP whereby the alkoxy anion saturates the HFP via addition to the carbon-carbon double bond resulting in the formation of compound **I,** which is a carbo-anion intermediate. The alkoxy anion is formed from methanol by releasing a proton, H^+. The anion intermediate **I** subsequently bonds with the free proton producing the target compound HME, **II**. There are also alternate reaction pathways resulting in the formation of two side products. By means of the elimination of a fluorine ion from reaction product **I**, an alkenyl ether, 1,2,3,3,3-pentafluoro-1-methoxyprop-1-ene, is formed denoted as compound **III** in Figure 2.1. The second side reaction occurs in the presence of water whereby an alkyl tetrafluoropropionate, methyl 2,3,3,3-tetrafluoropropionate, is formed illustrated by the annotation **IV** via hydrolysis.

The free hydrogen proton and fluorine anion may also react to form hydrogen fluoride (HF) and via the reaction with catalyst in Reaction 2.4 mentioned above, undesired potassium fluoride (KF) salt may form. Water is also produced from this reaction, which subsequently accelerates the hydrolysis of HME and the alkenyl ether (Il'in et al., 2004).

2.3 Reactor selection and development

2.3.1 Development and application of microreactors

Previously, it was believed that the only suitable approach to performing solution phase synthesis was conventional batch processes. The general focus being on a stationary reacting vessel with a means of agitation (Junkers, 2014).

Microreactors have changed the approach to chemical synthesis. In the past, research into synthetic pathways to produce new materials was performed and optimized in a batch system. If the product was a market driver and demand grew, the synthesis process would need to be readjusted to the larger batch scale. In a conventional batch system, this translates to larger units and this often restricts growth as many expansions are space-limited. Microreactors reduce capital and operating costs while having a less significant environmental impact by reducing the size of the chemical plant (Hessel, 2010). Figure 2.2 shows two typical microreactors, specifically falling-film microreactors.

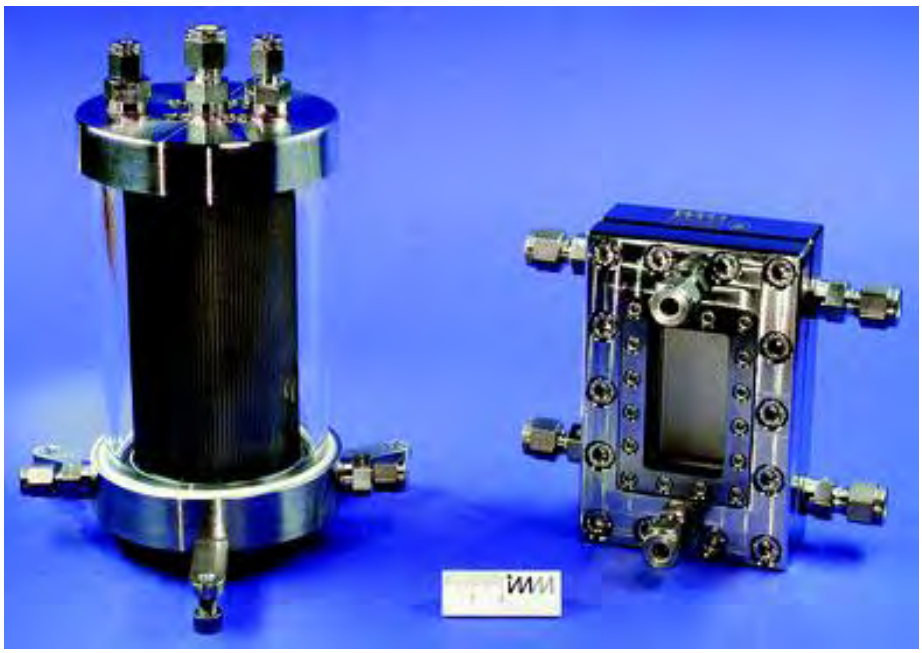

Figure 2.2: Cylindrical and rectangular falling-film microreactors (Maskos, 2015)

This was one of the factors that influenced the development of micro-structured reactors. Due to continuous operation of these units, the same output of a batch system can be produced in a shorter time requiring less space (Hessel, 2010).

Microreactor technology can enable alternate reaction paths including hazardous reactions due to increased safety, solvent free reactions and fluorination due to the enhanced process control available (Pohar, 2009).

The properties of a micro-structured device that allow more efficient processes are enhanced heat and mass transfer. Due to the high surface area to volume ratio in a microreactor, heat released in an exothermic reaction is absorbed much easier than in a batch system. In a batch system, cooling only takes place at the surfaces of the reactor which generates a temperature gradient from the surface to the centre of the reaction vessel. To give a holistic picture, a 1 m^3 reaction vessel has a surface area to volume ratio 3000 times smaller than a standard microchannel. At a laboratory level, microreactors are largely incorporated into the processes to synthesize new chemicals and in the development of processes for scale-up (Hessel, 2010).

Due to the larger thermal gradient in a batch system, it is more prone to develop hotspots. This can favour undesirable side reactions or even result in decomposition. Due to the micro-reactors heat efficiency, this will not be experienced. This allows greater precision in temperature control which becomes more prevalent when attempting to scale-up a process (Pohar, 2009).

Generally in batch systems, a synthesis process that works well in a laboratory scale may have process control issues on a larger scale. This may limit the operability of the unit. In microreactor technology, scale-up generally only affects the operation time of the system with no further process development necessary. Higher capacities can be achieved with microreactor technology by operation of multiple units as opposed to difficult and generally expensive scale-up of other technologies. This also creates a more robust process because a single unit can be isolated from the process to maintain continuous operation. This is in contrast to the operation of a single scaled-up batch unit (Pohar, 2009).

As with many developments of technology, safety implications play a highly influential role. In batch systems, highly exothermic reactions are difficult to control with runaway reactions a likely possibility. The relatively small inner volume of a microchannel in a microreactor coupled with high heat exchange efficiency often guarantees safe and stable operation (Hessel, 2010).

The mass transfer is often considered the core element of the reaction vessel. This becomes increasingly important with the possibility of side reaction occurring, making control of the molar ratios of the reactants fundamental in suppressing undesired reactions. The large interfacial

area in a microreactor facilitates a greater amount of mass transfer than in a batch system with mechanical agitation (Hessel, 2010).

A crucial factor facilitating the development of microreactors is that microreactors are considered to be the most applicable unit operation, when reactions that necessitate high mass or heat transfer rates in order to control a reaction rate or synthesis route (Hessel, 2010).

Common applications of microreactors include direct fluorination of organic compounds, nitration of organic and aromatic compounds, catalytic reactions, exothermic gaseous catalytic reactions, catalytic hydrogenations and dehydrogenation and liquid phase catalytic reactions (De Mello & Wootton, 2002).

A summary of the more prominent applications of microreactors include ethylene oxide synthesis conducted by Kestenbaum et al. (2002). The authors had previously worked on a batch system and compared their results with the use of a microreactor to an existing industrial batch process. They concluded that the microreactor was more applicable to the process due to the improved heat transfer characteristics observed. In addition, due to the inherent safer operation in using a microreactor, they could use greater compositions of ethylene in pure oxygen feed which is classified as explosive. This could not be achieved in the industrial application. The authors also reported that higher volumetric production rates were achieved with the microreactor technology. Figure 2.3 illustrates the system used in the ethylene oxide synthesis.

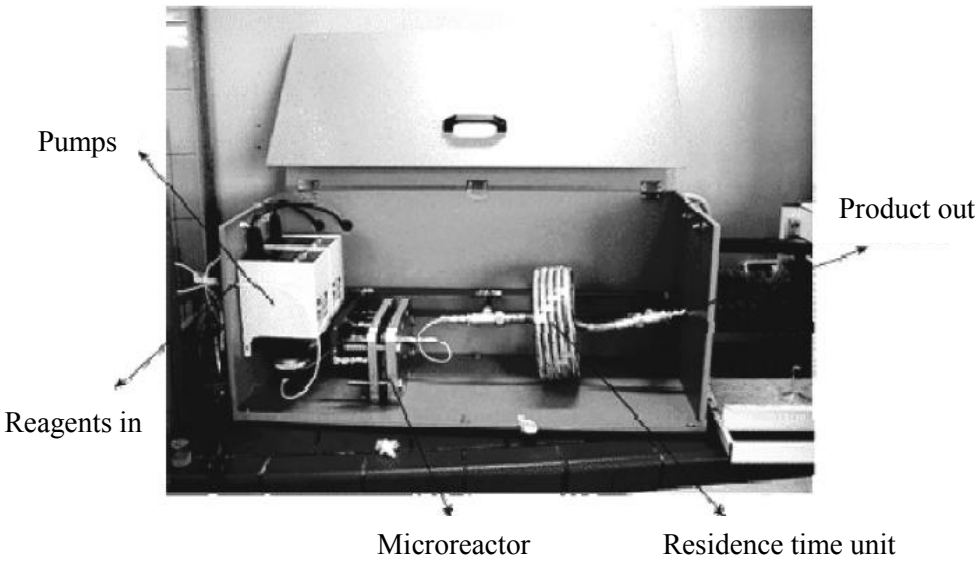

Figure 2.3: Experimental system for the synthesis of ethylene oxide (Kestenbaum et al., 2002)

In a review on the intensification of photocatalytic processes by van Gerven et al. (2007), microreactors were found to be the most applicable unit operation to facilitate photochemical and photocatalytic reactions. The authors based their claim on the high surface to volume ratio synonymous with microreactor technology. This was evident as in the case of photochemical reactions, effective contact in the reaction leads to efficient illumination. It was also reported that there was better control of important parameters such as temperature and flow due to the effective heat and mass transfer. In such applications, microreactors can produce up to 10 times greater product per unit volume than conventional batch systems.

A study by Kraii et al. (2008) showed a production rate of 61 $kg \cdot m^{-3} \cdot min^{-1}$ was achieved in the synthesis of biodiesel as compared to 42 $kg \cdot m^{-3} \cdot min^{-1}$ reported for the typical batch process. It was also reported that the microreactor is more efficient since the cleaning of the reactor between the batches can be omitted.

De Mas et al. (2009) performed an investigation into increasing productivity of microreactors for gas-liquid reactions. The direct fluorination of toluene in acetonitrile was selected as a model reaction and the synthesis carried out at ambient conditions. The throughput of a single-channel microreactor was increased by one order of magnitude relative to previous published results. This was achieved by the simultaneous increase of the superficial gas and liquid velocities. The authors reported that the contact between the two phases was enhanced with the increased gas and liquid velocities thus compensating for the reduced liquid residence time. Figure 2.4 shows the microreactor used for the gas-liquid reactions testing the effect of increased gas and liquid flow rates.

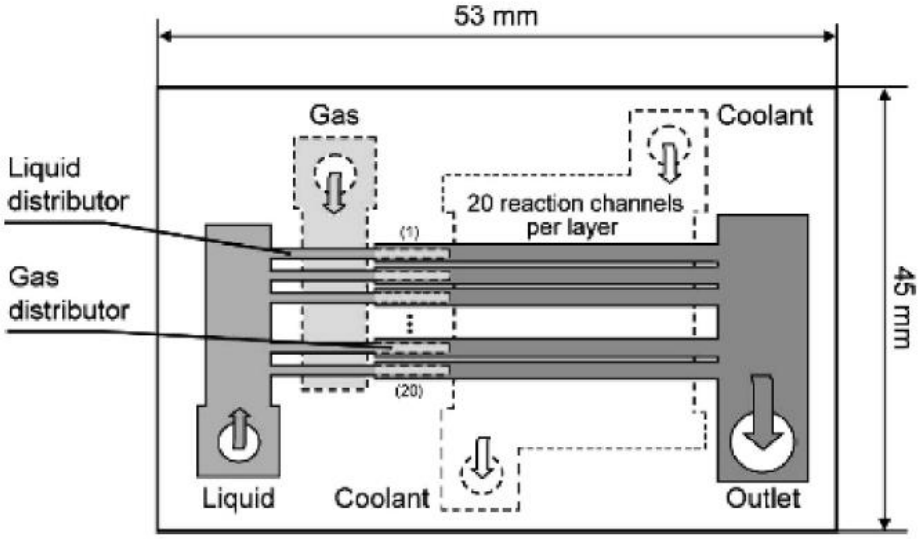

Figure 2.4: Microreactor used to test the effect of increased gas and liquid flow rates (De Mas et al., 2009)

Another favourable application for the microreactor is the synthesis of fluorine-containing organic compounds. The use of the microreactor; eliminates the safety hazards associated with the handling of fluorine, it allows for efficient mixing and improved temperature control (Chambers & Spink, 1999).

2.3.2 Selection and design of reactors for fine chemical synthesis

Characteristically, fine chemicals are produced in batch reactors. Consequently, product quantities below 1000 tons per year are common. However, due to the great monetary value of the product as intermediate materials for the production of speciality chemicals, these processes do not prescribe to the usual economies-of-scale (Pagliaro, 2014).

The reactors commonly employed for these applications are continuous stirred tank reactors in a semi-batch set-up with a homogenous catalyst with excess reactant needed to drive the reaction. This is not an efficient process as intensive separation and purification is thereafter required for the isolation of the fine chemical being produced. This also leads to excessive waste generation (Pagliaro, 2014). Figure 2.5 shows a typical set-up of a batch reactor.

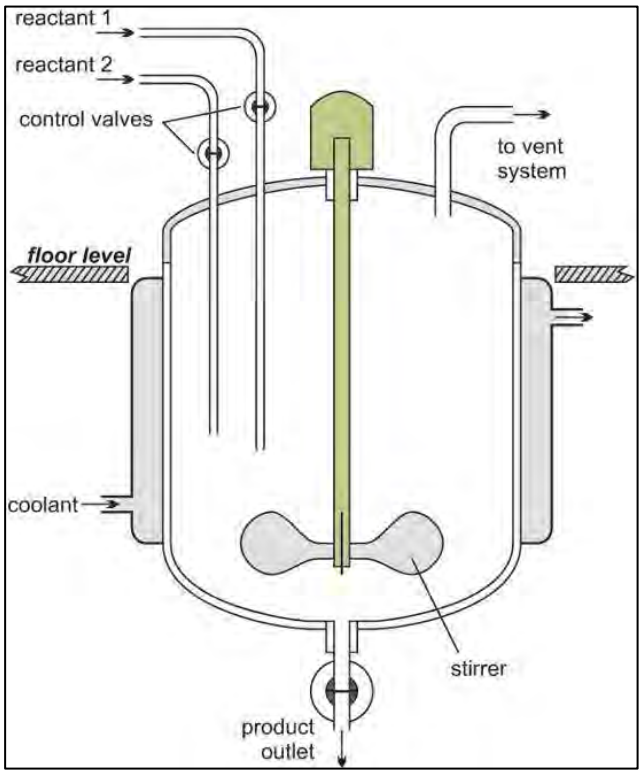

Figure 2.5: Typical set-up of a batch reactor (Holton, 2013)

In recent years, glass reactors have been commonly used in fine chemical production such as reactors produced by Radley's or QVF. These reactors generally have a reaction vessel with the capacity to accommodate between 5-20 dm^3. The glass material is corrosion resistant and allows for the reaction to be observed. The units can generally cater for temperatures from 213.15 K to 503.15 K (Radleys, 2014). Figure 2.6 shows a QVF Duran 20 dm^3 glass reactor.

Figure 2.6: QVF Duran 20 dm^3 glass reactor (Star, 2010)

The successful operation of a batch reactor relies predominantly on the design of the temperature control system of the reaction vessel. Typically, the batch reaction vessel is jacketed and with the use of a heat transfer fluid, the temperature inside the vessel is controlled. Limitations exist in that fluids having high vapour pressures must be avoided as it creates a pressurized system. Batch systems are generally not favoured for high pressure applications. The most commonly used heat transfer fluid is water due to its inherent property of high heat capacity (Edwards, 2005).

The ability to maintain temperature is often difficult when attempting to scale-up a batch system. The ratio of heat transfer area to reactor volume is lower at greater reactor sizes. Therefore, as the vessel size and hence volume is increased while scaling up, there is less area for heat transfer in proportion to the scaled-up reactor size. Due to a higher volume and therefore greater rate of heat generation, the bigger unit will experience much greater difficulty in temperature control as it will not sustain the same heat removal rate (Edwards, 2005).

Endothermic reactions exhibit, to some degree, self-regulation in temperature and therefore thermal stability in a reaction vessel. The heat removal ability is dependent on the resistances to heat transfer, temperature differences and the surface area for heat transfer. This is important when dealing with exothermic reactions as the increase in reaction temperature results in a higher reaction rate. In addition to the higher reaction rate, there is the risk of a runaway reaction if the appropriate heat removal rate cannot be achieved.

Often one of the reagents needs to be added at a very low flow rate to control the reaction rate and hence temperature generation. Some applications try to obtain an isothermal system by boiling off one of the components to remove heat via the latent heat of vapourisation in the reacting system. The vapourised component will have to be condensed and returned to the system as decreasing the level in the reactor will reduce the heat transfer area. These methods are very intensive when attempting to scale-up batch processes (Edwards, 2005).

Stirred batch reactors equipped with coils or external jackets inherently have the issue of thermal lag as a result of the reaction mixture, heat transfer fluid in the jacket or coils and the material of the coil or reaction vessel.

When a reactor is not filled to capacity, not only is the heat transfer area reduced but this may lead to inefficient agitation as well as exothermic reaction temperature instabilities (Edwards, 2005).

Metal reactors, such as the units produced by Parr and Autoclave Engineers, are also used in the manufacture of fine or speciality chemicals. These units allow for higher temperature ranges to be achieved as well as being able to withstand higher pressures. They are commonly applied in semi-batch application with similar capacities to those of the glass reactors (Autoclave, 2014). Figure 2.7 shows a typical metal reactor manufactured by Parr Instrument Company.

Figure 2.7: Metal reactor with floor stand (Parr, 2015)

Roberge et al. (2005) claims that 50% of reactions in the fine or speciality chemical industry will find benefit from converting from the commonly used batch system, as mentioned above, to continuous processes based predominantly on microreactor technology. The only drawback is the possible presence of solid phase components which limits the application of this new technology. Some of the main drivers of this technology is improved control of reaction conditions, ease of scale-up and applications in pilot productions as well as large scale productions where a gain in yield and safety from the use of microreactors is realised (Roberge et al., 2005).

It was previously claimed that solution-synthesis reactions can only be carried out with conventional batch systems with overhead stirring used as the means of agitation of the components. This is an example of how microreactors have revolutionised the industry of fine chemicals manufacture, as continuous processes can now be carried out with micro-structured devices allowing for enhanced mass and heat transfer compared to batch processes (Junkers, 2014).

2.4 Selection and design of separation systems for fine chemical synthesis

2.4.1 Separation process heuristics

To facilitate the development of processes or improve existing processes, heuristics are often employed in the design and sequencing of separators. Heuristics are empirical and serve as guidelines for the selection of separation units and the order thereof. Some common heuristics that are most predominantly applied in industry are discussed below (Rousseau, 1987).

Generally, the most difficult task of a process involves the separation of the constituent components of a mixture. The physical and chemical data available for the components should be gathered to serve as an indication for the separation methods that are applicable. As an example, properties such as the component boiling point and solubility in different solvents indicate if distillation, extraction or a combination of both are applicable (Rousseau, 1987).

The removal of corrosive or potentially harmful components should be undertaken as early as possible. This extends to components that may cause problems downstream such as salt scaling downstream units or heated dissolved gases in a fluid increasing the vapour pressure of a fluid causing cavitation (Rousseau, 1987).

Constituent components of a mixture that are in large fraction should be removed first. The removal of such components will reduce the processing costs as well as the sizing of downstream units that will now process lower volumes (Seader and Henley, 1998).

The most difficult separation should be done at the end of the process. When the difference in properties such as the boiling points or densities is not significant or if there is a presence of an azeotrope, the separation should be conducted at the end of the process in the absence of other non-key components (Rousseau, 1987).

It is advisable to avoid adding foreign components to the separation sequence. The extra components that must be added, such as in azeotropic distillation, will need to be recovered often resulting in another separation problem (Rousseau, 1987).

The use of extreme operating conditions should be avoided. Excessive temperatures and pressures are dangerous as well as increasing the operating costs of the process (Rousseau, 1987).

Due to the vast experience associated with the design and operation of conventional distillation, this particular separation technique should always be considered for fluid separations. Distillation columns use energy to facilitate separation as opposed to a separating agent. Therefore thermodynamic efficiencies can be high as well as the addition of new components to the system avoided (Rousseau, 1987).

2.4.2 Distillation design

The plate hydraulic design in a distillation column forms an integral part of the design process as a tray should: provide sufficient vapour liquid contact; induce high efficiency by means of sufficient liquid hold-up which increases mass transfer; have the required area and spacing such that the pressure drop and entrainment are within acceptable boundaries and providing adequate downcomer area for the fluid to flow easily from tray to tray. The design principles used for the distillation column design are discussed in this section (Sinnott, 2005).

The conditions at which flooding is expected sets the upper limit of the vapour velocity in the column. It is important to maximize the vapour velocity as this translates into higher plate efficiencies. It is recommended that the vapour velocity is between 70-90%, preferably 85% of the flooding velocity which is determined as shown below where K_1 is a constant determined from Figure 2.8 (Sinnott, 2005).

$$u_f = K_1 \sqrt{\frac{\rho_l - \rho_v}{\rho_v}} \tag{2.5}$$

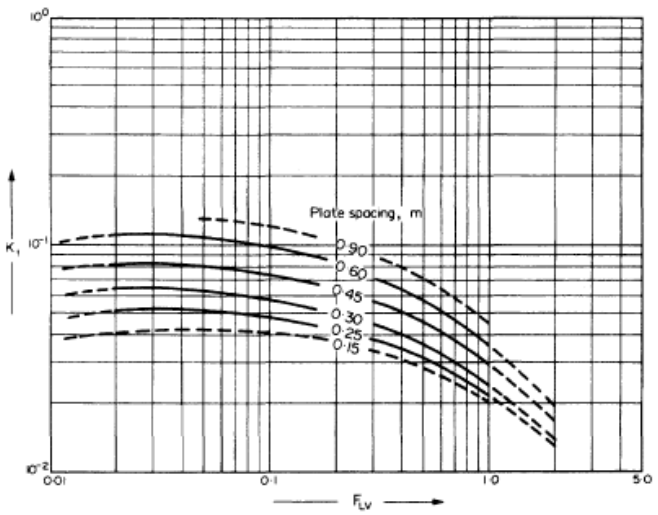

Figure 2.8: Flooding velocity for sieve plates (Sinnott, 2005)

The liquid-vapour flow factor, F_{LV}, required in Figure 2.8 is determined as shown below where L_W and V_W are the liquid and vapour mass flowrates, respectively (Sinnott, 2005).

$$F_{LV} = \frac{L_W}{V_W}\sqrt{\frac{\rho_v}{\rho_L}} \tag{2.6}$$

The percentage flooding in the column trays is determined by Equation 2.7. The actual velocity is based on the net area of the column (Sinnott, 2005).

$$percentage\ flooding = \frac{actual\ velocity}{vapour\ velocity} \tag{2.7}$$

The fractional entrainment can be estimated using Figure 2.9 which is a function of the liquid-vapour flow factor with percentage flooding as a parametric parameter. The upper limit of an allowable fractional entrainment is given as 0.1 as the effect on plate efficiency is negligible in this region (Sinnott, 2005).

The lower limit of the vapour velocity, known at the weep point, is defined as the point below which liquid leakage through the holes of the tray become excessive. The minimum design vapour velocity is defined in Equation 2.8. The constant, K_2, is determined from Figure 2.9. The vapour velocity calculated at the weep point, as shown below, is the minimum value to ensure stable operation (Sinnott, 2005).

$$\breve{u}_h = \frac{K_2 - 0.9\,(25.4 - d_h)}{{\rho_v}^{0.5}} \tag{2.8}$$

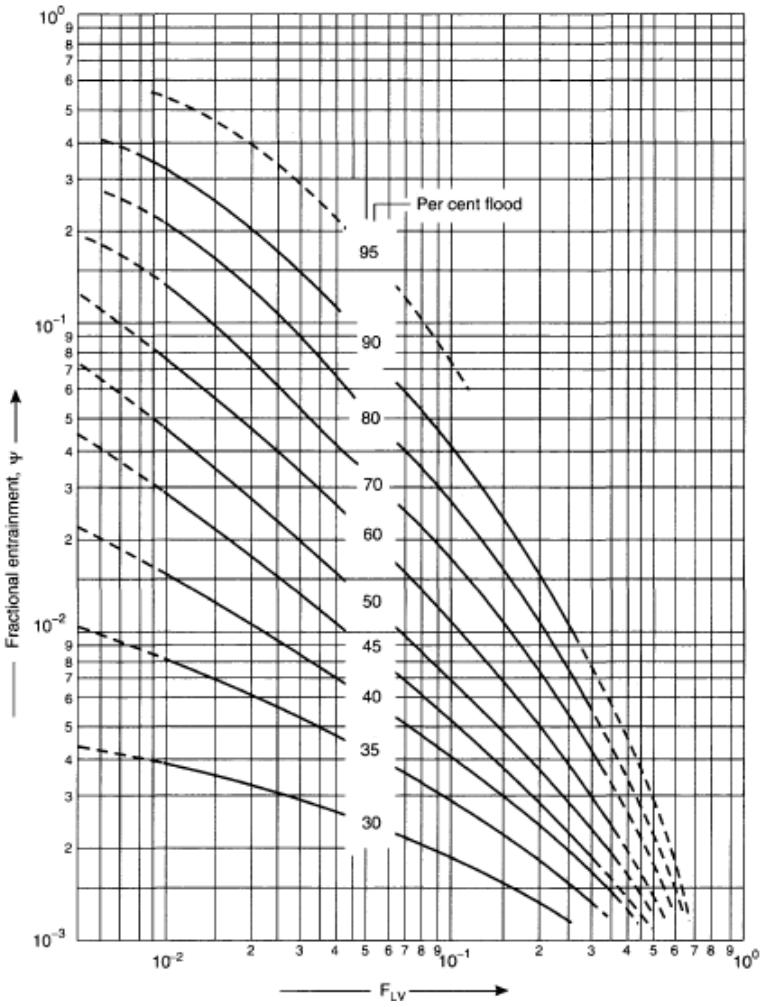

Figure 2.9: Entrainment correlation for sieve plates (Sinnott, 2005)

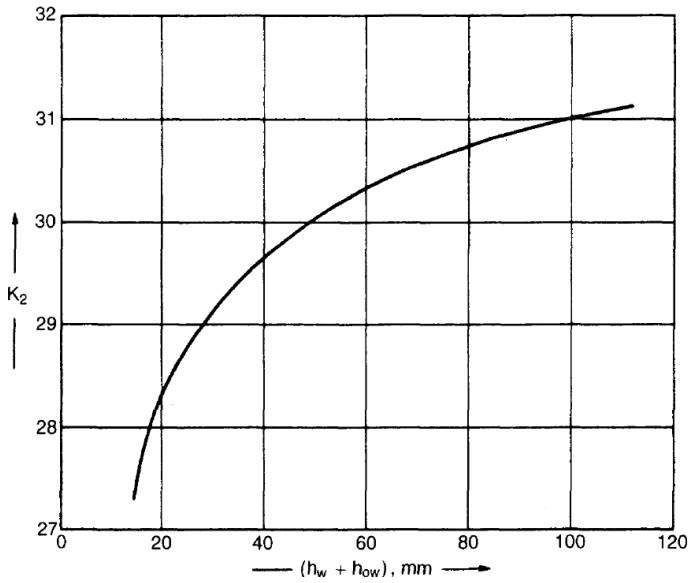

Figure 2.10: Weep-point correlation (Sinnott, 2005)

Equation 2.9 defines the height of liquid over the weir as a function of the liquid flowrate (L_w), weir length (l_w) and density of the liquid (p_l). This value is used in conjunction with Figure 2.10 to determine the constant K_2 for Equation 2.8 (Sinnott, 2005).

$$h_{ow} = 750 \left[\frac{L_w}{\rho_L l_w}\right]^{\frac{2}{3}} \tag{2.9}$$

The weir height influences the amount of liquid that is present on the tray which is one of the factors that determines the plate efficiency. The higher the weir, the greater the liquid hold up and efficiency but at the expense of an increased pressure drop of the tray. For columns operating at atmospheric conditions, literature recommends a weir height between 40 mm and 90 mm, preferably 50 mm (Sinnott, 2005).

The ratio of the downcomer area and column area is used to find the corresponding ratio of weir length to the diameter of the column as shown in Figure 2.11. Using the calculated column diameter, the corresponding weir length can be determined. The recommended weir length is between 0.6 and 0.85 of the column diameter (Sinnott, 2005).

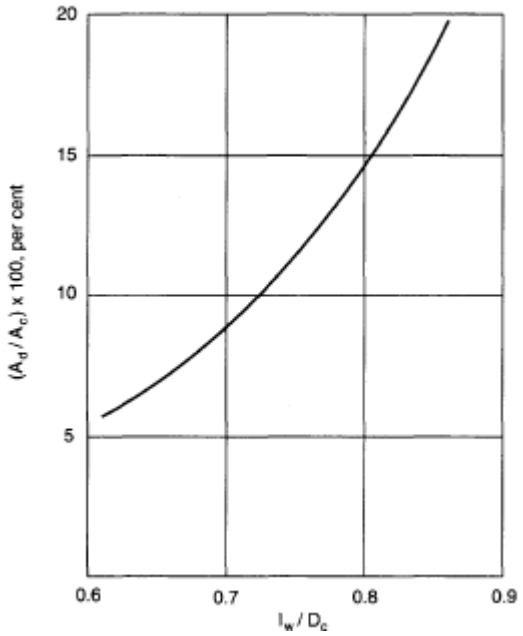

Figure 2.11: Relation between downcomer area and weir length (Sinnott, 2005)

In most applications an additive model is used to predict the total pressure drop across a tray by considering the pressure drop for the flow of vapour through the holes in a dry tray as well as the static head of liquid on a tray. A residual term is often included to account for the difference between the observed experimental pressure drop and the theoretical addition mentioned above.

The residual term accounts for the energy required to form bubbles of vapour as well as taking into account that the static head on a plate is assumed to be of a clear liquid whereas the liquid may be aerated, referred to as liquid froth. The total head loss per tray is defined in Equation 2.10 with dry plate head loss and residual head loss defined below.

$$h_t = h_d + (h_w + h_{ow}) + h_r \tag{2.10}$$

Equation 2.11 defines the pressure drop expected when the vapour flows through a dry plate as a function of the respective fluid densities (ρ_l and ρ_v), velocity through the holes (u_h) and an orifice coefficient (C_o). The orifice coefficient is determined from Figure 2.7.

$$h_d = 51\left[\frac{u_h}{C_o}\right]\frac{\rho_v}{\rho_l} \tag{2.11}$$

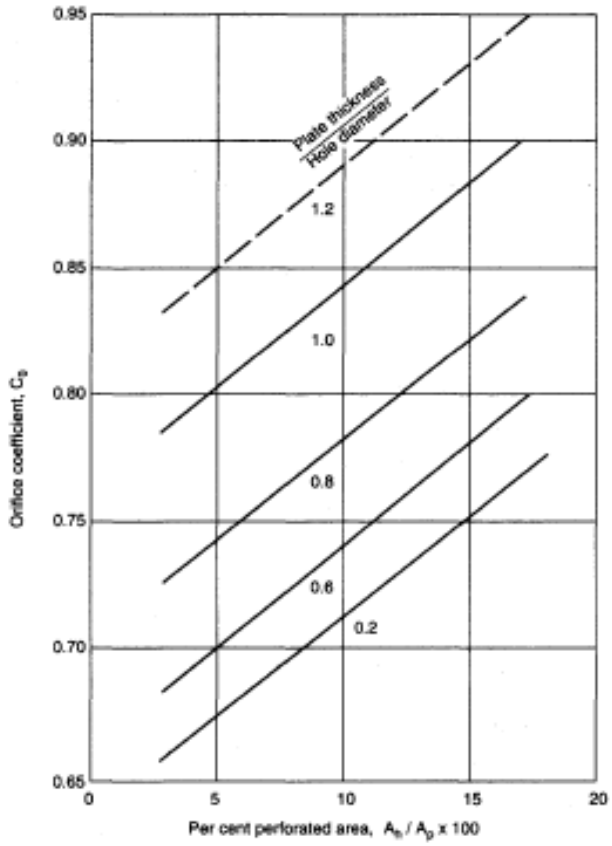

Figure 2.12: Orifice coefficient for sieve plates (Sinnott, 2005)

Literature proposes many correlations to increase the accuracy of the residual head term. However, as a result of the residual head being an insignificant correction to the total pressure drop over a tray, it is recommended that a simple equation, such as in Equation 2.12, be used for ease of design proposed by Hunt *et al*. (1955).

$$h_r = \frac{12.5\ x\ 10^3}{\rho_l} \tag{2.12}$$

In order to prevent flooding of the column, the downcomer back-up, which is the back-up of liquid in the downcomer between adjacent trays, needs to be significantly less than the top of the weir on the above tray. The pressure drop over a tray induces the back-up of liquid in the downcomer which leads to the definition of the downcomer back-up as a function of weir height (h_w), height of liquid over the weir (h_{ow}), total pressure drop on the plate (h_t) and head loss in downcomer (h_{dc}) as shown in Equation 2.13 (Sinnott, 2005).

$$h_b = (h_w + h_{ow}) + h_t + h_{dc} \tag{2.13}$$

The criterion often employed to prevent flooding of the trays is defined in Equation 2.14. It is recommended that the downcomer back-up does not exceed half the combined distance of the weir height and tray spacing (Sinnott, 2005).

$$h_b < \frac{1}{2}(l_t + h_w) \tag{2.14}$$

The head loss in the downcomer is, in large part, due to the constriction of flow on the outlet of the downcomer. Equation 2.15 can be used to estimate this head loss and is a function of the liquid flowrate in the downcomer (L_{wd}), the liquid density (ρ_l) and the downcomer area (A_d) (Sinnott, 2005).

$$h_{dc} = 166 \left[\frac{L_{wd}}{\rho_l A_m}\right]^2 \tag{2.15}$$

2.4.3 Prediction of VLE for systems containing fluorinated ethers: Analytical solution of groups (ASOG)

Analytical solution of groups (ASOG) is a group contribution method based on the Wilson equation that represents the group activity coefficient for a system. ASOG allows for the prediction of vapour-liquid equilibrium data. The method divides molecules into functional groups and the model assumes that the properties of the solution are determined by the interaction of the group pair. The methods prescribed by Tochigi et al. (2001) is claimed to be one of the most accurate methods of predicting interphase equilibria as the temperature dependence of the parameters required are considered (Correa et al., 1999). The equations below show the systematic approach to determine the activity coefficient of a component (Tochigi et al., 2001).

A liquid mixture is considered to be a solution of different groups according to the ASOG analysis. The properties of these groups are used to determine the activity coefficients of the actual components of a mixture. Equation 2.16 is used to determine the activity coefficient of component *i* from $ln\gamma_I{}^{FH}$ which accounts for the size and shape of the molecules and $ln\gamma_I{}^{G}$ which is a residual term which considers the interactions between groups.

$$ln\gamma_i = ln\gamma_I{}^{FH} + ln\gamma_I{}^{G} \tag{2.16}$$

The size contribution term of the activity coefficient is a function of $v_i{}^{FH}$, which is the number of atoms in molecule *i*, and x_j,which is the composition of component *j* in the liquid solution. The definition of this term is shown in Equation 2.17 (Correa et al., 1989).

$$ln\gamma_i{}^{FH} = 1 + ln\left[v_i{}^{FH} / \sum_{j=1}^{n} x_j v_j{}^{FH}\right] - v_i{}^{FH} / \sum_{j=1}^{n} x_j v_j{}^{FH} \tag{2.17}$$

The group contribution term of the activity coefficient is given in Equation 2.18 where $v_{k,i}$ represents the number of atoms in group *k* of the molecules of component *i*, $\Gamma_k$is the activity coefficient of group *k* and $\Gamma_k{}^{(i)}$ is the activity coefficient of pure component *i* (Correa et al., 1989).

$$ln\gamma_i{}^{G} = \sum v_{k,i}\left(ln\Gamma_k - ln\Gamma_k{}^{(i)}\right) \tag{2.18}$$

The term $ln\Gamma_k$ which is required in Equation 2.18 is defined below where X_l is the mole fraction of group *l* in solution and $a_{k/l}$ is the interaction parameter for a pair of groups, *k* and *l* (Correa et al., 1989).

$$ln\Gamma_k = 1 - ln\left[\sum_l X_l a_{k/l}\right] - \sum_l\left[X_l a_{k/l} / \sum_m X_l a_{l/m}\right] \tag{2.19}$$

Equation 2.20 and 2.21 are parameters used to determine the activity coefficient of a particular group as defined in Equation 2.19 (Correa et al., 1999).

$$X_k = \sum_{i=1}^{n} x_i v_{k,i} / \left[\sum_l \sum_{j=1}^{n} x_j v_{l,j}\right] \tag{2.20}$$

$$a_{k/l} = exp\left(m_{k/l} + n_{k/l}/T\right) \tag{2.21}$$

$a_{k/l}$ is a Wilson parameter that is dependent on temperature. It is also a function of $m_{k/l}$and $n_{k/l}$ which are group pair parameters that are only dependant on a particular group pair. ν_i^{FH} represents the number of atoms in molecule, *i*, whereas $\nu_{k,i}$ is the total number of atoms in group *k* of a particular molecule *i* . The group pair parameters from literature associated with the HME and methanol system pertinent to this project are listed below (Tochigi et al., 2001).

Table 2.1: ASOG group pair parameters, $m_{K,L}$

$m_{k,l}$	CF_2	CH_2	CHF	O(Ether)	OH
CF_2	0	-4.047	0.3534	-4.8242	-4.3746
CH_2	3.0905	0	3.0882	-1.3836	-41.2503
CHF	0.6892	-4.0432	0	-2.9943	6.1226
O(Ether)	5.2945	0.7666	2.0982	0	0.9348
OH	-28.2351	4.7125	-0.3794	-6.71	0

Table 2.2: ASOG group pair parameters, $n_{k,l}$

$n_{k,l}$	CF_2	CH_2	CHF	O(Ether)	OH
CF_2	0	1086.9	-267.8	1680.1	-1414.8
CH_2	-937.9	0	-981.1	606.4	7686.4
CHF	-269.7	1088.1	0	1074.5	-2182.7
O(Ether)	-2440.8	-444	-412.7	0	-152.2
OH	-635.4	-3060	-3958.4	-150.8	0

The calculated uncertainty on prediction associated with using ASOG is 0.016 on composition and 0.98 K on temperatures. The objective function that was used to minimise the error in determining the group pair parameters is shown below (Tochigi et al., 2001).

$$F_{obj} = \sum_{n=1}^{NDP}\left[\left(\frac{\gamma_{1,calc}-\gamma_{1,exp}}{\gamma_{1,exp}}\right)^2+\left(\frac{\gamma_{2,calc}-\gamma_{2,exp}}{\gamma_{2,exp}}\right)^2\right] \quad (2.22)$$

2.4.4 Decanter design

Decanters are implemented in industry to separate liquids when sufficient differences in their respective densities exist. Essentially, decanters are tanks that provide the required residence time for liquid droplets in the interface between two liquids to rise or settle to the interface of the liquid layer of higher density, at the bottom, or lower density, at the top. These tanks are usually cylindrical in shape due to the design being economical to fabricate (Sinnott, 2005).

The sizing of the decanter is based on the velocity of the continuous phase being less than the settling velocity of the liquid droplets in the dispersed phase. The continuous phase generally refers to the liquid with the higher density and dispersed phase refers to the liquid with the lower density. Assuming plug flow, the continuous phase velocity is calculated as shown in Equation 2.23 where A_i is the interfacial area and L_c is the volumetric flowrate of the continuous phase (Sinnott, 2005).

$$u_c = \frac{L_c}{A_i} < u_d \tag{2.23}$$

The settling velocity of the droplets is determined using Equation 2.24 where d_d is the diameter of the droplet, μ_c is the continuous phase viscosity, ρ_c and ρ_d are the densities of the continuous phase and dispersed phase, respectively and g is the gravitation acceleration constant of 9.81 $m \cdot s^{-2}$. A droplet size of 150 μm may be assumed based on generally larger droplet sizes existing in current industrial applications. A settling velocity of $4x10^{-3}$ $m \cdot s^{-1}$ is assumed if a greater velocity is calculated (Sinnott, 2005).

$$u_d = \frac{{d_d}^2 g(\rho_d - \rho_c)}{18\mu_c} \tag{2.24}$$

For cylindrical vessels, the height is calculated as twice the diameter. The diameter is determined from the interfacial area term, A_i, as shown below.

$$A_i = \pi d \tag{2.25}$$

The dispersion band height, between the two liquids, is assumed to be 10% of the total height. The calculated settling velocity can be used in conjunction with this height to determine the residence time, t_r, of the droplets as shown below.

$$t_r = \frac{dispersion\ height}{u_d} \tag{2.26}$$

As a final assessment, the droplet diameter is calculated for the dispersed phase to ensure no continuous phase droplets will be entrained in the dispersed phase. The droplet diameter is calculated at the end of the calculation and the results are satisfactory if the value is below the assumed size of 150 μm. If this is not satisfied, the flowrate of the liquid to the unit may be adjusted as well as changing the temperature of the liquid which subsequently alters the fluid density (Sinnott, 2005).

2.5 Elements of high-level statistical experimental design: central composite design

A comprehensive way to investigate the effect of different factors at different levels is to use a full factorial design. This design uses all possible combinations between the factors at the different levels and the combination yielding the best result can be determined by inspection once the experimental responses are tabulated (Istadi and Amin, 2006).

There are however limitations to using this method of experimental design. The method does not give an absolute optimum as the best result is taken as one of the levels of the factors that are investigated (i.e. the optimum can often lie between investigated levels). A possible method to alleviate this would be to undertake a larger number of runs using the same range but this brings about another limitation. The total number of trials is given by raising the number of factors to the power of the number of levels implemented. This exponential growth in number of trials is a major limiting factor in experimentation (Istadi and Amin, 2006).

The central composite method can be used as it builds a quadratic model for the response variable that is investigated without the need to complete a full factorial design. Linear regression is used to obtain the optimum levels from the factors investigated (Istadi and Amin, 2006).

Figure 2.13 shows the distribution of rotatable design points. Nodes 1-8 represent the cubic design points and nodes 9-14 represent the axial design points. Centre points are at the coordinates (0,0,0) and account for the variability in the experiment. Multiple centre points can be used to test the reproducibility of experiments as well as aid in the statistical analysis of the quadratic regression. Central design points are the trials that are run at the midpoint of the ranges of the factors that are being investigated. For the sake of repeatability, these runs are conducted multiple times (Lazic, 2004).

To obtain the axial points in the experimental design, Equation 2.27 is employed. The X_{max} and X_{min} values are representative of the upper and lower bounds of the ranges of the factor being investigated.

$$X_i = \frac{\alpha(X_{max} - X_{min}) + X_{max} + X_{min}}{2} \tag{2.27}$$

where the alpha value is given by Equation 2.28 with k being the number of variables investigated.

$$\alpha = \left(2^k\right)^{\frac{1}{4}} \tag{2.28}$$

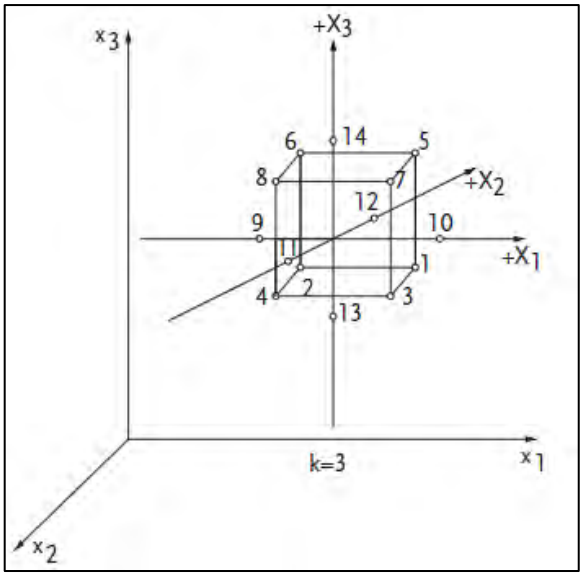

Figure 2.13: Graphical representation of the distribution of rotatable design point (Lazic, 2004)

2.5.1 Surface response methodology

The analysis of experimental data obtained from a central composite design is most conveniently undertaken using surface response methodology (SRM). The response variable is modelled using a quadratic polynomial equation shown in general form in Equation 2.29 (Istadi and Amin, 2006)

$$Y = \beta_O + \sum_{j=1}^{k} \beta_j X_j + \sum_{j=1}^{k} \beta_{jj} {X_j}^2 + \sum_{i<j}^{k} \beta_{ij} X_i X_j \qquad (2.29)$$

Y is the predicted response variable, $\beta_o$is the intercept coefficient, β_j are the linear terms, $\beta_{jj}$are the squared terms, B_{ij} are the interaction terms, and X_i and X_j represent the independent variables which are the factors investigated in the experiment. The coefficients can also be determined by making use of multi-linear regression.

The coefficients of Equation 2.29 can be determined using Equations 2.30-2.33 listed below (Lazic, 2004).

$$\beta_0 = a_1 \sum_{u=1}^{N} Y_u - a_2 \sum_{i=1}^{k} \sum_{u=1}^{N} X_{iu}^2 \times Y_u \qquad (2.30)$$

$$\beta_j = a_3 \sum_{u=1}^{N} X_u \times Y_u \tag{2.31}$$

$$\beta_{ij} = a_4 \sum_{u=1}^{n_j} X_{iu} \times X_{ju} \times Y_u \tag{2.32}$$

$$\beta_{jj} = a_5 \sum_{u=1}^{n_j} X_{iu}^2 \times Y_u + a_6 \sum_{i=1}^{k} \sum_{u=1}^{N} X_{iu}^2 \times Y_u - a_7 \sum_{u=1}^{N} Y_u \tag{2.33}$$

Y_u is the response variable of the experimentation. The coefficients ($a_1 - a_7$) are given in Table 2.3.

Table 2-3: Coefficient values for the quadratic response equation (Lazic, 2004)

Number of factors, k	Number of trials, N	Coefficients						
		a_1	a_2	a_3	a_4	a_5	a_6	a_7
2	13	0.2000	0.1000	0.1250	0.2500	0.1250	0.0187	0.1000
3	20	0.1663	0.0568	0.0732	0.125	0.0625	0.0069	0.0568
4	31	0.1428	0.0357	0.0417	0.0625	0.0312	0.0037	0.0357
5	52	0.0988	0.0191	0.0231	0.0312	0.0156	0.0015	0.0191
6	91	0.0625	0.0098	0.0125	0.0156	0.0078	0.0005	0.0098
7	163	0.0398	0.0052	0.0066	0.0078	0.0039	0.0002	0.0052

2.5.2 Statistical analysis

Vector X contains the different levels of factors that are investigated. In the search for optimal reaction conditions one usually examines the stationary points of the regressed function. The partial derivatives of the predicted response are equivalent to zero at the stationary point. The stationary point can represent a maxima, minima or saddle point of the system. The response variable is modelled by a quadratic equation and this model can be expressed in matrix notation (Istadi and Amin, 2006).

$$Y = \beta_o + X'b + X'BX \tag{2.34}$$

The variables in the above equation are shown below. Independent variables to the equations below have already been defined in section 2.5 (Istadi and Amin, 2006).

$$\mathrm{X} = \begin{bmatrix} X_1 \\ X_2 \\ X_3 \end{bmatrix} \tag{2.35}$$

$$B = \begin{bmatrix} \beta_1 \\ \beta_2 \\ \beta_3 \end{bmatrix} \tag{2.36}$$

$$B = \begin{bmatrix} \beta_{11} & \frac{\beta_{12}}{2} & \frac{\beta_{13}}{2} \\ \frac{\beta_{21}}{2} & \beta_{22} & \frac{\beta_{23}}{2} \\ \frac{\beta_{31}}{2} & \frac{\beta_{32}}{2} & \beta_{33} \end{bmatrix} \tag{2.37}$$

The stationary point (X_o) of the system can be determined using the equation below. Using this result, the predicted response at the calculated stationary point (Y_0) can be estimated (Istadi and Amin, 2006).

$$X_o = -\frac{1}{2}B^{-1}b \tag{2.38}$$

$$Y_0 = \beta_0 + \frac{1}{2}X_0{}'b \tag{2.39}$$

The sign as well as magnitude of eigenvalues are used to determine the characteristic of the stationary point. The eigenvalues will show the stationary point as a minimum if both are positive, a maximum if both are negative or a saddle point if the signs differ. The roots of the determinant of the matrix B equated to zero yield the eigenvalues (Istadi and Amin, 2006).

2.6 Mass transfer characteristics in a FFMR

Mass transfer between a gas and liquid in a falling film, as experienced in a FFMR, concentrates largely on the dependence of the liquid-side mass transfer coefficient on molecular diffusivity. There have been numerous studies in literature on the subject and several mass transfer models are proposed that offer an understanding on the absorption of a gas into a liquid medium. Most common of these proposed models are the film model, surface renewal model, penetration model and eddy diffusivity theory. For the purposes of this study, the focus is on the penetration model with its applicability elaborated upon below (Chen, 2009).

Assuming a flat surface profile in the FFMR (the entire microchannel surface is wetted), the Reynolds number can be defined by the equation below (Chen, 2009).

$$Re_L = \frac{4\delta_L j_L}{\upsilon} \tag{2.40}$$

δ_L is used to denote the thickness of the liquid film in a microchannel, j_L is the mean velocity of the liquid film and υ is the kinetic viscosity of the liquid. The liquid film thickness and mean velocity can be expressed, by definition according to Nusselt theory, by the equations shown below (Chen, 2009).

$$\delta_L = \sqrt[3]{\frac{3Q_L\upsilon}{nbg}} \tag{2.41}$$

$$j_L = \frac{g{\delta_L}^2}{3\upsilon} \tag{2.42}$$

The validity of the penetration model can be determined by the calculation of the Fourier number. The Fourier number is defined as the ratio of the residence time to the diffusion time. If the Fourier number is less than one, which is interpreted as the residence time being greater than the diffusion time, the penetration model is deemed applicable. This also indicates that mass transfer has not established steady-state. The definition of the Fourier number is shown below (Chen, 2009).

$$F_o = \frac{t_L}{\tau_D} = \frac{L}{j_L}\frac{D}{{\delta_L}^2} \tag{2.43}$$

If the penetration model is applicable, the liquid-side mass transfer coefficient can be defined by Equation 2.44. If the Fourier number is greater than unity, the film model is often preferred. In this circumstance, the liquid-side mass transfer coefficient can be defined by Equation 2.45 (Chen, 2009).

$$k_L = 2\sqrt{\frac{u_{surf}D}{\pi L}} = 2\sqrt{\frac{1.5j_L D}{\pi L}} \tag{2.44}$$

$$k_L = \frac{D}{\delta_L} \tag{2.45}$$

The liquid-side mass transfer coefficient can also be determined experimentally. Figure 2.14 shows an element of the liquid flow down a microchannel.

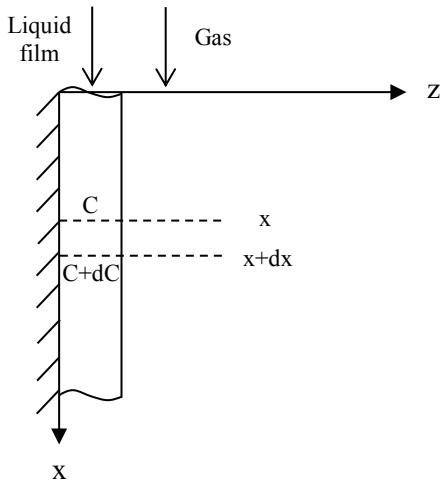

Figure 2.14: Finite element illustration of a liquid film in a

Equation 2.47 is derived by performing a mass balance over this finite element where C represents the concentration of the gas absorbed into the liquid and C^* is the saturated solubility for the liquid. There are two boundary conditions for the scenario analysed with the initial concentration at the liquid inlet being zero and the concentration at the end of the microchannel being the outlet or final concentration. This is significant as it is the easiest concentration in the concentration profile to be measured (Chen, 2009).

$$k_L(C^* - C)bdx = Q_L dC \tag{2.46}$$

Through the process of integration and application of the boundary conditions stated above, the liquid-side mass transfer coefficient can be expressed as shown below (Chen, 2009).

$$k_L = \frac{Q_L}{bL} \ln\left(\frac{C^*}{C^* - C_{out}}\right) \tag{2.47}$$

3

CHAPTER THREE

3. MATERIALS, APPARATUS AND PROCEDURES

This chapter first highlights the materials used and how the purity was assessed to ensure that a greater accuracy in the results was obtained.

In order to ensure that the experimentation was successfully carried out, it was important that the apparatus used be correctly calibrated and operated. Therefore this chapter also describes the procedures for the calibration and operation of the apparatus used.

3.1 Materials

This project is not possible without actual bench-scale experimentation for the reactor as there is no kinetic data available in literature for the reaction of the system studied. There is also no LLE data for the methanol and HME system which further warrants the need for experimentation.

The project required the materials listed below:

Table 3.1: Components used in the project with respective purities

Component	Purity
Hexafluoropropene	99.8%
Nitrogen	99.8%
Methanol	>99%[a]
Potassium Hydroxide	-
Water	-
Propanol	>99%[b]
Acetone	>99% [b]
Ethanol	>99% [b]
2-Butanol	>99% [b]
1,1,1- trichloroethane	>99% [b]

[a]Purity determined via refractive index
[b]Purities determined via GC analysis

The reactants, as depicted in Equation 2.1, for the synthesis of HME were methanol and HFP. KOH, which was used in the form of white solid pellets, was the alkali hydroxide catalyst for the reaction. Nitrogen was used as an inert diluent in the HFP feed stream to change the inlet mole fraction of HFP and allow the effect on the yield and mole fraction of HME in the reactor effluent to be investigated. The HFP was 99.8% pure as determined by gas-chromatography analysis according to Lokhat (2012).

Refractive index was used as a means to screen for impurities in methanol. Comparisons to literature are shown in Appendix A.6 in Table 6.1 and Table 6.2.

Distilled water (1.3 $\mu S \cdot cm^{-1}$) was used as a solvent in the liquid-liquid extraction process due to its ability to selectively extract the residual methanol. Water was also used as a cooling and heating utility fluid for the temperature control systems associated with each reactor.

Propanol was used as the internal standard for quantification of reaction products on the gas chromatograph. Acetone, 2-butanol, ethanol and 1,1,1- trichloroethane were also examined as potential internal standards by investigating their relative retention times as well as their miscibility with the crude product. However, only propanol provided the necessary resolution and exhibited appropriate miscibility. HFP used for the experiment was obtained from the South African Nuclear Energy Corporation (NECSA).

3.2 Apparatus

3.2.1 Semi-batch gas-liquid reactor

The synthesis of HME, in the preliminary work, was undertaken in a stirred tank gas-liquid reactor. This was a semi-batch reactor in which a sparger introduced a gas-stream of HFP into a liquid mixture of methanol and KOH. The maximum capacity of the reactor used was approximately 2 litres. Components in the gaseous phase in the headspace of the unit were vented. However, any methanol that evaporated was condensed and returned to the unit. The reactor was equipped with an impeller which ensured the system was kept homogenous through agitation. The impeller speed, which was measured in revolutions per minute, needed to be set high enough such that mass transfer was not the limiting step of the reaction and that the operation remained in the kinetic regime.

It was probable that there was not sufficient absorption of feed gas in the liquid through a single pass in the reactor. Gases that moved into the headspace of the column were vented. The reactant gas could have been recycled back into the reactor; however, such an arrangement was not used (Conway, Kyle and Rielly, 2002).

The reaction temperature needed to be controlled at a constant level as it was one of the factors under investigation in the experimentation process. The semi-batch gas-liquid reactor unit used a combination of an internal cooling coil and an external heating jacket to achieve the desired temperature of the reactor contents. The internal cooling coil used water at approximately 276.15 K as a cooling utility and the external heating jacket was connected to a water bath at 303.15 K.

The flowrate of the hot utility was uncontrolled. A solenoid valve on the cold utility line was interfaced with a PID temperature controller which adjusted the flowrate of cold water through the coils to maintain the reaction temperature in the vessel. Photograph 3.1 shows the semi-batch gas-liquid reactor used for the preliminary experimentation.

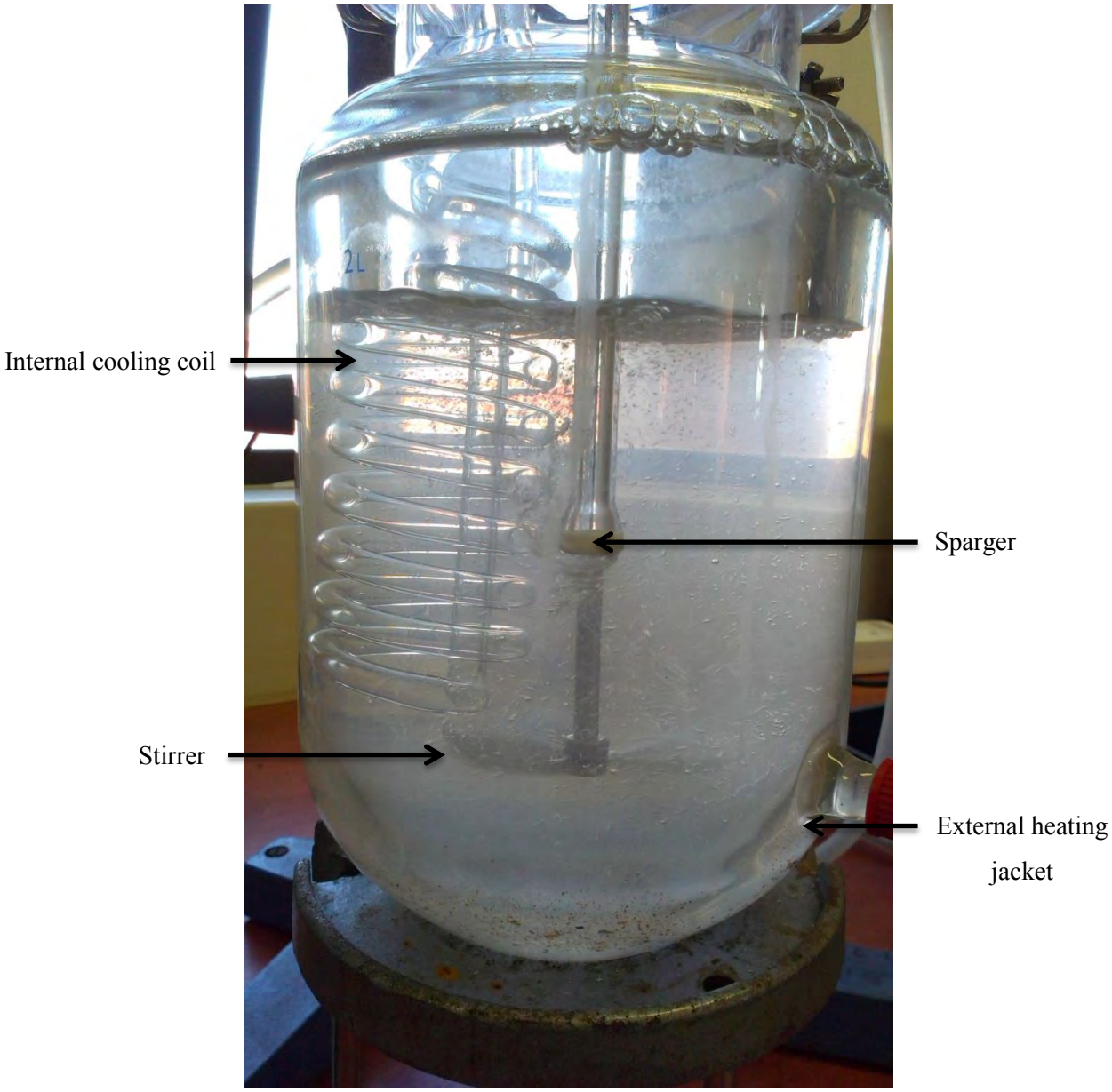

Photograph 3.1: Semi-batch gas-liquid reactor equipped with a gas sparger, internal cooling coil, external heating jacket and stirrer

3.2.2 Liquid-liquid extraction

In order to increase the purity of the crude product, it had to be first separated from the unreacted methanol in the reactor effluent. Liquid-liquid extraction was used via the addition of cold water to the mixture. The alcohol, methanol, had a greater affinity for the water and partitioned with the aqueous phase. The ether product, by virtue of its higher density, settled at the bottom of the mixture. This heterogeneous mixture was placed in a separating funnel and the bottom later was removed when the two distinct liquid layers formed (Rendall et al., 1958).

Photograph 3.2: Separating funnel containing the crude reactor product mixed with cold water

3.2.3 Fractional distillation

In systems where the difference in boiling points between the components is not significant, a fractionating distillation column is commonly used to separate the various liquid fractions (Vogel, 1989).

The fractionating column comprised of a long vertical tube, known as a Vigreux column, which contained the upward flow of vapour which emanated from the still pot. Some of the vapour condensed during this process and flowed back down the column. The vapour was brought into

contact with this condensate and a heat interchange occurred. This allowed the vapour to be absorbed by the more volatile components from the liquid in the system, in an attempt to establish vapour-liquid equilibrium. Charge was added to a still pot at the bottom of the Vigreux tube. Cooling coils, which used water at room temperature as a coolant, condensed the vapours that left the tube. The section of the apparatus above the cooling coils was open to the atmosphere which kept the column at atmospheric pressure. The contact between vapour and liquid phases results in equilibrium being reached on respective stages in the column. To ensure there was sufficient liquid in the column, the vapour travelling up the column was condensed and returned as reflux. A temperature plateau indicated that equilibrium was reached and that the condensate could be drawn off (Vogel, 1989).

Initially, the column was run under total reflux (i.e. no condensate was drawn off). The still pot was heated slowly until the vapour reached the boiling point of the lightest constituent component. The take-off rate should be kept low and when there was an increase in the temperature of the vapour from the constant temperature of the boiling point of the previous fraction, it was indicative of the boiling point of the next fraction being reached.

In order for an efficient separation to be achieved, both a vapour and liquid phase must exist in the column. There should also be a significant surface area, to facilitate contact between the vapour and liquid, to increase mass and heat transfer to establish VLE. Lagging or an insulating medium was also required as to prevent external cooling which may have lowered liquid temperatures and caused condensation of vapours. The temperature control, which helped maintain a continuous composition profile, became increasingly difficult with increasing boiling points of the different fractions. This resulted in extra cooling being required to ensure sufficient reflux was maintained (Vogel, 1989).

The Vigreux column contained several indentation angled downwards at approximately 45^{o} which allowed redistribution of the liquid from the column walls to the centre of the column. As mentioned before, this created a greater surface area which enhanced the mass and heat transfer. Photograph 3.3 shows the fractionating column that was used (Vogel, 1989).

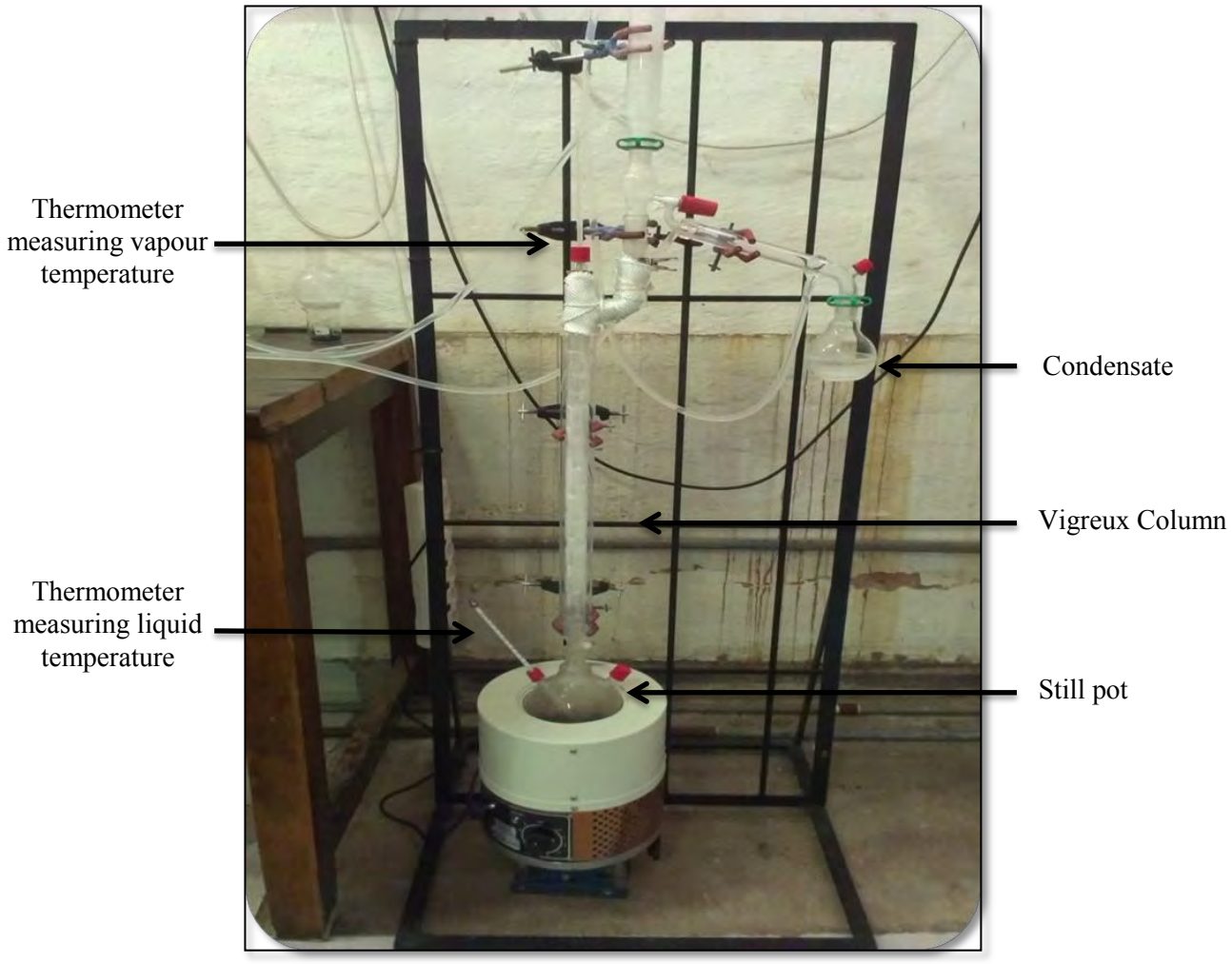

Photograph 3.3: Fractional distillation column used to isolate HME from extract from the liquid-liquid extraction process

3.2.4 Falling-film microreactor

Falling-film microreactors operate with numerous falling films of liquid in microchannels that are under the influence of gravitational force. The typical residence times on these units range from a few seconds to a few minutes. The properties unique to the use of FFMR's are increased heat and mass transfer as well as improved temperature control (Knorr, 2012).

Liquid films on the microchannels were created by the liquid feed being introduced into the unit and the channels being allowed to flood. Once flooded, the liquid was then drawn off. Under normal operation, a liquid feed entered through the top of the microreactor and flowed down the channels while simultaneously being drawn off at a higher rate than the feed. This prevented flooding of the unit and maintained the liquid film in the channels. Under steady-state operation a

gas stream entered through the bottom of the reactor and flowed up the channels and exited at the top of the reactor (Knorr, 2012).

The FFMR had a reaction plate behind the channels through which cooling water flowed and this facilitated temperature control of the reaction in the channels.

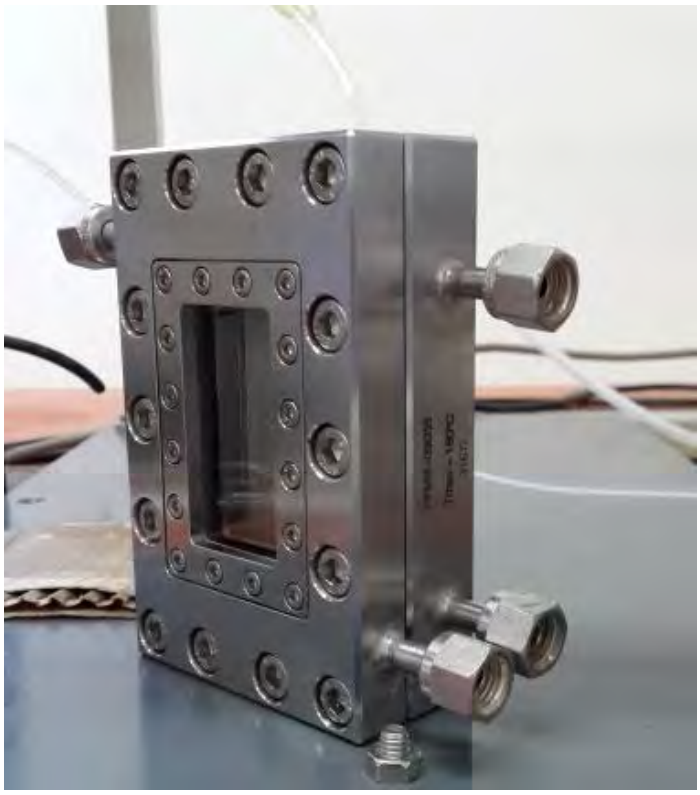

Photograph 3.4: FFMR used for the synthesis of HME

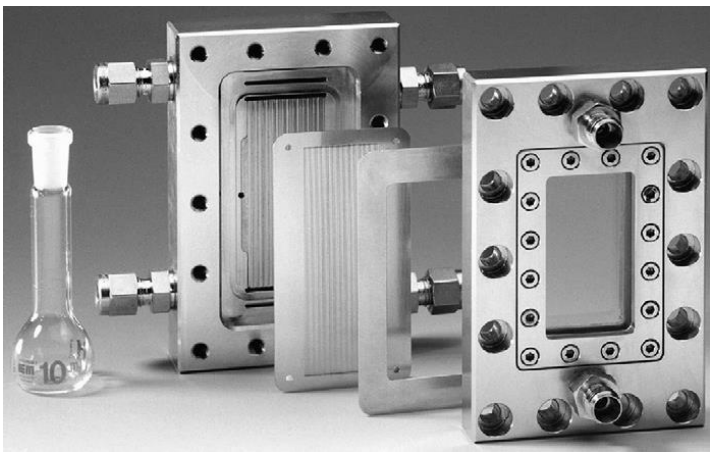

Figure 3.1: Exploded view of a FFMR (Al-Rawashdeh et al., 2008)

Figure 3.1 illustrates the exploded view of the FFMR described in this chapter. From the left, the first component was an integrated heat exchanger which used cooling water, as a utility, to maintain a constant temperature during operation. The next unit was the reaction plate with micro-channels through which the gas flowed and interacted with the liquid films on the channels. The third unit was a washer and the unit on the right was the reactor housing (Al-Rawashdeh et al., 2008).

3.2.5 GC and GC-MS

Qualitative and quantitative composition analysis of the feed and product gas mixtures was performed by means of gas chromatography and mass spectrometry. This technique is the most widely applied technique for the analysis of multi-component hydrocarbon mixtures (Raal and Muhlbauer, 1998).

A Shimadzu 2010 GC, equipped with a flame ionization detector, which uses a Restek® capillary column (30 m × 0.25 mm) coated within a 0.25μm layer of polyethylene glycol was used for all quantitative analysis. Helium served as the carrier gas. A Shimdazu QP 2010 Plus Quadropole GC-MS equipped with a Zebron® capillary column (30 m × 0.25 mm) coated within a 0.25μm layer of ZB-5MS Phenomenex® was used for the qualitative analysis.

Gas chromatography is used for the analysis of constituent components in a sample mixture that can be vapourised without decomposing. This analytic technique can be applied to both qualitative and quantitative analysis for components in a mixture. The compounds flow through the GC column in a gaseous state after vapourisation of the liquid sample. The gaseous compounds divide between a stationary phase, which is commonly a liquid or solid phase, and a mobile phase, which is a gas phase, commonly helium, hydrogen or nitrogen (helium in this application). An analyser at the end of the column quantifies the concentration of the components in the mobile phase (Seader and Henley, 1998).

Qualitative analysis involves the identification of chemical composition in a sample mixture. This is achieved by considering the retention time of a particular species to be a fixed characteristic with the column temperature and carrier gas flowrate as the constant controlled conditions. However, identification cannot be solely based on the retention time as it is not a unique property of a substance. Gas chromatography and Mass Spectrometry (MS) are often combined to alleviate this limitation as MS can be used to identify the chemical structure of a compound (Seader and Henley, 1998).

Quantitative analysis finds limitations in that the detectors at the end of the column have varying responses to different compounds. In addition it is not possible to inject the exact same volume each time an analysis is to be performed. An internal standard method is implemented to overcome these limitations (Seader and Henley, 1998).

An internal standard is a chemical that is not present in the sample mixture but possesses similar characteristics and that can be adsorbed without influencing the chromatographic peaks of the components in the sample. It serves as the reference component and aids in achieving accurate quantitative measurements with regards to the concentrations of constituent components. The use of an internal standard requires a calibration to be undertaken and this is elaborated upon in the section 3.3.

The temperature program used for the analysis kept a constant temperature of 303.15 K for 4 minutes and then increased to a temperature of 553.15 K at a heating rate of 10 K $\cdot min^{-1}$. This final temperature was kept constant for 5 minutes resulting in a complete run time of 34 minutes.

3.3 Procedures

3.3.1 Semi-batch gas-liquid reactor

Experimentation performed on the GLR was during the Laboratory/Industry project course as mentioned in the introduction.

3.3.1.1 Pre-run procedures

- Soapy water or leak detection solution (SNOOP) was used to ensure there were no gas-leaks along the tubing of the gas-feed tanks of HFP and nitrogen.
- The gas-sparger was placed in water and nitrogen set to its maximum flow through the sparger to allow any solid build-up from previous runs (KOH or KF) to be dissolved and removed from the outlet of the sparger.
- The cooling coil water bath temperature was set to 274.15 K.
- The external heating jacket water bath was set at 303.15 K.
- The condenser water bath was set to 278.15 K.

3.3.1.2 Synthesis of HME

The reaction to synthesize HME, as mentioned in Reaction 2.1, was initially performed in a semi-batch stirred tank gas-liquid reactor. A gas-sparger introduced a pre-determined concentration of HFP and nitrogen into the 1.5 dm^3 of methanol with dissolved KOH catalyst in the reactor. This volume of methanol was chosen such that the headspace in the reactor was minimized as well as the gas sparger and temperature probe to be sufficiently submerged.

Gaseous reaction components in the headspace were vented during the reaction but not before it passed through a condenser with water, which cooled the vapours, at 278.15 K. The condensed vapour was returned to the reactor.

The stirrer speed was set to a maximum of 450 rpm to ensure sufficient agitation of the liquid content in the reaction vessel. The highest speed was selected such to ensure mass transfer was not the rate limiting step.

The duration of the reaction was 30 minutes after which the HFP flow was ceased and the nitrogen flow purged the system. The system was purged for 5 minutes with the purpose of removing any remaining HFP in the reactor. Liquid-liquid extraction, as explained in section 3.2.2, was performed on the crude reactor product which isolated HME from the unreacted methanol.

The masses of the empty sample bottles used for storing crude samples for GC and GC-MS analysis and the beaker the bulk crude sample from the reactor was extracted to were weighed. These masses are used to determine the yield of HME as elaborated in section 3.5.

A 26 cm^3 sample of crude product was extracted using a micropore filter to remove all possible solids formed as the sample was used for GC analysis. The micropore filter removed any solids with a particle size smaller than 1 μm. A 26 cm^3 sample bottle was filled to capacity such that negligible headspace remained in the bottle to reduce evaporation of the sample. The masses of the empty sampling bottles used were required as the difference of this mass and the mass of the crude sample in the bottle will yield the mass of the crude sample analysed. The GLR experimental set-up diagram is illustrated in Figure 3-1 with a photograph provided in Photograph 3.5.

Photograph 3.5: The experimental set-up of the GLR system used in the preliminary study of the synthesis of HME

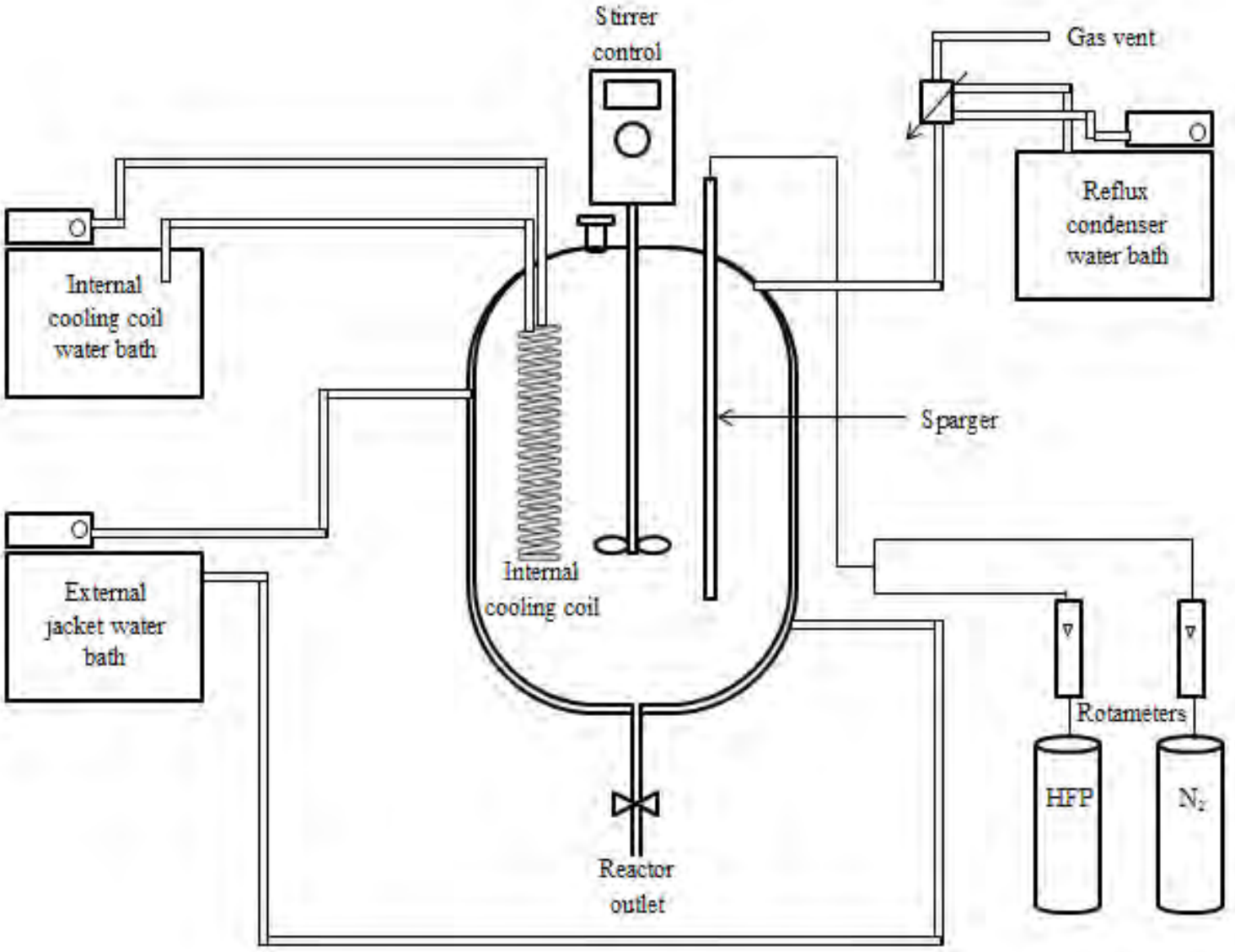

Figure 3.2: Schematic diagram of the semi-batch process to produce HME

3.3.1.3 Liquid-liquid extraction

The 1.5 litre crude sample was mixed with iced water in the ratio 1:3, agitated and then placed into a separating funnel and allowed to settle. By virtue of a higher density, the organic layer (consisting of predominantly HME) settled to the bottom of the separating funnel with the aqueous layer (consisting of predominantly methanol and water) settling above.

The organic layer was then extracted through the bottom of the separating funnel and the HME purity increased further using fractional distillation explained in section 3.2.3. The distinction of the organic layer and the aqueous layer is shown below.

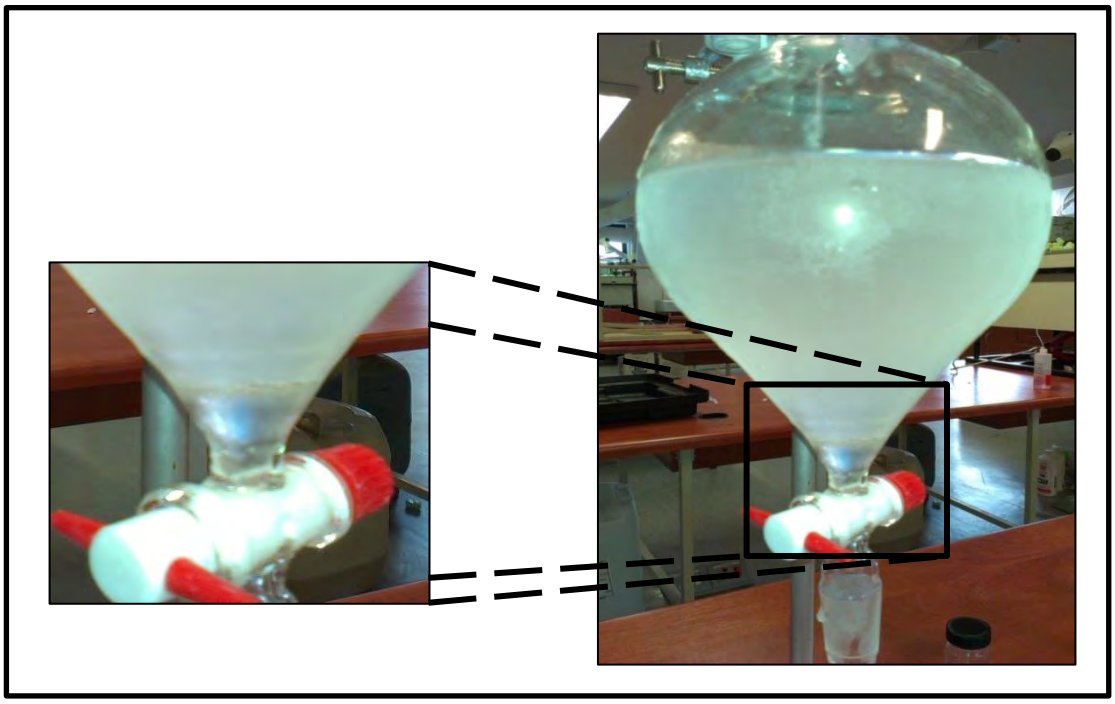

Photograph 3.6: The separation of the aqueous layer consisting of predominantly methanol and water (top) and organic layer consisting of predominantly HME (bottom)

3.3.1.4 Fractional distillation

In order to increase the purity of HME, fractional distillation was performed on the organic layer from the liquid-liquid extraction process. A volume of 500 cm^3 of the organic layer from the liquid-liquid extraction process was placed in the still pot of the fractionating column. A low heating rate was set on the still pot. The increments of the still pot temperature control were Low, 1, 2, 3, 4, and 5. The lowest setting was selected as a high heating rate would have resulted in inefficient separation at the expense of a longer time period required for equilibrium to be

established. The column was run under total reflux for approximately an hour. This was to allow sufficient time for equilibrium to be reached in the column indicated by a temperature plateau. During this period, no condensate was drawn off and returned as reflux to the column. The fractional distillation was run for a total of 12 hours. A temperature plateau of 319.15 K was indicative of the HME fraction of the organic layer being isolated. A more volatile component was, however, present in the organic layer that boiled off at 318.15 K. The GC analysis shows this component to be of negligible composition compared to the HME fraction. The cut times and temperature plateaus are tabulated in Table A-4.1 in Appendix A.

3.3.2 Falling-film microreactor

3.3.2.1 Pre-run procedures

- Foam was used to ensure there were no gas-leaks along the tubing of the gas-feed tanks of HFP and nitrogen.
- The cold bath was set to a pre-determined temperature required for the particular run.

3.3.2.2 Synthesis of HME

A 500 cm^3 feed solution of methanol with specific amounts of dissolved KOH was prepared to give the desired feed concentration. This was prepared as per the levels of catalyst concentration determined using the central composite design. The liquid flowrate in accordance to the required value in the experimental range was set. The feed pump was then switched on and the FFMR was allowed to flood. Once the channels of the FFMR were fully immersed in the feed solution, the outlet pump was switched on, at a flowrate higher than the feed flow, and the excess liquid was removed from the unit. The flooding and subsequent removal of the feed solution allows for the liquid films to form on the microchannels.

Once the excess liquid was removed, the gaseous feed of HFP was allowed to enter through the bottom of the reactor. The process was run for 10 minutes to allow sufficient time for steady-state to be achieved in the system. The liquid discharge extracted, during this time, was collected in an intermediate sample bottle. Independent tests were done to verify that 10 minutes was sufficient time for steady-state to be achieved as discussed in Chapter 5. Thereafter the solution was sent to a separate sample bottle to collect the reactor effluent for 30 minutes.

After the 30 minutes had elapsed, liquid-liquid extraction was performed on the crude product and GC and GC-MS analysis was used on the isolated HME. A schematic of the FFMR set-up is shown in Figure 3.3 with a photograph provided in Photograph 3.7.

3.3.3 Validation of the FFMR apparatus

The operation of the FFMR was validated by measuring the mass transfer of CO_2 in ethylene glycol solution and making a comparison with literature data.

The liquid phase mass transfer coefficient in the FFMR was determined using the methodology described in section 2.11. A 12 wt% solution of ethylene glycol was prepared and used as the liquid feed to the FFMR. Initially, the liquid feed-rate varied from 3 $cm^3 \cdot min^{-1}$ to 5 $cm^3 \cdot min^{-1}$ in increments of 1 $cm^3 \cdot min^{-1}$ at a constant inlet gas flowrate of carbon dioxide (CO_2) of 50 $cm^3 \cdot min^{-1}$. Three more experimental runs were then performed at the same levels of the inlet liquid flowrate but at a constant inlet gas flowrate of 80 $cm^3 \cdot min^{-1}$.

In order to develop the liquid film on the surface of the microchannel, the FFMR is first fed with the ethylene glycol solution at the predetermined inlet liquid flowrate for the experimental run being performed and the reactor was allowed to flood. Once the microchannels are fully immersed, the withdrawal pump is switched on and the liquid is drained from the FFMR. The withdrawal rate is always higher than the feed rate to prevent flooding of the microchannels.

The CO_2 is then allowed to enter the system for 20 minutes. In this time, the ethylene glycol with absorbed CO_2 is drawn off into a breaker containing 30 cm^3 of a 0.1 $mol \cdot dm^{-3}$ solution of sodium hydroxide (NaOH). Any CO_2 that does not absorb into the liquid in the microchannels is vented.

When the liquid product contacts the NaOH solution, reaction 3.1 occurs converting the absorbed CO_2 to the basic sodium carbonate (Na_2CO_3).

$$2NaOH + CO_2 \rightarrow Na_2CO_3 + H_2O \qquad (3.1)$$

The volume of product collected in the elapsed time was recorded. A standard solution of hydrochloric acid (HCl) of concentration 0.1 $mol \cdot dm^{-3}$ was used to perform a titration. An autotitrator (Metrohm 888 Titrando) was used to perform the titration. The concentration of CO_2 in the liquid leaving the FFMR, C_{out}, can be derived from the titration analysis of the mixture

using a phenolphthalein and methyl orange indicator. Equation 3.2 illustrates the equation to determine the required endpoints

$$C_{out} = \frac{V_{HCl}C_{HCl}}{Q_L t} \tag{3.2}$$

where V_{HCl} represents the volume of HCl solution consumed from the initial titration endpoint to the second endpoint, C_{HCl} is the concentration of HCl solution and t is the collecting time (Chen, 2009).

Photograph 3.7: The experimental set-up of the falling-film microreactor used to synthesise HME

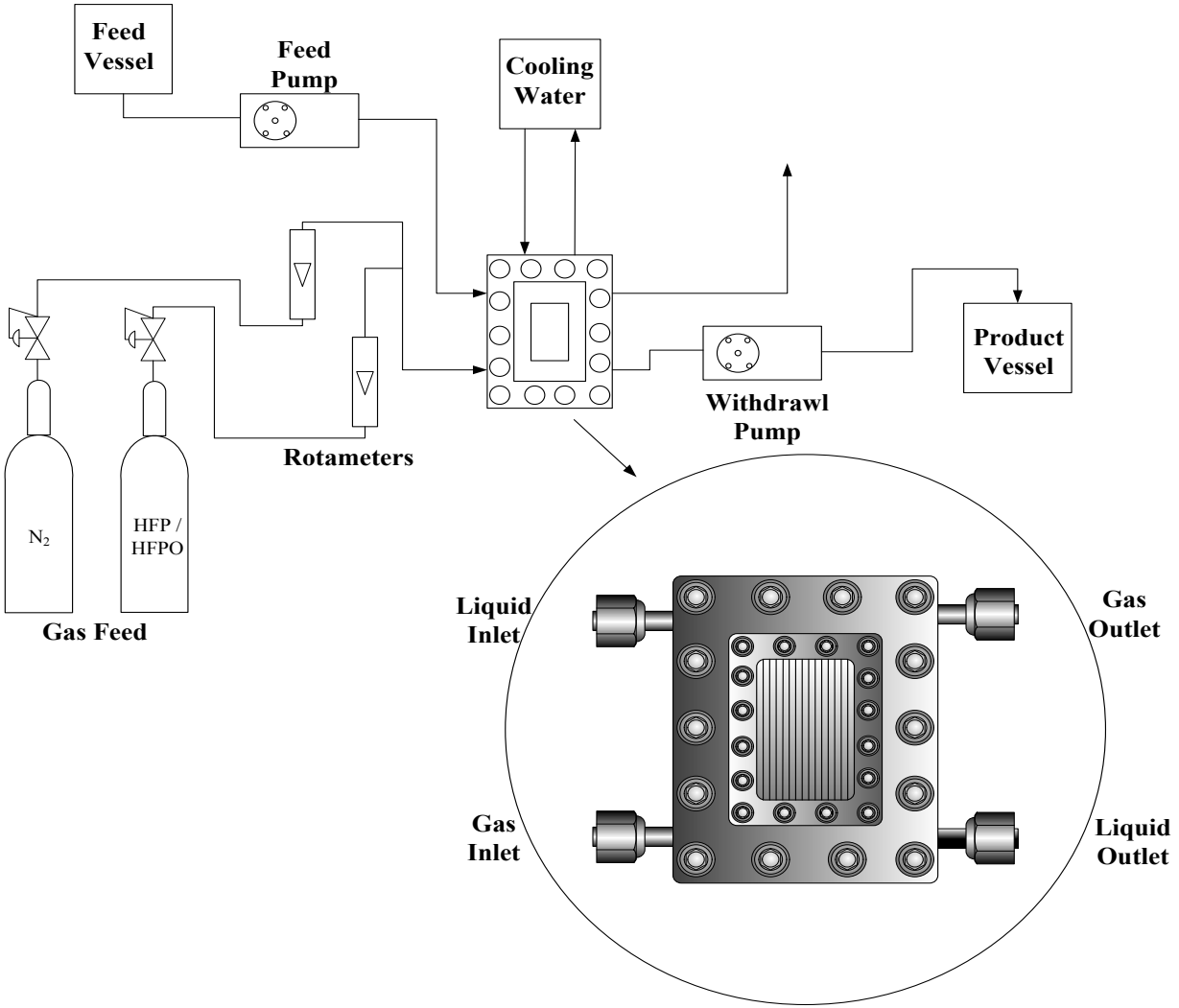

Figure 3.3: Schematic diagram of FFMR setup for continuous synthesis of HME

3.4 Analytical techniques

3.4.1 Gas chromatography and mass spectrometry

GC and GC-MS analysis were used to determine the composition of the different fractions analysed as well as the identity of the constituent components of the crude sample, respectively.

A GC-method was set-up such that analysed samples were exposed to the same chromatographic conditions. Using the GC calibrations in Appendix B and manipulations shown in Appendix C, the yield of HME was calculated using the area and mass ratios from the GC trace. In the case of the calibration, different mass ratios were determined by creating standard solutions of methanol and propanol such that the individual compositions were known. GC analysis revealed their respective area ratios. The gradient of the resulting graph, according to Equation 3.1, yields the internal response factor. The calibration for the GC is illustrated in Figure B-5.1 and elaborated in section 3.5.3. A similar procedure was performed to determine the internal response factor for HME and the internal standard propanol to determine the internal response factor for this system. During the experimental runs, the GC analysis determined the area ratios of methanol and HME with propanol. Thus, Equation 3.1 can again be applied using the constant internal response factor determined for the respective systems and the known mass of internal standard added to determine the mass of HME and methanol in the samples analysed. In the equation below $\frac{A_i}{A_{IS}}$ represents the area ratio of component *i* to the internal standard as per GC results, $F_{i,IS}$ represents the internal response factor and $\frac{M_i}{M_{IS}}$ is the mass ratio of component *i* and the internal standard.

$$\frac{A_i}{A_{IS}} = F_{i,IS} \cdot \frac{M_i}{M_{IS}} \tag{3.1}$$

A 1 μL syringe was used to inject the sample into the GC. Distilled water was used to remove any impurities in the syringe and a 0.5 μL sample was measured and injected into the GC. The Manual Peak Integration function in Lab Solution™ was used to find the relative areas of the peaks of the components in the sample analysed.

3.4.2 Surface response methodology

The yield of HME calculated was defined as the response variable and dependant on the factors investigated (i.e. temperature, catalyst concentration and HFP concentration for the semi-batch gas-liquid reactor experimental as well as temperature, HFP mole fraction, liquid feed flowrate and catalyst concentration for the FFMR experimental runs). Surface response methodology was used to investigate the relationship that exists between the factors pertinent to each reactor and the response variable.

Appendix F presents the programming code written in MatLab™ which uses the factors tabulated in Table A-2 and the HME yields and mole fraction in the reactor effluent to generate surface and contour plots. The levels of the factors determined by the central composite design and the corresponding HME yield determined at the different combinations of these factors were used to regress for the β-coefficients of Equation 2.7. The model with these coefficients was used to generate surface and contour plots for the interaction of any two factors with the remaining factors being held constant. These give a visual representation of the relationship between the combinations of factors being analysed.

3.5 Calibrations

3.5.1 Flowmeter calibration

3.5.1.1 Semi-batch gas-liquid reactor flowmeter calibration

The gaseous flows through the HFP and nitrogen flowmeters were calibrated using a bubble flow meter.

With regards to the HFP calibration, a rubber nipple was filled with a soapy solution and the reading on the flowmeter was set to 15. The rubber nipple was squeezed and the gas flowing into the bottom of the column formed a bubble which moved up the column. The duration for the bubble to move from the bottom of the column until a graduated mark, representing 200 cm^3, was recorded. This process was repeated to the final reading on the flowmeter of 150 in increments of 15. The procedure was repeated 3 times to assess the repeatability of the experimental results.

The nitrogen calibration followed the same procedure with the flowmeter number ranging between 0.2 and 2 in increments of 0.2. The above results have been tabulated in Tables B-1.1 and B-1.2 in Appendix B.

Figures B-1.2 and B-1.4 show systematic error as larger deviations are observed at higher flowrates. This is as a result of increasing difficulty in recording times at increased flowrates. The uncertainty on the nitrogen and HFP flowmeter calibrations were ±0.84 $cm^3 \cdot s^{-1}$ and ±2.2 $cm^3 \cdot s^{-1}$, respectively. Photograph 3.8 shows the bubble flowmeter used in the calibrations discussed.

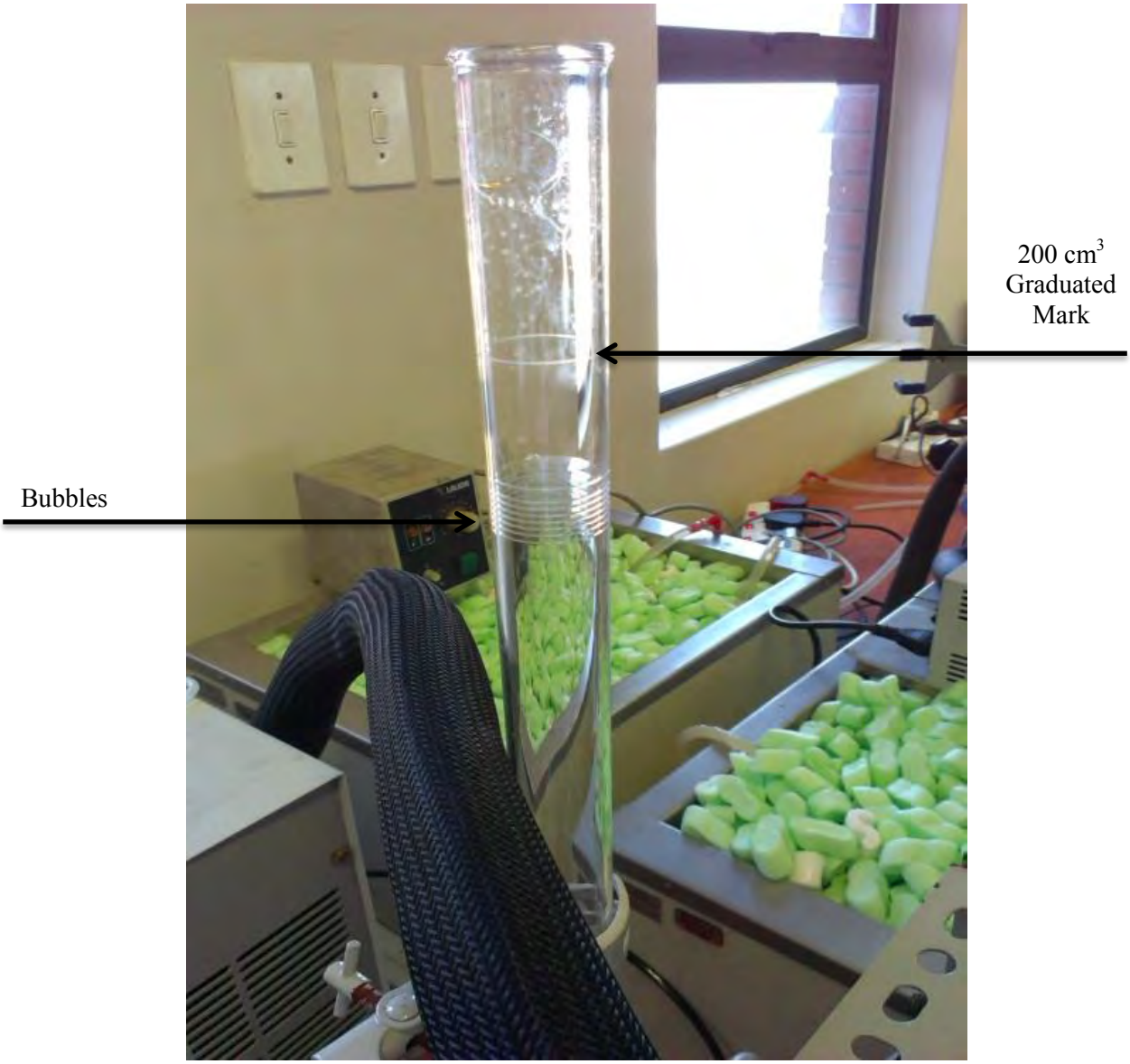

Photograph 3.8: The bubble flow meter used for the rotameter calibration

3.5.1.2 Falling-film microreactor flowmeter calibration

Similar to the calibration of the flowmeters for the semi-batch gas-liquid experimental runs, a bubble flow meter was used for the FFMR.

As described previously, for the HFP calibration, a rubber nipple was filled with soapy solution and the flowmeter number set to 15. The rubber nipple was squeezed and the gas flowing through the column formed a bubble with the gas flowing up the column. The time that the bubble took to move from a graduated mark at the bottom of the column to a chosen graduated mark along the column was recorded. This represented a volume of 10 cm^3. This process was repeated to a rotameter number of 75 in increments of 15. The procedure was done a total of 3 times to assess the repeatability of the results. The same procedure was repeated for the calibration of the nitrogen flowmeter.

The uncertainties on calibration on the HFP and nitrogen rotameters were ±0.0175 $cm^3 \cdot s^{-1}$ and ±0.013 $cm^3 \cdot s^{-1}$ respectively.

3.5.2 Temperature calibration

A Pt 100 temperature standard was used for the calibration of the Pt100 reactor temperature probe. The standard probe was connected to a display unit and was immersed in an oil bath together with the Pt 100 probe. The oil bath temperature was increased to a desired temperature and the system was allowed to reach thermal equilibrium. The temperatures of the standard probe and the Pt 100 probe were recorded. The procedure was repeated 3 times to assess the repeatability of the calibration results. The uncertainty of the calibration was determined to be ±0.17 K. Calibration results are shown in Appendix B.

3.5.3 GC calibration

Two GC calibrations were required for two different binary systems. The first calibration was for the methanol and internal standard (propanol) system and the second for the HME and internal standard system.

For the methanol and internal standard system 5 samples were prepared each containing 1 cm^3 of methanol and varied amounts of internal standard of 0.2 cm^3 to 1 cm^3 in increments of 0.2 cm^3. The

masses of the empty vial, vial with only methanol and vial with methanol and internal standard were measured so that the masses of methanol and internal standard could be determined. These samples were injected into the GC to obtain chromatograms from which the data was used to produce the calibration graphs. This was generated by plotting the respective mass ratio against the corresponding area ratio. The same procedure was followed for the HME and methanol calibration. All of the data and ranges have been tabulated in Appendix B. The uncertainty on the GC calibrations undertaken was ±0.06 for the methanol-internal standard system and ±0.027 for the distillate-internal standard system based on mass ratios.

An appropriate GC column oven temperature program had to be used to separate the components effectively. The temperature was kept constant at 303.15 K for 4 minutes and then increased to a temperature of 553.15 K and a heating rate of 10 $K \cdot min^{-1}$. This final temperature was kept constant for 5 minutes resulting in 34 minutes being the complete running time.

The initial period of 4 minutes at 303.15 K was chosen to resolve the methanol, HME and internal standard. The temperature ramp was done to allow any heavy components to exit the system before the next analysis.

4

CHAPTER FOUR

4. PRELIMINARY WORK: SEMI-BATCH GAS-LIQUID REACTOR

This chapter presents the results of experiments performed to synthesise HME using a semi-batch gas-liquid reactor. It also focuses on data analysis and discussion of the results. High level statistical analysis was also performed on the experimental results to allow a better understanding of the effect of the independent variables on the yield of HME.

4.1 Synthesis, isolation and identification of HME

4.1.1 Yields of HME

As part of the preliminary work conducted on this system, the synthesis of HME was carried out in a semi-batch gas-liquid reactor. This was performed in order to determine a suitable range of operating conditions for subsequent microreactor tests. The semi-batch apparatus contained 1.5 dm^3 of methanol and was charged with a gaseous feed of HFP diluted with nitrogen through a gas sparger. As the reaction proceeded, the unreacted or unabsorbed gaseous feed moved to the headspace of the reactor. The headspace may have also contained gaseous methanol as methanol may have been entrained in the exiting gas.

In order to prevent an increase in pressure in the reaction vessel and maintain the reaction at isobaric conditions, some of the gaseous components in the reactor were vented to atmosphere. It was vented out of the laboratory to avoid human contact. Any methanol entrained in the exiting gas was refluxed using an overhead condenser operating at 278.15 K. The methanol volume of 1.5 dm^3 was chosen so as to minimize the vapour headspace in the reactor and ensure complete immersion of the gas sparger and temperature probe.

The reactor was equipped with a stirrer which was set to a maximum rotational speed of 450 rpm. This was deemed appropriate to ensure operation in the kinetic regime.

Table 4.1 contains the reaction conditions and resultant HME yields for experiments undertaken in the semi-batch gas-liquid reactor as preliminary work. The centre-point experimental runs, as discussed in section 2.5, were repeated six times to test for reproducibility of the experimental data. There was a standard deviation in HME yield of ±2.8% for the centre-point runs.

Table 4.1: Reaction conditions and yields of HME

Run	HFP Mole Fraction	Catalyst Concentration, $mol \cdot dm^{-3}$	Temperature, K	Yield, %
1	0.74	0.71	298.15	56.13
2	0.74	0.71	288.15	50.54
3	0.74	0.48	298.15	29.48
4	0.74	0.48	288.15	31.31
5	0.49	0.71	298.15	29.13
6	0.49	0.71	288.15	29.80
7	0.49	0.48	298.15	31.77
8	0.49	0.48	288.15	29.83
9	0.41	0.60	293.15	29.86
10	0.83	0.60	293.15	30.89
11	0.62	0.40	293.15	27.44
12	0.62	0.80	293.15	27.02
13	0.62	0.60	284.75	26.03
14	0.62	0.60	301.55	30.42
15	0.62	0.60	293.15	30.91
16	0.62	0.60	293.15	31.53
17	0.62	0.60	293.15	31.56
18	0.62	0.60	293.15	29.83
19	0.62	0.60	293.15	34.17
20	0.62	0.60	293.15	25.76

The HME yields obtained at the different levels of factors investigated are also shown in Table 4.1. The yield was defined as the moles of HME produced per mole of HFP introduced into the system. The HME yields for the 20 experimental runs undertaken were in the range of 25.76-56.15%.

It is likely that incomplete conversion of HFP was realized. This could not be confirmed as the constituent components and compositions of the vapours leaving the system were not analysed.

One factor that may have a significant effect on the overall performance of the semi-batch system is a phenomenon referred to as 'salting out' (Schumpe, 1993). In this system, the presence of KOH catalyst causes a reduction in the saturation concentration of HFP in the solution and hence a reduction in the driving force for mass transfer. This has an inhibitory effect on the rate of reaction. An instance of this effect is evident in trial 12 with the highest catalyst mass used resulted in one of the lowest HME yields observed.

During the experimental runs, a build-up of solid salt precipitate on the gas-sparger was observed. Although the sparger was cleaned between runs, the build-up during the runs restricted the inlet flow of gas not allowing the desired flow of reactant gas to be achieved. Fluctuations of the float in the rotameter during the runs were indicative of solid build-up on the sparger inducing a back-pressure. This effect could have introduced some variance in the observed results although it is difficult to quantify the extent.

The trends from Figures 4.1-4.3 in conjunction with the data in Table 4.1 indicate that higher yields are observed at higher temperatures. The exothermic nature of the reaction suggests that the system temperature will increase as the reaction proceeds which was observed (Il'in et al., 2004). The system temperature was required to remain constant during the run as it was one of the experimental factors under investigation. Although there was temperature control on the system, as discussed in section 3.2.1, a temperature increase was observed. It was evident that the temperature control system could not cope with the amount of heat generated from the highly exothermic reaction. In addition, the formation of bubbles on the internal cooling coils reduced the effective area for heat transfer.

Photograph 4.1: Bubbles circulate the cooling coils impeding heat transfer

As a result of the exothermic nature of the reaction, as the reaction proceeded, the temperature of the reaction vessel increased. It was observed that after 30 minutes, the duration of an experimental run, the temperature ceased to increase. This served as an indication that the reaction had reached completion. It is improbable that this was due to insufficient HFP being introduced to the system as this had been continually fed. Likewise it was unlikely that the methanol had been completely consumed as the GC analysis indicated the presence of methanol after the reaction. To this effect, the most plausible reasoning is that HFP was no longer being dissolved into the methanol or the catalyst had been completely consumed. Since the catalyst was inorganic and non-volatile, it could not be detected using a Flame Ionizer Detector during GC analysis. By virtue of the manner in which the HME yield was defined, the magnitude of the yield will decrease if HFP is continually fed and no HME is produced.

4.1.2 Fractional distillation

In an attempt to increase the purity of HME, fractional distillation of the organic layer obtained after the liquid-liquid extraction (discussed in section 3.3.1.3) was attempted. The liquid and vapour temperatures in the column were recorded incrementally as shown in Table A-4.1. After the column was in operation for 12 hours, two temperature plateaus were observed at 318.15 K and 319.15 K. Literature suggests that laboratory distillation of complex mixtures should run between 8-10 hours (Vogel, 1989) however, after 12 hours, the still pot still contained approximately 250 cm^3 of the 500 cm^3 initially added to the unit. It was suggested at the time that this result may have been due to the existence of a multi-component azeotrope. The hypothesis was initially difficult to confirm as there is no substantial VLE data available on the system.

The Analytical Solution of Groups method was then used to generate VLE data for the methanol and HME system as elaborated upon in section 2.4.3. The generated VLE data revealed the presence of an azeotrope at 318.15 K which explains the temperature plateau observed during the fractional distillation.

4.1.3 Gas chromatography and mass spectrometry

GC-MS analysis was performed on the distillate obtained from the fractional distillation and the presence of HME was identified with an 88% level of confidence. The GC-MS mass spectrum used to identify HME is illustrated in Figures A-7.1 and A-7.2.The temperature of 319.15 K, at which the HME fraction was obtained, is not in agreement with the theoretical boiling point from literature of 327.15 K (Il'in et al., 2004). However, from the generation of VLE data using ASOG, the temperature at which the HME was obtained was the temperature corresponding to the methanol-HME azeotrope at atmospheric pressure.

Another observation during the fractional distillation was the fact that the still pot contents turned from clear to a viscous black liquid. This may have been as a result of decomposition of the heavier components in the still pot or due to the heavier boiling components being concentrated with the lighter fractions being removed. A GC analysis was performed on the still pot contents, to better understand the observation. The overlay of the chromatograph between the organic layer, initially charged to the still pot, and the sample after the colour change showed no new peaks. This indicates that no decomposition occurred.

The GC calibration was carried out using the internal standard method. Acetone, propanol, 2-butanol and 1,1,1–trichloroethane were tested as potential internal standards by first considering their miscibility in the crude product from the reactor. All the potential internal standards were miscible with the reactor product except for 1,1,1–trichloroethane as shown in Photograph 4.2.

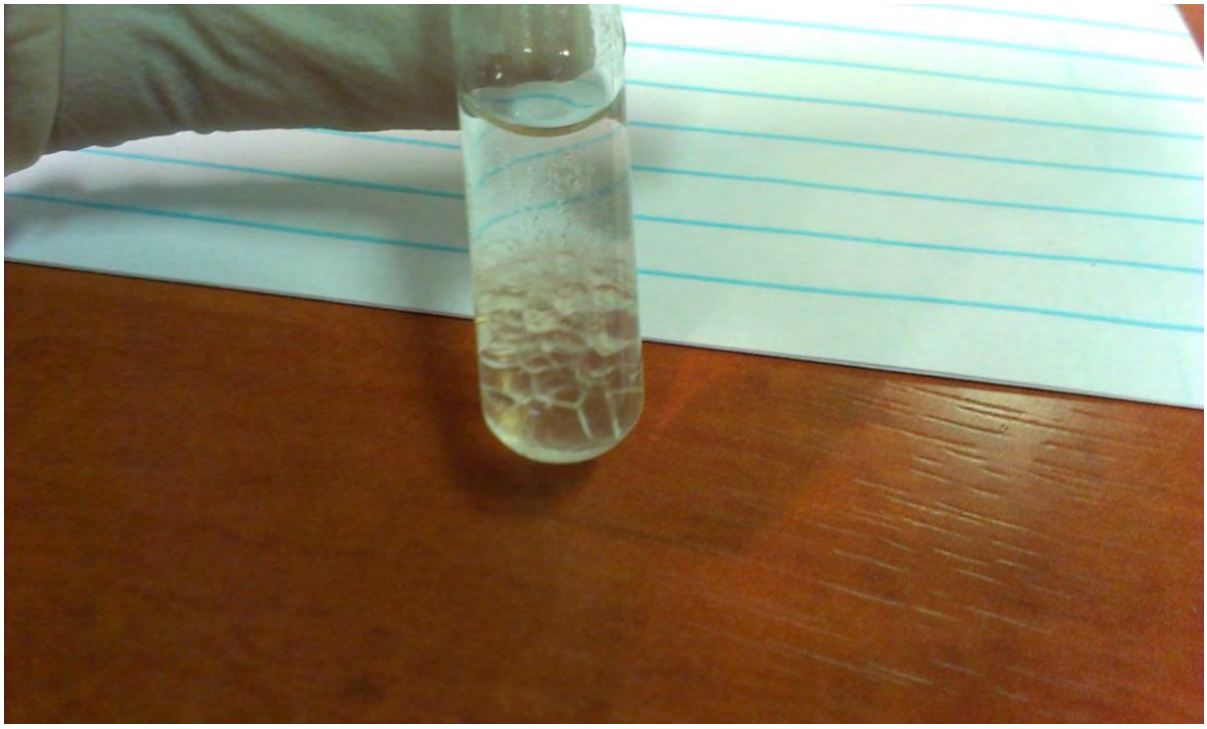

Photograph 4.2: 1,1,1-trichloroethane and crude sample immiscibility

The retention time in the GC and relative resolution of species was used as the next criteria in the selection of an appropriate internal standard. Propanol was selected as the internal standard as its peak in the chromatograph did not overlap with either the HME or methanol peaks. It becomes difficult to determine the area ratio and mass ratio of the individual peaks if they overlap. A subsequent GC analysis of pure methanol revealed no appreciable impurities were present.

4.1.4 Solid potassium fluoride precipitation

According to literature, there is an undesired side reaction, during the synthesis of HME, resulting in the formation of solid potassium fluoride (KF) precipitate as depicted in Equation 2.4 (Il'in et al., 2004). A significant observation was the negligible solid precipitation in the test region examined. This indicated that the reaction could possibly be carried out in a falling film microreactor, which is unable to operate if there is substantial solid formation. The presence of KF in solution was not confirmed.

The solubility of KF in methanol is 10.2 g·100 g methanol^{-1} at 298.15 K (Stenger, 1996). Considering the liquid volume of 1.5 dm^3 and the density of liquid methanol at ambient conditions, the mass of methanol in the reactor is 1186 grams. The liquid volume in the reactor was assumed to be pure methanol as this is the bulk of the contents. This implies that 121 grams of KF must form before precipitation is expected to occur. The presence of KF could not be identified in the GC and GC-MS analysis as it is an inorganic compound.

During the fractional distillation, there was precipitation of a white solid above the condensing section of the unit. The solid formed was suspected to be a mixture of KF and KOH originally present in the still-pot charge. Photograph 4.3 shows the solid formation on the upper portion of the condenser.

Photograph 4.3: Solid formation during the fractional distillation

4.1.5 Rate test on semi-batch gas-liquid reactor

Table 4.2: Incremental yields of HME in the semi-batch gas-liquid reactor

Data point	Time, min	Yield, %
1	0	0
2	5	66.62
3	10	66.74
4	15	67.33
5	20	61.83
6	25	61.38
7	30	49.81

The elapsed time for the experimental runs in the semi-batch gas-liquid reactor was 30 minutes. Samples were taken every 5 minutes from the initiation of the experimental run until 30 minutes using the experimental conditions of the centre point. The HME yields at these increments are shown in Table 4.2. As would be expected, the yield of HME initially was negligible. Between data points 2-4, there was no significant deviation in the yield obtained. The remaining data points show that the yield decreased. By virtue of the yield being defined as the moles of HME produced in proportion to the moles of reactant HFP fed, the observation can be justified by more HFP being fed than moles HME being produced. This test was performed merely as a verification of the steady-state operation of the reactor and not to measure kinetics or analyze the transient peroiod, therefore sampling during the initial reaction phase was not warranted.

The KOH catalyst may be consumed in the side reaction forming KF. However, there exists a practical limit to the amount of catalyst that can be added to the initial charge since salting out effects and by-product precipitation can inhibit the performance of the reactor (Schumpe, 1993).

4.2 Analysis of the interaction between factors with respect to HME yield

Surface response methodology (SRM) was utilized to generate surface and contour plots illustrated in Figures 4.1-4.3. SRM allowed for the relationship between 2 of the 3 factors investigated to be graphically represented with the remaining factor being held constant at its centre point as defined by the central composite design. The centre points for the factors were temperature at 293.15 K, HFP mole fraction at 0.62 and catalyst concentration at 0.6 $mol \cdot dm^{-3}$.

Figure 4.1 illustrates the relationship between the HFP mole fraction and the catalyst concentration with the temperature being held constant at 293.15 K. The results show that the

yield of HME was at its highest, in the test range, at the highest HFP mole fractions and catalyst concentrations. The lowest yields in the test region were observed at low catalyst concentrations regardless of the high HFP mole fraction. A similar observation is found at the lowest HFP mole fractions and high catalyst concentrations.

Theoretically it is expected that the higher the HFP mole fraction, the higher the yield of HME. This is expected as there would be a greater amount of reactant available for the reaction with the excess methanol in the reactor. Figure 4.1 shows good agreement with the theoretical expectation. It may be assumed that at high catalyst concentrations, a higher HME yield would be observed due to the catalyst increasing the rate of reaction as it decreases the activation energy of the reaction. However, lower yields were observed at higher catalyst concentrations. This can be explained by an effect called 'salting out'. This is when the solubility of a gas in a liquid decreases due to the addition of salts to the solution. This decrease in solubility results due to the increase of the activity coefficient of the dissolved gas, HFP, in the liquid phase. This results in an overall reduction in the driving force for mass transfer (Schumpe, 1993).

A saddle can also be observed in the test region which implies the maxima or minima lie outside the experimental range of the factors. Attempts to reach these optimum conditions may prove impractical or impossible (such as a mole fraction greater than 1).

Figure 4.2 illustrates the relationship between the catalyst concentration and temperature with the HFP mole fraction being kept constant at 0.62. The contours indicate that an absolute minimum appears to lie outside the test region at lower catalyst concentrations. This is expected in spite of the 'salting out' effect, since at extremely low catalyst concentrations not enough HME will be produced with the same amount of HFP being introduced and the overall yield will decrease by virtue of the definition of the yield.

The most plausible explanation for the high yields being observed at higher temperatures is the side reactions, shown in Equations 2.2 and 2.3, have lower relative reaction rates at higher temperatures compared to the main reaction stated in Equation 2.1. This is realizable if the activation energy of the side reactions is lower than the main reaction (Levenspiel, 2006).

Figure 4.3 shows the relationship between HFP mole fraction and temperature with the catalyst concentration being kept constant at 0.6 $mol \cdot dm^{-3}$. The theoretical expectations of the temperature and HFP mole fraction effect, as explained for the previous surface and contour plots, show good

agreement in Figure 4.3 i.e. high temperatures and high HFP mole fractions resulted in the highest HME yields.

An absolute minimum is found in this test region with the maximum appearing to lie at higher mole fractions of HFP and higher temperatures. This is however limited to a mole fraction of 1. There also exists a practical limit on the operating temperature since it has to be lower than the boiling point of methanol.

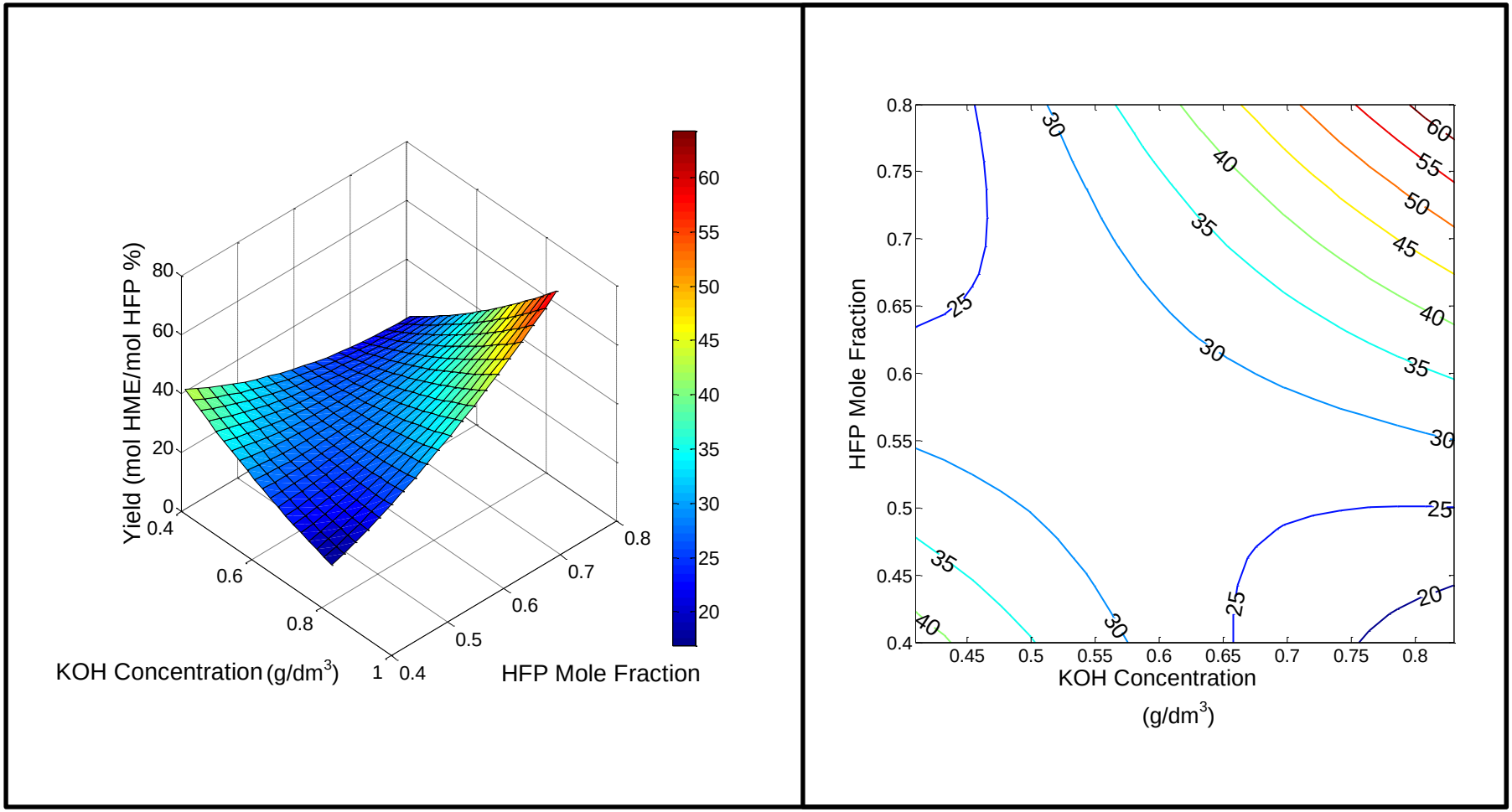

Figure 4.1: Surface and contour plot for HME yield for varying catalyst concentrations HFP mole fraction with a constant temperature of 293.15 K

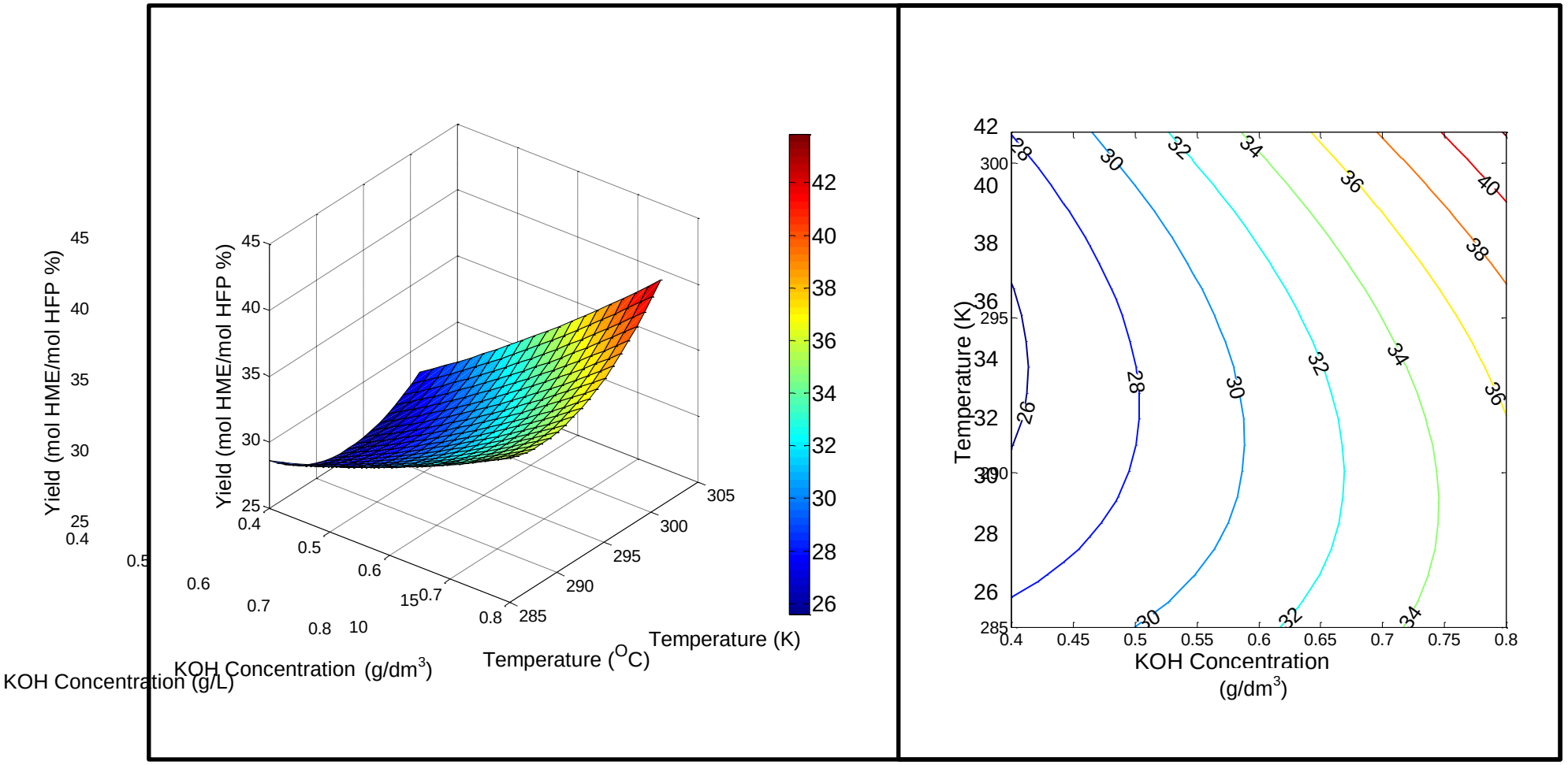

Figure 4.2: Surface and contour plot for HME yield for varying temperature and catalyst concentration with a constant HFP mole fraction of 0.62

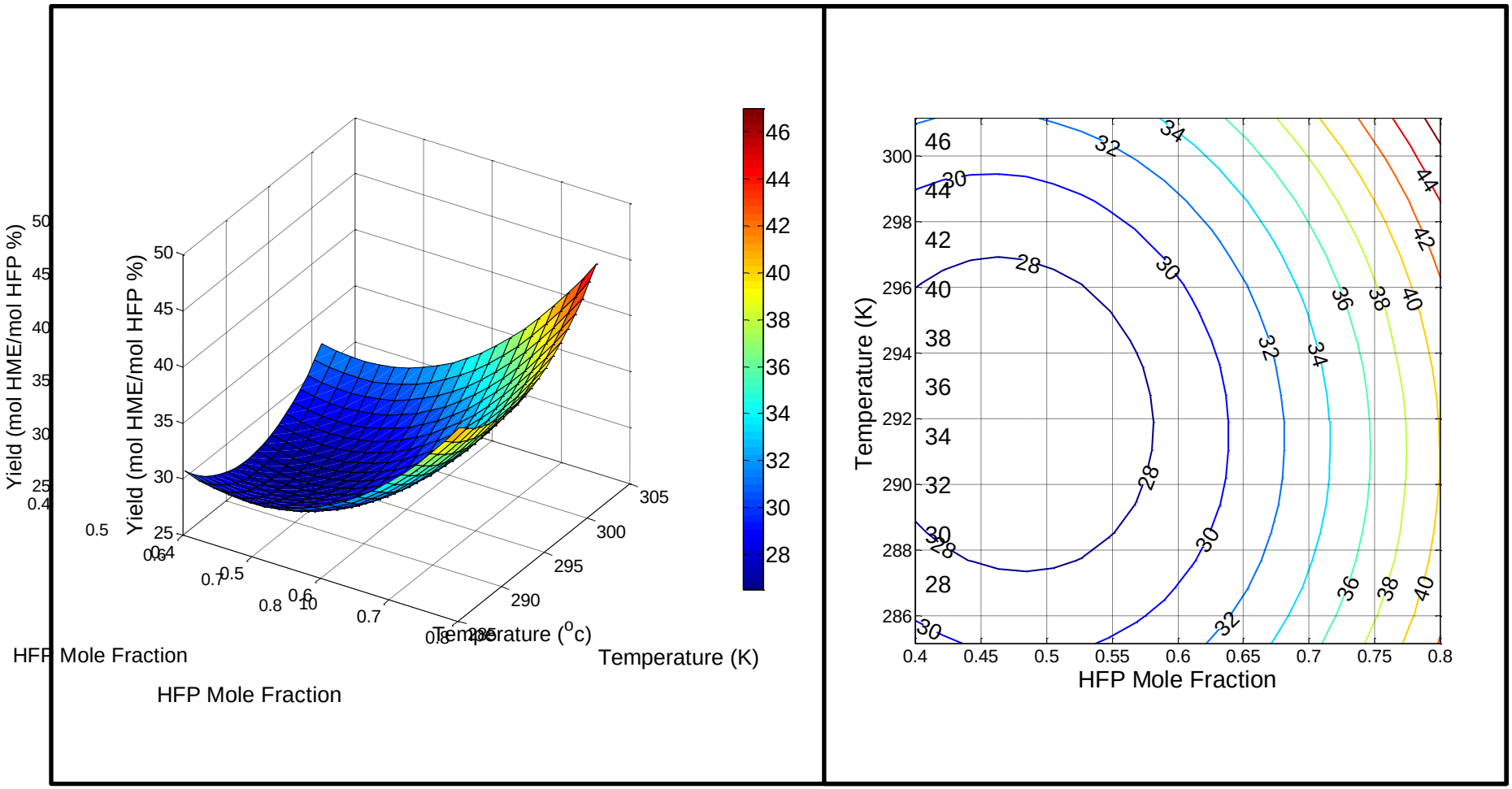

Figure 4.3: Surface and contour plot for HME yield for varying temperature and HFP mole fraction with a constant catalyst concentration of 0.62 mol·dm^{-3}

4.3 Statistical analysis

The reproducibility of the experiment is judged on the response variable, HME yield, determined for multiple runs using the conditions of the centre point. These were 6 identical experimental trials (Run 15-20 in Table 4.1) which realised a standard deviation of ±2.8%. Deviations in the yield have been elaborated in Section 4.1.1.

Table 4.3: Summary of statistical results obtained from MatLab™

Statistics	Result
R^2	0.60
R	0.77
F-statistic	1.44
p-value	0.29
Regression Mean Square	68.30
Residual Mean Square	47.47

An Analysis of Variance (ANOVA) table was generated and the results have been tabulated in Table A-2.1 in Appendix A-2. Some of the values from the ANOVA table have been highlighted in Table 4.3. It is desired that the *F*-value calculated is greater than the tabulated *F*-value for the specific degrees of freedom and confidence interval deemed appropriate (Istadi and Amin, 2006). Assuming a 95% confidence interval, the tabulated *F*-value, using data from Appendix A-4, indicates $F_{0.05,9,7} = 3.02$ (Dinov, 2013). The distributed *F*-value was determined from the table given in Appendix D. The ANOVA table generated yielded an *F*-value of 1.44 which is less than 3.02. This indicates that the results of the quadratic equation predicting the response variable is not satisfactory with a confidence interval of 95%. Analysis of the *F*-distribution table indicated the appropriate confidence to be approximately 75%.

The R^2 value defines the total variation of the yield about its mean. The R^2 value of 0.60 may indicate a broad distribution of data-points. This may be as a result of temperature fluctuations during the experimental runs (i.e. there was difficulty in maintaining a constant reaction temperature throughout the experimental run). There may also be inconsistencies in the results due to observed fluctuations in the inlet gas flow to the reactor. This value indicates that 60% of the total variation of the response variable, which is the HME yield, is viable results from the model prediction. The correlation coefficient, R, of 0.77 shows a satisfactory correlation between the predicted and experimental values of the yield (Istadi and Amin, 2006). The parity plot in Figure 4.4 illustrates the correlation between the observed and predicted yield. If a point lies on the 45^o line then the observed and predicted yields are equivalent. The further away the points move from this line, the poorer the correlation between the observed and the predicted response variables. The parity plot obtained showed a reasonable fit by the model.

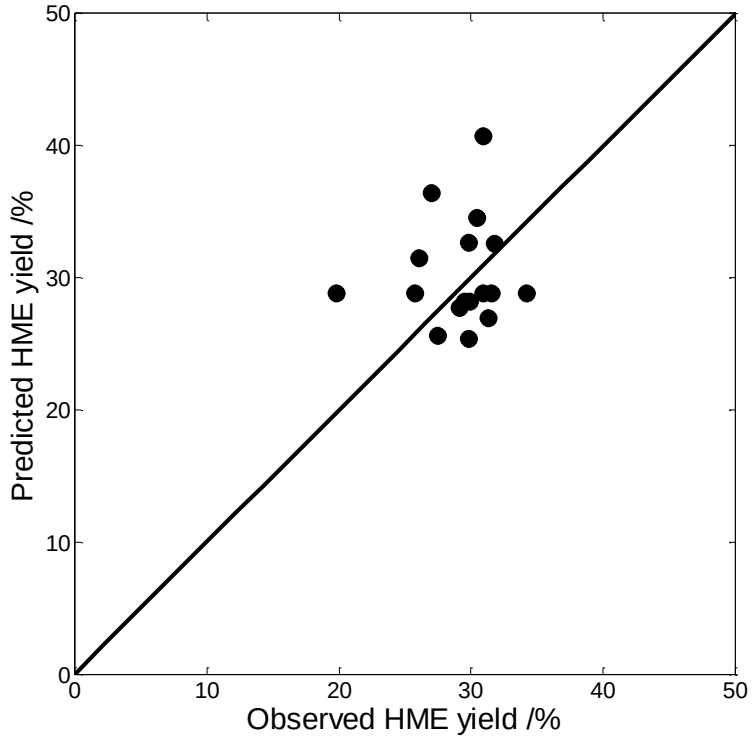

Figure 4.4: Parity plot for the predicted yield and the observed yield

The response variable prediction, shown in Equation 2.29, requires the regression of the β–coefficients which was programmed in MatLab™; the code shown in Appendix F. The resultant values for the coefficients with their *t*-value and *p*-value have been tabulated below. The standard errors on the regression are also shown.

Table 4.4: Coefficients obtained via regression and the accompanying statistics

Parameter	Coefficient	Term	Standard Error	*t*-value	*p*-value
β_0	219.7	intercept	120.86	1.82	0.10
β_1	-338.51	X_1	192.41	-1.76	0.11
β_2	-264.58	X_2	205.58	-1.29	0.23
β_3	-2.40	X_3	4.7077	-0.51	0.62
β_{12}	407.58	X_1X_2	169.33	2.41	0.04
β_{13}	0.52	X_1X_3	3.8963	0.13	0.90
β_{23}	1.06	X_2X_3	4.2349	0.25	0.81
β_{11}	91.40	X_1^2	116.22	0.79	0.45
β_{22}	14.54	X_2^2	129.69	0.11	0.91
β_{33}	0.041	$X3^2$	0.0079	0.52	0.61

X_1, X_2 and X_3 represent HFP mole fraction, catalyst concentration and temperature, respectively as defined in the MatLab™ code. β_1, β_2 and β_3 are the coefficients that represent the linear effect of the corresponding factor as shown above. β_{12}, β_{13} and β_{23} show the interaction effect between the

factors as defined in the above table. β_{11}, β_{22} and β_{33} are the second order terms which show the quadratic response of the particular factor. The *t*-value and *p*-value assess the significance of the β-coefficients (Istadi and Amin, 2006).

The coefficient's effect on the system can be judged by the *p*-value with which it is associated. The lower the magnitude of the *p*-value, the larger the contribution of the corresponding coefficient (Istadi and Amin, 2006).

The results indicate that the interaction between HFP mole fraction and catalyst concentration (X_1X_2) had the largest effect on the yield of HME at a 96% (*p*-value of 0.04) confidence level of significance. The linear temperature term (X_1) had the next most significant effect with an 89% (*p*-value of 0.11) confidence level of significance. The linear term for catalyst concentration (X_2) had a 77% confidence level of significance with a *p*-value of 0.23. The remaining interactions were not statistically significant (Istadi and Amin, 2006).

The eigenvalues were calculated for the response variable and the results were $\lambda_1 = 260.3, \lambda_2 = -154.4\ and\ \lambda_3 = 0.04$. The signs of the eigenvalues are different which indicates a saddle characteristic of the stationary point will exist in the test region. This indicates that unique optimums may not be identified in the test region (Istadi and Amin, 2006). This result further emphasizes the need for a wider test range to be investigated which may not always be practical (i.e. HFP mole fraction greater than one or operating at a higher temperature than the boiling point of methanol)

5

CHAPTER FIVE

5. DESIGN OF REACTION SECTION OF THE PROPOSED PROCESS - SYNTHESIS OF HME USING FALLING-FILM MICROREACTOR TECHNOLOGY

This chapter presents the results of the experiments performed on the falling-film microreactor. The results obtained have been analysed and discussed. This chapter also focuses on yield and the mole fraction of HME, separately, as the response factor in order to optimise the design of the reactor section of the proposed process. The chapter also comprises of statistical analysis performed on the experimental results.

5.1 Experimental results

The reactor needed to be designed and optimized by analysis of experimental results as there is no kinetic information on the methanol and HME system in microreactors available in literature.

5.1.1 Yields of HME

Table 5.1 contains the reaction conditions of each experimental run performed in the FFMR and the corresponding yield of HME. The yields of the side products which are an alkenyl ether, 1,2,3,3,3-pentafluoro-1-methoxyprop-1-ene, and an alkyl tetrafluoropropionate, methyl 2,3,3,3-tetrafluoropropionate, are also tabulated.

A comparison between Tables 4.1 and 5.1 reveals that higher yields of HME were observed in the FFMR than the GLR. This was an expected outcome due to the FFMR offering more efficient control over the temperature of the reaction zone as well as improved gas-liquid mass transfer (Knorr, 2012). This is a positive outcome and has further implications with regards to scale up. The continuous operation of the FFMR is a definite advantage over the conventional route, given that the performance of the microreactor meets and exceeds that of the conventional semi-batch

apparatus. Scale-up is also achieved much more easily with the microreactor unit since capacity and throughput is increased merely by placing identical modules in parallel (Vankayala et al., 2007).

Table 5.1: Reaction conditions with product and side reaction yields in the FFMR

Exp. No.	HFP mole fraction	KOH concentration, $mol \cdot dm^{-3}$	Liquid flow, $cm^3 \cdot min^{-1}$	Temp, K	Product yield, %		
					Hexafluoropropyl methyl ether	Alkenyl ether	Alkyl tetrafluoropropionate
1	0.34	0.34	1.75	280.15	11.60	0.32	1.10
2	0.34	0.34	4.25	280.15	48.32	3.91	4.22
3	0.70	0.34	1.75	280.15	38.88	2.15	4.00
4	0.70	0.34	4.25	280.15	56.93	6.99	5.06
5	0.34	0.52	1.75	280.15	33.12	2.21	3.59
6	0.34	0.52	4.25	280.15	39.78	2.82	3.26
7	0.70	0.52	1.75	280.15	81.59	6.35	9.96
8	0.70	0.52	4.25	280.15	23.33	1.44	1.84
9	0.34	0.34	1.75	290.15	42.94	3.58	3.47
10	0.34	0.34	4.25	290.15	49.85	1.48	3.79
11	0.70	0.34	1.75	290.15	40.38	3.01	3.78
12	0.70	0.34	4.25	290.15	52.36	1.60	4.58
13	0.34	0.52	1.75	290.15	29.90	1.04	2.95
14	0.34	0.52	4.25	290.15	37.48	1.73	3.64
15	0.70	0.52	1.75	290.15	37.41	2.44	3.18
16	0.70	0.52	4.25	290.15	46.88	2.91	3.92
17	0.52	0.43	3	275.15	61.53	5.10	5.12
18	0.52	0.43	3	295.15	51.76	3.28	3.76
19	0.52	0.25	3	285.15	53.30	5.39	4.52
20	0.52	0.61	3	285.15	44.73	2.58	3.74
21	0.17	0.43	3	285.15	34.91	1.88	3.26
22	0.88	0.43	3	285.15	61.67	5.39	5.51
23	0.52	0.43	0.5	285.15	28.45	2.84	0.75
24	0.52	0.43	5.5	285.15	55.13	1.87	4.30
25	0.52	0.43	3	285.15	51.98	1.04	4.68
26	0.52	0.43	3	285.15	67.20	2.85	3.98
27	0.52	0.43	3	285.15	59.44	5.12	4.98
28	0.52	0.43	3	285.15	53.55	3.30	4.63
29	0.52	0.43	3	285.15	68.00	2.74	5.95
30	0.52	0.43	3	285.15	59.36	3.80	5.04

5.1.2 Effect of inlet gas flowrate on reactor performance

As aforementioned, the yield of HME was defined as the ratio of the amount of HME formed and the quantity of HFP introduced into the system. An independent set of tests were performed to determine the influence that the inlet gas flowrate had on the HME yield. Pure HFP was introduced to a methanol solution which contained 0.43 $mol \cdot dm^{-3}$ catalyst. The liquid flowrate was 2 $cm^3 \cdot min^{-1}$ and the reaction temperature was 285.15 K. The inlet gas flowrate of HFP was

varied between 0.3 $cm^3 \cdot s^{-1}$ and 1.5 $cm^3 \cdot s^{-1}$ in increments of 0.3 $cm^3 \cdot s^{-1}$. The observed effects on the mass fraction of HME in the product as well as the yield of HME are illustrated in Figure 5.1.

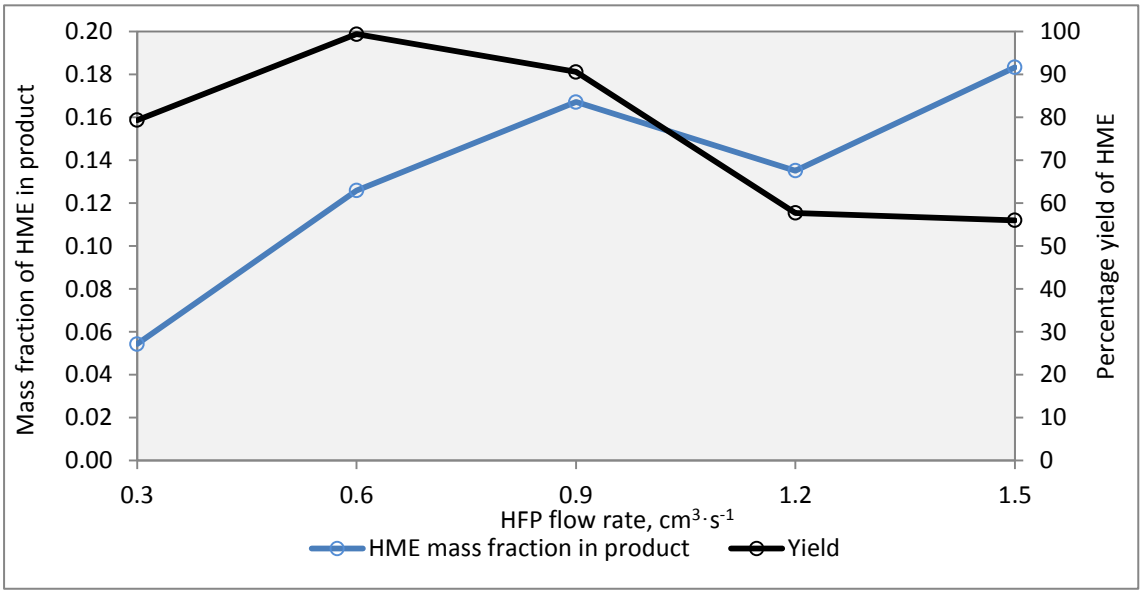

Figure 5.1: The effect of the inlet gas flowrate of HFP on the yield and mass fraction of HME in the product stream

The HME mass fraction in the product was observed to have increased with an increased inlet gas flowrate. The HME yield, however, initially increased with the increasing HFP inlet gas flowrate and began to decrease beyond an inlet gas flowrate of 0.6 $cm^3 \cdot s^{-1}$. It appears that beyond this value, the reaction became mass transfer limited and the excess HFP gas merely passed through the system unconverted. However, since the mass fraction of the HME in the reactor effluent was a critical factor determining the ease of product purification (to be discussed in Chapter 6), operating at sub-optimal HME yields may be unavoidable in the commercial process.

5.1.3 Mass transfer characteristics in a FFMR

As explained in section 3.3.3, the mass transfer coefficient was determined as per the penetration model (Equation 2.44) as well as experimentally (Equation 2.47). The results have been represented graphically in Figure 5.2 below.

Due to the limitation of the maximum liquid flow that can be achieved by the equipment, the experimentation was performed with the highest liquid flowrate that could be achieved. This was 5 $cm^3 \cdot min^{-1}$ which corresponds to a mean velocity in the microchannels of 0.037 $m \cdot s^{-1}$. This did not overlap with the range at which the literature data was available; however, it can be observed

that there is very close agreement between the two datasets predicting the liquid-side mass transfer coefficient with the penetration model.

The experimental data was generated at three different levels of liquid flowrate (3, 4 and 5 $cm^3 \cdot min^{-1}$) and at a constant gas flow of 50 $cm^3 \cdot min^{-1}$ and then 80 $cm^3 \cdot min^{-1}$. Again, the range tested was not the same as the experimental data from literature, however, a similar trend is observed showing good agreement with literature.

The Fourier number for the experiments performed lay in the range of 0.24-0.47. According to literature, the Fourier number being less than unity indicates that the penetration is applicable. It also suggests that mass transfer has not established equilibrium.

In literature and in the experimental runs, it was observed that the prediction of the liquid-side mass transfer coefficient was greater for the experimental data than the prediction by the penetration model. A possible cause of the deviation was the liquid surface (gas-liquid interface) not being uniform. This could have been caused by the pulsation of the feed-pump. This effect could have increased the interfacial area and resulted in an increased absorption of the gas than predicted by the model.

It can be observed that the measured mass transfer coefficient is in the range of 5.7 to $6.7 \cdot 10^{-5}$ $m \cdot s^{-1}$ for the runs at 50 $cm^3 \cdot min^{-1}$ and 5.8 to $6.8 \cdot 10^{-5}$ $m \cdot s^{-1}$ for the experimental runs at 80 $cm^3 \cdot min^{-1}$. The Reynolds numbers in the experimental range were below 14.72 which indicates laminar flow as it is less than 150. Literature suggests that for a falling film in a conventional reactor, the mass transfer coefficient is less than $1.5 \cdot 10^{-5}$ $m \cdot s^{-1}$ in the laminar flow regime. This shows that there is much more significant gas-liquid mass transfer rate in a FFMR than in other falling film systems.

The close agreement of the experimental and literature data shows that the FFMR was operated correctly which also serves as an indication that the data obtained was reliable.

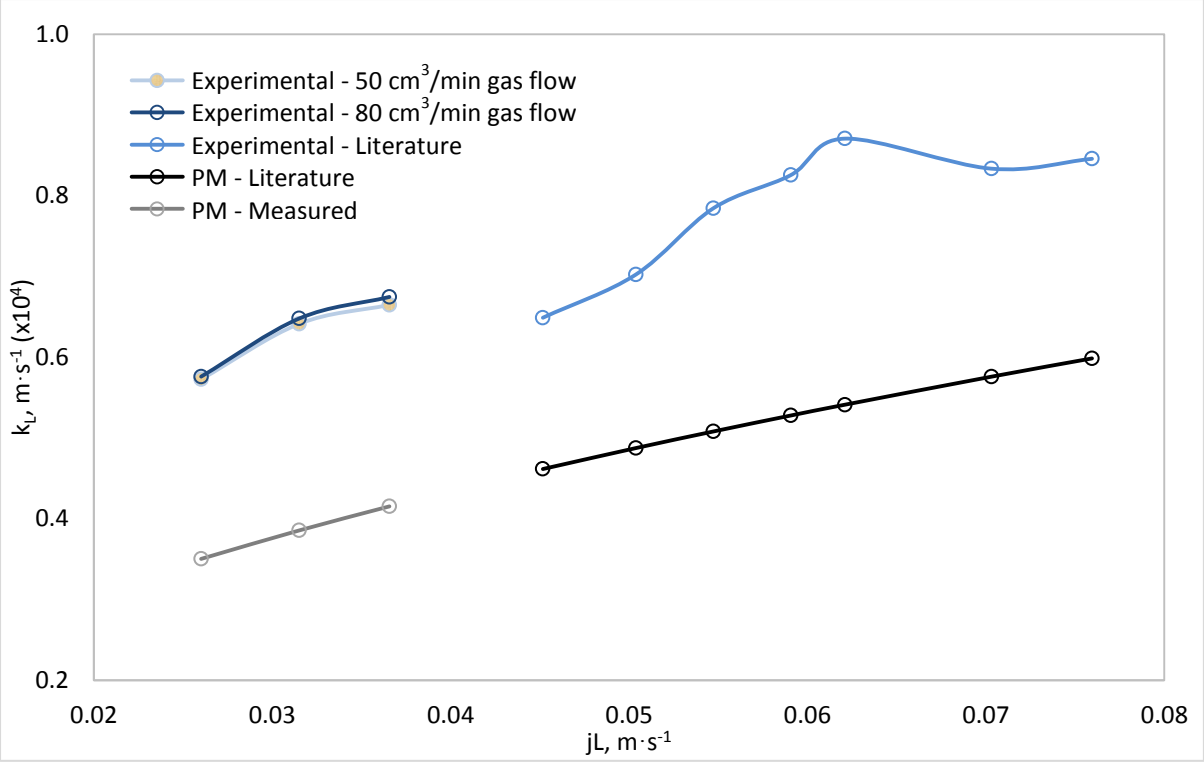

Figure 5.2: Comparison of measured liquid phase mass transfer coefficient and model predictions

5.1.4 Independent rate tests

The experimental runs in the FFMR were carried out for a period of 30 minutes each with 10 minutes allowed prior to this time for steady-state to be established. For a particular experimental run, using the centre-point experimental conditions, the yield was determined, incrementally, from the commencement of the reaction until 21 minutes had elapsed.

As observed in Table 5.2, the yields of HME achieved were similar at an average of 20.4 % with a standard deviation of 0.77 %. This independent test showed that the 10 minute period was adequate to allow the reaction to reach steady-state. This also indicates that the reaction rate was high with steady-state being achieved within 3 minutes. This is essential for applications involving FFMRs as they operate most efficiently at high rates of reaction (Knorr, 2012).

Table 5.2: Incremental yields of HME in the FFMR

Run	Time, min	Yield, %
1	3	20.04
2	6	21.82
3	9	20.53
4	12	20.45
5	15	20.78
6	18	19.60
7	21	19.59

5.1.5 Mole fraction of HME in the liquid product

Table 5.3 contains the reaction conditions employed for the experiments carried out in the FFMR and the corresponding mole fractions of HME in the product. It was found that higher HME mole fractions were a prerequisite for ease of isolation of the target compound via liquid-liquid extraction and distillation. These aspects of the proposed process are discussed further in Chapter 6.

Table 5.3: Reaction conditions with HME mole fraction in the FFMR

Exp. No.	HFP mole fraction	KOH concentration, $mol \cdot dm^{-3}$	Liquid flow, $cm^3 \cdot min^{-1}$	Temp, K	HME Mole Percentage, %
1	0.34	0.34	1.75	280.15	0.3
2	0.34	0.34	4.25	280.15	0.6
3	0.70	0.34	1.75	280.15	2.3
4	0.70	0.34	4.25	280.15	1.4
5	0.34	0.52	1.75	280.15	1.0
6	0.34	0.52	4.25	280.15	0.5
7	0.70	0.52	1.75	280.15	1.6
8	0.70	0.52	4.25	280.15	1.2
9	0.34	0.34	1.75	290.15	1.3
10	0.34	0.34	4.25	290.15	0.6
11	0.70	0.34	1.75	290.15	2.4
12	0.70	0.34	4.25	290.15	1.3
13	0.34	0.52	1.75	290.15	0.9
14	0.34	0.52	4.25	290.15	0.5
15	0.70	0.52	1.75	290.15	2.2
16	0.70	0.52	4.25	290.15	1.1
17	0.52	0.43	3	275.15	1.6
18	0.52	0.43	3	295.15	1.3
19	0.52	0.25	3	285.15	1.4
20	0.52	0.61	3	285.15	1.1
21	0.17	0.43	3	285.15	0.3
22	0.88	0.43	3	285.15	2.6
23	0.52	0.43	0.5	285.15	4.3
24	0.52	0.43	5.5	285.15	0.8
25	0.52	0.43	3	285.15	1.3
26	0.52	0.43	3	285.15	1.0
27	0.52	0.43	3	285.15	1.5
28	0.52	0.43	3	285.15	1.4
29	0.52	0.43	3	285.15	1.7
30	0.52	0.43	3	285.15	1.5

5.2 Analysis of the effects of reaction conditions on the performance of the FFMR using surface response methodology

5.2.1 Optimum HME yields

The surface and contour plots illustrated in Figures 5.5-10 were generated using Surface Response Methodology (SRM). SRM enabled the relationship between two of the four factors investigated to be graphical represented while the remaining two factors were kept constant at their centre-point value. The centre-point values were determined by the central composite design. The centre point values for the feed liquid flowrate, HFP mole fraction, reaction temperature and catalyst concentration were 3 $cm^3 \cdot min^{-1}$, 0.52, 285.15 K and 0.43 $mol \cdot dm^{-3}$, respectively.

Figure 5.3 shows the relationship between the liquid flowrate and catalyst concentration with the temperature and HFP mole fraction kept constant at 285.15 K and 0.52, respectively. The highest yields were observed at high liquid flowrates and lower catalyst concentrations. Conversely, the lowest yields for this interaction were observed with a low liquid flowrate and high catalyst concentration.

It would have been expected that higher catalyst concentrations would have resulted in an increased yield of HME due to the catalyst decreasing the activation energy of the reaction. The observed trend can be explained by an effect called ‘salting out’. This is the reduction of the solubility of a gas in a liquid due to the addition of salts to the solution. This decrease resulted due to the increase of activity coefficient of the dissolved gas, HFP, in the liquid phase. This resulted in an overall reduction in the driving force for mass transfer (Schumpe, 1993).

The higher flowrate of the liquid feed is observed to result in higher yields. The test region examined did not reveal an optimum interaction set of conditions resulting in the highest yield. The observed trends, however, indicate that moderate catalyst concentration and higher flowrates are favourable.

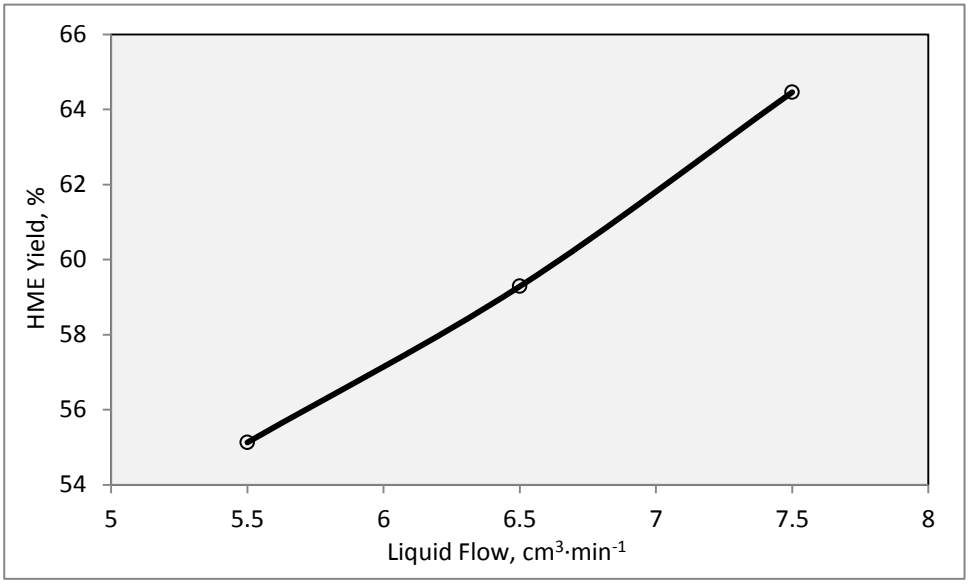

Figure 5.3: Independent test to assess the influence of the liquid flow on the yield of HME in the FFMR

The highest liquid flowrate used in the test region was 5.5 $cm^3 \cdot min^{-1}$. The results show that the higher liquid flowrates result in the highest yields being realised. An independent test was performed, using the conditions of experimental run 24 (HFP mole fraction of 0.52, catalyst concentration of 0.43 $mol \cdot dm^{-3}$, liquid flowrate of 5.5 $cm^3 \cdot min^{-1}$ and temperature of 285.15 K) to examine the effect of increased liquid flowrate beyond that which was tested using the central composite design. Figure 5.3 shows the results of this test with the yield increasing proportionally with the increase in liquid flowrate. According to the design limitations in the operating manual of the FFMR, the flow should not exceed an operating limit of 8.3 $cm^3 \cdot min^{-1}$. Although a higher yield can be realised if the flow is increased, it should not be considered a viable option as the mole fraction of HME in the reactor product stream will decrease with higher flowrates. This will therefore make downstream separation of the target compound difficult. This is elaborated in section 5.2.2.

Figure 5.6 examines the relationship between the temperature and catalyst concentration with the HFP mole fraction and liquid flowrate kept constant at 0.52 and 3 $cm^3 \cdot min^{-1}$, respectively. The highest yields were observed at higher temperatures in conjunction with lower catalyst concentrations. This was also evident for the combination of lower temperatures and higher catalyst concentrations.

The most likely reason for the evident temperature effect is that the side reactions shown in Equations 2.2 and 2.3 have lower reaction rates at higher temperatures than the main reaction stated in Equation 2.1. This is realizable if the activation energy of the side reactions is lower than the main reaction. As further justification, a further trend can be observed in Table 5.1 whereby the side reaction yields are generally decreasing with increasing temperature.

The contours also form a saddle for this interaction indicative of the optimum combination of these factors lying outside the test region.

Figure 5.7 illustrates the relationship between the HFP mole fraction and catalyst concentration with temperature and liquid flow held constant at 285.15 K and 3 $cm^3 \cdot min^{-1}$, respectively. The highest yields are observed at moderate catalyst concentrations and high HFP mole fractions. The general trend indicates that the higher yields are realised at the higher mole fractions of HFP which is in agreement to theoretical expectations. This is due to the higher amount of HFP being fed to the reactor resulting in more HFP being available for the reaction with the liquid feed. The lowest yields observed were at the lowest mole fractions of HFP being fed to the reactor as well as highest catalyst concentrations. This is in agreement with expectations as discussed above.

Figure 5.8 shows the relationship between the liquid flowrate and HFP mole fraction with the temperature and catalyst concentration held constant at 285.15 K and 0.43 $mol \cdot dm^{-3}$, respectively. As would be expected from the previous trends and theoretical explanations, the highest yields were observed at the highest HFP mole fractions and liquid flowrates. Conversely, the lowest yields in this interaction were observed at the lowest liquid flowrate and HFP mole fraction. According to the contour plot, it appears as if the maximum for this interaction lies outside the test region.

Figure 5.9 illustrates the interaction between the temperature and HFP mole fraction with the liquid flowrate and catalyst concentration held constant at 3 $cm^3 \cdot min^{-1}$ and 0.43 $mol \cdot dm^{-3}$, respectively. The surface and contour plots indicate that the yields of HME are at their highest at high mole fractions of HFP and higher reaction temperatures. This is in accordance with the explanations and trends above. The lowest yields were obtained at low mole fractions of HFP and low temperatures which are also in good agreement. The behaviour of the interaction shows a saddle as observed in the contour plot.

Figure 5.10 shows the graphical representation of the liquid flowrate and temperature with the HFP mole fraction and catalyst concentration held constant at 0.52 and 0.43 $mol \cdot dm^{-3}$,

respectively. The highest yields were found to exist at a combination of high temperature and high liquid flowrate.

The results from this section indicate that the FFMR should be operated with a pure HFP feed (i.e. mole fraction of 1) at ambient temperature. Although higher temperatures favour higher mole fractions and yields of HME in the reactor effluent, it is more economically viable to operate at ambient temperature. Moderate catalyst concentrations should be used in the process of approximately 0.4 $mol \cdot dm^{-3}$. As aforementioned, an integral aspect of the process is to maximise the mole fraction of HME, and therefore, low liquid flowrates should be used (0.5-1.5 $cm^3 \cdot min^{-1}$ is recommended for the test region). As stated above, lower flowrates increase the HME mole fraction exiting the reactor, however, consideration needs to be taken for the required throughput required by the plant. In this range, approximately sixteen reaction plates are required to produce 250 $kg \cdot month^{-1}$ HME. Multiple reaction plates can be installed in a single FFMR. An exploded view of an FFMR, developed in SolidWorks, with eight parallel reaction plates is illustrated in Figure 5.4. It is recommended that two FFMR's be run in parallel with eight reaction plates each.

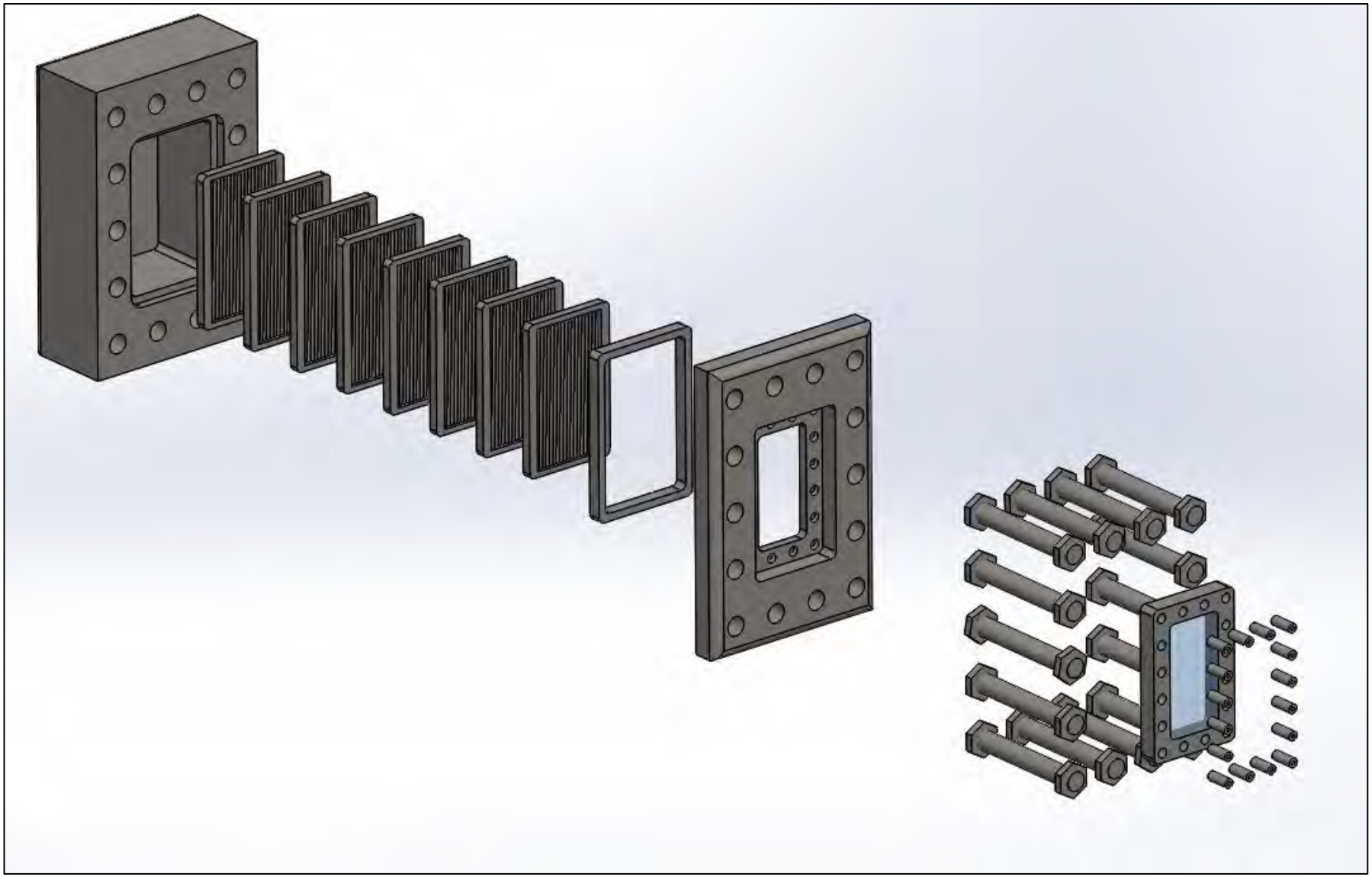

Figure 5.4: Exploded view of parallel reaction plates in the FFMR developed in SolidWorks

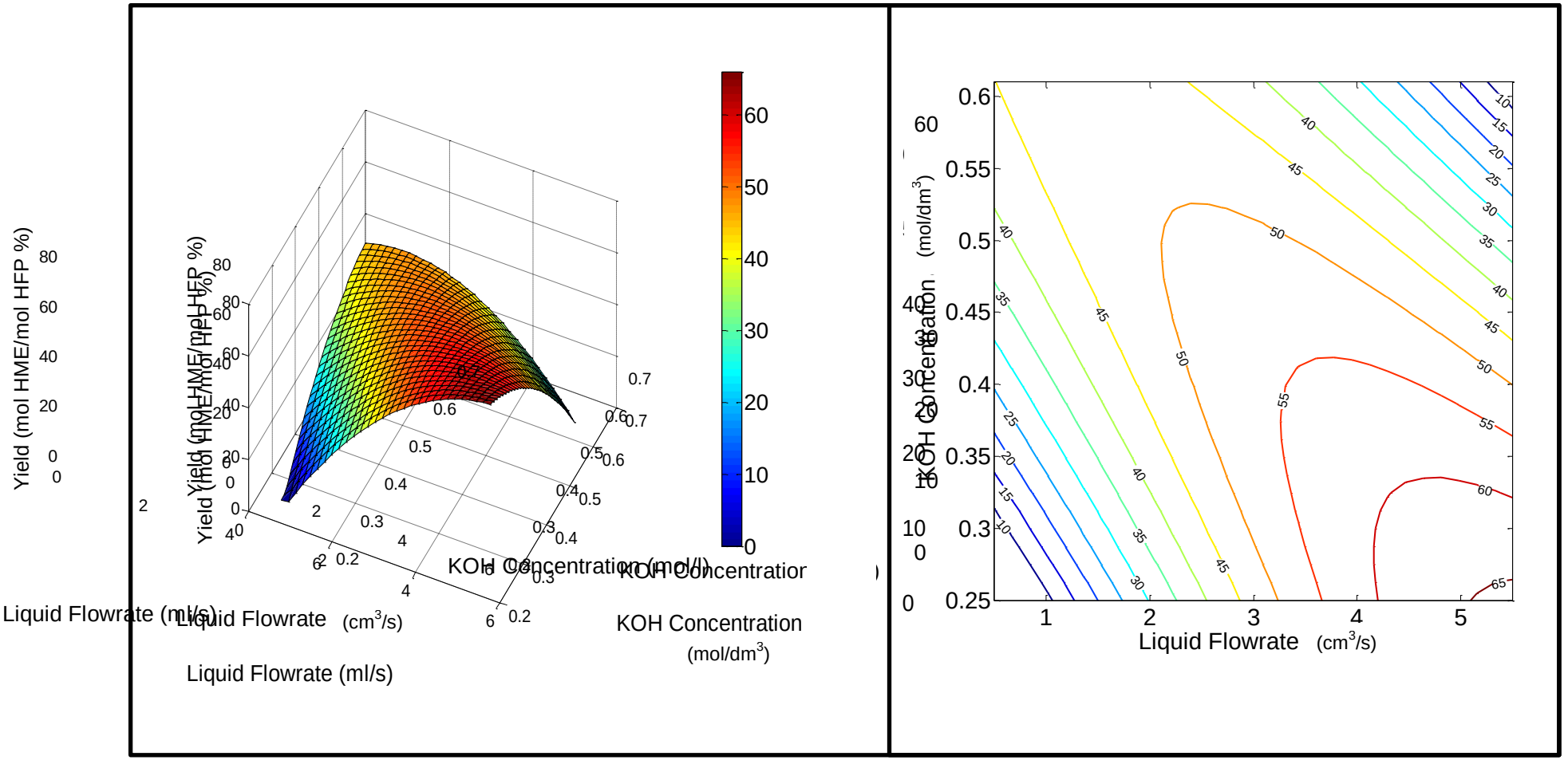

Figure 5.5: Surface and contour plot for HME yield for varying liquid flowrate and catalyst concentration with a constant temperature of 285.15 K and HFP mole fraction of 0.52

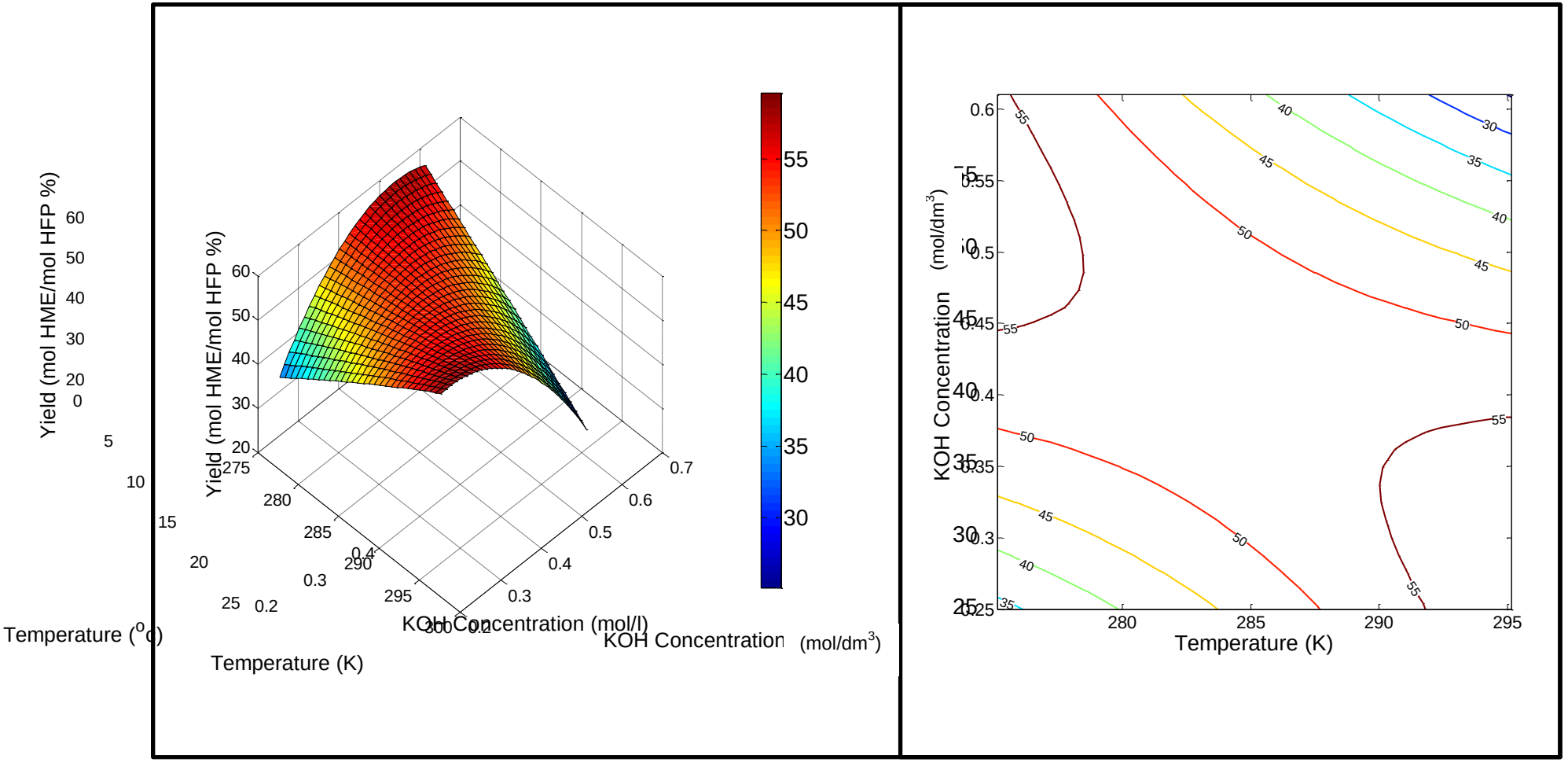

Figure 5.6: Surface and contour plot for HME yield for varying temperature and catalyst concentration with a constant liquid flowrate of 3 $cm^3 \cdot min^{-1}$ and HFP mole fraction of 0.52

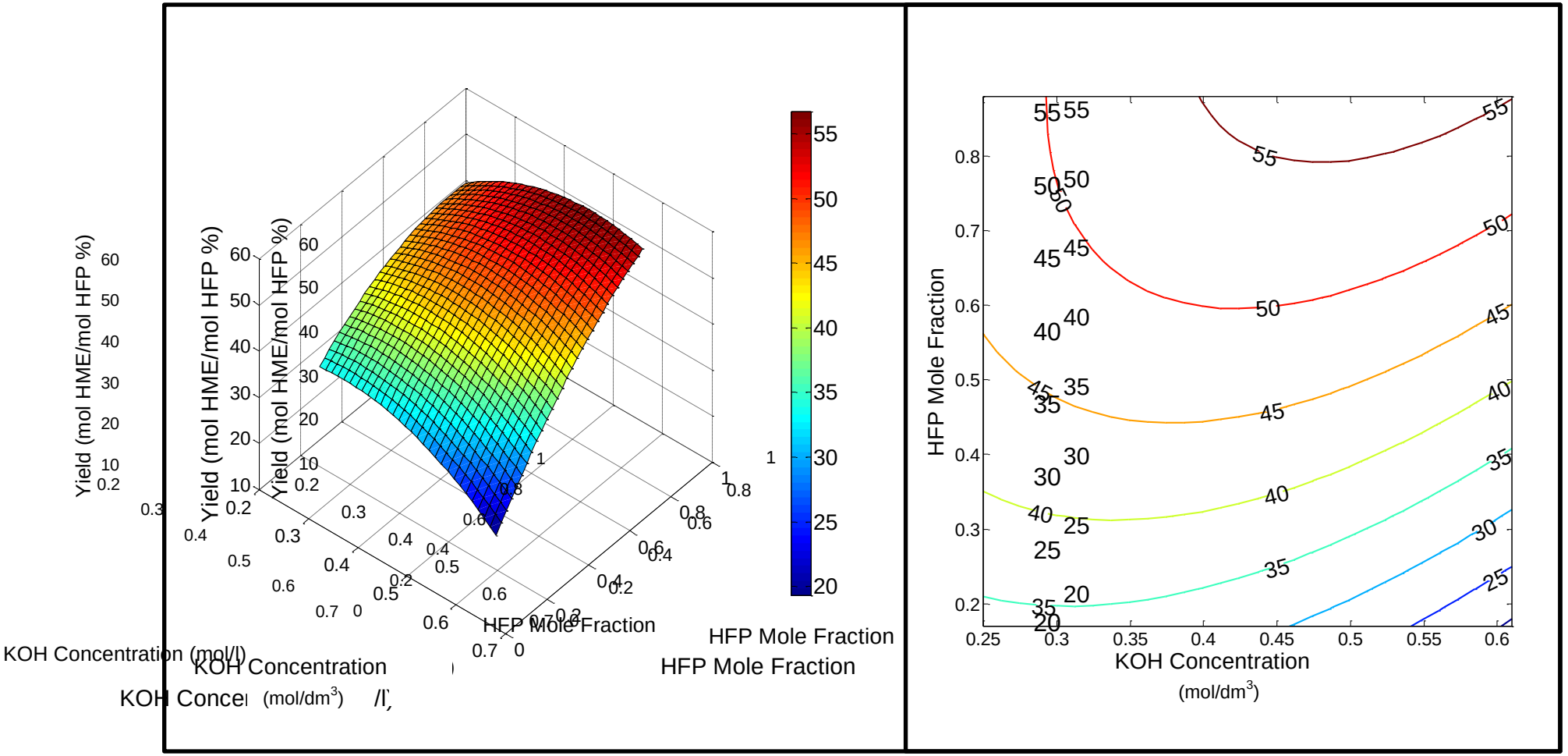

Figure 5.7: Surface and contour plot for HME yield for varying HFP mole fraction and catalyst concentration with a constant temperature of 285.15 K and liquid flowrate of 3 $cm^3 \cdot min^{-1}$

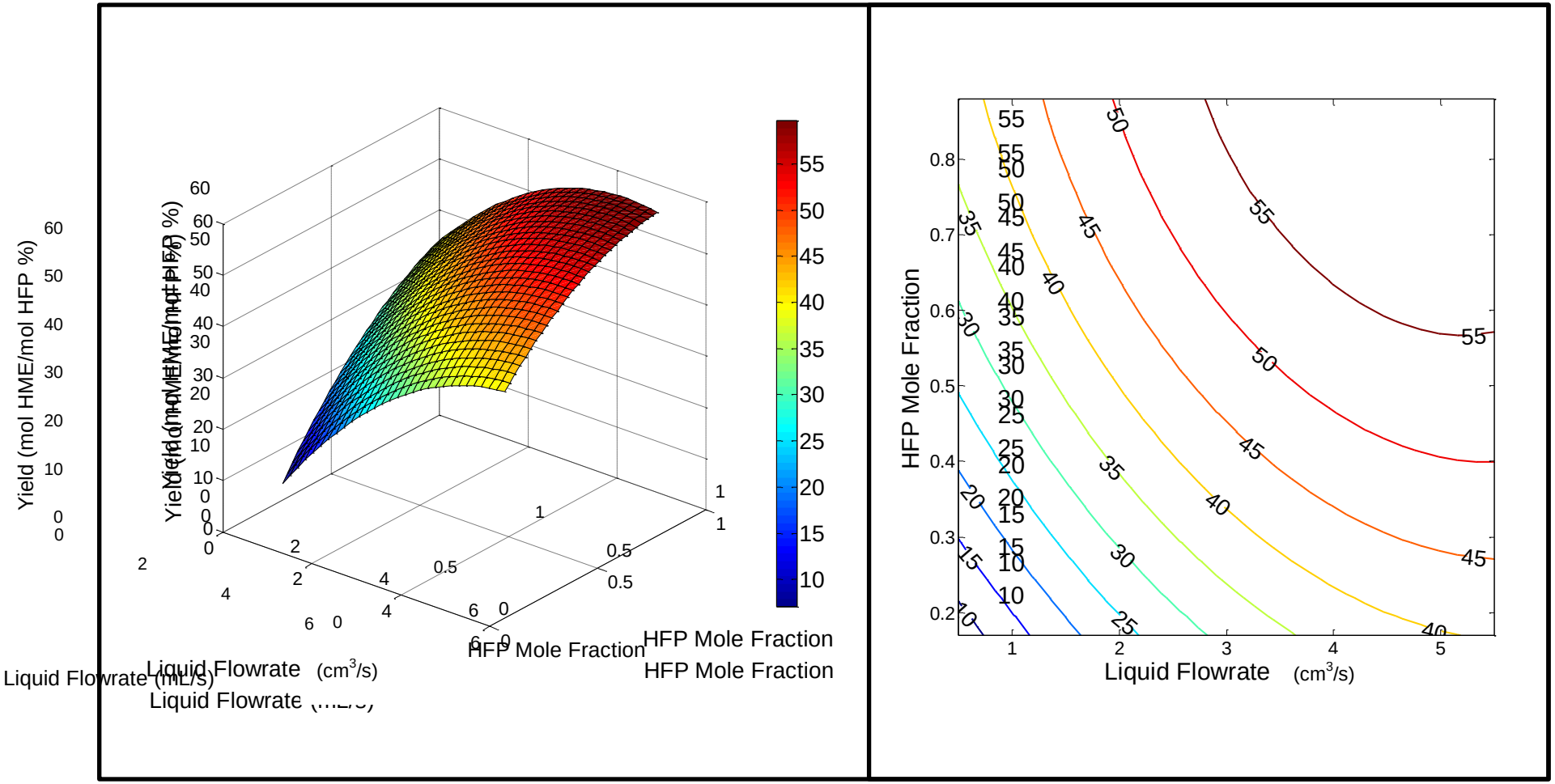

Figure 5.8: Surface and contour plot for HME yield for varying liquid flowrate and HFP mole fraction with a constant temperature of 285.15 K and constant catalyst concentration of 0.43 mol·dm^{-3}

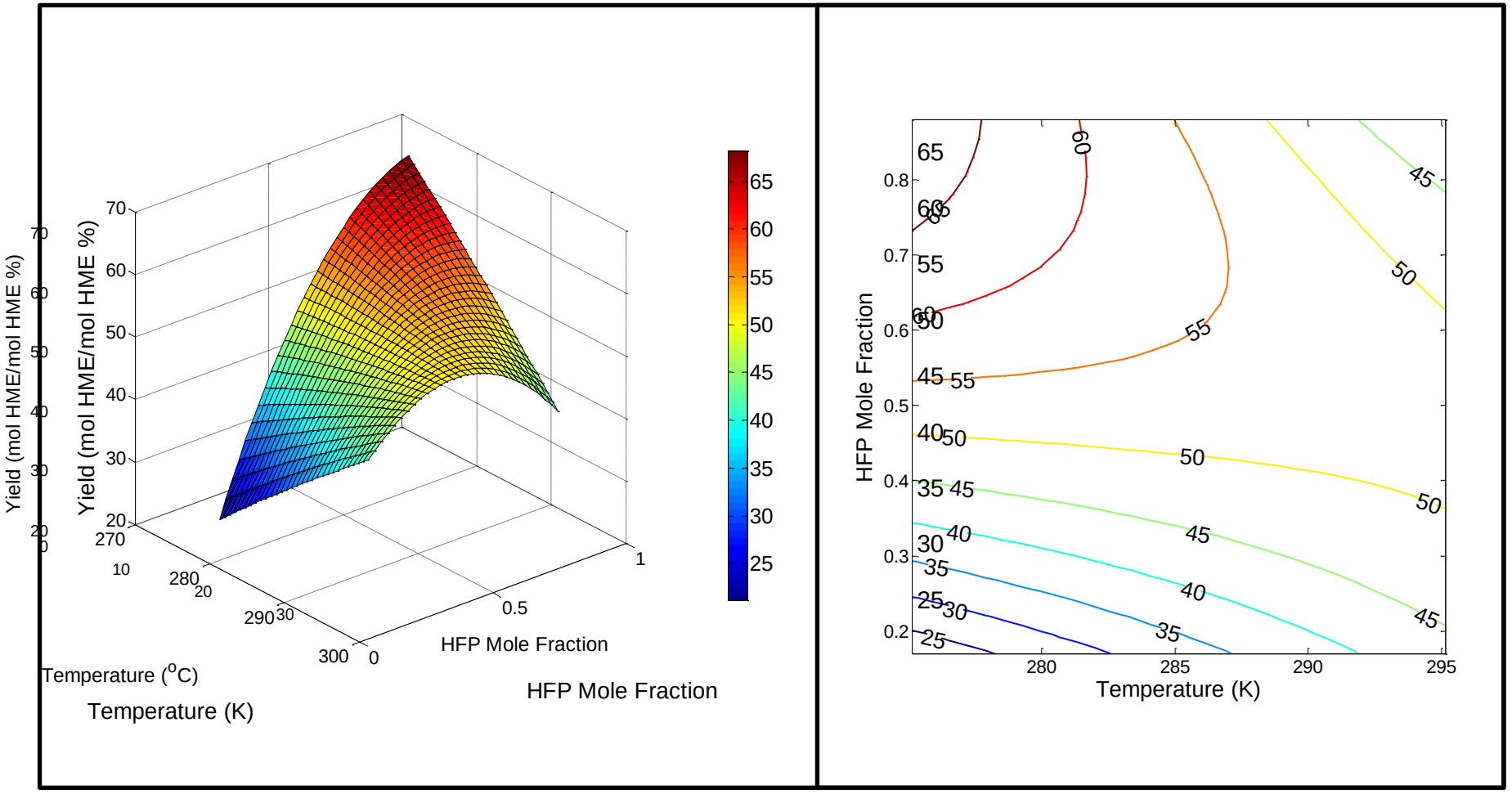

Figure 5.9: Surface and contour plot for HME yield for varying temperature and HFP mole fraction with a constant catalyst concentration of 0.43 mol·dm^{-3} and liquid flowrate of 3 cm^{3}·min^{-1}

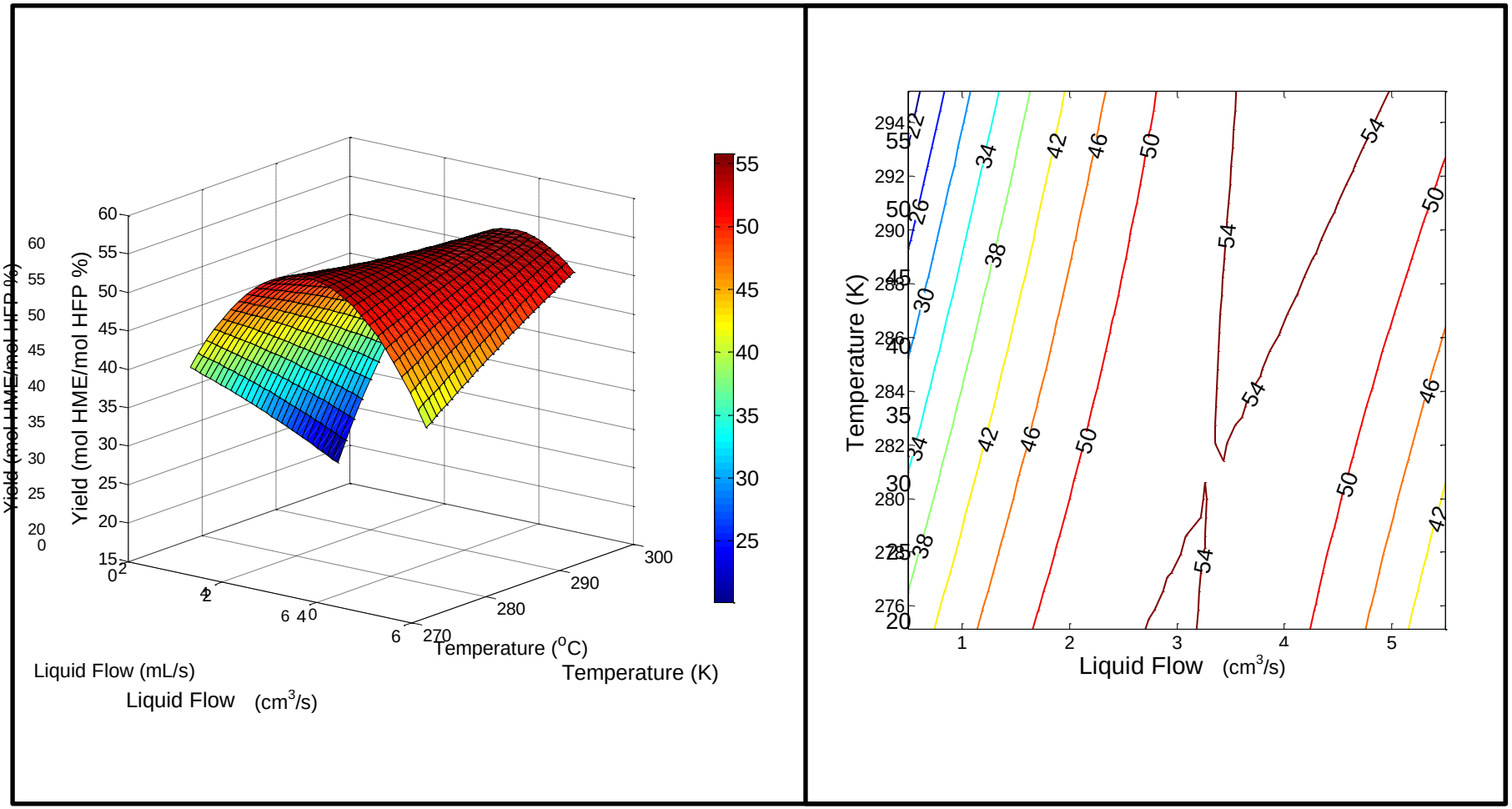

Figure 5.10: Surface and contour plot for HME yield for varying liquid flowrate and temperature with a constant catalyst concentration of 0.43 mol·dm^{-3} and HFP mole fraction of 0.52

5.2.2 Mole fraction of HME

5.2.2.1 Analysis of interactions

Surface response methodology was applied to determine the effect of operating conditions on the mole fraction of HME in the product. As will be shown in Chapter 6, higher exit HME mole fractions are beneficial and enable the use of conventional separation technologies for the isolation of the target compound.

It is important to note that the product from the FFMR contains the synthesized HME, unreacted methanol, unused catalyst and the by-products formed due to side reactions.

Figure 5.11 shows the interaction of the liquid flowrate and temperature with the HFP mole fraction and catalyst concentration held constant at 0.52 and 0.43 $mol \cdot dm^{-3}$, respectively. It can be observed that the highest HME mole fractions are achieved at high temperatures and low liquid flowrates. Due to the lower reaction rates of the side reactions at higher temperatures as explained in the previous section, it is expected that the mole fraction of HME in the product will increase at higher temperatures. The pronounced effect of the liquid flowrate can be observed with high flowrates resulting in the lowest mole fractions of HME. At increased flowrates, a higher amount of methanol with dissolved catalyst was being introduced into the system. Although the yield is higher as seen in the previous section, as a result of increased liquid flow, the increased flow dilutes the synthesized HME in the product.

Figure 5.12 shows the interaction of temperature and HFP mole fraction with the catalyst concentration and liquid flowrate constant at 0.43 $mol \cdot dm^{-3}$ and 3 $cm^3 \cdot min^{-1}$, respectively. The individual effect of the HFP mole fraction is significant in the graphical representation. This is as a result of a greater amount of HFP being available for the formation of HME (i.e. a higher gas phase concentration of HFP in the reaction zone results in an improved driving force for mass transfer and hence a larger amount of HFP in the liquid). The temperature did not have a significant effect in this interaction, however, the trend of a lower mole fraction of HME at lower temperatures can still be observed.

Figure 5.13 represents the interaction of liquid flowrate and HFP mole fraction with temperature and catalyst concentration kept constant at 285.15 K and 0.43 $mol \cdot dm^{-3}$, respectively. The illustration shows good agreement to the theoretical expectations of high HFP mole fractions and

low liquid flowrates as discussed above. Conversely, the lowest mole fractions of HME are observed at high liquid flowrates and low HFP mole fractions.

Figure 5.14 shows the interaction of catalyst concentration and HFP mole fraction with a constant temperature and liquid flowrate at 285.15 K and 3 $cm^3 \cdot min^{-1}$, respectively. The individual effect of the HFP mole fraction is again pronounced in this interaction with the highest mole fractions of HME predicted at the highest HFP mole fractions. Moderate concentrations of catalyst maximise the mole fraction of HME as expected. This is due to the low catalyst concentrations not being sufficient for the HFP and methanol reaction while high catalyst concentrations result in the 'salting out' effect reducing overall conversion of HFP and methanol to HME (Schumpe, 1993).

Figure 5.15 shows the interaction of temperature and catalyst concentration with a constant liquid flowrate and HFP mole fraction at 3 $cm^3 \cdot min^{-1}$ and 0.52, respectively. As seen in the previous interactions, the individual effects of the liquid flowrate and HFP mole fraction were much more pronounced as compared to temperature and catalyst concentration effects. The interaction between the two factors however revealed an optimum at approximately 288.15 K and a concentration of 0.4 $mol.dm^{-3}$.

Figure 5.16 shows the last interaction which is liquid flowrate and catalyst concentration with a constant HFP mole fraction and temperature at 0.52 and 285.15 K, respectively. This illustration again shows good agreement with the above discussed theoretical expectations. The individual effect of the liquid flowrate is much more pronounced than the catalyst concentrations with the high HME mole fractions observed at low liquid flowrates. The highest HME mole fractions were also observed at moderate catalyst concentrations.

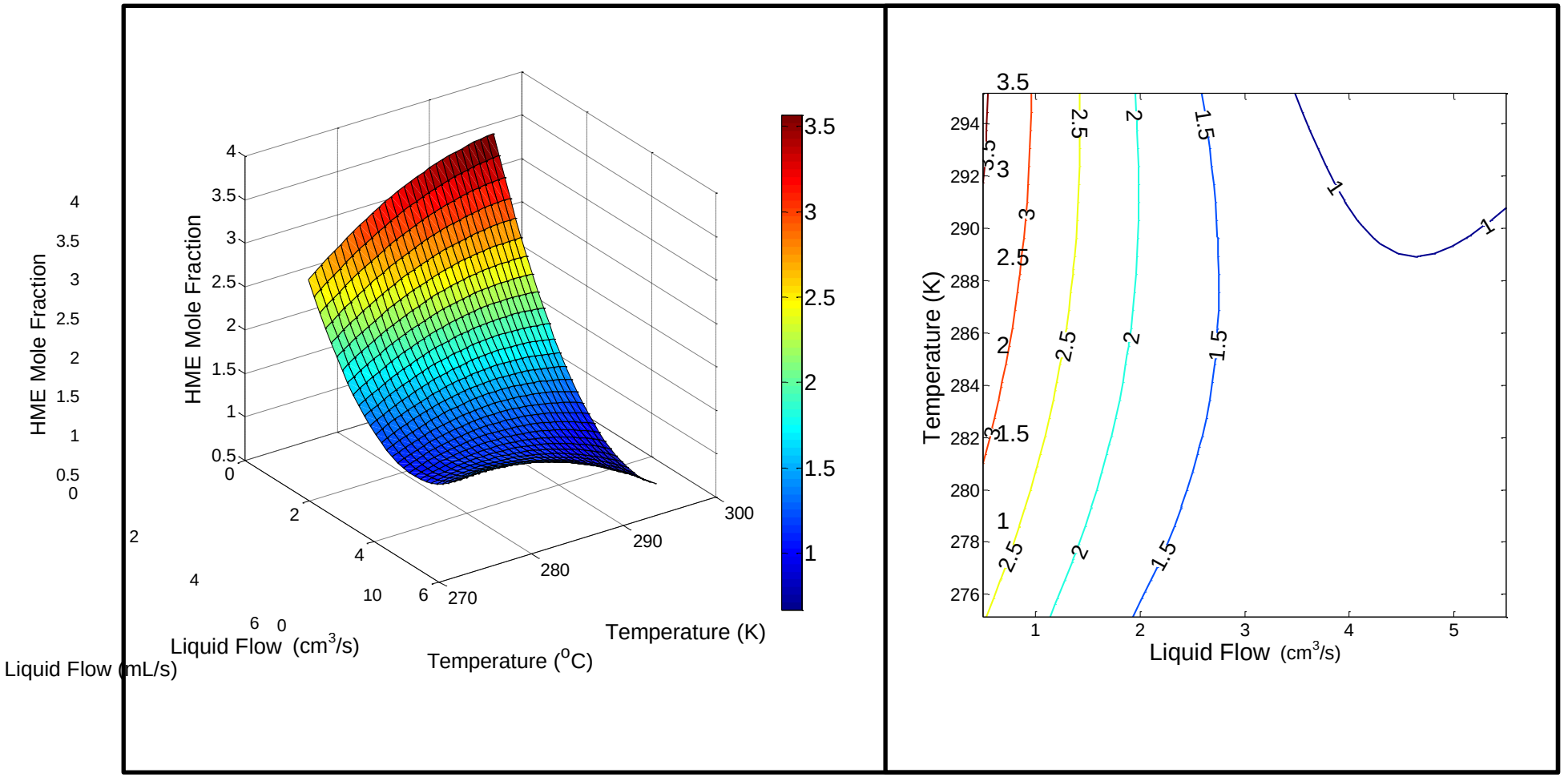

Figure 5.11: Surface and contour plot for HME mole fraction for varying liquid flowrate and temperature with a constant catalyst concentration of 0.43 mol·dm^{-3} and HME mole fraction of 0.52

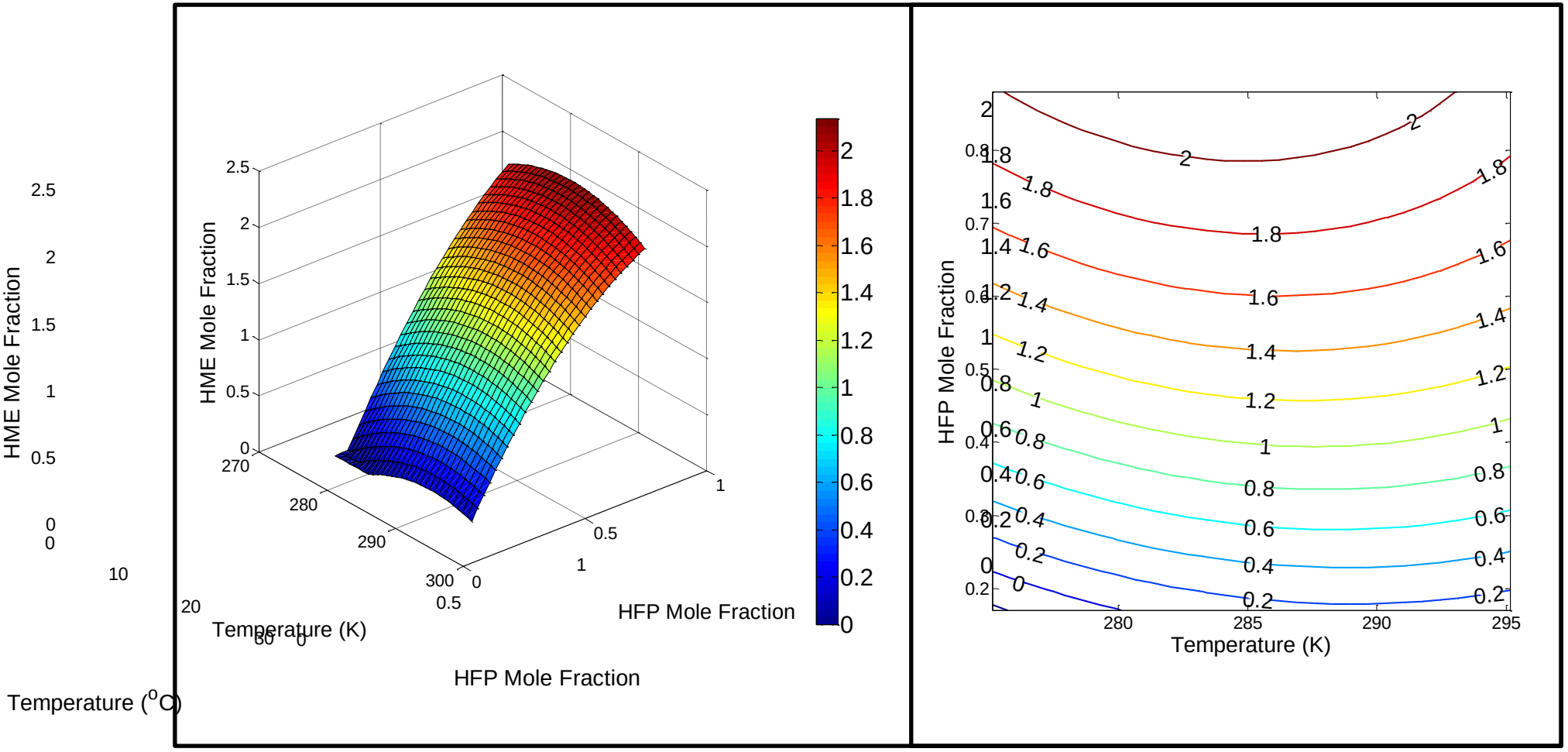

Figure 5.12: Surface and contour plot for HME mole fraction for varying temperature and HFP mole fraction with a constant catalyst concentration of 0.43 mol·dm^{-3} and liquid flowrate of 3 cm^{3}·min^{-1}

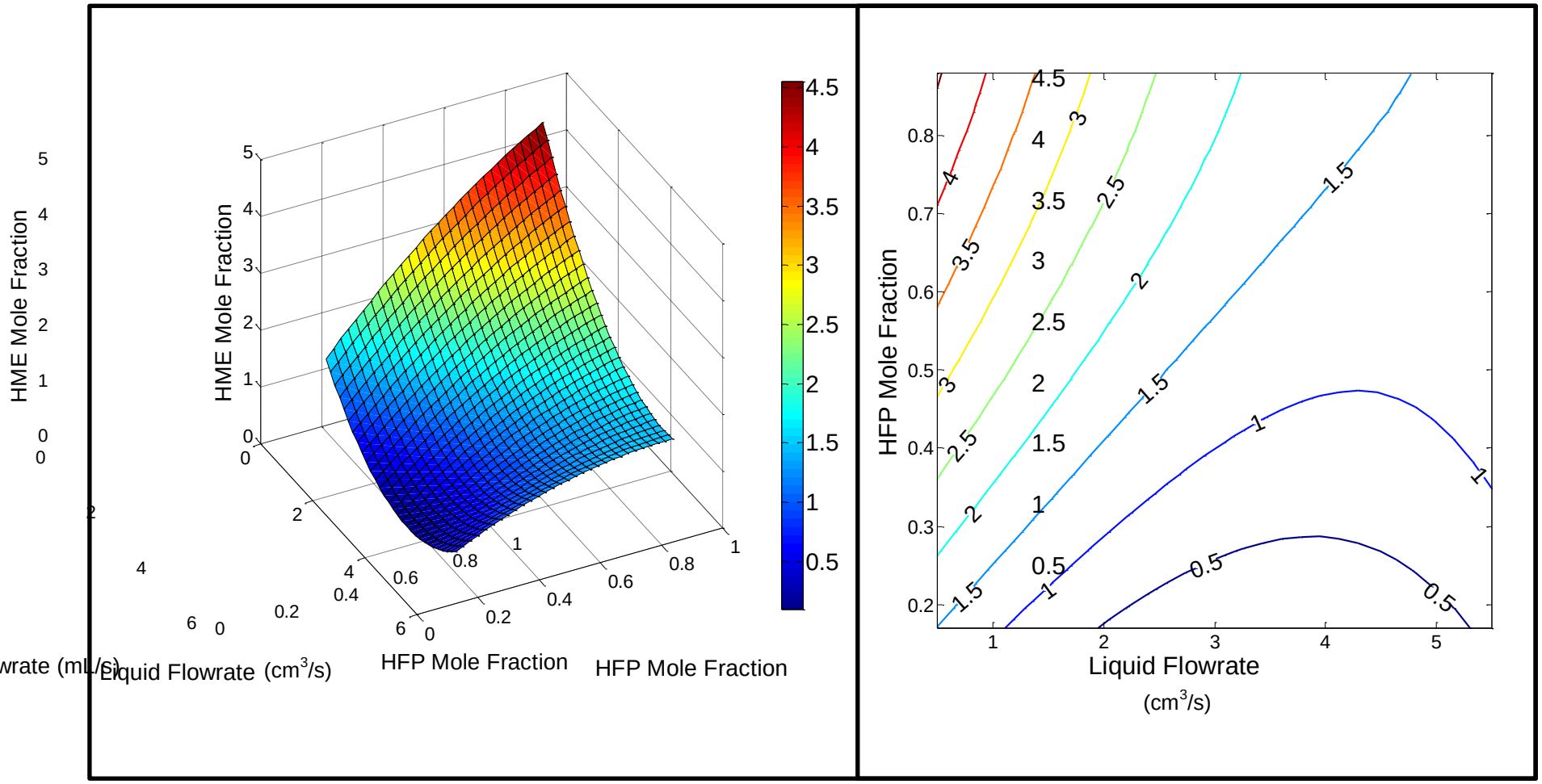

Figure 5.13: Surface and contour plot for HME mole fraction for varying liquid flowrate and HFP mole fraction with a constant temperature of 285.15 K and constant catalyst concentration of 0.43 mol·dm^{-3}

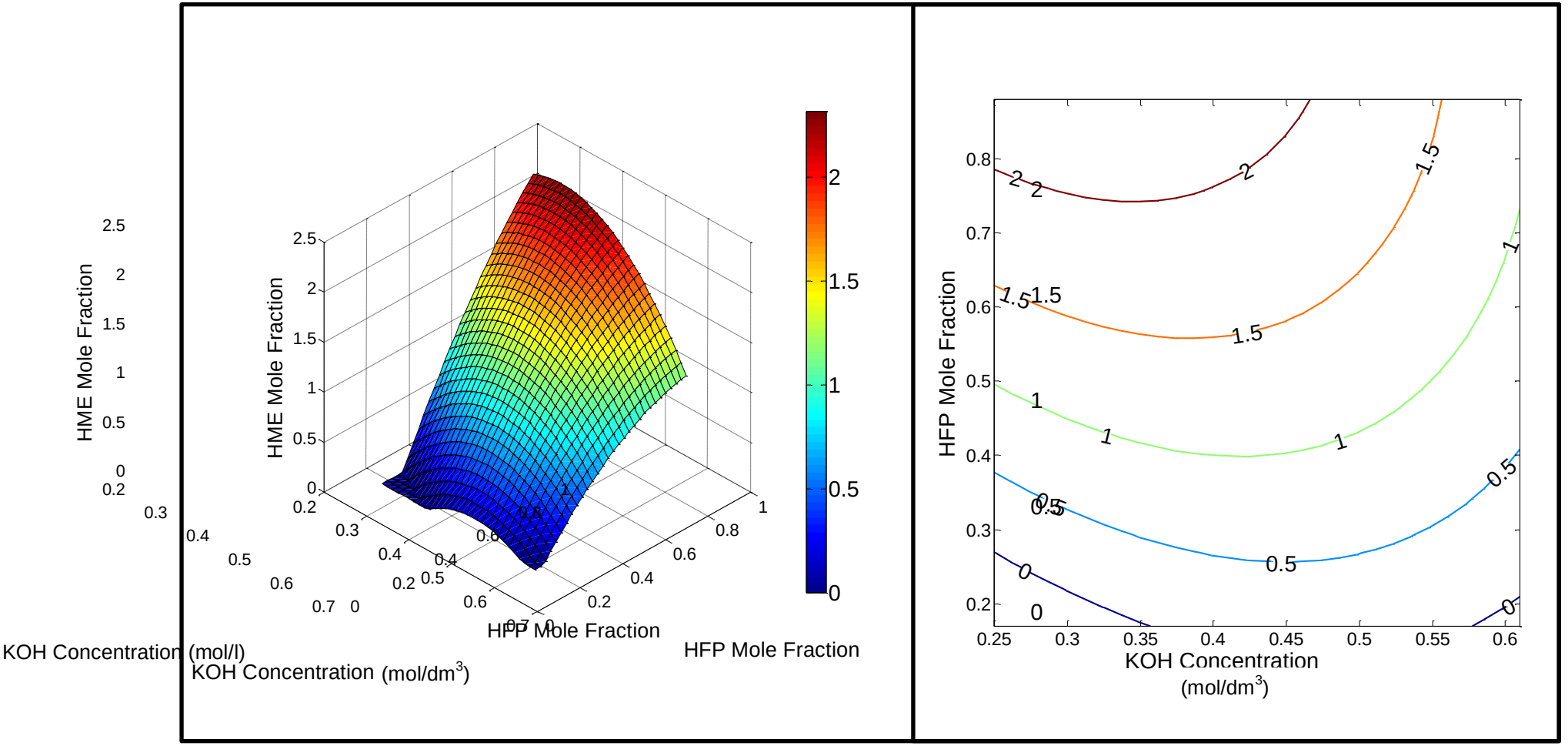

Figure 5.14: Surface and contour plot for HME mole fraction for varying HFP mole fraction and catalyst concentration with a constant temperature of 285.15 K and liquid flowrate of 3 $cm^3 \cdot min^{-1}$

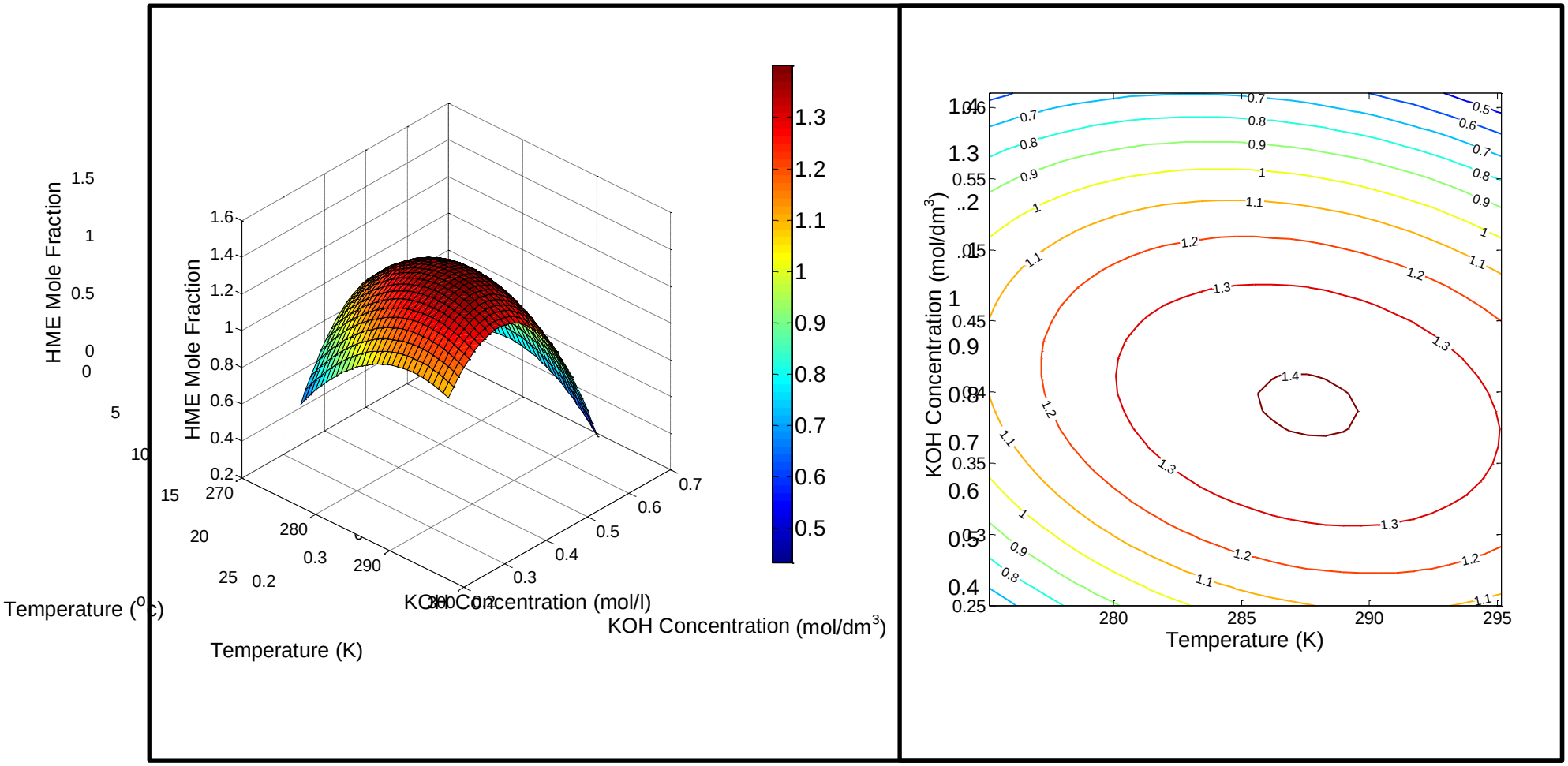

Figure 5.15: Surface and contour plot for HME mole fraction for varying temperature and catalyst concentration with a constant liquid flowrate of 3 $cm^3 \cdot min^{-1}$ and HFP mole fraction of 0.52

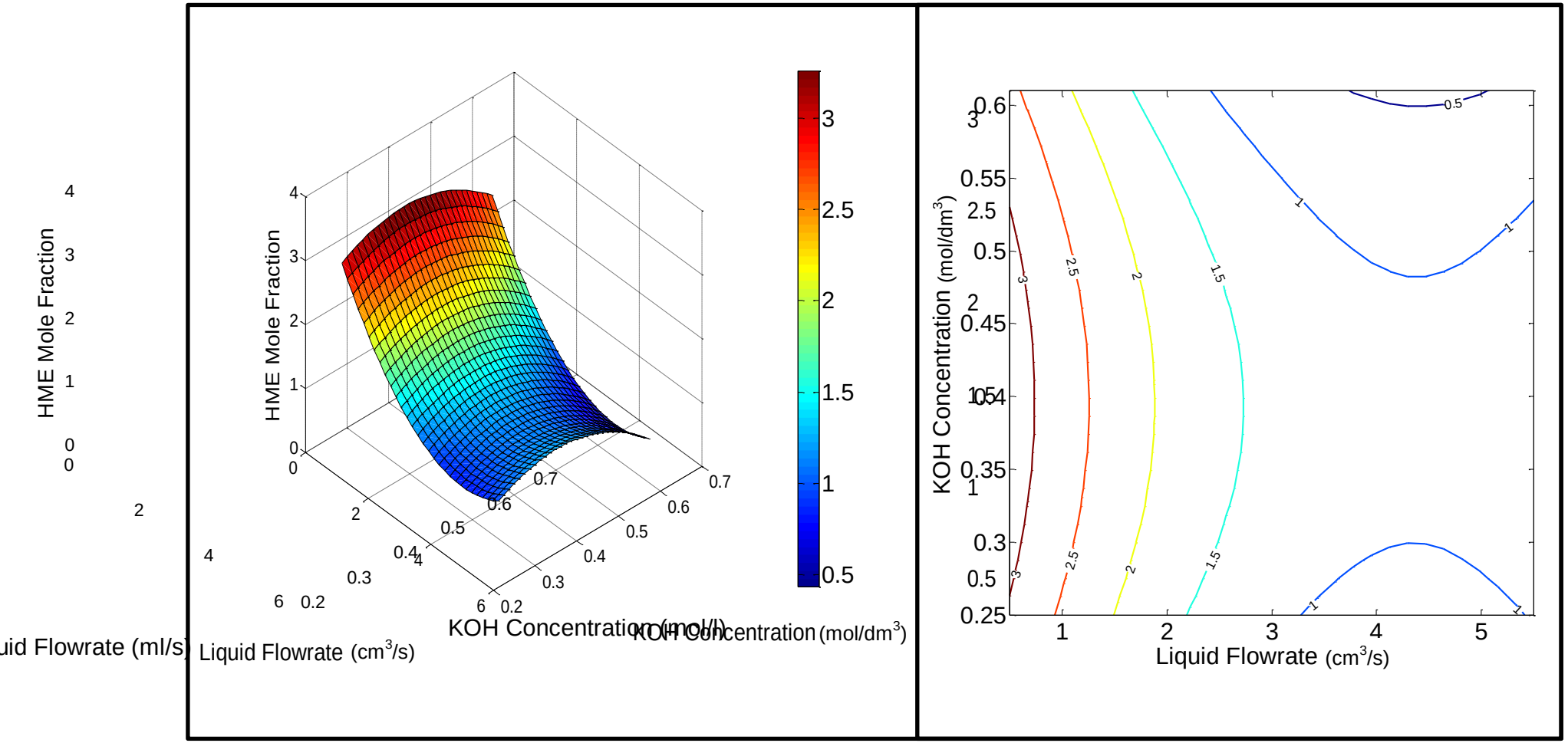

Figure 5.16: Surface and contour plot for HME mole fraction for varying liquid flowrate and catalyst concentration with a constant temperature of 285.15 K and HFP mole fraction of 0.52

5.2.2.2 High liquid residence time tests

As a possible means of further increasing the exit HME mole fraction, the application of increased liquid residence times were investigated. This effect is equivalent to increasing the channel length of the reactor. However, since only a single reactor was available for experimentation, it was decided to carry out these tests using a reactors-in-series approach. In this approach the liquid product from an initial run is used as feed for a subsequent run, which simulates transferral of material to another section of a long reactor channel. The two should be theoretically equivalent provided that the gas phase concentration of HFP remains constant.

As observed in Figure 5.17, the mole fraction increases with a greater number of runs through the reactor and reaches a plateau. This suggests that operating with more than 3 reactors in series (i.e. a reactor with a channel length equal to 3 times the channel length of the experimental reactor) will not be practical as negligible change is observed. The experimental conditions of the centre-point experimental runs were used for this independent test.

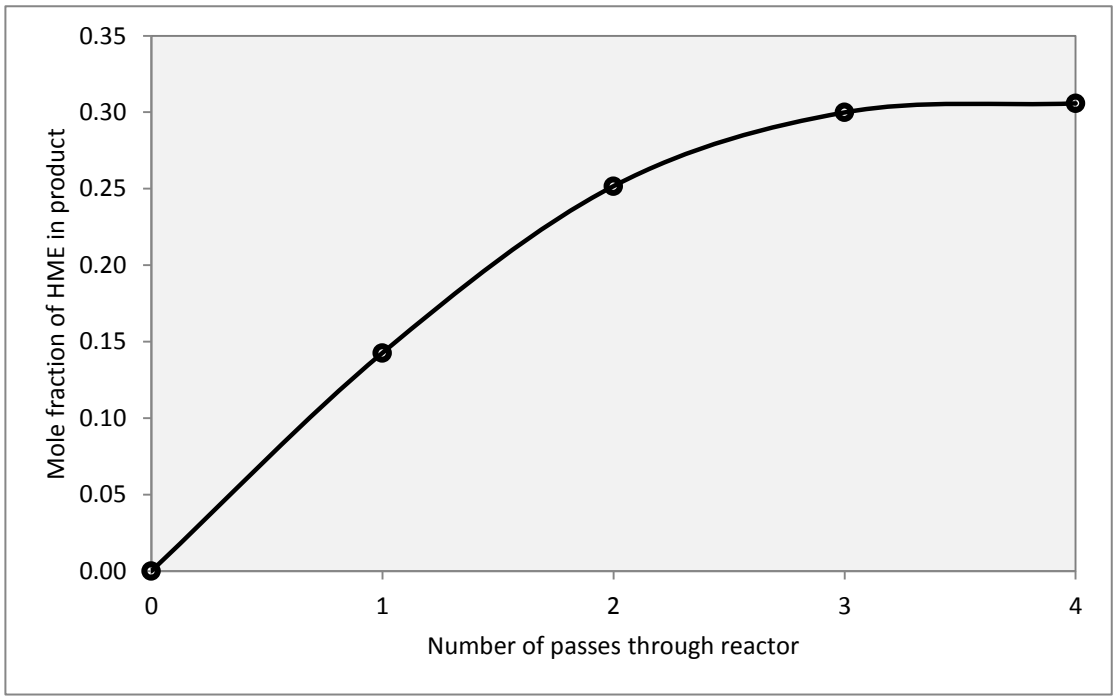

Figure 5.17: The effect of simulated high liquid residence time on the mole fraction of HME in the product

5.3 Statistical analysis

5.3.1 HME yield as the response factor

The reproducibility of the experiment is judged on the response variability of the multiple runs carried out at the centre-point. Six centre point runs were performed which have been tabulated in Table 5.1 (Experimental runs 25-30). The standard deviation between the centre point experimental runs was approximately 6.7%. There exists no outlier in the sample set of centre points and therefore the deviation is high within the inter-quartile range.

Table 5.4: Summary of statistical results obtained from analysis of variance in MatLab™

Statistics	Result
R^2	0.85
R	0.92
F-statistic	6.04
p-value	0.0007
Regression Mean Square	224.87
Residual Mean Square	37.21

The significant results from the generated ANOVA table using MatLab™ including the regression coefficients have been tabulated in Table 5.4. It is desired that the *F*-value generated for the data set is greater than the *F*-value found for the given degrees of freedom and confidence level (Istadi and Amin, 2006). A 95% confidence interval was assumed and the tabulated F-value using degrees of freedom from Appendix A.2, gives $F_{0.05,14,15} = 2.42$ (Dinov, 2013).

The *F*-value of the data set is 6.04 which is greater than 2.42 which indicates a statistically significant regression at a 95% level of confidence. Due to an increased level of control on process parameters on the FFMR as compared to the GLR, a data set of greater statistical relevance resulted from experiments carried out in the FFMR.

The R^2 value shows the total variation of the response variable about its mean. The R^2 value of 0.85 indicates a good agreement between the experimental values and predicted values. This value indicates that 85% of the total variation of the response variable, which is the HME yield, is viable results from the model. The correlation coefficient, R, of 0.92 gives a good correlation between the predicted and experimental values of the response variable (Istadi and Amin, 2006).

The parity plot below graphically shows the correlation between the observed yield and the predicted yield. The model generated a satisfactory prediction.

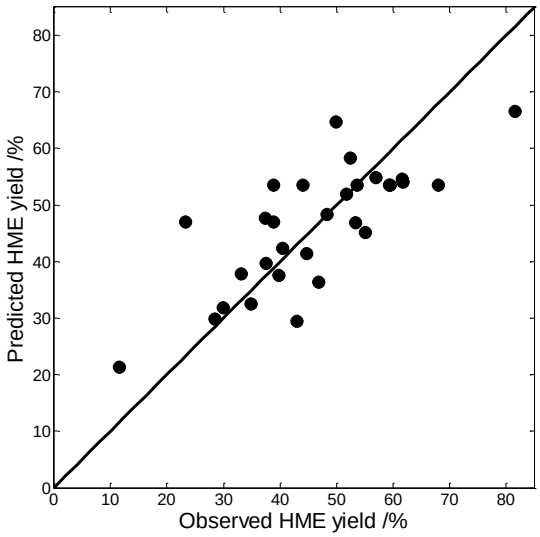

Figure 5.18: Parity plot for the predicted yield and the observed yield

Similar to Chapter 4.3, the response variable prediction, shown in Equation 2.7, requires the regression for the β–coefficients which was performed using MatLab™ and the code is shown in Appendix F. The resultant values for the coefficients with their *t*-value and *p*-value are tabulated below.

Table 5.5: Coefficients obtained via regression and the accompanying statistics

Parameter	Coefficient	Term	Standard Error	*t*-value	*p*-value
β_0	-126.68	intercept	42.20	-3.00	0.01
β_1	95.61	X_1	61.97	1.54	0.14
β_2	265.30	X_2	113.43	2.34	0.03
β_3	5.84	X_3	2.17	2.69	0.02
β_4	28.85	X_4	8.85	3.26	0.01
β_{12}	86.69	X_1X_2	100.22	0.86	0.40
β_{13}	-4.48	X_1X_3	1.71	-2.62	0.02
β_{14}	-3.32	X_1X_4	6.85	-0.48	0.64
β_{23}	-9.69	X_2X_3	3.43	-2.83	0.01
β_{24}	-24.62	X_2X_4	13.86	-1.78	0.10
β_{34}	-0.32	X_3X_4	0.24	-1.31	0.21
β_{11}	-32.78	X_1^2	36.44	-0.90	0.38
β_{22}	-150.02	X_2^2	110.70	-1.36	0.20
β_{33}	0.06	X_3^2	0.05	1.24	0.24
β_{44}	-1.20	X_4^2	0.74	-1.63	0.12

X_1, X_2, X_3 and X_4 represents mole fraction of HFP, catalyst concentration, temperature and liquid feed flowrate as defined in the MatLab™ code in Appendix F. β_1, β_2,β_3 and β_4 are the

coefficients that represent the linear effect of the corresponding factor as shown above. β_{12}, β_{13}, β_{14}, β_{23}, β_{24} and β_{34} show the interaction effect between the factors as defined in the above table. β_{11}, β_{22}, β_{33} and β_{44} are the second order terms which show the quadratic response of the particular factor. The *t*-value and *p*-value assess the significance of the β-coefficients (Istadi and Amin, 2006).

The *p*-value serves as an indication of a coefficients influence on the system. They are indirectly proportional as the lower the *p*-value the greater the effect of that particular factor (Istadi and Amin, 2006).

The most significant effect on the yield was the liquid flowrate at a confidence interval of 99% (*p*-value of 0.01). This pronounced effect can also be observed on the surface contour plots with liquid flowrate as one of the varied factors. The interaction between catalyst concentration and temperature had the same level of significance as the liquid flowrate. The linear term for temperature as well as in the interaction between HFP mole fraction and temperature had a 98% confidence interval (*p*-value of 0.02). The linear term for concentration had a 97% confidence interval (*p*-value of 0.03). These high confidence intervals, or low *p*-values observed, indicate that the levels of the factors investigated can be expanded further however this may not always be practical.

The eigenvalues calculated above indicate the characteristic of the stationary point. If all the eigenvalues are positive, the stationary point predicts an absolute minimum, if all the eigenvalues are negative an absolute maximum results. If the signs differ, the stationary point is a saddle and the absolute optimums lie outside the test range (Istadi and Amin, 2006).

The eigenvalues were calculated for the response variable and the results are listed below. Due to the fact that the eigenvalues have differing signs, the stationary point, as shown in Equation 2.15, will be a saddle. This indicates, as shown with the generally low *p*-values, that the experimental range should be wider to obtain optimum interaction points.

Table 5.6: Eigenvalues based on the regressed coefficients

Eigenvalue	Result
$\boldsymbol{\lambda_1}$	-165.1
$\boldsymbol{\lambda_2}$	-20.6
$\boldsymbol{\lambda_3}$	2.0
$\boldsymbol{\lambda_4}$	-0.2

5.3.2 HME mole fraction as the response factor

Six centre point runs were performed which have been tabulated in Table 5.3 (Experimental runs 25-30) as these are used to assess the reproducibility of the experimental data. The standard deviation between the centre point experimental runs was approximately 0.24%. Outliers exist in the data set and are the mole fractions of HME less than 0.6% and in excess of 2%.

Table 5.7: Summary of statistical results obtained from analysis of variance in MatLab™

Statistics	Result
R^2	0.82
R	0.91
F-statistic	4.96
p-value	0.002
Regression Mean Square	1.11
Residual Mean Square	0.22

An ANOVA table was generated and the relevant results tabulated in Table 5.7. It is desirable if the *F*-value calculated is greater than the tabulated value of the *F*-value (Istadi and Amin, 2006). A 95% confidence interval was assumed for this dataset and, the tabulated *F*-value, using degrees of freedom from Appendix A.2, gives $F_{0.05,14,15} = 2.42$ (Dinov, 2013).

The distributed *F*-value was determined from Appendix D. The ANOVA table generated yielded an *F*-value of 4.96. This is greater than 2.42 which indicates that the results of the quadratic predicting the response variable is sufficiently satisfactory with a confidence interval of 95%.

The total variation of the HME mole fraction about its mean is assessed by the R^2 value. The R^2 value of 0.82 indicates a good agreement between the experimental values and predicted values. This value indicates that 82% of the total variation of HME mole fraction is viable results from the model. The correlation coefficient, R, of 0.91 gives a good correlation between the predicted and experimental values of the response variable (Istadi and Amin, 2006).

The parity plot in Figure 5.19 shows the correlation between the predicted and observed HME mole fractions.

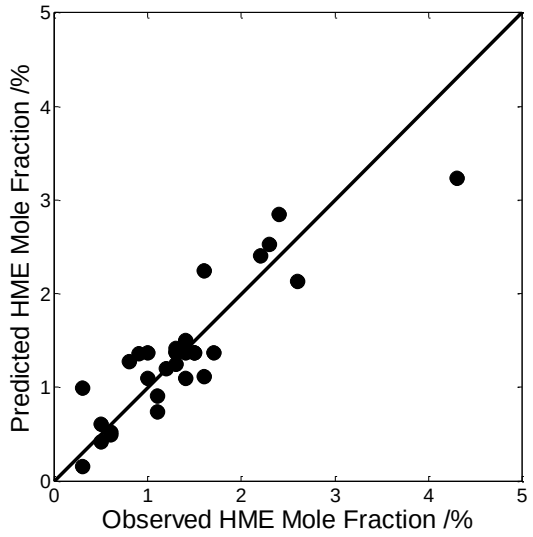

Figure 5.19: Parity plot for the predicted HME mole fraction and the observed HME mole fraction

In order to generate a model to predict the HME mole fraction, shown in Equation 2.7, regression for the β–coefficients is required which was done using MatLab™ and the code shown in Appendix F. The resultant values for the coefficients with their *t*-value and *p*-value have been tabulated below. The standard error on the values regressed for is also shown.

Table 5.8: Coefficients obtained via regression and the accompanying statistics

Parameter	Coefficient	Term	Standard Error	*t*-value	*p*-value
β_0	-4.31	intercept	3.28	-1.32	0.21
β_1	9.53	X_1	4.82	1.98	0.07
β_2	15.50	X_2	8.81	1.76	0.10
β_3	0.16	X_3	0.17	0.94	0.36
β_4	-0.70	X_4	0.69	-1.01	0.33
β_{12}	-6.02	X_1X_2	7.79	-0.77	0.45
β_{13}	-0.03	X_1X_3	0.13	-0.21	0.83
β_{14}	-0.61	X_1X_4	0.53	-1.15	0.27
β_{23}	-0.09	X_2X_3	0.27	-0.33	0.74
β_{24}	-0.04	X_2X_4	1.08	-0.04	0.97
β_{34}	-0.02	X_3X_4	0.02	-0.95	0.36
β_{11}	-1.88	X_1^2	2.83	-0.66	0.52
β_{22}	-14.21	X_2^2	8.60	-1.65	0.12
β_{33}	-0.002	X_3^2	0.004	-0.53	0.60
β_{44}	0.14	X_4^2	1.52	-1.53	0.15

X_1, X_2, X_3 and X_4 represents mole fraction of HFP, catalyst concentration, temperature and liquid feed flowrate as defined in the MatLab™ code in Appendix F. β_1, β_2,β_3 and β_4 are the coefficients that represent the linear effect of the independent variables. β_{12}, β_{13}, β_{14}, β_{23}, β_{24} and β_{34} show the interaction effect between the factors as defined in Table 5.8. β_{11}, β_{22}, β_{33} and β_{44} are the second order terms which show the quadratic response of the particular factor. The *t*-value and *p*-value assess the significance of the β-coefficients (Istadi and Amin, 2006).

The quadratic term for the liquid flowrate had the most significant effect on the HME mole fraction at a level of confidence of 97% (*p*-value of 0.03). The next most significant factor was the linear term for HFP mole fraction in the feed at a level of confidence of 93% (*p*-value of 0.07). The catalyst concentration was at a confidence level of significance of 90% (*p*-value if 0.1). The mole fraction of HME showed an overall tendency to have a trivial response to the temperature variations which can be explained by the temperature affecting the rate of side reactions of which there is insignificant yields as compared to the formation of HME which is elaborated upon in section 5.2.1.

The eigenvalues were calculated for the HME mole fraction prediction and the results are listed below. Due to the fact that the eigenvalues have different signs, the stationary point, as shown in Equation 2.15, will be a saddle.

Table 5.9: Eigenvalues based on the regressed coefficients

Eigenvalue	Result
$\boldsymbol{\lambda_1}$	-14.9
$\boldsymbol{\lambda_2}$	-1.25
$\boldsymbol{\lambda_3}$	0.20
$\boldsymbol{\lambda_4}$	-0.002

6

CHAPTER SIX

6. DESIGN OF THE RECOVERY AND PURIFICATION SECTION OF THE PROPOSED PROCESS

Thus far the operation of the reactor has been discussed. In order to achieve a high purity of the target compound, the reactor effluent will need to be separated and the HME purified to a marketable composition (>98 mol%) (Pagliaro, 2014). The sections below will elaborate on the removal of salt and any by-products formed in the reaction from the effluent as well as the extraction and recovery of excess methanol and purification of HME.

6.1 Salt recovery evaporator

The liquid effluent from the FFMR is pumped to a Salt Recovery Evaporator (SRE). The SRE is a steam-heated tubular evaporator with the process fluid entering the shell of the heat exchanger and the steam allocated to the tubes.

The steam will be used to boil the liquid to a temperature of approximately 348.15 K. This will vapourise HME and methanol, which is the majority of the liquid, as their boiling-points are 327.15 K and 338.15 K, respectively. The higher boiling components will therefore concentrate at the bottom of the evaporator. These higher boiling components are the two by-products from the reaction methyl 2,3,3,3 – tetrafluoropropionate (TFP) and (E)-1,2,3,3,3-pentafluoro-1-methoxy-prop-1-ene (PMP). The boiling point of TFP is 368.15 K. No experimental boiling point for PMP could be found in the available literature, however, by virtue of increased carbon-fluorine bonds as compared to TFP, it is assumed that it's boiling point is in excess of 368.15 K. Determining the magnitude of the boiling point will add minimal value in this particular circumstance. The moles of PMP formed are a factor of 100 times less than HME and insignificant in comparison to the amount of methanol in the reactor effluent, and therefore the PMP will have negligible effect on the system. Due to these low concentration of the heavy boiling components, it can be assumed there will be minimal carry-over. This allows such evaporation to be used as opposed to

conventional multicomponent separation techniques such as distillation. It was assumed that there will be negligible multicomponent interactions due to the low concentrations of the heavy boiling components. The main function of this unit is to recover the KOH and allow methanol and HME to pass through for further processing downstream.

The purge rate or blowdown required with a feed load designed to produce 250 $kg \cdot month^{-1}$ of HME is 3 $kg \cdot day^{-1}$. To maintain the overall mass balance in the system, the feed of fresh methoxide make-up may be increased. At the prescribed blowdown and inlet liquid flow, no precipitation of solid is expected and the dissolved salts will be removed in the purge. The salt will concentrate on be removed through this purge.

The duty on the SRE will be approximately 260 W with a LP steam utility requirement of 0.4 $kg \cdot hr^{-1}$. The evaporator will be equipped with a mesh screen to prevent entrainment of salt in the exiting vapour stream.

6.2 Liquid-liquid extraction

The vapour stream from the SRE is to be condensed and its temperature reduced to approximately 298.15 K. The condensed and cooled stream then enters a mixer and a subsequent settler where it is contacted with water at the same temperature. The extract from this train will contain the water and the majority of the methanol entering the unit, whereas the raffinate will contain the bulk of the HME and any residual methanol. The extract will then be fed to the Methanol Recovery Unit (MRU) and the raffinate to the HME Purification Unit (HPU). The operations of these units are discussed in section 6.3.

The extraction unit is a pivotal component of the process as the HME mole fraction needs to be concentrated to above 61 mol % due to the presence of an azeotrope in the HME-methanol system. This is discussed further in section 6.3.2.

There are no liquid-liquid equilibrium data available at present for the system investigated and therefore no design calculations could be performed on an extraction unit. However, simple laboratory experiments were conducted using product mixtures obtained from the FFMR in order to prove that such a unit was capable of concentrating the HME sufficiently for downstream processing.

As aforementioned, there is no available liquid-liquid equilibrium data available for the HME and methanol system. Laboratory experiments were performed to prove the viability of the liquid-liquid extraction process shown below. The scale-up of the laboratory experiments, which made use of a separating funnel which contained an agitated solution of HME, methanol and water as discussed in section 3.3.1.3, can be realised by a mixer and settler. The mixer will provide the sufficient agitation for the mixture and the settler will allow for the two liquid phases to separate. The design of the settler is discussed at the end of this section. The same HME purity level can be achieved on an industrial scale if the ratio of the fresh water to methanol and HME is maintained at 3:1 as in the laboratory tests. According to Cussler. (2001), the scale-up of an extraction process is straightforward as long as the ratio of the amount of solvent and the amount of feed is kept constant as has been proposed shown in Equation 6.1.

The extent of extraction (E) is defined below where m is the constant partition coefficient, L is the amount of solvent and H is the amount of feed. Since the partition coefficient is constant, keeping the ratio of solvent to feed constant results in the same extent of extraction during scale-up (Cussler, 2001).

$$E = \frac{mL}{H} \tag{6.1}$$

Figure 6.1 shows the HME mole fraction after a single wash for different initial HME mole fractions in the reactor effluent. It was observed that the higher the initial HME mole fraction, the higher the HME mole fraction after a single wash. This is beneficial is achieving the required composition to overcome the azeotrope at 61 mol% as mentioned.

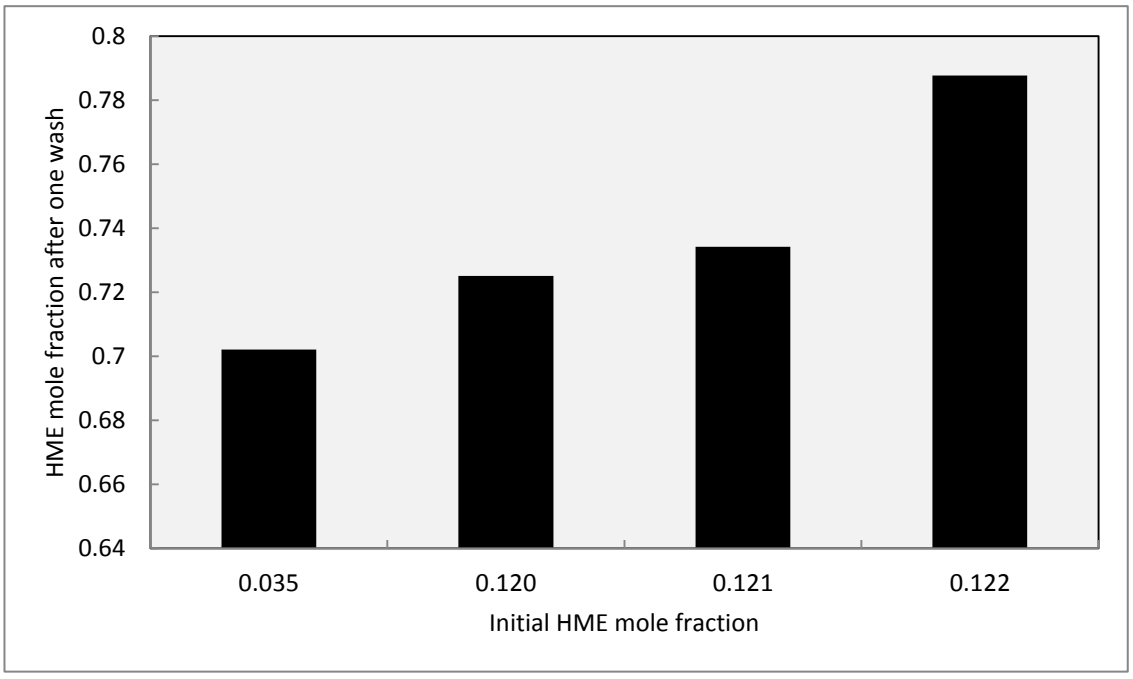

Figure 6.1: Effect of the initial HME mole fraction on the HME mole fraction after one wash

A further study was performed, on two independent samples, whereby multiple washes were done on the same sample with the results represented in Figure 6.2. As can be observed there is no further increase in the HME mole fraction after the initial wash. This served as a guideline for the proposed operation of a single mixer and settler in the process as opposed to a train of mixer-settlers.

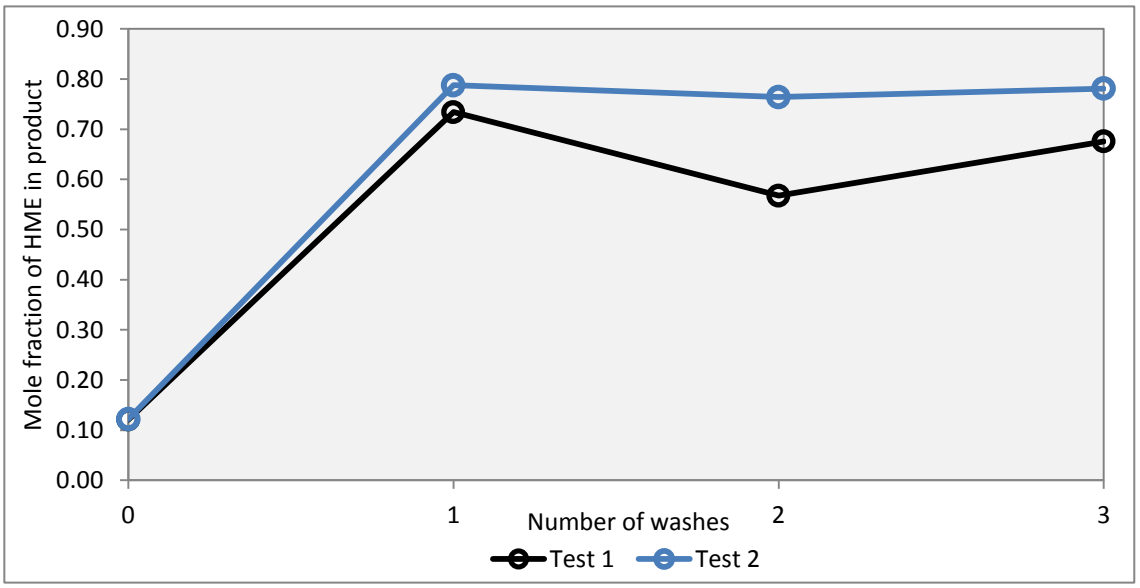

Figure 6.2: Independent tests to assess the effect of multiple washes on the HME mole fraction

A general design for the settler was performed to assess the size of the units that will be required. Settlers are often used in industry to separate liquid mixtures with differing densities which is the same principle by which the HME was separated from the methanol and water solution in the laboratory scale experiments (Sinnott, 2005).

The flowrate of methanol, HME and water are 183 kg·day^{-1}, 8.5 kg·day^{-1} and 577 kg·day^{-1}. These flowrates were calculated from the distillation design, discussed in the next section, to produce 250 kg·month^{-1} of HME. The ratio of the water to methanol and HME is 3:1 as in the laboratory experiments.

Initially, a droplet size of 150 μm was assumed, as recommended in literature, and using Equation 2.27, the dispersed phase settling velocity was calculated to be 0.02 m.s^{-1}. However, according to literature, a settling velocity of 4x10^{-3} m·s^{-1} is assumed if a greater velocity is calculated (Sinnott, 2005).

Using Equation 2.25, the interfacial area can be calculated and subsequently, with Equation 2.23, the diameter of the vessel required was calculated to be 0.3 m. The height of the cylindrical unit is recommended as twice the diameter resulting in a value of 0.6 m. A cylindrical vessel is recommended due to the relatively low flow rates in the system (Sinnott, 2005). The final check is the size of the HME droplets may be entrained in the methanol and water droplets that move to the top of the unit. Using Equation 2.27, a droplet size of 140 μm was calculated which less than the 150 μm, as is recommended, and therefore no entrainment is expected (Sinnott, 2005).

6.3 Methanol recovery and HME purification units

The property method chosen for both the methanol-water system and HME-methanol system for the simulation was NTRL-RK. This property method accounts for highly non-ideal systems which improves the viability of the simulation results. Although an alternative option, such as the Wilson model is effective for polar and non-polar systems, NRTL is derived from this model and is therefore more effective than Wilson. The NRTL activity coefficients accounts for liquid phase non-ideality while the Redlich-Kwong extension accounts for vapour phase deviations from ideality. The property method also contains binary interaction parameters. In the HME-methanol system, VLE data was generated using ASOG and inputted to Aspen™. The binary interaction parameters are then regressed for in Aspen for the NTRL-RK property method. NRTL-RK is also recommended for polar, non-electrolytic systems that are operated below 10 bar (Smith, Van Ness and Abbott, 2005).

6.3.1 Methanol recovery unit (MRU)

The extract containing methanol and water is separated in a conventional distillation column. There is a large excess of methanol in the system, and therefore, from an economic point of view, it is important to recover and recycle methanol. On a mole basis, the methanol is approximately 21 times in excess as compared to the amount of HME being produced.

The MRU was designed on Aspen™ which allowed for the general specifications of a column to be analysed. A DSWTU simulation was first performed to yield initial estimates of the number of stages in the column, feed stage location and the reflux ratio to be used in the more rigorous RadFrac simulation. Using the expected separation in the liquid-liquid extraction process, based on the laboratory experiments discussed in the previous section, the flow to the MRU is approximately 757 $kg \cdot day^{-1}$ containing approximately 25 wt% methanol and 75 wt% water. Methanol was selected as the light key and water as the heavy key for the required separation.

HME has a lower boiling point than methanol and therefore classified as the lighter than light key. A recommended value of 1.5 was used for the reflux ratio in the DSTWU simulation and the recovery of the heavy and light keys set to 99% (Seader and Henley, 1998)

The RadFrac simulation, using the initial estimates from the DSWTU simulation, was manually adjusted such that the desired recovery of methanol from the water was achieved. However, these are not necessarily the most efficient combination of the variables and therefore, using sensitivity analysis, the specified variables were optimised.

To optimize the relationship between the number of stages in the column and reflux ratio, a sensitivity plot was generated with number of stages varied as the independent variable and reflux ratio varied as a parametric variable with methanol purity being the dependent variable shown in Figure 6.3. The number of stages selected was 16 (15 trays) and the reflux ratio was 2, which is agreement with a common heuristic value of 2.5, resulting in a methanol purity of approximately 99% which also translates to a methanol recovery of approximately 99% (Seader and Henley, 1998). The results showed negligible HME in the bottoms stream with a water purity in excess of 99%. The HME in the distillate with methanol is recycled to the beginning of the process.

The feed stage was optimised by considering the column composition profile and was found to be at tray 11. If the composition profile was not smooth, it indicated that the feed stage is disrupting the equilibrium of the system which is inefficient hence the feed stage location was adjusted such that a smooth composition profile for the system can be realised. The composition profile for the main components in the separation, methanol and water, is shown in Figure 6.4. There is no horizontal profile in the plot indicative of no excess trays being selected for the design.

The column is designed to operate at atmospheric pressure of 1 bar and a feed temperature of 293.15 K. The bubble and dew point temperatures are 372.15 K and 337.15 K, respectively. The reboiler has a duty of 8.6 kW with a boil-up ratio of 1.06. The condenser has a duty of 7 kW. The approximate height of the unit, using a tray spacing of 0.2 m is 3.5 m (Seader and Henley, 1998).

An empirical correlation for stage efficiency, which is a function of viscosity, was used to determine an efficiency profile over the column. This allows a more realistic specification of the column to be determined as the non-idealities of practical application was considered (Seader and Henley, 2011).

It is desired that the downcomer area and plate spacing are designed such that the level of the liquid and froth in the downcomer is significantly below the outlet of the weir on the tray above (i.e. half the distance of the sum of the plate spacing and weir height). The column will flood if the back-up of liquid in the downcomer rises above the outlet of the weir. The calculated downcomer back-up was 0.11 m which is sufficiently below the maximum allowable height of 0.125 m (Sinnott, 2005).

The calculated vapour velocity through the tray holes was 5.13 $m \cdot s^{-1}$ which was greater than the minimum design vapour velocity was 4.86 $m \cdot s^{-1}$ which is indicative of no weeping expected to occur (Sinnott, 2005).

The upper limit of the flooding velocity was 2.9 $m \cdot s^{-1}$ which is in excess of the calculated velocity through the column if 2.47 $m \cdot s^{-1}$ as required as velocities in excess of the flooding velocity will not allow the liquid to fall down the column subsequently flooding the trays (Sinnott, 2005).

The recommended upper limit of fractional entrainment is 0.1 as the effect on column efficiency is negligible in this region. The calculated value for fractional entrainment for the designed column was 0.09 as required (Seader and Henley, 1998).

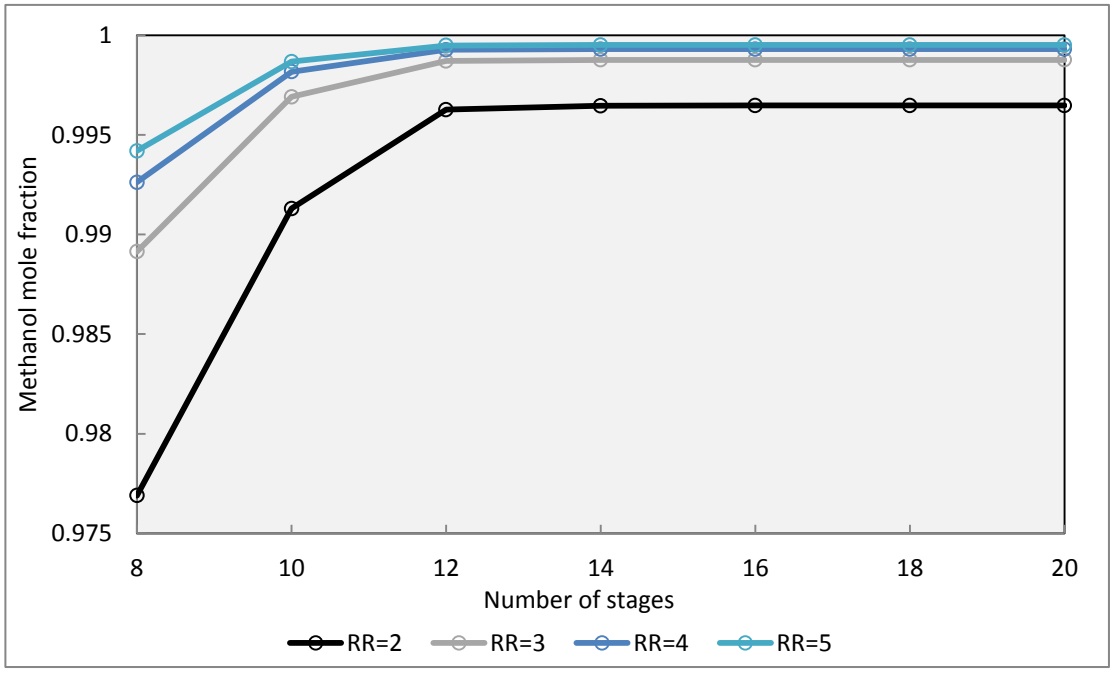

Figure 6.3: Parametric plot showing the different methanol mole fractions resulting from different combinations of reflux ratio and number of stages

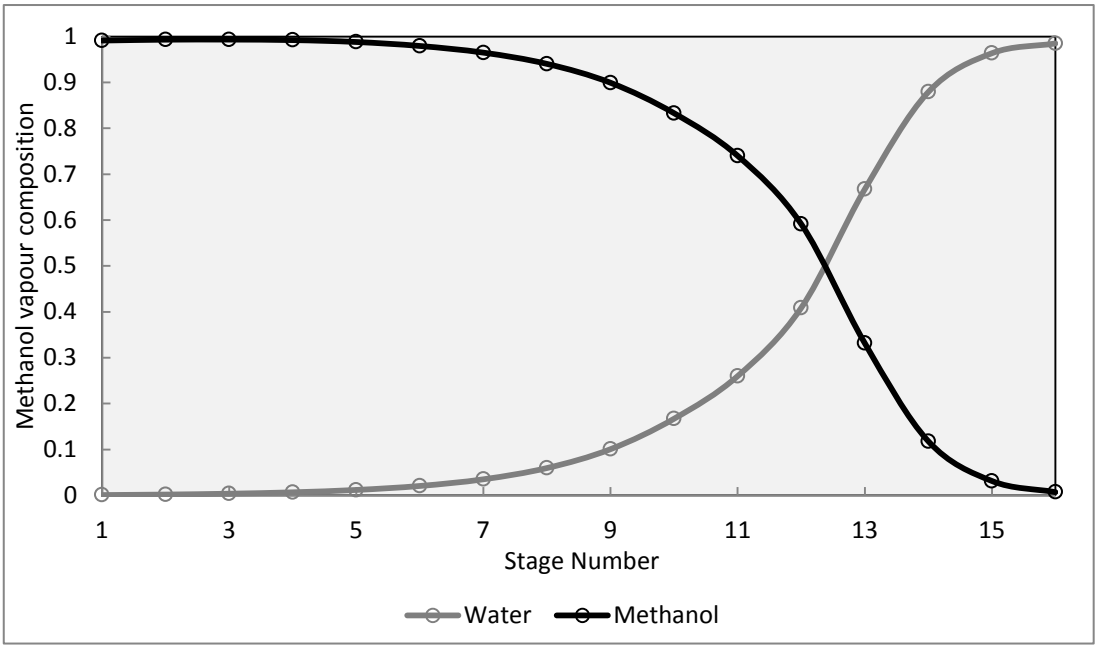

Figure 6.4: Vapour composition profile in the MRU

VAPOUR-LIQUID CONTACTING COLUMN

Equipment name		Methanol Recovery Unit (MRU)
Maximum diameter		0.4 m
Column height		3.5 m
PROCESS DATA AND PROPERTIES		
Stage (total/feed)	15/11	-
Total feed flow	31.5	kg/h
Feed quality	1.00	-
Distillate flow	8	kg/h
Bottoms flow	23.5	kg/h
Boil-up ratio	0.7	-
Operating temperature (top/feed/bottom)	336.85/293.15/360.65	K
Pressure (top/bottom)	1/1.09	bar
Vapour density (column average)	1.12	kg/m^3
Vapour dynamic viscosity (column average)	0.013	mPa.s
Liquid density (column average)	840	kg/m^3
Liquid dynamic viscosity (column average)	0.3	mPa.s
Liquid surface tension (column average)	0.35	N/m
Pressure drop across column	0.09	bar
CONSTRUCTION AND MATERIALS		
Shell and tray material	Carbon Steel	-
Shell diameter	0.4	m
Shell length	10.5	m
Shell thickness	6	mm
Design temperature	383.15	K
Design pressure	1.1	bar
Pipe branch diameter (top/bottom/feed)	10/10/10	mm
Tray type	Sieve	-
Number of trays	15	-
Hole size	2	mm
Hole area/active area	10	-
Tray spacing	200	mm
Weir length	320	mm
Weir height	50	mm
Pressure drop per plate	0.006	bar
Flooding velocity	2.9	m/s
Actual velocity	2.47	m/s
Downcomer area fraction	0.05	-
Downcomer velocity	0.003	m/s
Column area	0.13	m^2
Ψ (fractional entrainment)	0.09	-
Max vapour velocity through hole	5.13	m/s

6.3.2 HME purification unit (HPU)

To make the process feasible, the target compound needs to be at a marketable composition in excess of 98% according to John Hogg, a sales executive at Apollo Scientific Ltd in the United Kingdom. Apollo is one of the few companies that produce HME albeit on a small scale using a batch process (Hogg, J, 2014, 27 May, John.Hogg@apolloscientific.co.uk)

One of the difficulties of the development of this process is the lack of information with regards to the HME and methanol system. From communication with the suppliers of HME globally and from a general research undertaken, there appears to be no vapour-liquid equilibrium (VLE) data defining this system.

According to the international suppliers as well as research by Il'in, (2004) as mentioned, fractional distillation is used to increase HME composition and therefore, on a larger scale, it appears practical to use a conventional distillation column for this application, however, with no VLE data, the column cannot be designed.

From the fractional distillation conducted, it was found that the temperature did not exceed 319.15 K. In the absence of VLE data, the observation was difficult to quantify. Analytic Solution of groups (ASOG) was employed in order to generate VLE data. ASOG is a group contribution method based on the Wilson equation that represents the group activity coefficient for a system. In order to generate VLE data, the method divides the respective molecules into their functional groups and uses defined group pair interaction parameters to generate the predicted VLE. UNIFAC uses a similar approach however the group pair interaction parameter for the carbon-fluorine bond is not defined. As a result, Aspen™, which uses UNIFAC, could not generate VLE data. ASOG also considers the temperature dependence of the parameters resulting in a greater accuracy in the predicted VLE.

Figure 6.5 and 6.6 shows the x-y and T-x-y graphs generated respectively for the HME-methanol system. Figure 6.6 shows a minimum boiling azeotrope in the system at approximately 318.15 K which is in agreement to the experimental observation mentioned above.

The important finding from the curves generated is the presence of the azeotrope in the system at approximately 61 mol%. This places emphasis on achieving a high mole fraction of HME out the reactor as well as the importance of the extraction unit which removes methanol from the feed increasing the mole fraction of HME.

The VLE data generated using ASOG was inputted to Aspen™. The binary interaction parameters for the NRTL-RK equation of state were then calculated in Aspen™ for the generated VLE data. This allows are more realistic simulation to be realised. A near perfect separation can be achieved as long as the feed to the HPU is above 61 mol% HME.

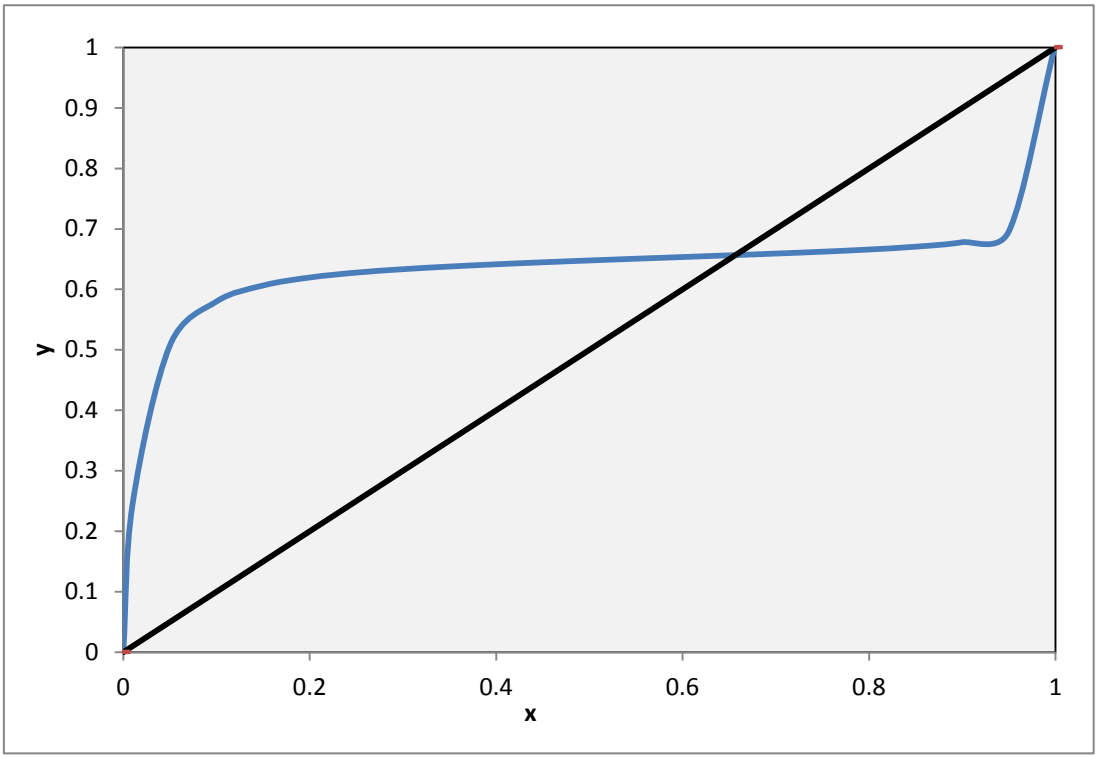

Figure 6.5: x-y plot for the methanol-HME system using HME as the composition basis

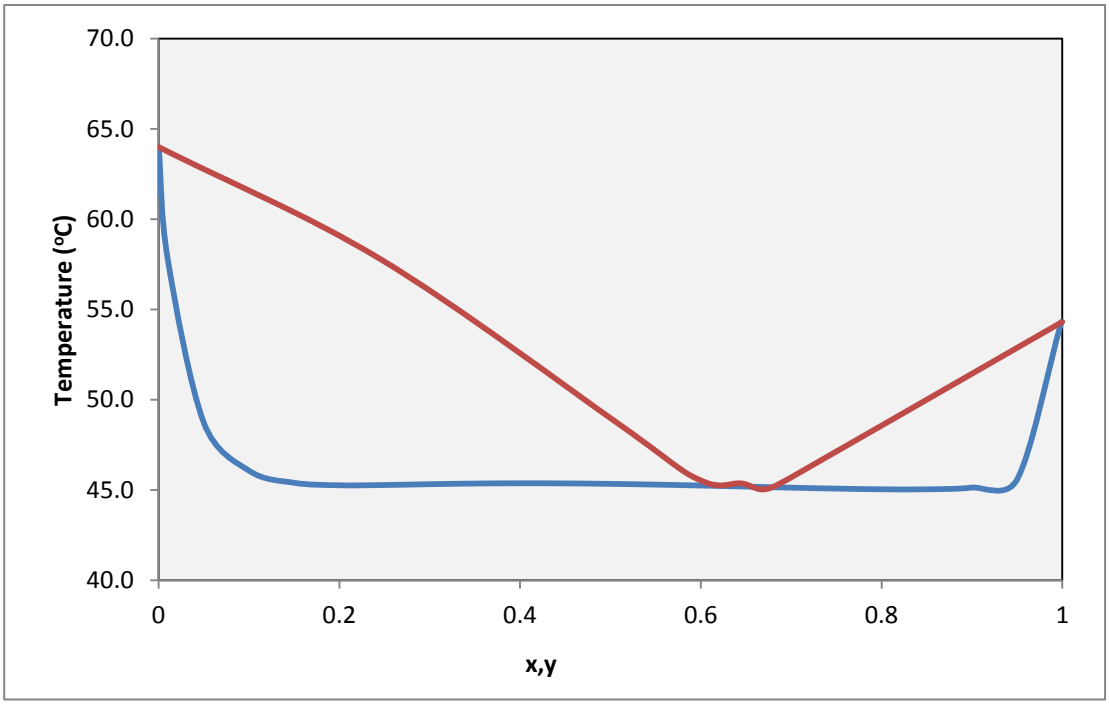

Figure 6.6: T-x-y plot for the HME methanol system using HME as the composition basis

The general specifications of the design of the HPU were acquired from an Aspen™ simulation. A DSTWU simulation used a recommended reflux ratio of 2.5 and a 99% recovery of HME in the distillate and 99% methanol in the bottoms to yield initial estimates for number of stages, reflux ratio and feed stage location for the more rigorous RadFrac design (Seader and Henley, 1998).

The results from the liquid-liquid extraction laboratory experiments discussed in the previous section served as a basis to determine the flowrates to the distillation columns. The flow of methanol and HME to the HPU is approximately 13 $kg \cdot day^{-1}$ with a prudent assumption of 0.65 mol% HME present.

The specifications mentioned above were manually adjusted to give the desired marketable purity of HME of 98 mol%. This does not represent the optimised design, and therefore, a sensitivity analysis was performed on the specifications to allow to most efficient combination of these factors to be determined.

Figure 6.7 represents a sensitivity plot investigating the combined effect of the reflux ratio and number of stages on the purity of HME in the distillate. As observed, the most efficient combination appears to be 16 stages (15 trays) and a reflux ratio of 5 which yields a purity in excess of 98 mol%. There is a high recovery of HME in the distillate of approximately 99% with negligible HME in the bottoms stream.

The optimum feed stage location was at tray 9. This allowed a smooth composition profile to be established in the column. The column may not operate efficiently if the composition profile is not smooth. There is no horizontal profile in the plot indicative of no excess trays being selected for the design. Figure 6.8 shows the composition profile for this unit (Seader and Henley, 1998).

The column was designed to operate at atmospheric pressure and an inlet feed temperature of 293.15 K. The duties on the condenser and reboiler are relatively low at 225 W and 230 W, respectively. The bubble and dew point temperatures were 336.15 K and 326.15 K, respectively. The approximate height of the HPU assuming a tray spacing of 0.2 m is 3.5 m (Seader and Henley, 1998).

As with the design of the MRU, an efficiency profile was generated to allow a more realistic design to be realised.

It is desired that the downcomer back-up height is significantly lower than the top of the weir on the tray above. If this height is exceeded, the column will begin to flood resulting in an inefficient separation. It is recommended that the downcomer back-up height is less than half the sum of the tray spacing, 0.2 m, and weir height, 50 mm, which is 0.125 m. This condition was met with the calculated value of the downcomer back-up of 0.1 m being below 0.125 m (Sinnott, 2005).

In order to prevent weeping in the column the calculated vapour velocity should be greater than the minimum design velocity. No weeping is expected to occur in the HRU with the vapour velocity of 2 $m \cdot s^{-1}$ being greater than the minimum requirement of 1.86 $m \cdot s^{-1}$ (Sinnott, 2005).

The upper limit of the flooding velocity was calculated as 1.23 $m \cdot s^{-1}$. This was greater than the calculated velocity through the HRU of 1.05 $m \cdot s^{-1}$ which indicated flooding of the trays is not expected to occur (Sinnott, 2005).

In order to prevent a reduction in column efficiency, it is recommended that the upper limit of the fractional entrainment be 0.1. A fractional entrainment of 0.02 was calculated indicative of a negligible influence on the column efficiency is expected (Sinnott, 2005).

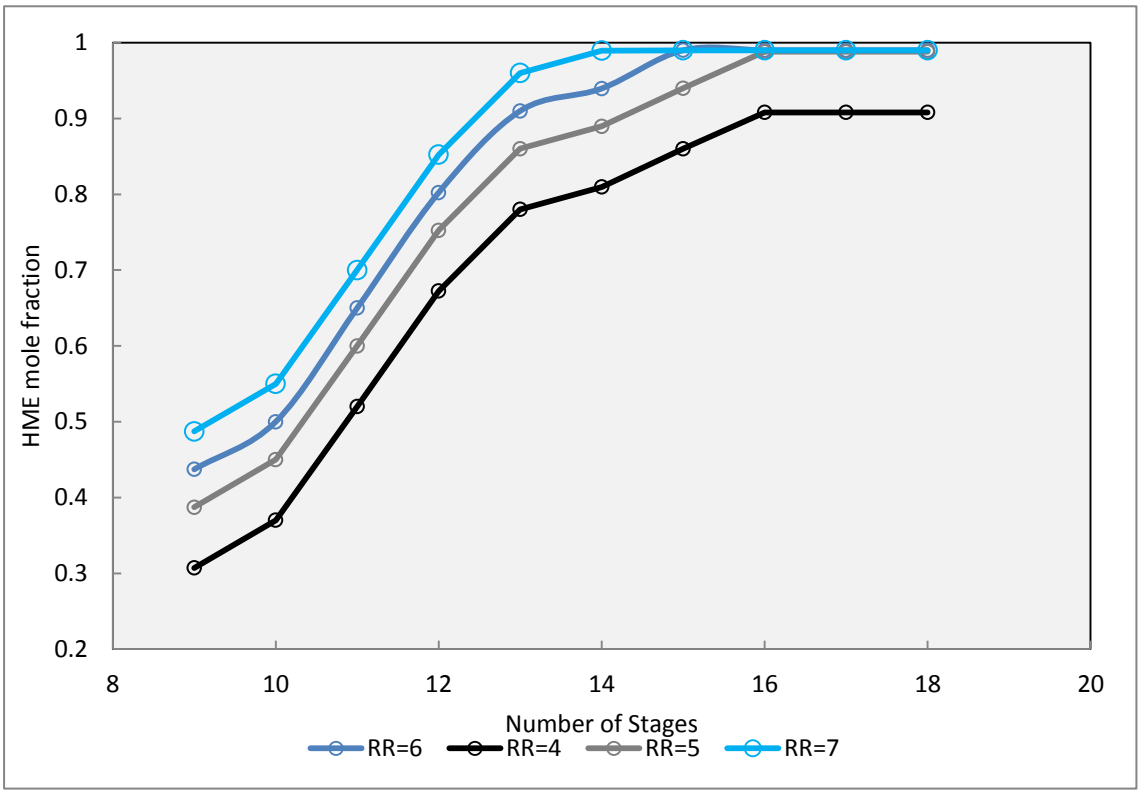

Figure 6.7: Parametric plot showing the different HME mole fractions resulting from different combinations of reflux ratio and number of stages

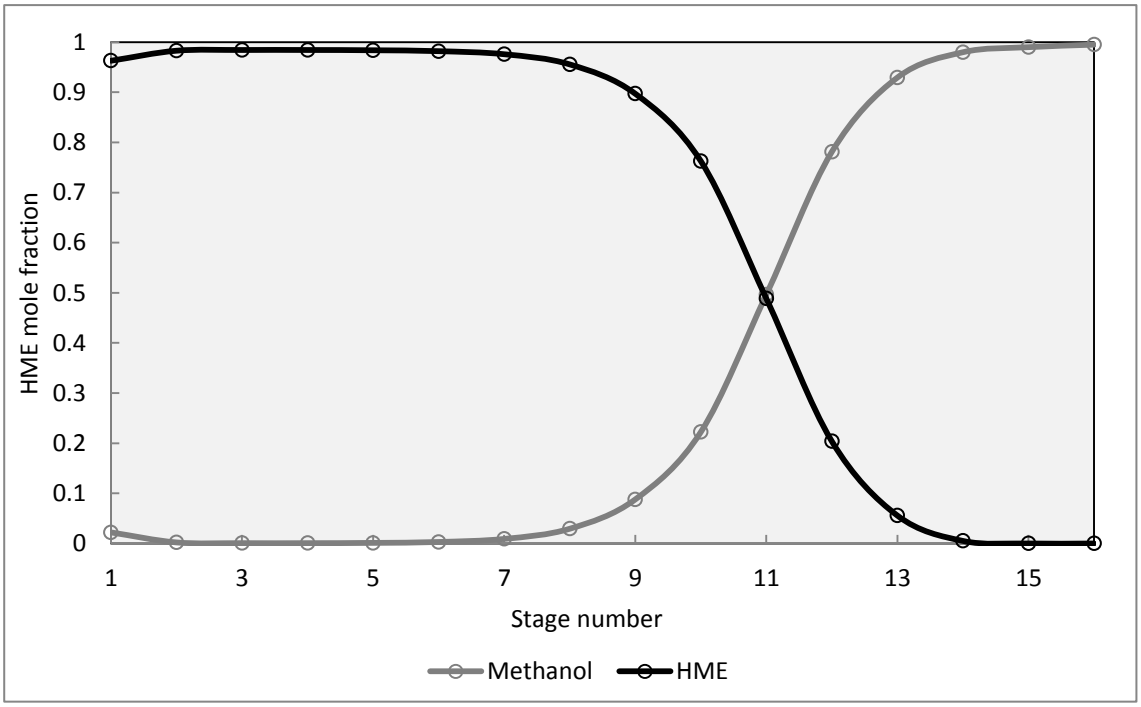

Figure 6.8: Vapour composition profile in the HPU

VAPOUR-LIQUID CONTACTING COLUMN

Equipment name		HME Purification Unit (HPU)
Maximum diameter		0.3 m
Column height		3.5 m
PROCESS DATA AND PROPERTIES		
Stage (total/feed)	15/10	-
Total feed flow	13	kg/day
Feed quality	1.00	-
Distillate flow	8.3	kg/day
Bottoms flow	4.7	kg/day
Boil-up ratio	2.78	-
Operating temperature (top/feed/bottom)	323.15/293.15/337.15	K
Pressure (top/bottom)	1/1.08	bar
Vapour density (column average)	6.3	kg/m^3
Vapour dynamic viscosity (column average)	0.01	mPa.s
Liquid density (column average)	1050	kg/m^3
Liquid dynamic viscosity (column average)	0.3	mPa.s
Liquid surface tension (column average)	0.016	N/m
Pressure drop across column	0.08	bar
CONSTRUCTION AND MATERIALS		
Shell and tray material	Carbon Steel	-
Shell diameter	0.3	m
Shell length	10.5	m
Shell thickness	6	mm
Design temperature	343.15	K
Design pressure	1.1	bar
Pipe branch diameter (top/bottom/feed)	6/6/6	mm
Tray type	Sieve	-
Number of trays	15	-
Hole size	2	mm
Hole area/active area	15	-
Tray spacing	200	mm
Weir length	300	mm
Weir height	50	mm
Pressure drop per plate	0.005	bar
Flooding velocity	1.23	m/s
Actual velocity	1.05	m/s
Downcomer area fraction	0.08	-
Downcomer velocity	0.0012	m/s
Column area	0.07	m^2
Ψ (fractional entrainment)	0.02	-
Max vapour velocity through hole	2	m/s

6.4 Mass Balance

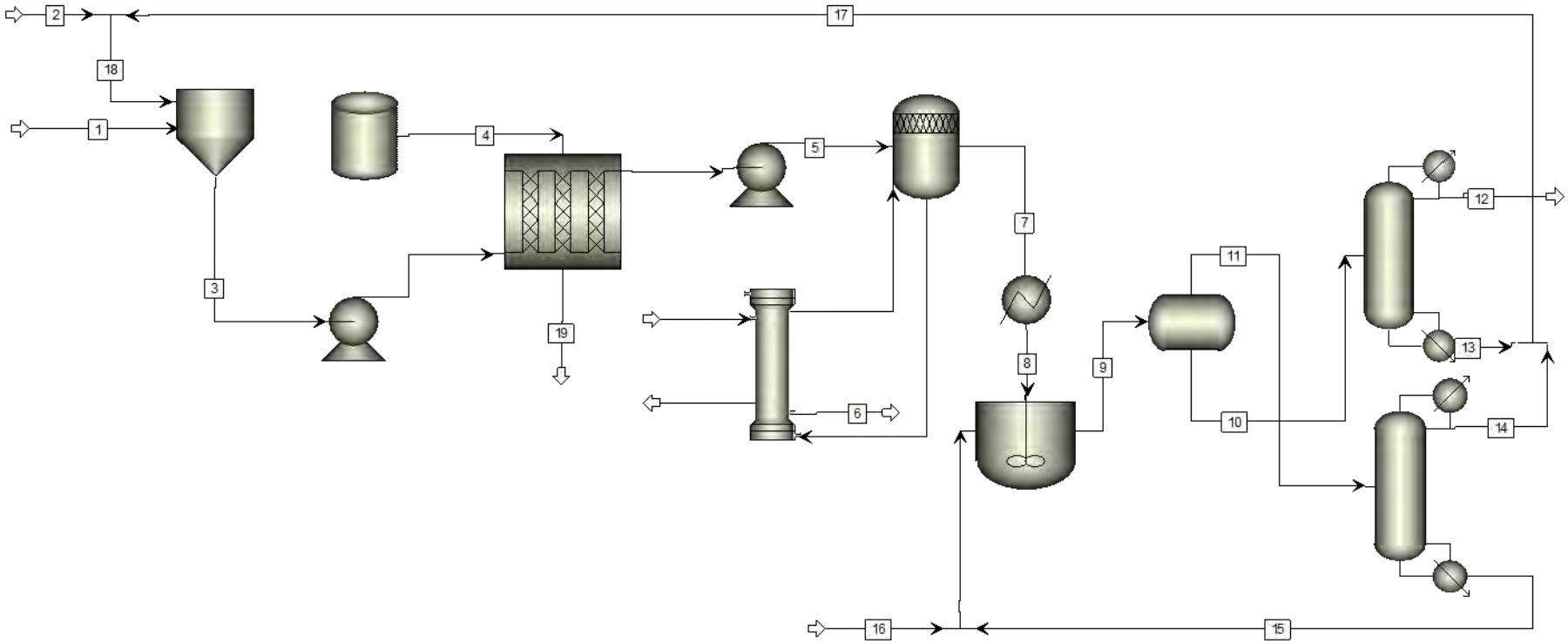

Figure 6.9: Schematic of proposed process with accompanying stream numbers

Table 6.1: Mass balance information for the proposed process

	1	2	3	4	5	6	7	8	9
Mass flow, kg·day^{-1}									
HME	0	0	0.1	0	8.2	0	8.2	8.2	8.3
Methanol	0	4.81	183	0	183	0	183	183	183
Water	0	0	1.78	0	2	2	0	0	577
PMP	0	0	0	0	0.19	0.19	0	0	0
TME	0	0	0	0	0.7	0.7	0	0	0
KOH	0.19	0	0.19	0	0.08	0.08	0	0	0
HFP	0	0	0	100	0	0	0	0	0
Total Flow, kg·day^{-1}	0.19	4.81	188	100	194	2.97	191.20	191.20	768.33
Total Flow, mol·day^{-1}	3.25	150	5914	549	5882	118	5764	0	37821
Temperature, K	298.15	298.15	298.15	298.15	298.15	348.15	348.15	298.15	298.15

Table 6.2: Mass balance information for the proposed process continued

	10	11	12	13	14	15	16	17	18	19
Mass flow, kg·day^{-1}										
HME	8.3	0	8.2	0.1	0	0	0	0.1	0.1	0
Methanol	4.78	178	0.083	4.7	176	1.79	0	181	186	0
Water	0	577	0	0	1.78	575.22	2	1.78	1.78	0
PMP	0	0	0	0	0	0	0	0	0	0
TME	0	0	0	0	0	0	0	0	0	0
KOH	0	0	0	0	0	0	0	0	0	0
HFP	0	0	0	0	0	0	0	0	0	4.253
Total flow, kg·day^{-1}	13.08	755.25	8.28	4.80	178.24	577.01	2.00	183.04	187.85	4.25
Total flow, mol·day^{-1}	195	37626	47.6	147	5613	32013	111	5761	5911	23
Temperature, °C	298.15	298.15	323.15	337.15	336.15	360.15	278.15	360.15	298.15	298.15

6.5 Proposed process and instrumentation to control critical parameters

In order to run the proposed design optimally, process control is proposed based on the critical parameters of the design. Figure 6.10 illustrates the process control and instrumentation diagram with the philosophy of control elaborated in this section.

6.5.1 Feed system

There are flow indicators (FI101 and FI102) on the KOH flow and combined fresh and recycled methanol flow, respectively. The flow control valves both receive the desired set-point of 5 $kg \cdot day^{-1}$ and 187.85 $kg \cdot day^{-1}$ from a ratio controller to ensure that the desired catalyst concentration is achieved before being fed to the FFMR. The amount of fresh methanol added is dependent on the amount being recycled to maintain a constant flow of 183 $kg \cdot day^{-1}$ when running at design feed rates of 188 $kg \cdot day^{-1}$. There is also a flow indicator (FI104) on the HFP flow to the reactor.

It is critical to the operability of the FFMR that the microchannels do not flood. Therefore, there is a level control that will reduce the feed flow of methanol with dissolved catalyst and HFP proportionally.

6.5.2 Reactor Section

There is a withdrawal pump on the outlet of the FFMR. There are pressure indicators on the suction and discharge of the pump to ensure that the required NPSH is available and that the discharge flowrate is high enough to prevent liquid accumulation in the reactor channels under normal operation.

6.5.3 Salt recovery unit

The vapour-liquid separation drum has level control to prevent liquid carry-over or entrainment such that no dissolved salts are migrated in the system which could cause downstream scaling. The level controller (LI 105) gives a set-point to the flow controller (FI 120) on the outlet of the unit. This will increase the valve opening at increased liquid levels in the vessel and decrease valve opening at lower liquid levels. There is also level control on the salt recovery evaporator. Increased levels in the heat exchanger will facilitate liquid entrainment and carryover which will flood the vapour-liquid separation drum. The level in this heat exchanger should be controlled by

manipulation of the flow of utility used for heating (steam has been recommended). This control indirectly controls the level in the vapour-liquid separation drum as manipulation of FC120 will influence the level in the heat exchanger.

There is a temperature indicator on the line leaving the SRU to monitor if the desired vapour temperature is being achieved to allow boil off HME and methanol. The second temperature reading is to ensure that the temperature after the heat exchanger is below saturation temperature of both components as there should be a pure liquid feed to the LLE section of the process.

6.5.4 Liquid-liquid extraction

There is feedback control proposed on the separation tank to maintain a desired level. This is achieved but control on the flow of the HME and methanol mixture and combined water stream to the unit. The flows will be controlled based on the desired ratio of the feeds of 4:1 (proportion of water to combined feed of HME and methanol) as per design. There is similar level control on the decanter which controls the flow from the separation vessel. Manipulation of this flow control valve will affect the level in the separation vessel which will in turn invoke the level control of the separation vessel as explained above.

The fresh water make-up flow is dependent on the bottoms flow from the MRU. The control scheme will manipulate the fresh water control valve if there is a fluctuation in the bottoms flowrate which changes the steady-state design requirement of fresh water of 2 $kg \cdot day^{-1}$.

6.5.5 Distillation section

There is a similar control philosophy applied to both distillation units (HPU and MRU). It is proposed that three temperature indicators be placed near the bottom of the units at different heights to monitor the temperature profile in the column. A temperature approach of these indicators can be used to detect flooding in the column. The liquid level at the bottom of the column should be controlled on the utility flowrate of the reboiler (i.e. increase the flowrate at high levels and decrease utility flow at lower levels). The distillate flowrate will be controlled on the utility flowrate of the condenser (i.e. increase flow to increase distillate flowrate or decrease utility flow to increase the distillate flowrate).

On the HPU unit there will be a composition analyzer on the feed and distillate of the unit. The feed analyzer is to ensure the HME composition is higher than the azeotrope at 61 mol%. There is

a purge line that will open if the composition decreases below 61 mol% to avoid off-specification product and upset to steady-state that will result. The analyzer on the distillate line will increase the condensation rate to increase reflux in the unit if the target specification of 98 mol% is not being achieved. This control overrides the effects of the distillate rate flow which also controls the condensation rate.

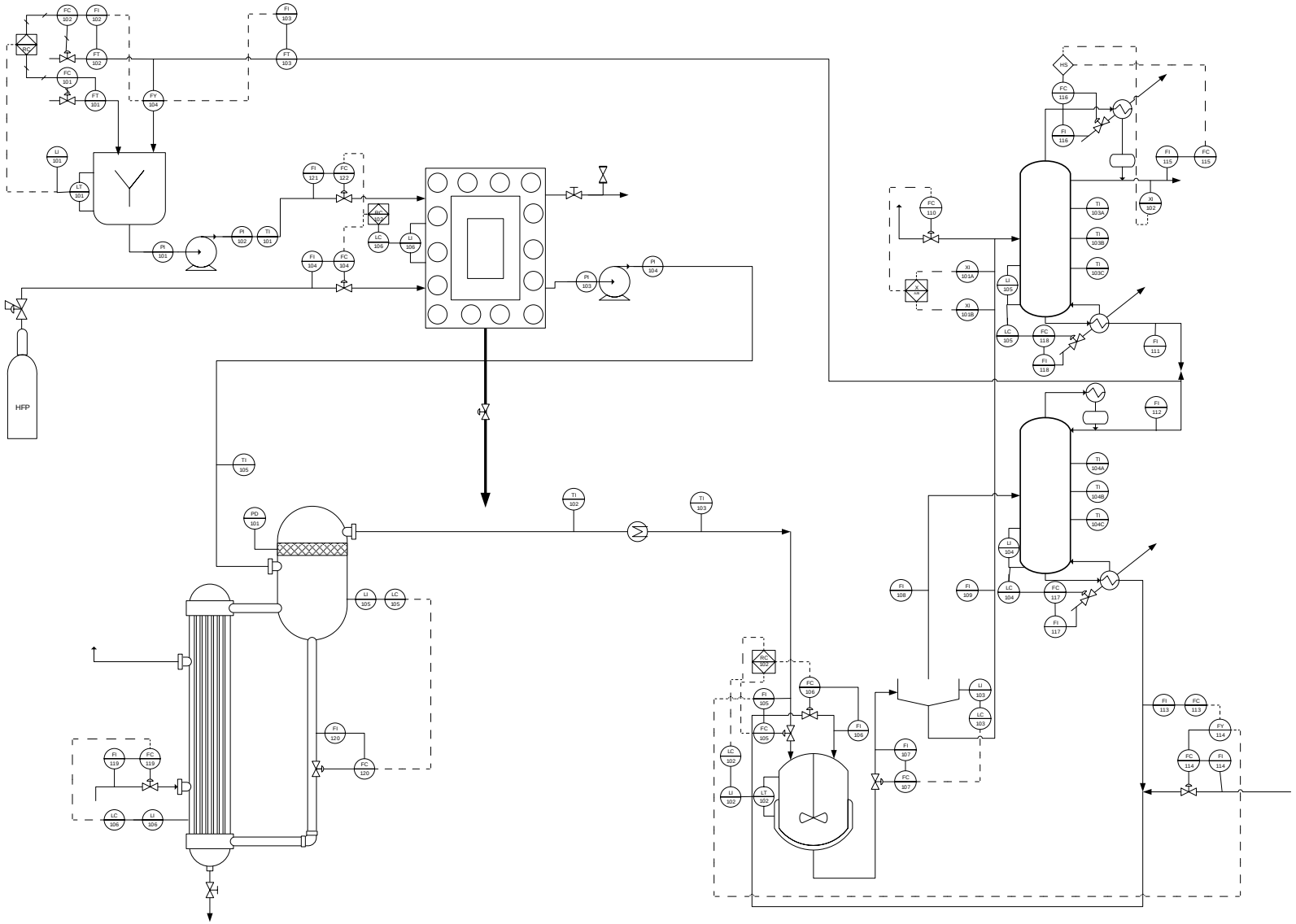

Figure 6.10: Process and instrumentation diagram for proposed control

7

CHAPTER SEVEN

7. PROCESS OVERVIEW

In Chapter 5 and 6, the individual unit operations have been discussed. In section 2.4.1, design heuristics have been discussed and served as guidelines for the development of the entire process.

It is recommended that corrosive or potentially harmful components be removed in the first separation stage as to not damage pipelines and downstream equipment. The first separation process is the salt recovery evaporator that removes dissolved salts from the reactor effluent. If the salt is in the process stream to the distillation column, scale is likely to form on the column. This was observed in the fractional distillation of the reactor product as mentioned in Chapter 4.

Another recommendation is to remove components in a mixture that are in large fraction. This served as a guideline to implement the liquid-liquid extraction immediately after the SRE and therefore the methanol, which is in large excess in the reactor effluent, was extracted as discussed in section 6.2.

A further recommendation is to perform the most difficult separations at the end of a process in the absence of other non-key components. The separation may be defined as difficult when the difference in properties such as the boiling points or densities is not significant or if there is a presence of an azeotrope. The separation of HME and methanol, via distillation, is performed at the end of the process due to the presence of an azeotrope in the HME-methanol system. At this point in the process, other non-key components have already been removed from the feed to the HPU.

Due to the vast experience associated with the design and operation of conventional distillation, this particular separation technique should always be considered for fluid separations. This influenced the use of distillation for the HME and methanol separation as well as the methanol and water separation.

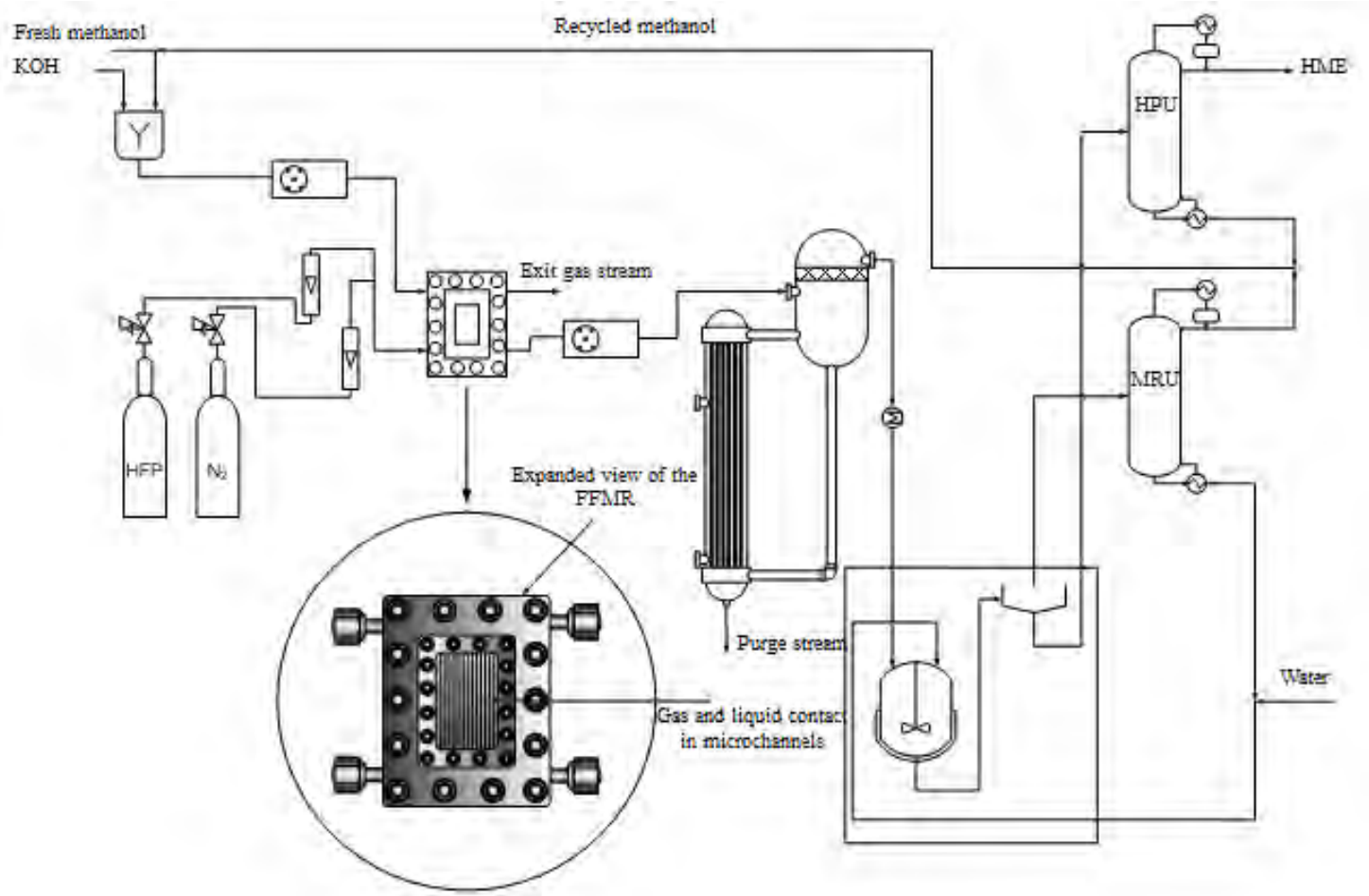

Figure 7.1: Complete process for the synthesis and purification of HME

7.1 Operating envelope for the major proposed unit operations

7.1.1 Falling-film microreactor

The FFMR should be operated at ambient conditions, which reduces energy usage through utilities. In order to allow the desired throughput of 250 kg·month^{-1} of HME to be achieved, the design feed rate of 188 kg·day^{-1} of the KOH and methanol mixture needs to be maintained. In order to obtain the optimum mole fraction of HME in the liquid product of the reactor, a ratio of 1:36 with respect to KOH catalyst and methanol needs to sustained (i.e. 5 kg·day^{-1} of KOH and 183 kg·day^{-1} of the combined flow of fresh and recycled methanol).

It is important for the correct operation of the FFMR that the microchannels do not flood. The withdrawal pump flowrate should always be higher than the feed pump to achieve this other than during start-up of the unit when the channels would have to be flooded and drained in order to obtain complete wetting and a uniform film.

7.1.2 Salt recovery evaporator

The main purpose of the SRE is to prevent salt from migrating through the process which may result in downstream scaling of the separation equipment which was observed during experimentation as explained in section 4.1.4. The temperature of the gaseous stream of methanol and HME leaving the SRE should be higher than the boiling point of methanol of 337.85 K. If the unit is operated at a lower temperature, it may prove inefficient with the valuable components staying in the liquid phase and being removed by the purge.

7.1.3 Liquid-liquid extraction

The purpose of the LLE section of the process is to separate the methanol from the HME such that the HME can be concentrated to above its azeotropic composition of 61 mol% in the HME-methanol system. If any process upsets results in the HME composition in the feed being less than the azeotropic composition, it will need to be purged as it will not be able to be concentrated to its marketable specification purity of 98 mol% in the HPU.

In order to achieve the desired extraction, the water needs to be in a 4:1 proportion to the combined feed of HME and methanol from the SRE.

The water in the system is in a closed loop circulating between the MRU and LLE section of the process. However, a small portion of water may be entrained in the feed to the HPU and some

water will be present in the distillate of the MRU which requires a make-up of fresh water to the LLE section of the process of approximately 2 $kg \cdot day^{-1}$. This entrained water will leave the system via the purge in the SRE.

7.1.4 HME purification unit

The operating intent of the HPU is to separate residual methanol and HME to produce a 98 mol% HME distillate product. The bottoms stream containing methanol will be combined with the distillate of the MRU and recycled to the feed.

In order to achieve a 98 mol% purity of HME in the distillate of the HPU, the feed to the column has to be greater than the azeotropic composition of 61 mol%. If any process upsets results in a lower composition than the minimum feed specification, the feed should be purged and not enter the column as it will reduce the purity of the product.

7.1.5 Methanol recovery unit

The purpose of the MRU is to separate methanol and water emanating from the bottom of the decanter in the LLE section of the process. The methanol will be combined with the bottoms of the HPU and recycled to the feed to the process.

If there is inefficient separation in the MRU, the purge at the SRE should be increased to remove the excess water from the system.

8

CHAPTER EIGHT

8. CONCLUSIONS

8.1 Preliminary study on the semi-batch gas-liquid reactor

The most important observation from the preliminary experimentation was the negligible KF formation for the range of reaction conditions that were investigated. This was attributed to insufficient KF being formed during the reaction to surpass the solubility limit of KF in methanol. This allowed the reaction to be carried out in a falling-film microreactor thereafter.

The experimental results revealed that higher mole fractions of inlet gas, HFP, resulted in higher yields and mole fractions of HME being realised as there was more HFP available for reaction with the excess methanol that was available in the reactor.

It was also shown that greater yields and mole fractions of HME were achieved at higher reaction temperatures. This observation is suspected due to the side reactions having greater reaction rates at lower temperatures than the main reaction producing HME.

Due to the salting-out effect, higher initial catalyst (KOH) concentration inhibited the synthesis of HME due to the decreased solubility of the HFP in the methanol.

The above observations served as a basis for establishing experimental test regions for the levels of the factors investigated in the FFMR.

8.2 Synthesis of HME in a FFMR and subsequent process development for the isolation of HME

Higher yields and mole fractions were obtained in the FFMR experimental runs as compared to the preliminary work on the semi-batch gas-liquid reactor. Similar observations with regards to the trends were observed in both reactors for the HFP inlet mole fraction, reaction temperature and catalyst concentration as discussed in section 7.1.

The effect of the inlet liquid flowrate was also investigated in the FFMR. The highest liquid flowrates resulted in the highest yields, however it was found that this subsequently resulted in the lowest mole fractions of HME in the reactor effluent. It was confirmed through laboratory experimentation that a higher mole fraction of HME in the reactor exit stream resulted in a more concentrated product after liquid-liquid extraction.

The operation of the FFMR should be done at ambient temperature with an inlet gas flow of pure HFP. A moderate catalyst concentration of approximately 0.4 $mol \cdot dm^{-3}$ is recommended. In order to maximise the mole fraction of HME in the reactor effluent, a low inlet liquid flow of methanol with dissolved catalyst of approximately 0.5-1.5 $cm^3 \cdot min^{-1}$ is recommended. In this range, approximately 16-22 reaction plates are required to produce 250 $kg \cdot month^{-1}$ HME. Multiple reaction plates can be installed in a single FFMR.

The results from an independent test performed to investigate the effect of increased liquid residence time in the FFMR revealed the most effective operation is realised by operation of 3 reactors in series (or a channel length equivalent to thrice the length of the experimental reactor)

A Salt Recovery Evaporator (SRE), which is a steam-heated tubular evaporator, will be used to remove dissolved KF, side-reaction products or any water that may be in the reactor effluent. LP steam in the tubes will raise the temperature of the liquid pool in the unit to 348.15 K which will cause the HME and methanol to vapourise and leave the unit while the remaining components will be concentrated. A purge of 2 $kg \cdot day^{-1}$ will be sufficient to remove these high-boiling components from the system.

The laboratory experiments, with regards to liquid-liquid extraction with water, reveal that scale-up on an industrial scale to a mixer and settler unit is plausible in the absence of LLE data from literature for a comprehensive design. The tests indicate that only one mixer and settler is required to overcome the azeotropic composition of HME, in the HME-methanol system, of 61 mol%.

Two distillation columns are required for the process proposed. A column to separate water and methanol, MRU, and a second column to separate HME and methanol, HPU, both emanating from the liquid-liquid extraction process.

The design of the MRU proved feasible with a 10.5 m column in height with 16 trays, with the feed on tray 11, being required. The 757 $kg \cdot day^{-1}$ feed to the unit is at 293.15 K contains approximately 25 wt% methanol and 75 wt% water. The optimised design required a reflux ratio of 2 and will operate at atmospheric pressure to achieve a recovery of methanol of approximately 99%. The duties of the reboiler and condenser are reasonable at 8.6 kW and 7 kW, respectively.

The design of the HPU also proved feasible with a column height of 10.5 m containing 15 trays with the feed stage on the 9^{th} tray. The unit will process a 13 $kg \cdot day^{-1}$ inlet feed stream of 65 mol% HME and 35 mol% methanol entering at 293.15 K. The column is designed to operate at atmospheric pressure and a reflux ratio of 5. The duties of the condenser and reboiler are relatively low at 225 W and 230 W, respectively. HME is removed in the distillate at a marketable purity of 98 mol%. The unit will produce 250 $kg \cdot month^{-1}$ of HME.

9

CHAPTER NINE

9. RECOMMENDATION

The focus in this project, from an experimental standpoint, was on the FFMR. In order to develop a complete process, experimental observations and theoretical calculations served as a basis for the separation unit design. Therefore, it may prove viable to experimentally determine the VLE and LLE data for the systems of interest.

The rotameters should be calibrated using a larger volume bubble flow meter to reduce the deviations incurred at higher flowrates due to the consequential higher velocities during calibration.

An ultrasonic bath should be used to remove solid build-up from the gas sparger if experimentation on the semi-batch gas-liquid reactor is to be performed.

Analysis on solid formation during fractional distillation to determine the presence of KF may be performed. This can be achieved by first making a standard solution of KOH using distilled water and recording the resultant pH. The solid formed during the fractional distillation should then be dissolved in the same volume of distilled water used previously. If the pH of the solid formed in distilled water decreases, it indicates the presence of KF due to it being acidic as compared to KOH which is basic.

The effluent gas stream from the FFMR was not analysed and therefore could not be quantified. An analysis of this stream may offer a greater understanding and possibly further optimization of this process. The possibility of recovering HFP from the vapour and employing a recycle could be investigated.

The reproducibility of the results may be further tested by undertaking further experimental runs at the optimum conditions determined.

Crude samples should be evaporated to identify the presence of any dissolved solids.

REFERENCES

Al-Rawashdeh, M.M., Hessel, V., Lob, P., Mevissen, K. and Schonfield, F. (2008) 'Pseudo 3-D simulation of a falling-film microreactor based on realistic channel and film profiles', *Chemical Engineering and Science*, vol. 63, pp. 5149-5159.

Autoclave (2014) *Autoclave Engineers*, [Online], Available: http://www.autoclaveengineers.com/products/stirred_reactor/ [9 October 2014].

Chambers, R. D. & Spink, R. C.,(1999). 'Microreactors for elemental fluorine'. *Chemical Community,* pp. 883-884.

Chi, K.-W. & Furin, G. G., (1999). 'A facile synthesis of partly-fluorinated ethers using perfluoropropoxyethylene and aliphatic alcohols'. *Bull. Korean chemical society,* 20(2), pp. 220-222.

Conway, K., Kyle, A. and Rielly, C.D. (2002) 'Gas-liquid-solid Operation of a Vortex-ingesting Stirred Tank Reactor', *Trans IChemE, Vol 80, Part A*, pp. pages 839-845.

Correa, A., Tojo, J., Correa , J. and Blanco, A. (1999) 'New analytical solution of group method parameters for the prediction of vapour liquid equilibria', *Ind. Engineering chemical resources*, vol. 28, pp. 609-911.

Correa, A., Tojo, J., Correa, J.M. and Blanco, A. (1989) 'New Analytical solution of groups method parameters for the prediction of vapour-liquid equilibrium', *Ind. Engineering Chemical Resources*, vol. 28, pp. 609-611.

Cussler, E.L. and Moggridge, G.D. (2001) '*Chemical product design'*, London: Cambridge University Press.

de Mas, N., Gunther, A., Schmidt, M. & Jensen, K., (2009). 'A microfabricated scaled-out multilayer gas-liquid microreactor with integrated velocimetry sensors' *Eng. Chem. Res.,* Volume 48, pp. 698-710.

De Mello, A. & Wootton, R., (2002).' *But what it is good for? Applications of microreactor technology for the fine chemical industry'.* [Online]

Available at: http://pubs.rsc.org/en/content/articlehtml/2002/LC/B200736N [Accessed 1 June 2015].

Dinov, I. (2013) '*Statistics Online Computational Resource'*, [Online], Available: http://www.socr.ucla.edu/applets.dir/f_table.html [16 May 2013].

Edwards, J., 2005. '*Chemical Processing'.* [Online] Available at: http://www.chemicalprocessing.com/articles/2005/554/?start=1 [Accessed 1 June 2015].

Hessel, V., (2004). 'Microreactor technology: Applications in Pharma/Chemical Processing'. *Chem Eng Technol,* 5(26), pp. 531-544.

Holton, J., (2013). '*The essential chemical industry'.* [Online] Available at: http://www.essentialchemicalindustry.org/processes/chemical-reactors.html [Accessed 23 June 2015].

Hudlicky, T. et al., (2000). 'Practical preparation of potentially anesthetic fuorinated ethyl methyl ether by means of bromine trifluoride and other methods'. *Fluorine Chemistry,* Volume 102, pp. 363-367.

Il'in, A.A., Bakhmutov, Y.L., Ivanova, L.M., Furin, G.G., Tolstikova, T.G. and Sukhinin, V.S. (2004) 'Synthesis and Use of Partially Fluorinated Dialkyl Ethers Derived from Hexafluoropropylene', *Russian Journal of Applied Chemistry, Vol 77*, pp. pages 98-101.

Istadi and Amin, N.A.S. (2006) 'Optimization of process parameters and catalyst compositions in carbon dioxide coupling of methane over CaO-MnO/CeO catalyst using response surface methodology', *Fuel processing Technology, Vol 87*, pp. pages 449 - 459.

Junkers, M. (2014) '*Microreactor Technology'*, [Online], Available: http://www.sigmaaldrich.com/technical-documents/articles/chemfiles/microreactor-technology.html [9 October 2014].

Kato, R. & Nishiumi, H., (2003). 'Stationary state model in reforming HCFC22 to difluoromethylether'. *The Canadian journal of chemical engineering,* Volume 81, pp. 1-6.

Kestenbaum, H. et al., (2002). 'Process intensification through microreactor application'. *Ind. Eng. Chem. Res,* Volume 41, p. 710.

Knorr, A. (2012). '*Federal Institute for materials research and testing'*, 01 January, [Online], Available: http://www.bam.de/en/geraete_objekte/fg22_fallfilm_mikro_reaktor.htm [02 August 2013].

Kraai, G. et al., (2008). 'Two-phase (bio) catalytic reaction in a microreactor'. *Chem. Int ,* Volume 47, pp. 384-389.

Kurnia, K.A., Mutalib, M.M. and Murugesan, T. (2011) 'Densitie, refractive indices and excess molar properties for binary mixtures of protic ionic liquids in methanol at T=293.15K to T=313.15K', *Molecular Liquids*, pp. 211-219.

Kurnia, K.A., Taib, M.M., Mutalib, A. and Murugesan, T. (2011) 'Densities, refractive indices and excess molar properties for minary mixtures of protic ioninc liquids with methanol at T=293.15 to T=313.15K', *Molecular Liquids*, vol. 159, no. 3, pp. 211-219.

Lazic, Z.R. (2004). '*Design of Experiements in Chemical Engineering'* , Weinheim: Wiley-VCH.

Levenspiel, O. (2006). '*Chemical Engineering Engineering'*, 3rd edition, New York: Wiley India Pvt. Limited.

Lokhat, D. (2012). '*Gas-Phase Epoxidation of Hexafluoropropylene'*, Durban.

Maskos, M., (2015). '*Fraunhofer'*. [Online] Available at: http://www.imm.fraunhofer.de/en/product_areas/m4chemistry/project_myprochem.html [Accessed 23 June 2015].

Murata, J., Tamura, M. & Sekiya, A., (2002). 'Selective synthesis of fluorinated ethers by addition reaction of alcohols to fluorinated olefins in water'. *The royal society of chemistry,* Volume 4, pp. 60-63.

Pagliaro, M. (2014). '*Speciality Chemicals'*, [Online], Available: http://www.specchemonline.com/articles/view/green-chemistry-in-fine-chemicals-pharmaceuticals#.VDaGk_mSxIE [10 October 2014].

Parr, (2015). '*Parr Instrument company'*. [Online] Available at: http://www.parrinst.com/products/stirred-reactors/series-4555-10-20-l-floor-stand-reactors/ [Accessed 23 June 2015].

Pelchem (2011). '*Fluorochemical Expansion Initiative'*, [Online], Available: http://www.pelchem.com/FEI.html [21 February 2014].

Pohar, A. & Plazl, I., (2009). 'Process intensification through microreactor application'. *Biochem Engineering,* 23(4), pp. 537-544.

Raal, J. and Muhlbauer, A. (1998) 'Phase equilibira - measurement and computation', *Taylor and Fraccis*, pp. 302-309.

Radleys (2014). '*Radleys'*, [Online], Available: http://www.radleys.co.uk/pages/products/pilot/ [10 October 2014].

Rendall, J. L. (1958). 'Fluorinated carbon compounds'. Google Patents.

Roberge, D., Ducry, L., Bieler, P., Cretton P and Zimmermann, B. (2005). '*Chemical Engineering and Technology'*, 1st edition, Weinheim: Wiley.

Rousseau, R. (1987). '*Handbook of Separation Process Technology'*, 2nd edition, New York: Wiley.

Scholle, T. (2009). '*Statiscal Design and Process Control'*, [Online], Available: http://faculty.ycp.edu/~tscholle/EGR305/f-table0.05.html [18 May 2013].

Schumpe, A. (1993). 'The estimation of gas solubilities in salt solutions', *Chemical Enginnering Science*, vol. 48, pp. 153-158.

Seader, J.D. and Henley, E.J. (1998). '*Separation Process Principles'*, Hoboken: John Wiley & Sons Inc.

Sinnott, R.K. (2005). '*Coulson and Richardson's chemical engineering design'*, 4th edition, London: Elsevier.

Smith, J.M., Van Ness, H.C. and Abbott, M.M. (2005). '*Introduction to chemical engineering thermodynamics'*, New York: McGraw Hill.

Star, (2010). '*Star Industried'*. [Online] Available at: http://www.starind.com/About [Accessed 23 June 2015].

Stenger, V.A. (1996). 'Solubilities of Various Alkali Metal and Alkaline eart Metal compounds in methanol', *J. Chem. Eng. Data*, vol. 41, pp. 1111-1113.

Tochigi, K., Yoshida, K., Kurihara, K., Ochi, K., Murata, J., Yasumoto, M. and Sako, T. (2001). 'Prediction of vapour-liquid equilibrium for syustems containing hydrofluoroethers suing ASOG group contribution method', *Elsevier*, vol. 183, pp. 173-182.

van Gerven , T., Mul, G., Moulijn, J. & Stankiewicz, A., (2007). 'A review of intensifcation of photocatalyticc processes'. *Chem. Eng. Process,* 46(9), pp. 781-789.

Vankayala, B.K., Lob, P., Hessel, V., Menges, G., Hofmann, C., Metzke, D., Krtschil, U. and Kost, H.-J. (2007). 'Scale-up of Process Intensifying Falling film microreactors to pilot production scale', *International journal of chemical reactor engineering*, vol. 5, no. A91, pp. 1-10.

Vogel, I. (1989). '*Vogel's textbook of practical organic chemistry'*, 5th edition, London: Pearson Education.

A

APPENDIX A

A. RAW DATA

A.1 Steady state test – FFMR

Table A-1.1: Areas obtained from the gas chromatograph for the different components

Time, min	Area			
	Methanol	HME	Tetrafluoropropionate	Propanol
3	44498308	812674	52526	49273531
6	48088410	917719	60526	53062436
9	39469183	730074	43849	65339070
12	36697848	683752	32438	73707302
15	52402069	999261	36860	49662736
18	45766597	827805	31645	54224798
21	47524706	864694	42357	54094726

Table A-1.2: Sequential calculation of the yield

Time, min	Crude Mass, g	IS Mass, g	AR HME/IS	HME Mass, g	HME Mass Fraction	Mass HME in Crude	Moles HME	Moles HFP	Yield, %
3	0.829	0.479	0.016	0.025	0.030	0.14	0.0008	0.0039	20
6	0.87	0.522	0.017	0.028	0.032	0.31	0.0017	0.0078	22
9	0.754	0.659	0.011	0.023	0.030	0.44	0.0024	0.0117	21
12	0.662	0.694	0.009	0.020	0.030	0.58	0.0032	0.0156	20
15	0.918	0.451	0.020	0.028	0.031	0.74	0.0040	0.0195	21
18	0.853	0.521	0.015	0.025	0.029	0.83	0.0046	0.0234	20
21	0.861	0.502	0.016	0.025	0.029	0.97	0.0053	0.0272	20

A.2 Statistical data

Table A-2.1 Analysis of variance table - GLR

Source	DoF	SS	MS	*F*-value	*p*-value
Regression	9	614.7	68.3	1.44	0.29
Residual	10	474.7	47.47	-	-
Total	19	1089.4	-	-	-

Table A-2.2: Analysis of variance table – HME yield as response factor on FFMR

Source	DoF	SS	MS	*F*-value	*p*-value
Regression	14	3148.3	224.9	6.04	0.0007
Residual	15	558.2	37.2	-	-
Total	29	3706.5	-	-	-

Table A-2.3: Analysis of variance table – HME mole fraction as response factor on FFMR

Source	DoF	SS	MS	*F*-value	*p*-value
Regression	14	15.6	1.1	4.96	0.002
Residual	15	3.4	0.2	-	-
Total	29	19.0	-	-	-

A.3 Experimentation

Table A-3.1: Factors with corresponding levels - GLR

FACTORS	INTERVAL STEP	-1.68	-1	0	1	1.68
HFP Rotameter Number	20	26	40	60	80	93.64
HFP flow, $cm^3 \cdot min^{-1}$	218	716	864	1082	1300	1449
Nitrogen flow, $cm^3 \cdot min^{-1}$	218	1033	885	667	449	300
Catalyst Mass, $mol \cdot dm^{-3}$	12	41	49	62	74	83
Temperature, K	278.15	285.15	288.15	293.15	298.15	301.55

A total inlet flowrate of a combined feed of nitrogen and HFP was chosen to be 1750 $cm^3 \cdot s^{-1}$. Using the difference of this total flow and the determined amount of HFP flow, the nitrogen flow required could be determined. The conversion of rotameter number for the HFP to the actual volumetric flow was done using the calibration in Appendix B.

Table A-3.2: Factors with corresponding levels - FFMR

Factors	-2	-1	0	1	2
Temperature, K	275.15	280.15	285.15	290.15	295.15
Concentration, $mol \cdot dm^{-3}$	0.25	0.34	0.43	0.52	0.61
HFP Flow	0.25	0.52	0.78	1.05	1.32
Nitrogen Flow	1.25	0.98	0.72	0.45	0.18
Liquid Flow, $cm^3 \cdot min^{-1}$	0.50	1.75	3.00	4.25	5.50

A.4 Fractional distillation

Table A-4.1: Raw data obtained during fractional distillation

Time Elapsed, min	Vapour Temperature, K	Liquid Temperature , K
0	296.15	295.15
6	296.15	298.15
12	296.15	300.15
18	296.15	303.15
24	296.15	305.15
30	296.15	309.15
36	296.15	312.15
42	296.15	317.15
48	296.15	320.15
54	296.15	322.15
60	296.15	324.15
66	298.15	324.65
72	311.15	325.15
78	315.15	325.15
84	316.15	325.15
90	317.15	325.15
96	318.15	325.15
108	318.15	325.15
120	319.15	325.15
180	319.15	325.15
240	319.15	325.15
300	319.15	325.15
360	319.15	325.15
420	319.15	333.15
480	319.15	333.15
540	319.15	333.15
660	319.15	333.15
720	319.15	333.15

A.5 Gas chromatography results

Table A-5.1: Data from the GC analysis for crude samples from the GLR

Sample	Component	Retention Time, min	Area	Height	Composition
1	Methanol	1.687	30790700	7712264.1	32.16
	HME	1.788	2158128.7	1447628.9	2.25
	Side Product	1.863	12974.9	11842.2	0.01
	Propanol (IS)	2.648	62782218	3750061.1	65.57
2	Methanol	1.736	23355116	7029598.9	27.77
	HME	1.846	2391371.7	1573550.4	2.84
	Side Product	1.922	9366.7	7773.1	0.01
	Propanol (IS)	2.688	58339204	3684933.2	69.37
3	Methanol	1.752	35789092	8365339.9	42.76
	HME	1.845	2440732.9	1816243.7	2.92
	Side Product	0	0	0	0
	Propanol (IS)	2.638	45464413	3432785.1	54.32
4	Methanol	1.747	34961815	8387170.5	43.01
	HME	1.84	2653400.9	1938489.9	3.26
	Side Product	0	0	0	0
	Propanol (IS)	2.625	43672768	3379039.9	53.73
5	Methanol	1.747	34961815	8387170.5	43.01
	HME	1.84	2653400.9	1938489.9	3.26
	Side Product	0	0	0	0
	Propanol (IS)	2.625	43672768	3379039.9	53.73
6	Methanol	1.765	41292723	8897634.1	48.39
	HME	1.847	1251482.6	827426.3	1.47
	Side Product	0	0	0	0
	Propanol (IS)	2.638	42780515	3347375.4	50.14
7	Methanol	1.76	34513307	8541180.5	43.92
	HME	1.849	1427755.7	1057432.7	1.82
	Side Product	0	0	0	0
	Propanol (IS)	2.643	42648895	3339339	54.27
8	Methanol	1.765	39843915	8808901.3	45.57
	HME	1.848	1833448.9	1310358.6	2.10
	Side Product	0	0	0	0.00
	Propanol (IS)	2.651	45757258	3443054.2	52.33
9	Methanol	1.756	35966736	8255970.2	44.48
	HME	1.848	1083800.1	728345.1	1.34
	Side Product	1.924	19444.3	8741	0.02
	Propanol (IS)	2.628	43791746	3403935.3	54.16

10	Methanol	1.75	34640547	8463342.3	43.44
	HME	1.842	2454040.7	1689946	3.08
	Side Product	1.917	9623.9	5588.2	0.01
	Propanol (IS)	2.623	42642346	3346540.5	53.47
11	Methanol	1.756	33174089	8454023.1	42.23
	HME	1.849	2317974.5	1690990.8	2.95
	Side Product	0	0	0	0.00
	Propanol (IS)	2.635	43060945	3360871.8	54.82
12	Methanol	1.759	34510888	8521106.6	44.52
	HME	1.848	1350999.1	1004598.1	1.74
	Side Product	0	0	0	0.00
	Propanol (IS)	2.638	41660662	3350711.5	53.74
13	Methanol	1.752	37474000	8727179.4	43.82
	HME	1.837	2264603	1790198.7	2.65
	Side Product	1.912	7385	4145.3	0.01
	Propanol (IS)	2.644	45763599	3437027.6	53.52
14	Methanol	1.753	34601665	8660493.4	43.24
	HME	1.844	1692113.2	1189973.6	2.11
	Side Product	1.928	10136.5	4498.3	0.01
	Propanol (IS)	2.638	43721577	3398825.6	54.63
15	Methanol	1.727	35408635	8558369	43.26
	HME	1.817	1945186.4	1488401.1	2.38
	Side Product	1.892	2539.7	3155.3	0.00
	Propanol (IS)	2.609	44489787	3392454.9	54.36
16	Methanol	1.74	28703637	8005315.7	42.49
	HME	1.844	1263577.2	846670.5	1.87
	Side Product	0	0	0	0.00
	Propanol (IS)	2.601	37590067	3268189.9	55.64
17	Methanol	1.752	36539340	8540074	43.85
	HME	1.842	1314832.7	1236589.8	1.58
	Side Product	0	0	0	0.00
	Propanol (IS)	2.639	45477645	3448282.3	54.57
18	Methanol	1.731	36552698	8256325	43.56
	HME	1.852	1265852.8	1013395.6	1.79
	Side Product	0	0	0	0.00
	Propanol (IS)	2.625	39658524	3396589.8	54.30
19	Methanol	1.748	38935620	8623589	42.87
	HME	1.848	1425698.8	1023658.9	1.26
	Side Product	0	0	0	0.00
	Propanol (IS)	2.598	45263259	3302569.4	55.10
20	Methanol	1.753	29836540	8362598	43.83
	HME	1.839	1856325.5	1023658.9	1.60
	Side Product	0	0	0	0.00
	Propanol (IS)	2.650	38526598	3285963.3	54.57

TABLE A-5.2: Data from the GC analysis for crude samples from the FFMR

Experiment	Peak	Retention Time, min	Area	Height	Concentration
1	Methanol	1.673	21293996	5726562	18.79143
	HME	1.794	869239.2	527502.4	0.76708
	AE	1.908	21312.3	9026.5	0.01881
	IS	2.736	91060869	4304230	80.35899
	AT	4.678	72168.6	26304.9	0.06369
2	Methanol	1.776	49844591	9248191	44.43153
	HME	1.846	843401.6	559753.4	0.75181
	AE	1.967	60816.5	29511.3	0.05421
	IS	2.704	61369356	3847395	54.70472
	AT	4.712	64758.3	27808.2	0.05773
3	Methanol	1.731	30197238	7500834	28.93314
	HME	1.839	3128922	1972885	2.99794
	AE	1.914	154090.6	90409.3	0.14764
	IS	2.717	70605718	4030960	67.65007
	AT	4.712	283055.5	99494.3	0.27121
4	Methanol	1.724	29680880	8380514	35.27767
	HME	1.827	1422857	820467.5	1.69116
	AE	1.903	155495.1	60999.7	0.18482
	IS	2.643	52764606	3697422	62.71419
	AT	4.691	111192.2	52410.1	0.13216
5	Methanol	1.756	40714567	9176132	44.03787
	HME	1.839	1283329	894639.3	1.38808
	AE	1.913	76147.2	51752	0.08236
	IS	2.647	50257328	3668345	54.35955
	AT	4.697	122171	47006.3	0.13214
6	Methanol	1.758	45623542	9378519	48.93359
	HME	1.833	726639.5	450311.5	0.77936
	AE	1.909	45927	27943	0.04926
	IS	2.635	46787149	3548618	50.18161
	AT	4.693	52382	24076	0.05618
7	Methanol	1.761	45731933	9378047	46.52451
	HME	1.839	3719685	2628777	3.78415
	AE	1.912	257594.4	188793.1	0.26206
	IS	2.64	48187841	3584917	49.02298
	AT	4.711	399379.3	144713.1	0.4063
8	Methanol	1.761	46390397	9286782	45.9507
	HME	1.838	2084437	1332325	2.06468
	AE	1.912	114602.7	70878.7	0.11352
	IS	2.653	52222868	3689161	51.72789
	AT	4.701	144579.4	69332.9	0.14321

9	Methanol	1.755	36594411	8736345	35.41652
	HME	1.845	1998944	1471289	1.9346
	AE	1.92	148549.3	113717.7	0.14377
	IS	2.712	64442037	3935828	62.3678
	AT	4.711	141880.1	65901.7	0.13731
10	Methanol	1.774	46998706	9164000	48.79309
	HME	1.846	849626	630301.5	0.88206
	AE	1.921	22497.3	12779.7	0.02336
	IS	2.657	48394794	3562026	50.24248
	AT	4.714	56839.3	30058.9	0.05901
11	Methanol	1.761	41355575	8826225	42.68607
	HME	1.846	3733252	2730348	3.85336
	AE	1.919	247645.1	180753.4	0.25561
	IS	2.661	51239639	3652926	52.88813
	AT	4.72	306959.2	149016.3	0.31683
12	Methanol	1.77	43748561	9048397	41.74206
	HME	1.847	2040176	1539517	1.9466
	AE	1.921	55523.9	40846.8	0.05298
	IS	2.704	58805872	3779818	56.10877
	AT	4.715	156783.3	78028.9	0.14959
13	Methanol	1.765	43296221	8748699	42.0777
	HME	1.846	1461688	1014514	1.42055
	AE	1.922	45469.4	29033.2	0.04419
	IS	2.685	57965588	3786933	56.33421
	AT	4.716	126917	59237.1	0.12335
14	Methanol	1.751	53201282	9514911	47.018
	HME	1.814	780393.9	586675.1	0.68969
	AE	1.889	31974	21395.2	0.02826
	IS	2.671	59070509	3773314	52.20508
	AT	4.688	66724	28250.6	0.05897
15	Methanol	1.764	40162137	8802124	42.39365
	HME	1.849	3823498	2785031	4.03594
	AE	1.922	222153.9	151827.7	0.2345
	IS	2.659	50243116	3612201	53.03475
	AT	4.719	285315.1	135359	0.30117
16	Methanol	1.72	42014194	9229053	41.12221
	HME	1.802	1776041	1015853	1.73833
	AE	1.876	98011.1	60578.7	0.09593
	IS	2.647	58150447	3799220	56.91589
	AT	4.679	130400.2	53514.4	0.12763

17	Methanol	1.771	46101652	9412338	52.19883
	HME	1.846	2241694	1702046	2.53817
	AE	1.92	165510.6	127756.3	0.1874
	IS	2.622	39646601	3371548	44.89007
	AT	4.711	163862.9	82206	0.18553
18	Methanol	1.748	32136518	8302326	30.44065
	HME	1.845	1487109	1096704	1.40863
	AE	1.92	83803.1	65907.5	0.07938
	IS	2.741	71768546	4052229	67.98127
	AT	4.71	95087.4	49365.5	0.09007
19	Methanol	1.765	43601434	9413728	46.9395
	HME	1.845	2039560	1442237	2.19571
	AE	1.92	183435.7	132368.6	0.19748
	IS	2.648	46912208	3567314	50.50374
	AT	4.712	151937.6	70177.3	0.16357
20	Methanol	1.775	48402054	9368344	51.80419
	HME	1.848	2298138	1564238	2.45967
	AE	1.922	117901.8	78101.1	0.12619
	IS	2.633	42445449	3423731	45.4289
	AT	4.712	169156.8	83162.3	0.18105
21	Methanol	1.774	48550023	9204702	46.48506
	HME	1.845	432309.1	295566.8	0.41392
	AE	1.921	20763.2	14348.8	0.01988
	IS	2.68	55403613	3758142	53.04715
	AT	4.709	35498.6	16662.2	0.03399
22	Methanol	1.761	42227504	9304961	49.9953
	HME	1.845	3881095	2731636	4.59503
	AE	1.918	301873.2	210751.1	0.3574
	IS	2.601	37747871	3338000	44.69163
	AT	4.716	304608.9	148464.5	0.36064
23	Methanol	1.757	38581695	8790552	42.80276
	HME	1.848	6796455	4840137	7.54003
	AE	1.919	602873.3	446216.9	0.66883
	IS	2.625	43999914	3487974	48.81377
	AT	4.705	157387.1	81058.4	0.17461
24	Methanol	1.751	40054499	9406547	49.97965
	HME	1.84	1027974	657212.5	1.2827
	AE	1.917	31076.5	17209.4	0.03878
	IS	2.6	38957539	3397523	48.61087
	AT	4.703	70530	33317	0.08801

25	Methanol	1.77	46068483	8847165	52.2836
	HME	1.846	2092605	1515812	2.37492
	AE	1.921	37190.4	27640.1	0.04221
	IS	2.616	39748622	3358480	45.11112
	AT	4.707	165785.4	82916.8	0.18815
26	Methanol	1.769	45420818	9379130	51.60392
	HME	1.845	1805675	1323204	2.05148
	AE	1.919	123093.9	87936	0.13985
	IS	2.619	40498884	3408360	46.01197
	AT	4.708	169682.2	79424.3	0.19278
27	Methanol	1.682	45694863	9257635	48.69564
	HME	1.757	2129189	1405079	2.26901
	AE	1.83	163079.8	107270.8	0.17379
	IS	2.557	45693588	3514592	48.69429
	AT	4.658	156960.1	78049.6	0.16727
28	Methanol	1.732	39114151	9156879	51.19414
	HME	1.817	1993585	1089762	2.60928
	AE	1.892	109297.4	88530.6	0.14305
	IS	2.563	35034881	3281467	45.85503
	AT	4.685	151658.8	70201.2	0.1985
29	Methanol	1.746	40824036	7988020	46.34922
	HME	1.845	1940663	984314.7	2.20331
	AE	1.921	69702	38230.7	0.07914
	IS	2.607	45095598	3525558	51.1989
	AT	4.702	149234.2	66155.2	0.16943
30	Methanol	1.762	55193551	9700075	56.55778
	HME	1.828	2703052	1944792	2.76986
	AE	1.901	154049.5	112348.2	0.15786
	IS	2.601	39335672	3347372	40.30794
	AT	4.706	201576.6	95327.3	0.20656

A.6 Screening of impurities in methanol

Table A-6.1: Refractive index results for first bottle of methanol used

Run	Refractive Index
1	1.3298
2	1.3297
3	1.3297
4	1.3299
5	1.3299

Table A-6.2: Refractive index results for second bottle of methanol used

Run	Refractive Index
1	1.3312
2	1.3312
3	1.3312
4	1.3312
5	1.3312

The literature value for the refractive index of methanol is 1.3294 (Kurnia, et al., 2011). The measured refractive index was done by the use of a refractometer (ATAGO RX-7000α).

A.7 HME identification

Table A-7.1: Table of peaks from GC-MS mass spectrum to identify HME

m/z	Absolute Intensity	Relative Intensity
29.1	542	5.42
31.1	1033	10.33
47.05	902	9.02
51.05	1104	11.04
60.05	246	2.46
63.05	282	2.82
69.05	2006	20.06
81.1	10000	100
82.1	945	9.45
101.05	1108	11.08
113.1	304	3.04
129.1	1679	16.79
151.1	526	5.26
163.1	2663	26.63

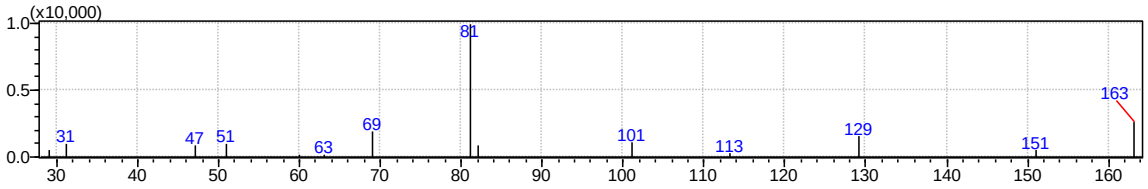

Figure A-7.1: GC-MS mass spectrum to identify HME - sample 1

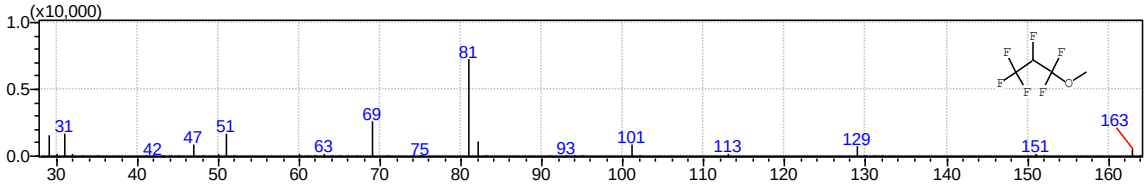

Figure A-7.2: GC-MS mass spectrum to identify HME –sample 2

A.8 Mass transfer characteristic

Table A-8.1: Calculation scheme for mass transfer characteristic

Run	1	2	3	4	5	6
Q_L, $cm^3 \cdot min^{-1}$	3	4	5	3	4	5
Q_g, $cm^3 \cdot min^{-1}$	50	50	50	80	80	80
V_{HCL}, cm^3	8.85	9.95	10.35	8.9	10.05	10.5
Time, min	20	20	20	20	20	20
C_{out}, $mol \cdot l^{-1}$ ($x10^3$)	1.48	1.24	1.04	1.48	1.26	1.05
k_L[a], $cm^3 \cdot s^{-1}$ ($x10^4$)	0.57	0.64	0.66	0.58	0.65	0.67
$\boldsymbol{\delta}_L$, m ($x10^4$)	0.94	1.03	1.11	0.94	1.03	1.11
j_L, $cm^3 \cdot s^{-1}$	0.026	0.032	0.037	0.026	0.032	0.037
F_0	0.48	0.32	0.24	0.48	0.32	0.24
k_L[b], $cm^3 \cdot s^{-1}$ ($x10^4$)	0.35	0.39	0.42	0.35	0.39	0.42

[a] Mass transfer coefficient – experimental
[b] Mass transfer coefficient - predicted

B

APPENDIX B

B. CALIBRATIONS

B.1 Nitrogen flowmeter calibration - GLR

Table B-1.1: Raw data from the calibration of the nitrogen flowmeter - GLR

Flowmeter reading	Run 1 time, s	Run 2 time, s	Run 3 time, s	Average time, s	Flowrate, $cm^3 \cdot min^{-1}$	Flowrate, $cm^3 \cdot s^{-1}$
0.2	36	36	35.6	35.9	334.6	5.6
0.4	20.5	20.4	21	20.6	581.6	9.7
0.6	15.5	15.8	15.4	15.6	770.9	12.8
0.8	12	11.7	11.8	11.8	1014.1	16.9
1	9.9	10.1	9.6	9.9	1216.2	20.3
1.2	8.2	8.5	8.2	8.3	1445.8	24.1
1.4	7.3	7.3	7.5	7.4	1629.0	27.1
1.6	6.3	6.3	6.3	6.3	1904.8	31.7
1.8	5.7	5.6	5.6	5.6	2130.2	35.5
2	5.3	5.4	5.2	5.3	2264.2	37.7

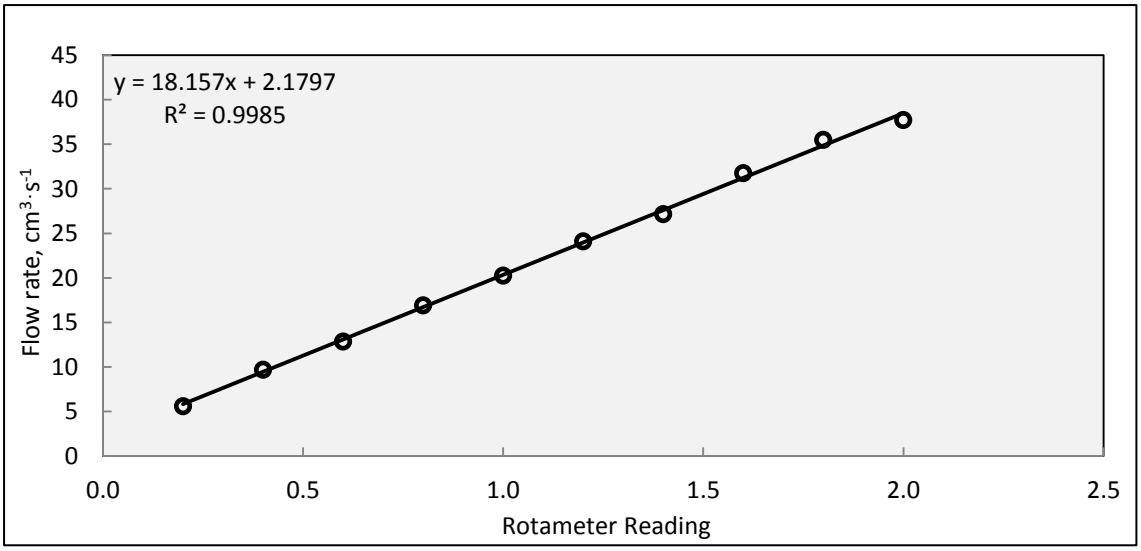

Figure B-1.1: The rotameter calibration for the flow of nitrogen - GLR

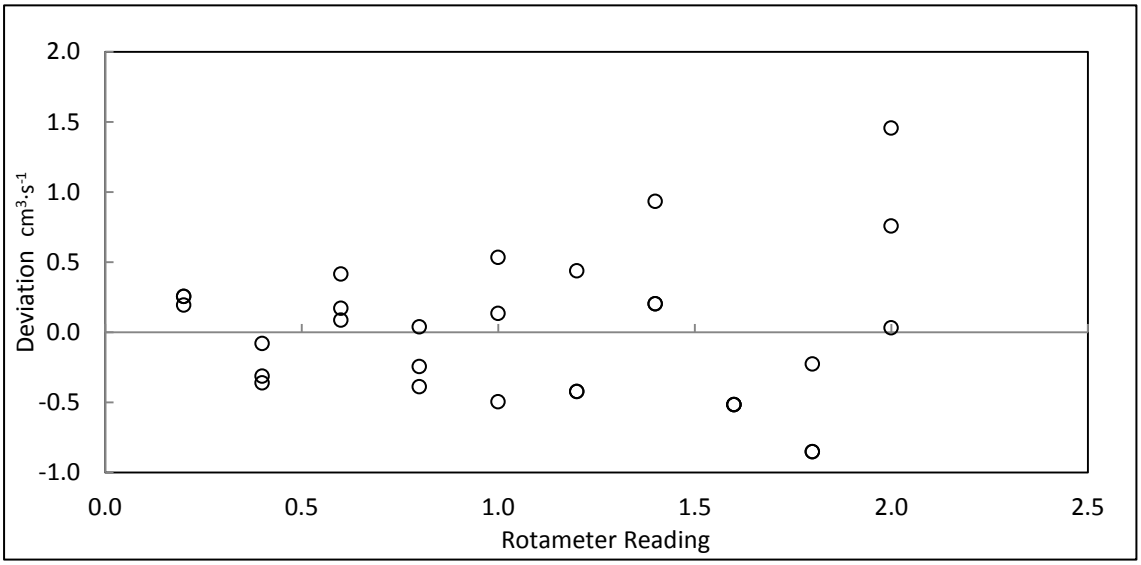

Figure B-1.2: Deviation plot for the 3 experimental runs done for the nitrogen flow meter calibration - GLR

B.2 HFP flowmeter calibration - GLR

Table B-2.1: Raw data from the calibration of the HFP flowmeter - GLR

Flowmeter reading	Run 1 time, s	Run 2 time, s	Run 3 time, s	Average time, s	Flowrate, $cm^3 \cdot min^{-1}$	Flowrate, $cm^3 \cdot s^{-1}$
15	22.28	21.97	22.28	22.2	541.1	9.0
30	16.5	16.19	16.22	16.3	736.0	12.3
45	12.91	12.85	12.78	12.8	934.1	15.6
60	10.87	10.57	10.81	10.8	1116.3	18.6
75	9.28	9.22	9.35	9.3	1292.6	21.5
90	8.34	8.34	8.34	8.3	1438.8	24.0
105	7.69	7.68	7.72	7.7	1559.1	26.0
120	6.65	6.84	6.97	6.8	1759.5	29.3
135	6.53	6.29	6.41	6.4	1872.1	31.2
150	5.94	5.87	5,72,	5.9	2032.2	33.9

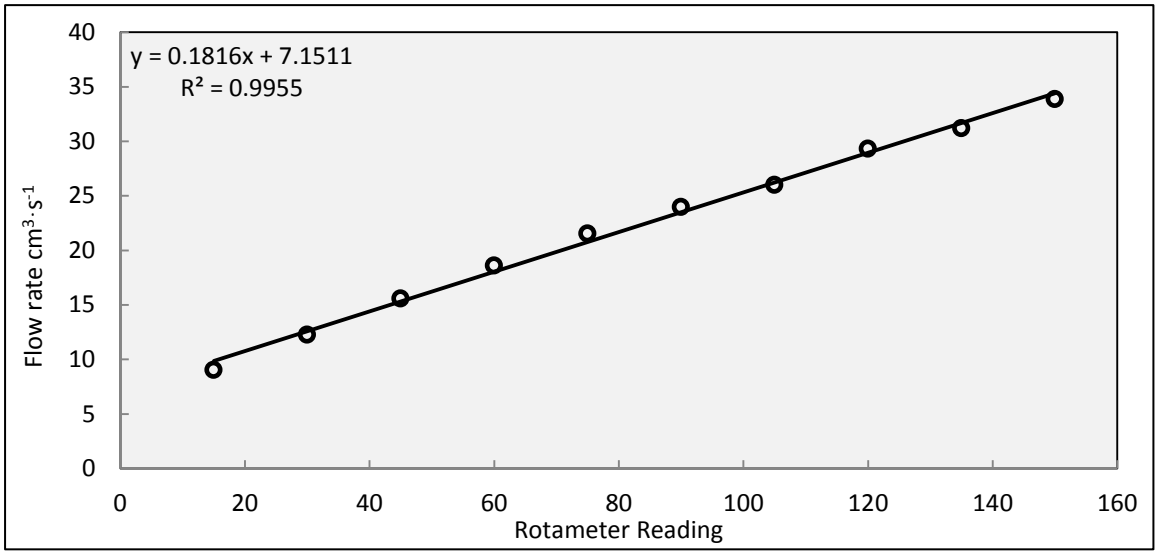

Figure B-2.1: The rotameter calibration for the flow of HFP - GLR

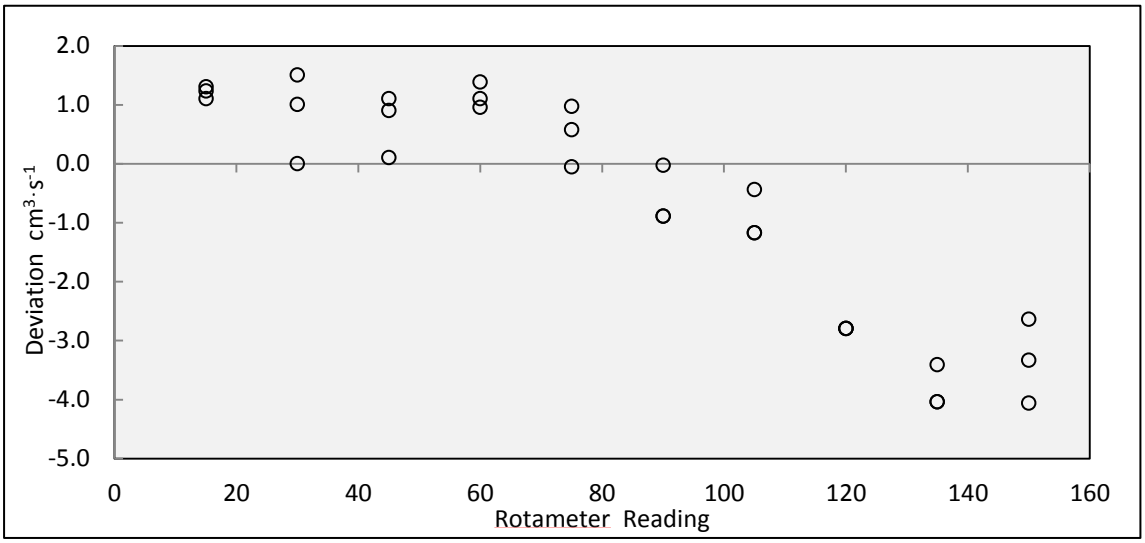

Figure B-2.2: Deviation plot for the 3 experimental runs for the HFP flow meter calibration - GLR

B.3 Nitrogen flowmeter calibration - FFMR

Table B-3.1: Raw data from the calibration of the nitrogen flowmeter - FFMR

Flowmeter reading	Run 1 time, s	Run 2 time, s	Run 3 time, s
15	35.87	36.25	35.12
30	17.06	17.32	17.34
45	12.07	12.28	12.25
60	8.89	8.81	8.78
75	7.34	7.31	7.25

Table B-3.2: Deviation between actual and predicated flowrates - FFMR

Run	Flowmeter reading	Actual	Predicted	Deviation, $cm^3 \cdot s^{-1}$
		Flowrate, $cm^3 \cdot s^{-1}$	Flowrate, $cm^3 \cdot s^{-1}$	
1	15	0.279	0.290	0.011
	30	0.586	0.563	-0.023
	45	0.829	0.836	0.008
	60	1.125	1.110	-0.015
	75	1.362	1.383	0.021
2	15	0.276	0.290	0.014
	30	0.577	0.563	-0.014
	45	0.814	0.836	0.022
	60	1.135	1.110	-0.025
	75	1.368	1.383	0.015
3	15	0.285	0.290	0.005
	30	0.577	0.563	-0.014
	45	0.816	0.836	0.020
	60	1.139	1.110	-0.029
	75	1.379	1.383	0.004

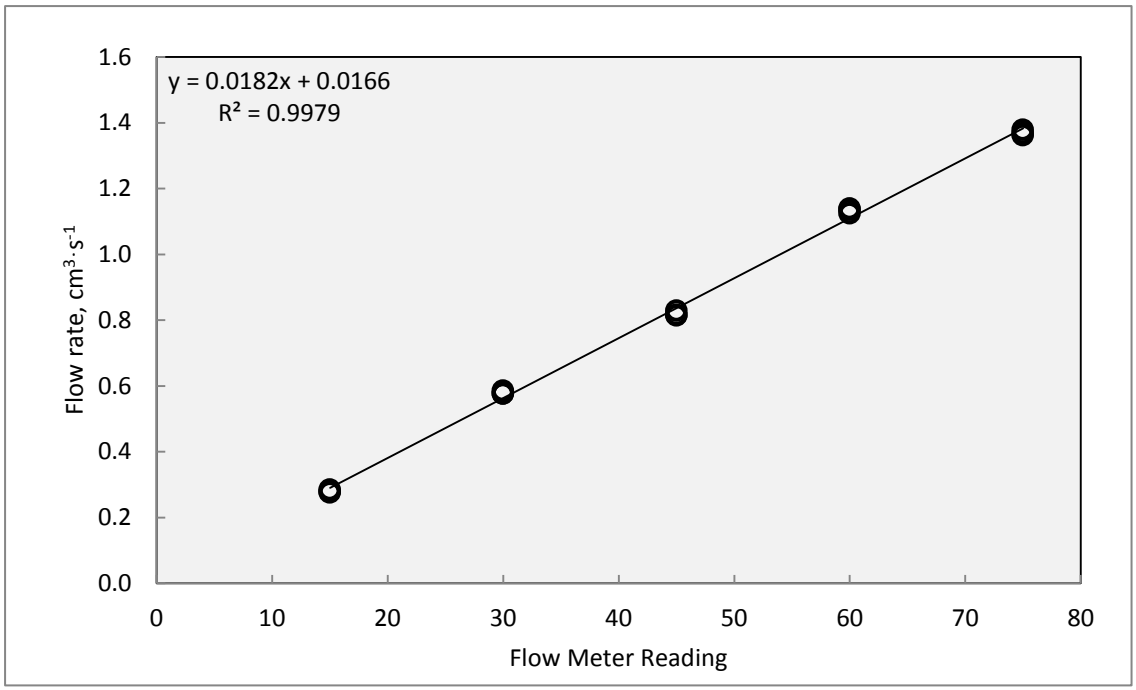

Figure B-3.1: Calibration plot for the flowrate of nitrogen

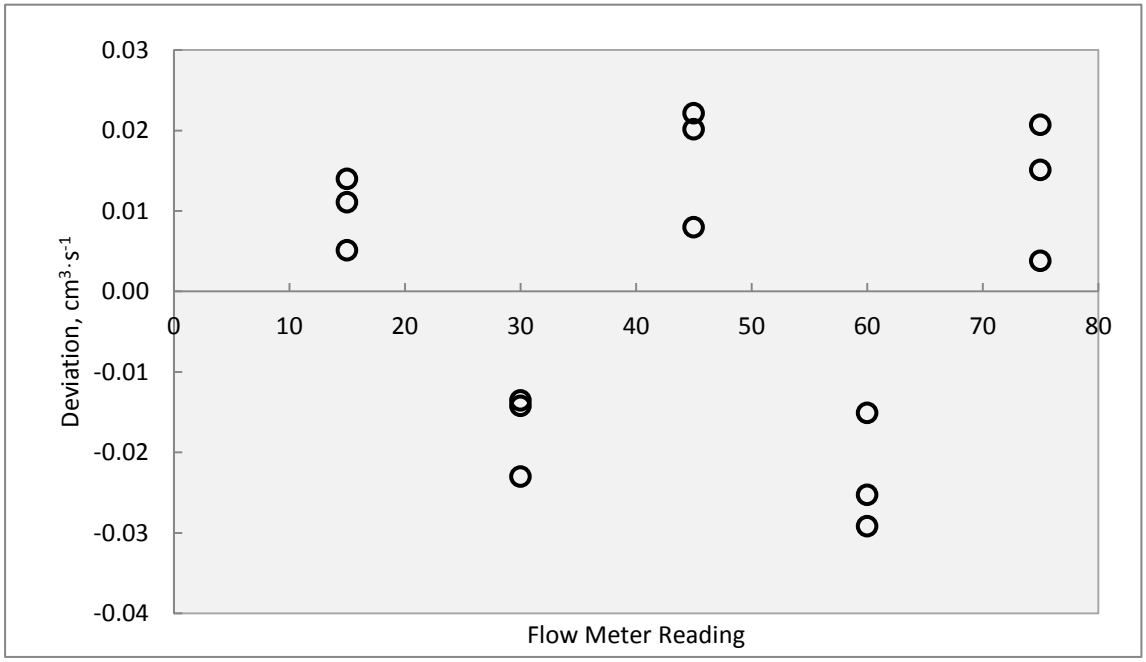

Figure B-3.2: Deviation plot for the calibration of the nitrogen rotameter

B.4 HFP flowmeter calibration – FFMR

Table B-4.1: Raw data from the calibration of the HFP flowmeter - FFMR

Flowmeter reading	Run 1 time, s	Run 2 time, s	Run 3 time, s
15	31.83	32.6	31.75
30	15.92	15.98	16.03
45	11.21	11.28	11.25
60	8.69	8.75	8.88
75	7.18	7.16	7.22

Table B-4.2: Deviation between actual and predicated flowrates - FFMR

Run	Flowmeter reading	Actual Flowrate, $cm^3 \cdot s^{-1}$	Predicted Flowrate, $cm^3 \cdot s^{-1}$	Deviation, $cm^3 \cdot s^{-1}$
1	15	0.314	0.337	0.023
	30	0.628	0.604	-0.024
	45	0.892	0.872	-0.020
	60	1.151	1.139	-0.012
	75	1.393	1.406	0.014
2	15	0.307	0.337	0.030
	30	0.626	0.604	-0.021
	45	0.887	0.872	-0.015
	60	1.143	1.139	-0.004
	75	1.397	1.406	0.010
3	15	0.315	0.337	0.022
	30	0.624	0.604	-0.019
	45	0.889	0.872	-0.017
	60	1.126	1.139	0.013
	75	1.385	1.406	0.021

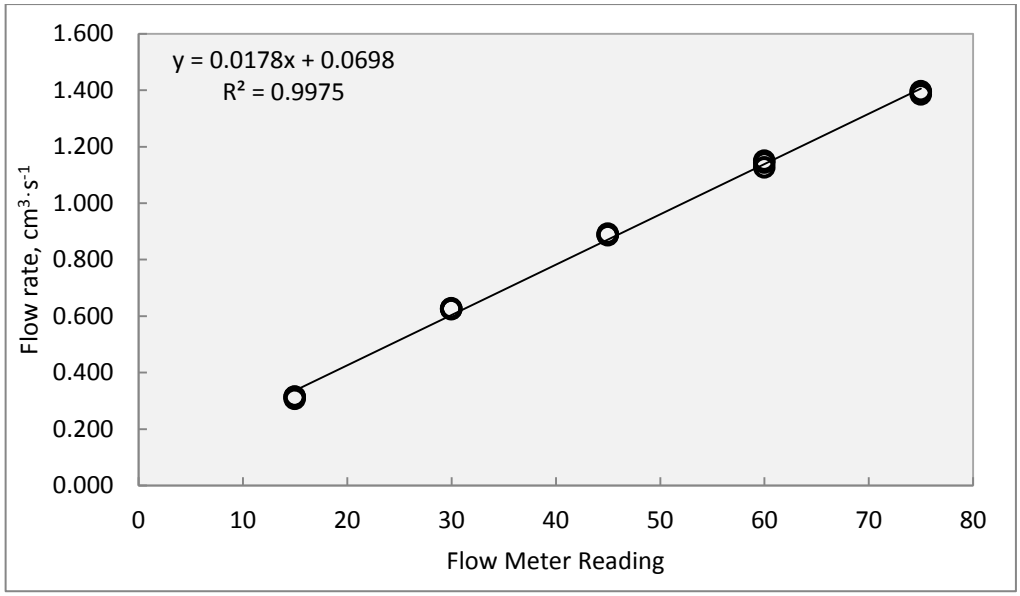

Figure B-4.1: Calibration plot for the flowrate of HFP

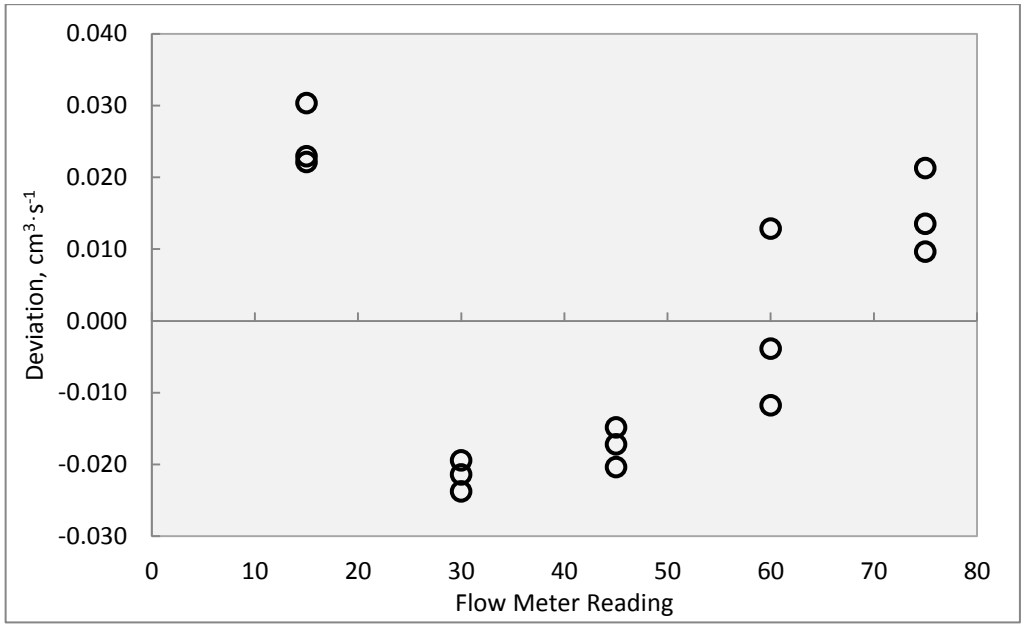

Figure B-4.2: Deviation plot for the calibration of the HFP rotameter

B.5 GC calibrations

Table B-5.1: Data for the calibration for methanol-propanol (IS) system

Run	Sample	Peak	Retention time	Area	Height	Concentration	Ratio
1	1	methanol	1.764	55057352	9975026	76.31	3.22
		IS	2.49	17086351	2554145	23.68	
	2	methanol	1.662	43394567	9634096	61.13	1.57
		IS	2.442	27588792	3024588	38.86	
	3	methanol	1.714	42327597	8700259	45.63	0.86
		IS	2.549	50419067	3349671	54.36	
	4	methanol	1.728	41690154	8635770	40.42	0.67
		IS	2.661	61448233	3911089	59.57	
	5	methanol	1.712	35828138	8489318	39.77	0.66
		IS	2.613	54247257	3759354	60.22	
2	1	methanol	1.732	57915252	10195528	76.04	3.17
		IS	2.462	18242633	2575648	23.95	
	2	methanol	1.747	50374646	9962972	61.56	1.60
		IS	2.546	31443801	3156894	38.43	
	3	methanol	1.709	45617161	9743273	50.09	1.00
		IS	2.569	45450827	3557865	49.90	
	4	methanol	1.719	41987631	8973990	40.42	0.67
		IS	2.656	61880746	3923430	59.57	
	5	methanol	1.683	32764784	8014828	38.52	0.62
		IS	2.595	52276867	3728347	61.47	
3	1	methanol	1.76	61249759	10283991	75.64	3.19
		IS	2.495	19716145	2665809	24.35	
	2	methanol	1.74	48915006	9626683	61.27	1.58
		IS	2.536	30917513	3121842	38.77	
	3	methanol	1.738	43032610	9305598	50.19	1.00
		IS	2.592	42697299	3524094	49.80	
	4	methanol	1.401	38419641	8263822	39.72	0.65
		IS	2.325	58300812	3858657	60.27	
	5	methanol	1.726	38183220	9047740	43.75	0.77
		IS	2.61	49088735	3667529	56.24	

Table B-5.2: Raw data in the preparation of samples to be analysed in the GC for calibration

Sample	Vial mass, g	Combined mass, g	IS volume, cm^3	Total mass, g	Methanol mass, g	IS mass, g	$\frac{M_{methanol}}{M_{IS}}$
1	2.76	3.551	0.2	3.694	0.791	0.143	5.53
2	2.793	3.585	0.4	3.891	0.792	0.306	2.58
3	2.765	3.537	0.6	4.009	0.772	0.472	1.64
4	2.765	3.555	0.8	4.178	0.79	0.623	1.27
5	2.725	3.504	1	4.148	0.779	0.644	1.21

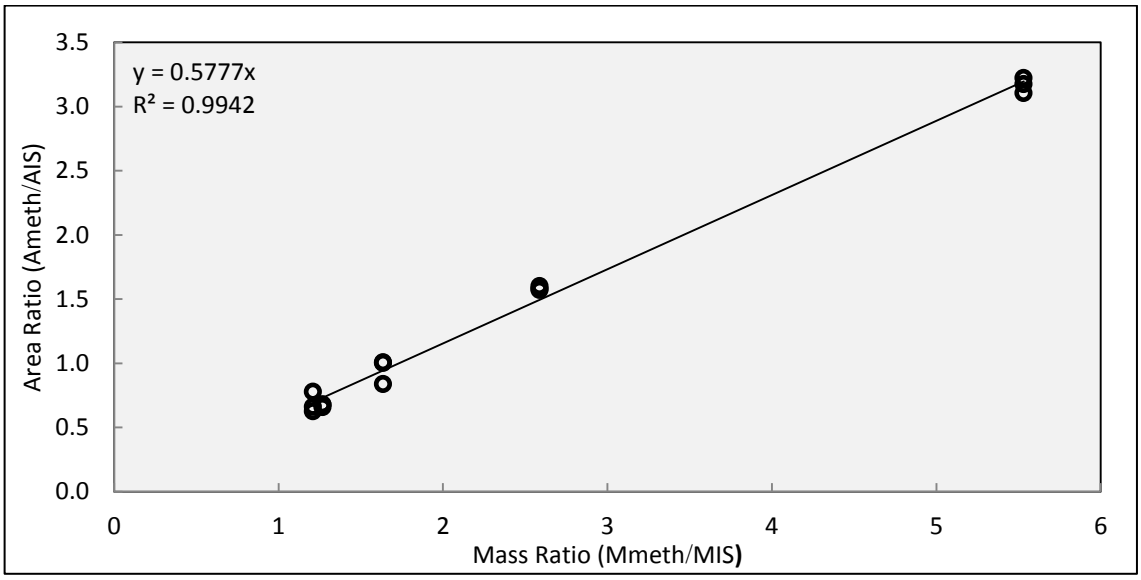

Figure B-5.1: Plot used to determine the internal response factor for methanol and propanol

Table B-5.3: Data for the samples prepared for GC analysis on crude-internal standard system

	Mass vial, g	Total mass, g	Mass dist, g	Volume IS, cm^3	Total Mass, g	Mass IS, g	Total mass, g	Mass Methanol, g
1	5.232	7.860	2.628	0.2	8.024	0.164	9.950	1.885
	5.363	7.909	2.546	0.2	8.065	0.156		
2	5.248	7.84	2.592	0.4	8.147	0.307	10.235	1.997
	5.396	7.928	2.532	0.4	8.238	0.310		
3	5.267	7.875	2.608	0.6	8.343	0.468	10.267	1.835
	5.387	7.970	2.583	0.6	8.432	0.462		
4	5.247	7.852	2.605	0.8	8.476	0.624	10.284	1.662
	5.385	8.013	2.628	0.8	8.622	0.609		
5	5.252	7.794	2.542	1	8.562	0.768	10.167	1.422
	5.393	7.98	2.587	1	8.745	0.765		

Table B-5.4: Data obtained that was used to plot Figure B-5.2

	Area Ratio (A_{HME}/A_{IS})	Mass Ratio (M_{HME}/M_{IS})
Run 1	4.90	15.06
	2.56	7.86
	1.79	5.21
	1.28	3.94
	1.00	3.19
Run 2	4.90	15.06
	2.55	7.89
	1.80	5.21
	1.26	3.94
	0.98	3.19
Run 3	4.64	15.09
	2.54	7.87
	1.80	5.21
	1.29	3.94
	1.00	3.19

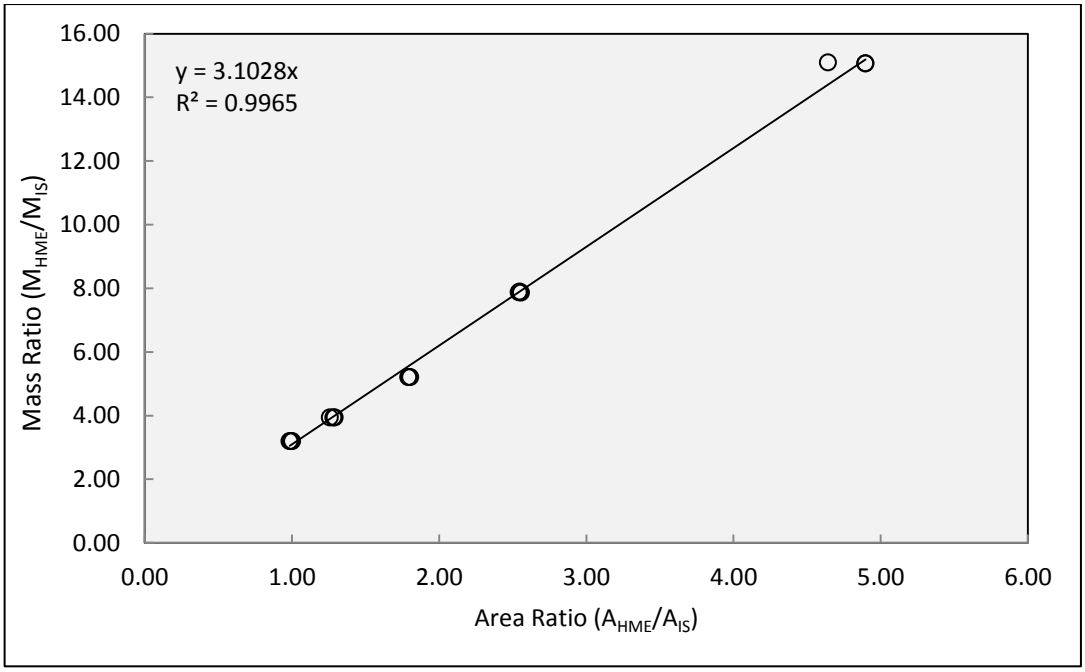

Figure B-5.2: Calibration plot for the crude and internal standard system

B.6 Temperature probe calibration

Table B-6.1: Raw data and results for temperature probe calibration

Standard Temperature, K	Display temperature, K	Predicted Temperature, K	Deviation, %
283	283.3	283.22	-0.08
283	282.8	282.72	0.10
293	292.7	292.64	0.12
293	293.3	293.24	-0.08
303	303.2	303.16	-0.05
303	303.3	303.26	-0.09
313	312.9	312.88	0.04
313	312.9	312.88	0.04

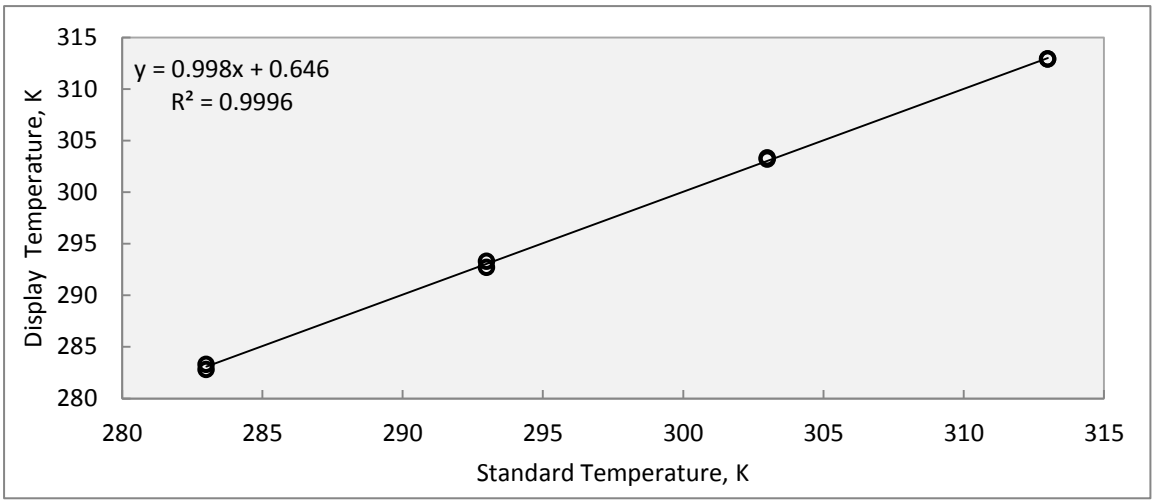

Figure B-6.1: Plot of the display temperature and the standard temperature for the calibration

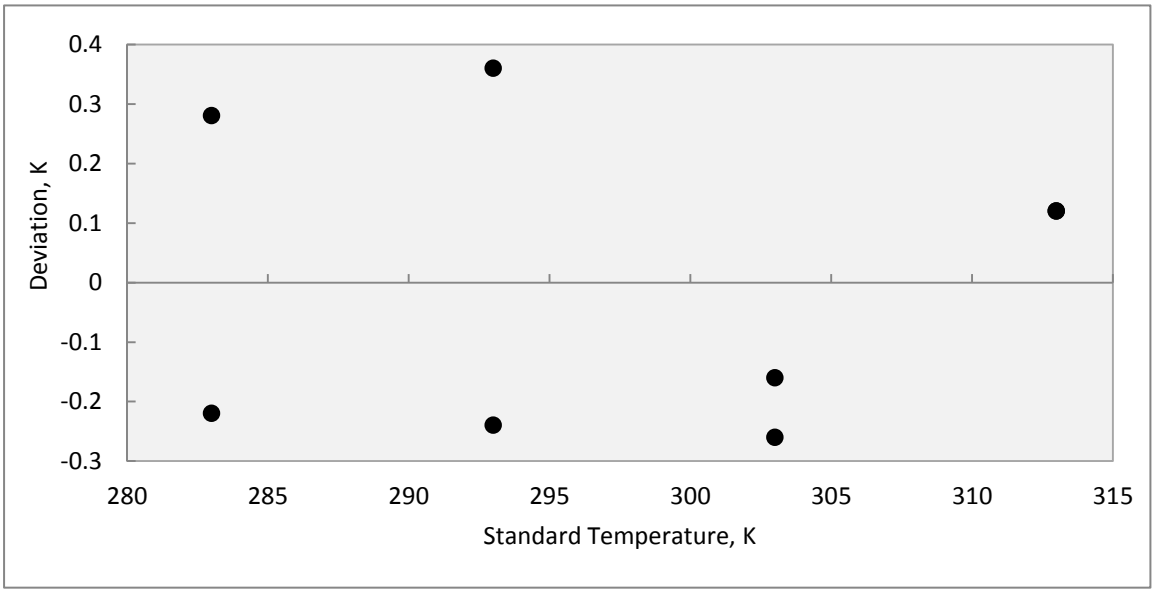

Figure B-6.2: Plot of the deviation of the calibration of the temperature probe

C

APPENDIX C

C. SAMPLE CALCULATIONS

C.1 GC calibrations

C.1.1Methanol-internal standard calibration

Calculations to obtain the data seen in Table B-5.4 for Sample 1 were obtained as follows:

Table C-1: Sequential calculations for methanol-internal standard calibration

M_v	M_{v+meth}	V_{IS}	$M_{v+meth+IS}$	M_{meth}	M_{IS}	M_{Ratio}
Measured	Measured	Measured	Measured	$= M_{v+meth} - M_v$	$= M_{v+meth+IS} - M_{v+meth}$	$= \frac{M_{meth}}{M_{IS}}$
2.76	3.551	0.2	3.694	$= 3.551 - 2.76$	$= 3.694 - 3.551$	$= \frac{0.791}{0.143}$
2.76	3.551	0.2	3.694	0.791	0.143	5.531

Figure B-5.1 was then constructed and the Internal Response Factor $(F_{meth,IS})$ then obtained

$$\frac{A_{meth}}{A_{IS}} = F_{meth,IS} \cdot \frac{M_{meth}}{M_{IS}}$$

This gave $F_{meth,IS} = 0.5777$, which is the gradient of the plot in Figure B-5.1 in Appendix B.

C.1.2 HME-internal standard calibration

Using Figure B-5.1, the methanol mass in the sample from the fractional distillation can be determined.

$$\frac{A_{meth}}{A_{IS}} = 0.5777 \cdot \frac{M_{meth}}{M_{IS}}$$

$$\therefore M_{meth} = M_{IS} \cdot \frac{A_{meth}}{0.5777 \cdot A_{IS}}$$

$$= (0.164) \cdot \left(\frac{6448331.9}{0.5777 \cdot 11627184.1}\right)$$

$$= 0.157 \text{ g}$$

The HME sample mass was determined as shown below:

$$M_{HME} = M_{sample} - M_{vial} - M_{meth} - M_{IS}$$

$$= 8.024 - 5.232 - 0.157 - 0.164$$

$$= 2.471\ g$$

The internal response factor for a HME-internal standard system was found from Figure B-5.2, which yielded a value of $F_{HME,IS} = 3.1028$.

C.2 Uncertainty on calibration

This sample calculation is done for nitrogen with similar procedures performed for the HFP rotameter calibrations as well as the GC calibrations.

The independent variable is used to calculate the calibration equation to determine the predicted output variable.

$$y_{predicted} = 0.018(15) + 0.017 = 0.29\ cm^3 \cdot s^{-1}$$

The difference between the predicted value and the experimental value is then found.

$$Difference = y_{experimental} - y_{predicted} = 0.29 - 0.279 \approx 0.011\ cm^3 \cdot s^{-1}$$

The largest magnitude difference found is divided by square root of 3 and the uncertainty on calibration results.

$$Uncertainty\ on\ calibration = \frac{0.022}{\sqrt{3}} \approx 0.013\ cm^3 \cdot s^{-1}$$

C.3 Calculating experimental yield

Using the calibrated equation from Figure B-5.1, the mass of the HME in the tested sample could be determined.

$$M_{HME} = M_{IS} \cdot \frac{A_{HME}}{F_{HME,IS} \cdot A_{IS}} = 0.557 \cdot \frac{0.01}{3.1028} = 0.016\ g$$

Then the mass fraction of the HME layer in the crude sample is shown below:

$$x_{HME} = \frac{M_{HME}}{M_{Crude}} = \frac{0.016}{0.953} = 0.017$$

Knowing the mass fraction of the crude sample after the GC analysis, the total mass can be found as shown below,

$$M_{HME,Total} = x_{HME} \cdot M_{Total}$$
$$= (0.017) \cdot (46.265) = 0.801\ \text{g}$$

The moles of HFP fed to the reactor is shown below,

$$n_{HME} = \frac{M_{HME}}{MM_{HME}} = \frac{0.801}{182.06} = 0.004\ mol$$

Moles of HFP introduced into reactor at system conditions assuming ideal gas is given by,

$$n_{HFP} = \frac{P \cdot \dot{V}}{R \cdot T} \cdot t = \frac{(101325) \cdot (5.15x10^{-7})}{(8.314) \cdot (25 + 273.15)} \cdot 30 = 0.038\ mol$$

The yield has been defined as the moles of HME produced in proportion to HME fed to the reactor.

$$\%\, Yield = \frac{0.004}{0.038} \cdot 100 = 11.6\,\%$$

C.4 Surface response methodology

The stationary point characteristic can be determined by finding the eigenvalue of the system. The eigenvalues are the roots of the determinant of the matrix B below.

$$\mathrm{B} = \begin{bmatrix} \beta_{11} & \frac{\beta_{12}}{2} & \frac{\beta_{13}}{2} \\ \frac{\beta_{21}}{2} & \beta_{22} & \frac{\beta_{23}}{2} \\ \frac{\beta_{31}}{2} & \frac{\beta_{32}}{2} & \beta_{33} \end{bmatrix}$$

$$\mathrm{B} = \frac{1}{-1618} \begin{bmatrix} 91.4 & 203.74 & 0.26 \\ 203.74 & 14.54 & 0.53 \\ 0.26 & 0.53 & 0.041 \end{bmatrix}$$

$$\det(\mathrm{B}) = \frac{1}{-1618} \begin{bmatrix} 91.4 - \lambda & 203.74 & 0.26 \\ 203.74 & 14.54 - \lambda & 0.53 \\ 0.26 & 0.53 & 0.041 - \lambda \end{bmatrix} = 0$$

$$\lambda_1 = 260.3, \lambda_2 = -154.4 \; and \; \lambda_3 = 0.04$$

D

APPENDIX D

D. SOURCE DATA

Table D-1.1: F-distribution data (Scholle, 2009)

/	DoF_1=1	2	3	4	5	6	7	8	9	10	12	15
DoF_2=1	161.4	199.5	215.7	224.6	230.2	234.0	236.8	238.9	240.5	241.9	243.9	245.9
2	18.51	19.00	19.16	19.25	19.30	19.33	19.35	19.37	19.38	19.40	19.41	19.43
3	10.13	9.552	9.277	9.117	9.014	8.941	8.887	8.845	8.812	8.786	8.745	8.703
4	7.709	6.944	6.591	6.388	6.256	6.163	6.094	6.041	5.999	5.964	5.912	5.858
5	6.608	5.786	5.409	5.192	5.050	4.950	4.876	4.818	4.772	4.735	4.678	4.619
6	5.987	5.143	4.757	4.534	4.387	4.284	4.207	4.147	4.099	4.060	4.000	3.938
7	5.591	4.737	4.347	4.120	3.972	3.866	3.787	3.726	3.677	3.637	3.575	3.511
8	5.318	4.459	4.066	3.838	3.688	3.581	3.500	3.438	3.388	3.347	3.284	3.218
9	5.117	4.256	3.863	3.633	3.482	3.374	3.293	3.230	3.179	3.137	3.073	3.006
10	4.965	4.103	3.708	3.478	3.326	3.217	3.135	3.072	3.020	2.978	2.913	2.845
11	4.844	3.982	3.587	3.357	3.204	3.095	3.012	2.948	2.896	2.854	2.788	2.719
12	4.747	3.885	3.490	3.259	3.106	2.996	2.913	2.849	2.796	2.753	2.687	2.617
13	4.667	3.806	3.411	3.179	3.025	2.915	2.832	2.767	2.714	2.671	2.604	2.533
14	4.600	3.739	3.344	3.112	2.958	2.848	2.764	2.699	2.646	2.602	2.534	2.463
15	4.543	3.682	3.287	3.056	2.901	2.790	2.707	2.641	2.588	2.544	2.475	2.403

E

APPENDIX E

E. LABORATORY SAFETY

Table E-1.1: Physical and toxicological properties of the chemicals used in this study

Property	HFP	Nitrogen	Methanol	KOH	Water	Propanol
CAS No.	116-15-4	7723-37-9	67-56-1	1310-58-3	7732-18-5	71-23-8
Molecular Formula	C_3F_6	N_2	CH_3OH	KOH	H_20	$CH_3CH_2CH_2OH$
Molecular mass, $g \cdot mol^{-1}$	150.02	28.01	32.04	56.11	18.02	60.1
Boiling point, K	243.55	77.35	1778.15	653.15	373.15	370.37
Vapour Pressure, bar	6.5	-	12.3 kPa@ 20°C	-	2.3 kPa@ 20°C	14.9 mmHg
Critical Temp, K	367.15	-	513.15	-	-	-
Critical Pressure, bar	29	-	-	-	-	-
Appearance	colourless gas	colourless gas	colourless liquid	white solid pellets	colourless liquid	colourless liquid
Flash Point Open Cup	Non-flammable	-	289.15	Non-flammable	Non-flammable	300.35
Flash Point Closed cup	Non-flammable	-	285.15	Non-flammable	Non-flammable	288.15
LC50, ppm	3060	-	64 000	-	-	67882.3

Table E-1.2: Physical and toxicological properties of the chemicals used in this study - continued

Property	Acetone	Ethanol	2-Butanol	HME	TFP	KF
CAS No.	67-64-1	64-17-5	78-92-2	382-34-3	382-93-4	7789-23-3
Molecular Formula	C_3H_6O	C_2H_6O	$CH_3CH_2CHOHCH_3$	C4H4F6O	$C_7H_3F_4O_3$	CH_3OH
Molecular mass, $g \cdot mol^{-1}$	58.08	46.07	74.12	182	344.08	32.04
Boiling point, K	329.35	351.65	372.65	327.45	448.15	337.65
Vapour Pressure, kPa	24 @ 20°C	5.7 @ 20°C	1.3 @ 20°C	-	1.1 mmHg @ 20°C	12.3 @ 20°C
Critical Temp, K	508.15	516.15	-	-	-	513.15
Critical Pressure, bar	-	-	-	-	-	-
Appearance	clear liquid	clear liquid	colourless liquid	clear liquid		clear liquid
Flash Point Open Cup	264.15	291.03	304.15	-	332.15	289.15
Flash Point Closed cup	253.15	286.03	297.05	-	-	285.15
LC50, ppm	44000	39000	6480	-	-	64000

F

APPENDIX F

F. MATLAB CODE

F.1 Semi-batch gas-liquid reactor

The code below pertains to the surface and contour plot generation for experimental runs in the GLR. The code has been adapted from similar programming performed by Lokhat. (2012). It has only been shown for one interaction pair with the same methodology used for other combinations of independent variables of the experiments.

F.1.1 Interaction of catalyst concentration and HFP mole fraction

```
close all
clear all
clc

%Raw data in the format X1,X2,X3,X1X2,X1X3,X2X3,X1^2,X2^2,X3^2

X=[0.74  0.71      298.15   0.5254   220.631  211.6865      0.5476   0.5041
88893.4225
0.74      0.71      288.15   0.5254   213.231  204.5865      0.5476   0.5041
83030.4225
0.74       0.48       298.15    0.3552    220.631  143.112  0.5476    0.2304
88893.4225
0.74       0.48       288.15    0.3552    213.231  138.312  0.5476    0.2304
83030.4225
0.49     0.71     298.15   0.3479   146.0935     211.6865     0.2401   0.5041
88893.4225
0.49     0.71     288.15   0.3479   141.1935     204.5865     0.2401   0.5041
83030.4225
0.49      0.48      298.15   0.2352   146.0935      143.112  0.2401   0.2304
88893.4225
0.49      0.48      288.15   0.2352   141.1935      138.312  0.2401   0.2304
83030.4225
0.41       0.6  293.15    0.246      120.1915       175.89    0.1681    0.36
85936.9225
0.83       0.6  293.15    0.498      243.3145       175.89    0.6889    0.36
85936.9225
0.62     0.4 293.15   0.248    181.753 117.26   0.3844   0.16     85936.9225
0.62     0.8 293.15   0.496    181.753 234.52   0.3844   0.64     85936.9225
```

```
0.62    0.6 285.15  0.372   176.793 171.09  0.3844  0.36    81310.5225
0.62    0.6 301.15  0.372   186.713 180.69  0.3844  0.36    90691.3225
0.62    0.6 293.15  0.372   181.753 175.89  0.3844  0.36    85936.9225
0.62    0.6 293.15  0.372   181.753 175.89  0.3844  0.36    85936.9225
0.62    0.6 293.15  0.372   181.753 175.89  0.3844  0.36    85936.9225
0.62    0.6 293.15  0.372   181.753 175.89  0.3844  0.36    85936.9225
0.62    0.6 293.15  0.372   181.753 175.89  0.3844  0.36    85936.9225
0.62    0.6 293.15  0.372   181.753 175.89  0.3844  0.36    85936.9225

];


X1 = [ones(size(X,1),1) X(:,1:9)]; % Adding a row of ones to the
beginning of the matrix

%Assigning each of the first 3 columns with the respective raw data

HFP=X(:,1);
Mass=X(:,2);
Temp=X(:,3);

%Creating a column of ones
ypred=ones(20,1);

%Response variable for the experimental runs assigned to variable y

y=[ 56.12503734
50.54027986
29.48271799
31.31443068
29.12794497
29.80472002
31.76503477
29.82601369
29.85733497
30.89466723
27.44131888
27.02073929
26.02948394
30.42226932
30.90809484
31.52662605
31.56281088
19.826077
34.17211783
25.75579633
];

%Built-in methods to generate an ANOVA table
%restats performs a multilinear regression of the reaction conditions,
X,
%and corresponding responses, y.

stats=regstats(y,X);
```

```
%Used to return an array of coefficients for the model equation

beta=stats.beta
%Generates a column of the predicted response variable as a function of
the
%respective reaction conditions using the calculated coefficients

for index=1:20
    ypred(index,1)= beta(1)+ beta(2)*HFP(index)  + beta(3)*Mass(index)  +
beta(4)*Temp(index)...
    +                beta(5)*(HFP(index))*(Mass(index))                 +
beta(6)*(HFP(index))*(Temp(index))                                      +
beta(7)*(Mass(index))*(Temp(index))...
    +       beta(8)*(HFP(index))^2       +       beta(9)*(Mass(index))^2
+beta(10)*(Temp(index))^2;
end


% Method to determine correlation coefficient
R = stats.rsquare

f = stats.fstat;

%Tabulating the ANOVA table
fprintf('\n')
fprintf('Regression ANOVA');
fprintf('\n\n')

fprintf('%6s','Source');
fprintf('%10s','df','SS','MS','F','P');
fprintf('\n')

fprintf('%6s','Regr');
fprintf('%10.4f',f.dfr,f.ssr,f.ssr/f.dfr,f.f,f.pval);
fprintf('\n')

fprintf('%6s','Resid');
fprintf('%10.4f',f.dfe,f.sse,f.sse/f.dfe);
fprintf('\n')

fprintf('%6s','Total');
fprintf('%10.4f',f.dfe+f.dfr,f.sse+f.ssr);
fprintf('\n')

%Generation of coefficients, standard error, t-statistic and p-value in
a
%table
t = stats.tstat;
CoeffTable = dataset({t.beta,'Coef'},{t.se,'StdErr'}, ...
                     {t.t,'tStat'},{t.pval,'pVal'})

%plotting  the  surface  contour  plot.  The  relationship  between  to
variables
%are shown while the other is kept constant.
```

```
%Generation values in the test region for two variables

FZ=20;
F=linspace(0.4,0.8,FZ)';

MZ=20;
M=linspace(0.41,0.83,MZ);

FM=repmat(F,[1,MZ]);
MM=repmat(M,[FZ,1]);

TM=zeros(FZ,MZ);

%Other variable/s kept constant
for a=1:FZ;
    for g=1:MZ;
        TM(a,g)=293.15;
    end
end

%The model to predict the response variable
YD=beta(1)+    beta(2).*FM    +    beta(3).*MM    +    beta(4).*TM    +
beta(5).*(FM).*(MM)   +   beta(6).*(FM).*(TM)   +   beta(7).*(MM).*(TM)   +
beta(8).*(FM).^2 + beta(9).*(MM).^2 +beta(10).*(TM).^2;

%to make any values that are negative, zero

for d=1:20;
    for e=1:20;
        YD_new(d,e)=YD(d,e);

        if YD(d,e)<0
            YD_new(d,e)= 0;
        end
    end
end

%Plotting and formatting the graph
surf(MM,FM,YD_new);
set(gca,'Xcolor',[0     0     0],'Ycolor',[0     0     0],'Zcolor',[0     0
0],'FontName','Arial','FontSize',16);
colorbar('FontName','Arial','FontSize',22,'Xcolor',[0 0 0],'Ycolor',[0 0
0],'location','eastoutside')

axis square %([30 70 40 90 20 100])
shading faceted
colormap jet
view(44,32)
xlabel('KOH                                                    Concentration
(g/dm^3)','FontName','Arial','FontSize',20,'FontWeight','normal','Color'
,[0 0 0])
ylabel('HFP                                                          Mole
Fraction','FontName','Arial','FontSize',20,'FontWeight','normal','Color'
,[0 0 0])
% Create zlabel
zlabel('Yield (mol HME/mol HFP %)','FontSize',20,'FontName','Arial');
```

```
%-----------------------------------------------

figure(2)

%Contour plot for the corresponding surface contour plot
[C,h]=contour(MM,FM,YD);
%Formatting the graph
clabel(C,h,'FontName','Arial','FontSize',20,'LabelSpacing',200,'Color',[
0 0 0]);
set(gca,'Xcolor',[0             0             0],'Ycolor',[0             0
0],'FontName','Arial','FontSize',16,'LineWidth',0.5);
set(h,'LineWidth',2);

axis square
shading interp
colormap jet
xlabel('KOH                                                    Concentration
(g/dm^3)','FontName','Arial','FontSize',20,'FontWeight','normal','Color'
,[0 0 0])
ylabel('HFP                    Mole                    Fraction','FontName',
'Arial','FontSize',20,'FontWeight','normal','Color',[0 0 0])

hold on


%-----------------------------------------------

figure(3)
%Parity plot for the response variable inputted and the predicted
response
%variable
plot(y,ypred,'ko','MarkerFaceColor','black','MarkerEdgeColor','black','M
arkerSize',12)

hold on

FFDx=linspace(0,100,50);
FFDy=linspace(0,100,50);


%Plotting a y=x line
plot(FFDx,FFDy,'k-','LineWidth',3)


%Formatting the graph
set(gca,'XColor','k','YColor','k','LineWidth',0.5)

set(gca,'Ytick',0:10:50)
set(gca,'Xtick',0:10:50)

set(gca,'YTickLabel',{'0';'1';'2';'3';'4';'5'},'FontName','Arial'...
    ,'FontSize',16,'FontWeight','normal')

set(gca,'XTickLabel',{'0';'1';'2';'3';'4';'5'},'FontName','Arial'...
    ,'FontSize',16,'FontWeight','normal')

%grid on
```

```
axis([0 6 0 6])
axis square

xlabel('Observed                              HME                              yield
/%','FontName','Arial','FontSize',20,'FontWeight','normal')
ylabel('Predicted                             HME                              yield
/%','FontName','Arial','FontSize',20,'FontWeight','normal')


B=zeros(3,3);

%Calculating the matrix values (as explained in the literature review)
%using the coefficients determined.
B(1,1)=(beta(8));
B(1,2)=(beta(5))/2;
B(1,3)=(beta(6))/2;
B(2,1)=(beta(5))/2;
B(2,2)=(beta(9));
B(2,3)=(beta(7))/2;
B(3,1)=(beta(6))/2;
B(3,2)=(beta(7))/2;
B(3,3)=(beta(10));

b=[beta(2); beta(3); beta(4)];

D=B^-1;

X0=-0.5*D*b;

X0T=X0';

Y0=beta(1)+0.5*X0T*b
```

F.2 Falling-film microreactor

The code used to generate the surface and contour plots for the HME yield are the same as the code used to generate the surface and contour plots for the HME mole fraction in the reactor effluent. The only alteration is the yields obtained are replaced with mole fractions as the response variable.

F.2.1 Interaction of catalyst concentration and liquid flowrate

```
close all
clear all
clc

%Raw data used for regression in the format
%X1,X2,X3,X4,X1X2,X1X3,X1X4,X2X3,X2X4,X3X4,X1^2,X2^2,X3^2,X4^2
%X represents the different independant variables
X=[0.34  0.339     280.15   1.75      0.11526  95.251   0.595     94.97085
0.59325 490.2625    0.12    0.12    78484.0225  3.06
0.34      0.339     280.15   4.25      0.11526  95.251   1.445     94.97085
1.44075 1190.6375   0.12    0.12    78484.0225  18.06
0.7 0.339    280.15  1.75     0.2373  196.105 1.225    94.97085     0.59325
490.2625    0.49    0.12    78484.0225  3.06
0.7 0.339    280.15  4.25     0.2373  196.105 2.975    94.97085     1.44075
1190.6375   0.49    0.12    78484.0225  18.06
0.34      0.518     280.15   1.75      0.17612  95.251   0.595     145.1177
0.9065  490.2625    0.12    0.27    78484.0225  3.06
0.34      0.518     280.15   4.25      0.17612  95.251   1.445     145.1177
2.2015  1190.6375   0.12    0.27    78484.0225  18.06
0.7 0.518    280.15  1.75     0.3626  196.105 1.225    145.1177     0.9065
490.2625    0.49    0.27    78484.0225  3.06
0.7 0.518    280.15  4.25     0.3626  196.105 2.975    145.1177     2.2015
1190.6375   0.49    0.27    78484.0225  18.06
0.34      0.339     290.15   1.75      0.11526  98.651   0.595     98.36085
0.59325 507.7625    0.12    0.12    84187.0225  3.06
0.34      0.339     290.15   4.25      0.11526  98.651   1.445     98.36085
1.44075 1233.1375   0.12    0.12    84187.0225  18.06
0.7 0.339    290.15  1.75     0.2373  203.105 1.225    98.36085     0.59325
507.7625    0.49    0.12    84187.0225  3.06
0.7 0.339    290.15  4.25     0.2373  203.105 2.975    98.36085     1.44075
1233.1375   0.49    0.12    84187.0225  18.06
0.34      0.518     290.15   1.75      0.17612  98.651   0.595     150.2977
0.9065  507.7625    0.12    0.27    84187.0225  3.06
0.34      0.518     290.15   4.25      0.17612  98.651   1.445     150.2977
2.2015  1233.1375   0.12    0.27    84187.0225  18.06
0.7 0.518    290.15  1.75     0.3626  203.105 1.225    150.2977     0.9065
507.7625    0.49    0.27    84187.0225  3.06
0.7 0.518    290.15  4.25     0.3626  203.105 2.975    150.2977     2.2015
1233.1375   0.49    0.27    84187.0225  18.06
0.52     0.429    275.15   3    0.22308 143.078 1.56     118.03935    1.287
825.45  0.27    0.18    75707.5225  9
0.52     0.429    295.15   3    0.22308 153.478 1.56     126.61935    1.287
885.45  0.27    0.18    87113.5225  9
```

```
0.52      0.25      285.15   3    0.13      148.278  1.56      71.2875  0.75
855.45  0.27    0.06    81310.5225  9
0.52     0.607   285.15   3   0.31564  148.278  1.56     173.08605   1.821
855.45  0.27    0.37    81310.5225  9
0.17     0.43     285.15   3    0.0731   48.4755  0.51     122.6145     1.29
855.45  0.03    0.18    81310.5225  9
0.88     0.43     285.15   3    0.3784   250.932  2.64     122.6145     1.29
855.45  0.77    0.18    81310.5225  9
0.52     0.43     285.15   0.5  0.2236   148.278  0.26     122.6145     0.215
142.575  0.27    0.18    81310.5225  0.25
0.52     0.43     285.15   5.5  0.2236   148.278  2.86     122.6145     2.365
1568.325    0.27    0.18    81310.5225  30.25
0.52     0.43     285.15   3    0.2236   148.278  1.56     122.6145     1.29
855.45  0.27    0.18    81310.5225  9
0.52     0.43     285.15   3    0.2236   148.278  1.56     122.6145     1.29
855.45  0.27    0.18    81310.5225  9
0.52     0.43     285.15   3    0.2236   148.278  1.56     122.6145     1.29
855.45  0.27    0.18    81310.5225  9
0.52     0.43     285.15   3    0.2236   148.278  1.56     122.6145     1.29
855.45  0.27    0.18    81310.5225  9
0.52     0.43     285.15   3    0.2236   148.278  1.56     122.6145     1.29
855.45  0.27    0.18    81310.5225  9
0.52     0.43     285.15   3    0.2236   148.278  1.56     122.6145     1.29
855.45  0.27    0.18    81310.5225  9


];



X1 = [ones(size(X,1),1)  X(:,1:14)]; % Adding a row of ones to the
beginning of the matrix

%defining a column of the each of the 4 independant variables
FRAC=X(:,1);
CONC=X(:,2);
TEMP=X(:,3);
FLOW=X(:,4);

%Defining a columns of ones
ypred=ones(30,1);

%Assigning variable y with the response variable from experimentation
y=[ 11.60287969
48.32060228
38.87511458
56.93495529
33.11829389
39.78000259
81.58758008
23.33019093
42.93894042
49.84724741
40.37908833
52.35594554
29.90078968
37.47673543
37.41386218
46.88364004
```

```
61.53492175
51.76111132
53.29850275
44.72735489
34.90780363
61.66544974
28.45207202
55.12967207
44.01894679
38.88201478
59.44413374
53.54868663
67.99831355
59.35758571

];


%Built-in methods to generate an ANOVA table
%restats performs a multilinear regression of the reaction conditions,
X,
%and corresponding responses, y.

stats=regstats(y,X);

beta=stats.beta

for index=1:30
     ypred(index,1)= beta(1)+ beta(2)*FRAC(index)  + beta(3)*CONC(index)
+ beta(4)*TEMP(index)+beta(5)*FLOW(index)...
    +                beta(6)*(FRAC(index))*(CONC(index))                +
beta(7)*(FRAC(index))*(TEMP(index))                                      +
beta(8)*(FRAC(index))*(FLOW(index))+beta(9)*(CONC(index))*(TEMP(index))+
beta(10)*(CONC(index))*(FLOW(index))+beta(11)*(TEMP(index))*(FLOW(index)
)...
    +      beta(12)*(FRAC(index))^2      +      beta(13)*(CONC(index))^2
+beta(14)*(TEMP(index))^2+beta(15)*(FLOW(index))^2;
end

R = stats.rsquare

f = stats.fstat;

fprintf('\n')
fprintf('Regression ANOVA');
fprintf('\n\n')

fprintf('%6s','Source');
fprintf('%10s','df','SS','MS','F','P');
fprintf('\n')

fprintf('%6s','Regr');
fprintf('%10.4f',f.dfr,f.ssr,f.ssr/f.dfr,f.f,f.pval);
fprintf('\n')

fprintf('%6s','Resid');
fprintf('%10.4f',f.dfe,f.sse,f.sse/f.dfe);
fprintf('\n')
```

```
fprintf('%6s','Total');
fprintf('%10.4f',f.dfe+f.dfr,f.sse+f.ssr);
fprintf('\n')



t = stats.tstat;
CoeffTable = dataset({t.beta,'Coef'},{t.se,'StdErr'}, ...
                     {t.t,'tStat'},{t.pval,'pVal'})



concZ=30;
conc=linspace(0.25,0.61,concZ)';

flowZ=30;
flow=linspace(0.5,5.5,flowZ);

concM=repmat(conc,[1,flowZ]);
flowM=repmat(flow,[concZ,1]);

molFracM=zeros(concZ,flowZ);
tempM=zeros(concZ,flowZ);

for a=1:concZ;
    for g=1:flowZ;
        molFracM(a,g)=0.52;
        tempM(a,g)=285.15;
    end
end

%The model to predict the response variable
YD=beta(1)+  beta(2).*molFracM  +  beta(3).*concM  +  beta(4).*tempM  +
beta(5).*flowM          +          beta(6).*(molFracM).*(concM)          +
beta(7).*(molFracM).*(tempM)        +        beta(8).*(molFracM).*(flowM)
+beta(9).*(concM).*(tempM)                                                +
beta(10).*(concM).*(flowM)+beta(11).*(tempM).*(flowM)+
beta(12).*(molFracM).^2               +              beta(13).*(concM).^2
+beta(14).*(tempM).^2+beta(15).*(flowM).^2;

%to make any values that are negative, zero
for d=1:30;
    for e=1:30;
        YD_new(d,e)=YD(d,e);

        if YD(d,e)<0
            YD_new(d,e)=0;
        end
    end
end



surf(flowM,concM,YD_new);
set(gca,'Xcolor',[0     0     0],'Ycolor',[0     0     0],'Zcolor',[0     0
0],'FontName','Arial','FontSize',16);
```

```
colorbar('FontName','Arial','FontSize',22,'Xcolor',[0 0 0],'Ycolor',[0 0
0],'location','eastoutside')

axis square
shading faceted
colormap jet
view(44,32)
xlabel('Liquid                                                    Flowrate
(ml/s)','FontName','Arial','FontSize',22,'FontWeight','normal','Color',[
0 0 0])
ylabel('KOH                                                  Concentration
(mol/l)','FontName','Arial','FontSize',22,'FontWeight','normal','Color',
[0 0 0])

% Create zlabel
zlabel('Yield (mol HME/mol HFP %)','FontSize',20,'FontName','Arial');

%-------------------------------------------

figure(2)

%Contour plot for the corresponding surface contour plot
[C,h]=contour(flowM,concM,YD,[10:5:70]);
%Formatting the graph
clabel(C,h,'FontName','Arial','FontSize',12,'LabelSpacing',200,'Color',[
0 0 0]);
set(gca,'Xcolor',[0             0             0],'Ycolor',[0             0
0],'FontName','Arial','FontSize',22,'LineWidth',0.5);
set(h,'LineWidth',2);

axis square
shading interp
colormap jet
xlabel('Liquid                                                    Flowrate
(ml/s)','FontName','Arial','FontSize',22,'FontWeight','normal','Color',[
0 0 0])
ylabel('KOH                                                  Concentration
(mol/l)','FontName','Arial','FontSize',22,'FontWeight','normal','Color',
[0 0 0])

hold on

figure(3)
%Parity plot for the response variable inputted and the predicted
response
%variable
plot(y,ypred,'ko','MarkerFaceColor','black','MarkerEdgeColor','black','M
arkerSize',12)

hold on

FFDx=linspace(0,100,50);
FFDy=linspace(0,100,50);

%Plotting a y=x line
plot(FFDx,FFDy,'k-','LineWidth',3)

%Formatting the graph
```

```
set(gca,'XColor','k','YColor','k','LineWidth',0.5)

set(gca,'Ytick',0:10:90)
set(gca,'Xtick',0:10:90)

set(gca,'YTickLabel',{'0';'10';'20';'30';'40';'50';'60';'70';'80';'90'},
'FontName','Arial'...
    ,'FontSize',16,'FontWeight','normal')

set(gca,'XTickLabel',{'0';'10';'20';'30';'40';'50';'60';'70';'80';'90'},
'FontName','Arial'...
    ,'FontSize',16,'FontWeight','normal')

%grid on

axis([0 85 0 85])
axis square

xlabel('Observed                              HME                              yield
/%','FontName','Arial','FontSize',22,'FontWeight','normal')
ylabel('Predicted                              HME                              yield
/%','FontName','Arial','FontSize',22,'FontWeight','normal')

B=zeros(4,4);

%Calculating the matrix values (as explained in the literature review)
%using the coefficients determined.
B(1,1)=(beta(12));
B(1,2)=(beta(6))/2;
B(1,3)=(beta(7))/2;
B(1,4)=(beta(8))/2;
B(2,1)=(beta(6))/2;
B(2,2)=(beta(13));
B(2,3)=(beta(9))/2;
B(2,4)=(beta(10))/2;
B(3,1)=(beta(7))/2;
B(3,2)=(beta(9))/2;
B(3,3)=(beta(14));
B(3,4)=(beta(11))/2;
B(4,1)=(beta(8))/2;
B(4,2)=(beta(10))/2;
B(4,3)=(beta(11))/2;
B(4,4)=(beta(15));

b=[beta(2); beta(3); beta(4); beta(5)];

D=B^-1;

X0=-0.5*D*b;

X0T=X0';

Y0=beta(1)+0.5*X0T*b
```

```
48.48
51.55

];


%Built-in methods to generate an ANOVA table
%restats performs a multilinear regression of the reaction conditions,
X,
%and corresponding responses, y.


stats=regstats(y,X);

beta=stats.beta

for index=1:30
    ypred(index,1)= beta(1)+ beta(2)*FRAC(index) + beta(3)*CONC(index) +
beta(4)*TEMP(index)+beta(5)*FLOW(index)...
    +                beta(6)*(FRAC(index))*(CONC(index))                +
beta(7)*(FRAC(index))*(TEMP(index))                                      +
beta(8)*(FRAC(index))*(FLOW(index))+beta(9)*(CONC(index))*(TEMP(index))+
beta(10)*(CONC(index))*(FLOW(index))+beta(11)*(TEMP(index))*(FLOW(index)
)...
    +      beta(12)*(FRAC(index))^2       +      beta(13)*(CONC(index))^2
+beta(14)*(TEMP(index))^2+beta(15)*(FLOW(index))^2;

end

R = stats.rsquare

f = stats.fstat;

fprintf('\n')
fprintf('Regression ANOVA');
fprintf('\n\n')

fprintf('%6s','Source');
fprintf('%10s','df','SS','MS','F','P');
fprintf('\n')

fprintf('%6s','Regr');
fprintf('%10.4f',f.dfr,f.ssr,f.ssr/f.dfr,f.f,f.pval);
fprintf('\n')

fprintf('%6s','Resid');
fprintf('%10.4f',f.dfe,f.sse,f.sse/f.dfe);
fprintf('\n')

fprintf('%6s','Total');
fprintf('%10.4f',f.dfe+f.dfr,f.sse+f.ssr);
fprintf('\n')



t = stats.tstat;
CoeffTable = dataset({t.beta,'Coef'},{t.se,'StdErr'}, ...
```

```
                    {t.t,'tStat'},{t.pval,'pVal'})



molFracZ=30;
molFrac=linspace(0.17,0.88,molFracZ)';

flowZ=30;
flow=linspace(0.5,5.5,flowZ);

molFracM=repmat(molFrac,[1,flowZ]);
flowM=repmat(flow,[molFracZ,1]);

tempM=zeros(molFracZ,flowZ);
concM=zeros(molFracZ,flowZ);

for a=1:molFracZ;
    for g=1:flowZ;
        tempM(a,g)=285.15;
        concM(a,g)= 0.43;
    end
end

%The model to predict the response variable
YD=beta(1)+  beta(2).*molFracM  +  beta(3).*concM  +  beta(4).*tempM  +
beta(5).*flowM          +          beta(6).*(molFracM).*(concM)          +
beta(7).*(molFracM).*(tempM)        +        beta(8).*(molFracM).*(flowM)
+beta(9).*(concM).*(tempM)                                                +
beta(10).*(concM).*(flowM)+beta(11).*(tempM).*(flowM)+
beta(12).*(molFracM).^2               +               beta(13).*(concM).^2
+beta(14).*(tempM).^2+beta(15).*(flowM).^2;

%to make any values that are negative, zero
for d=1:30;
    for e=1:30;
        YD_new(d,e)=YD(d,e);

        if YD(d,e)<0
            YD_new(d,e)=0;
        end
    end
end

%Plotting and formatting the graph
surf(flowM,molFracM,YD_new);
set(gca,'Xcolor',[0     0     0],'Ycolor',[0     0     0],'Zcolor',[0     0
0],'FontName','Arial','FontSize',16);
colorbar('FontName','Arial','FontSize',22,'Xcolor',[0 0 0],'Ycolor',[0 0
0],'location','eastoutside')

axis square
shading faceted
colormap jet
view(55,30);
% Create xlabel
xlabel('Liquid                                                    Flowrate
(ml/s)','HorizontalAlignment','right','FontSize',20,...
    'FontName','Arial');
```

```
% Create ylabel
ylabel('HFP Mole Fraction','FontSize',20,'FontName','Arial',...
    'HorizontalAlignment','left');

% Create zlabel
zlabel('Yield (mol HME/mol HFP, %)','FontSize',20,'FontName','Arial');
%-----------------------------------------

figure(2)

[C,h]=contour(flowM,molFracM,YD,[10:5:70]);
clabel(C,h,'FontName','Arial','FontSize',20,'LabelSpacing',200,'Color',[
0 0 0]);
set(gca,'Xcolor',[0            0            0],'Ycolor',[0            0
0],'FontName','Arial','FontSize',16,'LineWidth',0.5);
set(h,'LineWidth',2);

axis square
shading interp
colormap jet
xlabel('Liquid                                                    Flowrate
(ml/s)','FontName','Arial','FontSize',22,'FontWeight','normal','Color',[
0 0 0])
ylabel('HFP                                                         Mole
Fraction','FontName','Arial','FontSize',22,'FontWeight','normal','Color'
,[0 0 0])

hold on



figure(3)
%Parity plot for the response variable inputted and the predicted
response
%variable
plot(y,ypred,'ko','MarkerFaceColor','black','MarkerEdgeColor','black','M
arkerSize',12)

hold on

FFDx=linspace(0,100,50);
FFDy=linspace(0,100,50);

%Plotting a y=x line
plot(FFDx,FFDy,'k-','LineWidth',3)

%Formatting the graph
set(gca,'XColor','k','YColor','k','LineWidth',0.5)

set(gca,'Ytick',0:10:50)
set(gca,'Xtick',0:10:50)

set(gca,'YTickLabel',{'0';'10';'20';'30';'40';'50'},'FontName','Arial'..
.
    ,'FontSize',16,'FontWeight','normal')
```

```
set(gca,'XTickLabel',{'0';'10';'20';'30';'40';'50'},'FontName','Arial'..
.
    ,'FontSize',16,'FontWeight','normal')

%grid on

axis([0 50 0 50])
axis square

xlabel('Observed                          HME                          yield
/%','FontName','Arial','FontSize',22,'FontWeight','normal')
ylabel('Predicted                          HME                          yield
/%','FontName','Arial','FontSize',22,'FontWeight','normal')

B=zeros(4,4);

%Calculating the matrix values (as explained in the literature review)
%using the coefficients determined.
B(1,1)=(beta(12));
B(1,2)=(beta(6))/2;
B(1,3)=(beta(7))/2;
B(1,4)=(beta(8))/2;
B(2,1)=(beta(6))/2;
B(2,2)=(beta(13));
B(2,3)=(beta(9))/2;
B(2,4)=(beta(10))/2;
B(3,1)=(beta(7))/2;
B(3,2)=(beta(9))/2;
B(3,3)=(beta(14));
B(3,4)=(beta(11))/2;
B(4,1)=(beta(8))/2;
B(4,2)=(beta(10))/2;
B(4,3)=(beta(11))/2;
B(4,4)=(beta(15));

b=[beta(2); beta(3); beta(4); beta(5)];

D=B^-1;

X0=-0.5*D*b;

X0T=X0';

Y0=beta(1)+0.5*X0T*b
```